SOLID-STATE NMR STUDY OF DRUG INTERACTION WITH PHOSPHOLIPID BILAYERS

Chlorpromazine, olanzapine and articaine interacting with saturated and unsaturated phosphatidylserines and saturated phosphatidylcholines

Thesis submitted in fulfillment of the requirements for

the degree philosophiae doctor (PhD)

CHEN SONG

DEPARTMENT OF CHEMISTRY

THE FACULTY OF MATHEMATICS AND NATURAL SCIENCES

UNIVERSITY OF BERGEN

NORWAY, 2007

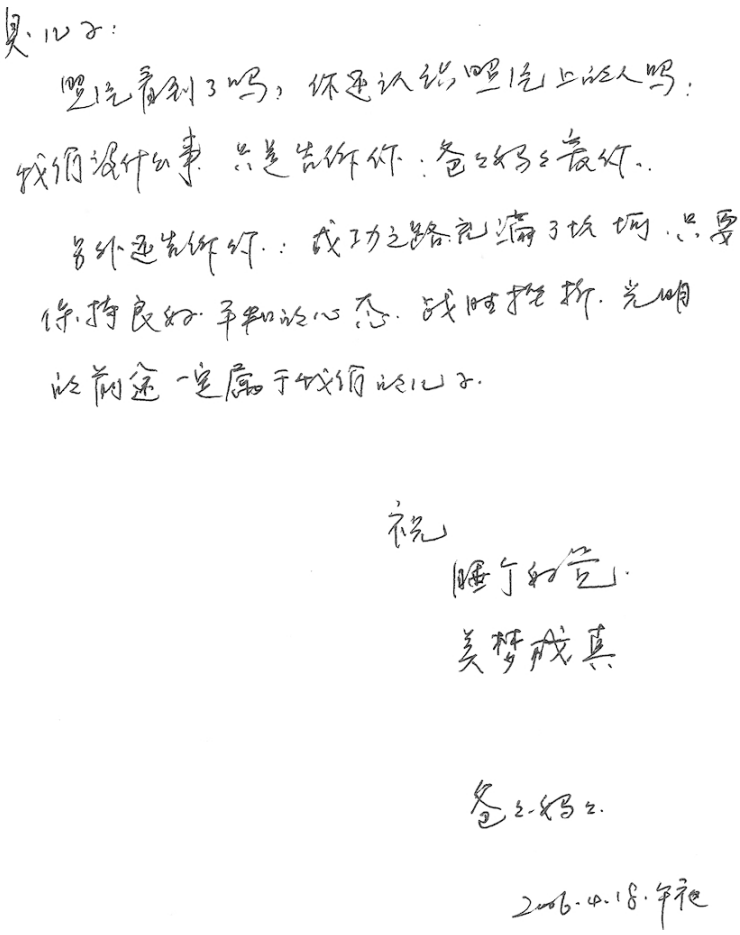
奥儿子：

望已看到了吗，你还认识照片上的人吗？

我们没什么事，只是告诉你：爸妈很爱你。

另外还告诉你：成功之路充满了坎坷，只要你持良好平和的心态，战时挫折，光明的前途一定属于我们的儿子。

祝

睡个好觉！

美梦成真

爸妈

2006.4.18.午祝

– *A letter from my mother (Beijing, 18 April 06)*

ACKNOWLEDGEMENTS

This work was carried out at Department of Chemistry, the Faculty of Mathematics and Natural Sciences, University of Bergen (UiB) during the period of 2004−2007. The financial support of this project was mainly provided from Lånekassen, and the one-year financial support (08,04−08,05) was from Førsteamanuensis Henning Lygre at Department of Dental Science, UiB.

First of all, I wish to give special thanks to my supervisor Førsteamanuensis Willy Nerdal for all of his appreciated guidance and versatile support through these many years (from 08,02). Willy has an open-door policy, which means I can stop by his office, whenever I want, he also has an open-mind policy, there are no stupid questions, so, if I have something on my mind, simply knock on his door. Willy also suggested many interesting points and perspectives to me and provided me with a reasonable degree of freedom in my work. Furthermore he skillfully revised this thesis. And I would like to express my sincere gratitude to my co-supervisor Prof. Holm Holmsen for his much valued support and advice. The contribution of my co-author Dr. Anja Underhaug Gjerde at Department of Biomedicine to this work is highly appreciated. I wish to thank Prof. Einar Sletten and Førsteamanuensis Nils Åge Frøystein for their helpful advices and contributions to my work.

I also thank my colleague Magnus Jensen for creating the friendly atmosphere in the office and constructive collaboration in the lab. There is no negativity in the air, even when he feels under impossible pressure at work. I am very grateful to all my former and current fellow students in Biophysics Chemistry group for their help and cheerful attitudes that made my time here more enjoyable, where I should name Katrin, Carsten, and Cecilie.

Many thanks to Avdelingsingeniør Atle Aaberg for his technical support and expert help (especially on weekends), when I worked in Bruker DMX 400 MHz spectrometer and Bruker 500 MHz Ultrashield Plus spectrometer labs.

I thank the staff in main office for taking care of many of those administrative tasks that made my time in Norway so much easier.

Finally, my unlimited gratitude is addressed to my family for their supports and love, especially my grandfather Yanren Song, who knew the value of a good education. I am fortunate to be part of such a caring family. I am very thankful for my wonderful wife Ziwen for all of her love, devotion, understanding and patience on my way to achieve this goal.

BERGEN, JUNE 2007

CHEN SONG

TABLE OF CONTENTS

ABBREVIATIONS

AA	arachidonic acid
AChR	nicotinic acetylcholine receptor
apoD	apolipoprotein-D
cAMP	cyclic adenosine monophosphate
cGMP	cyclic guanosine monophosphate
CK	creatine kinase
CMC	critical micelle concentrations
CP	cross polarization
CPZ	chlorpromazine
CSA	chemical shielding anisotropy
CW	continuous wave
DAG	diacylglycerol
DGK	diacylglycerol kinase
DHA	docosahexaenoic acid
DiGlcDAG	diglucosyldiacylglycerol
DMPC	1,2-Dimyristoyl-*sn*-Glycerol-3-Phosphatidylcholine
DOPC	1,2-Dioleoyl-*sn*-Glycerol-3-Phosphocholine
DPPC	1,2-Dipalmitoyl-*sn*-Glycerol-3-Phosphatidylcholine
DPPS	1,2-Dipalmitoyl-*sn*-Glycerol-3-Phosphatidylserine
DSC	differential scanning calorimetry
DSPC	1,2-Distearoyl-*sn*-Glycerol-3-Phosphatidylcholine
EPC	egg phosphatidylcholine
EPR	electron paramagnetic resonance
EPUFA	essential polyunsaturated fatty acids
ESR	electron spin resonance
IP_3	inositol 1,4,5-*tri*phosphate
K_{eff}	partition coefficient
MAS	magic-angle spinning
NMR	nuclear magnetic resonance
NO	nitric oxide
NOE	nuclear Overhauser effect
OLZ	olanzapine
PA	phosphatidic acid

PBPS	pig brain PS
PC	phosphatidylcholine
PE	phosphatidylethanolamine
PG	phosphatidylglycerol
PI	phosphatidylinositol
PIP_2	phosphatidylinositol 4,5-*bis*phosphate
PIP_3	phosphatidylinositol 3,4,5-*tri*phosphate
PKC	protein kinase C
PLA_2	phospholipase A_2
PLC	phospholipase C
PLD	phospholipase D
POPC	1-Palmitoyl, 2-Oleoyl-*sn*-Glycerol-3-Phosphatidylcholine
POPS	1-Palmitoyl, 2-Oleoyl-*sn*-Glycerol-3-Phosphatidylserine
PS	phosphatidylserine
PUFAs	polyunsaturated fatty acids
rf	radio frequency
SOPS	1-Stearoyl, 2-Oleoyl-*sn*-Glycerol-3-Phosphatidylserine
SDPS	1-Stearoyl, 2-Docosahexaenoyl-*sn*-Glycerol-3-Phosphatidylserine
SM	sphingomyelin
SPR	surface plasmon resonance
T_1	spin-lattice relaxation constant
T_2	spin-spin relaxation time constant
T_m	gel-to-liquid-crystalline phase-transition temperature
τ_c	correlation time

LIST OF PAPERS

I C. Song, A.U. Gjerde, H. Holmsen, W. Nerdal, Importance of polyunsaturated acyl chains in chlorpromazine interaction with phosphatidylserines: A ^{13}C and ^{31}P solid-state NMR study. *Biophys. Chem.* **117**(2) (2005) 101−109.

II C. Song, H. Holmsen, W. Nerdal, Existence of lipid microdomains in bilayer of dipalmitoylphosphatidylcholine (DPPC) and 1-stearoyl-2-docosahexenoyl phosphatidylserine (SDPS) and their perturbation by chlorpromazine: A ^{13}C and ^{31}P solid-state NMR study. *Biophys. Chem.* **120**(3) (2006) 178−187.

III C. Song, H. Lygre, W. Nerdal, Articaine interaction with DSPC bilayer: A ^{13}C and ^{31}P solid-state NMR study. *Submitted, 2007*.

IV C. Song, W. Nerdal, Olanzapine Interaction with DPPC/DPPS and DPPC/POPS bilayers: A ^{13}C and ^{31}P solid-state NMR study. *Submitted 2007*.

AIMS OF PRESENT STUDY

Several studies have demonstrated that the activity of membrane-bound proteins (receptors, channels, enzymes) is often dependent on the class of phospholipid, the particular acyl chains and the physical state of the phospholipids. On the other hand, a perturbation of lipid bilayer organization by amphiphilic molecules (e.g. chlorpromazine and olanzapine) could influence the activity or catalyzed processes of membrane-bound proteins, even without direct interaction between the protein and the amphiphile.

The main objective of the present study is about the interaction and perturbation of amphiphiles (a typical antipsychotic drug chlorpromazine, an atypical drug olanzapine, and a local anaesthetic articaine) on phospholipid bilayers as models of biological membranes by carbon−13 and phosphorus−31 solid-state Nuclear Magnetic Resonance (NMR).

1. INTRODUCTION

The biological membrane is a collage of many different proteins embedded in the fluid matrix of the lipid bilayer [1], the most of the membrane's specific functions, e.g. pumps, channels, energy transducers, are determined by proteins. In particular, the integral proteins which penetrate through the membrane are, for example, ionic channels, the proteins that provide active ionic transport etc. [2,3]. The lipid bilayer is the main fabric of the membrane, and its structure creates a semi-permeable membrane [4,5]. The hydrophobic core impedes the transport of hydrophilic structures, such as ions and polar molecules but enables hydrophobic molecules, which can dissolve in the membrane, to cross it with ease [6,7]. The complex array of phospholipids present in membranes of different tissues and organelles demonstrates the involvement in membrane-mediated events [8–10]. Several early examples have already shown that lipids behave not only as structural molecules but also as active biological molecules, functionally important components of cells [11–13]. Many drugs, e.g. antipsychotics and local anaesthetics, are amphiphilic molecules, known to partition preferentially in the plasma membrane, and perturb the packing of phospholipids in biological bilayers [14–16]. On the other hand, the activity of membrane-bound proteins can be influenced by the changes in the organization and dynamics of the membrane [17–19]. Therefore, one should expect that perturbation of the lipid organization by amphiphilic molecules (such as arise from the drug–lipid interaction) would subsequently influence the activity or catalyzed processes of membrane-bound proteins, even without direct interaction between the protein and the amphiphile.

1.1 Biomembranes

1.1.1 Composition of Lipid Bilayer

Most biological membranes contain a variety of lipids, including the various glycerophospholipids such as phosphatidylcholine (PC), phosphatidylethanolamine (PE), phosphatidylserine (PS), phosphatidylinositol (PI), phosphatidylglycerol (PG) and phosphatidic acid (PA) as well as sphingomyelin (SM) and, in some membranes, glycosphingolipids. This category is characterized as the open-chain compounds with a polar headgroup and one or two non-polar hydrocarbon chains linked to a glycerol by either an acyl (diacylglycerophospholipids, referred here to as phospholipids, also see *Section 1.1.4*) or an ether bond. Furthermore, cholesterol, ergosterol, stigmasterol and sitosterol are sterols (see *Scheme 1.1*), which consist of fused-ring compounds, also found in many membranes [6,7].

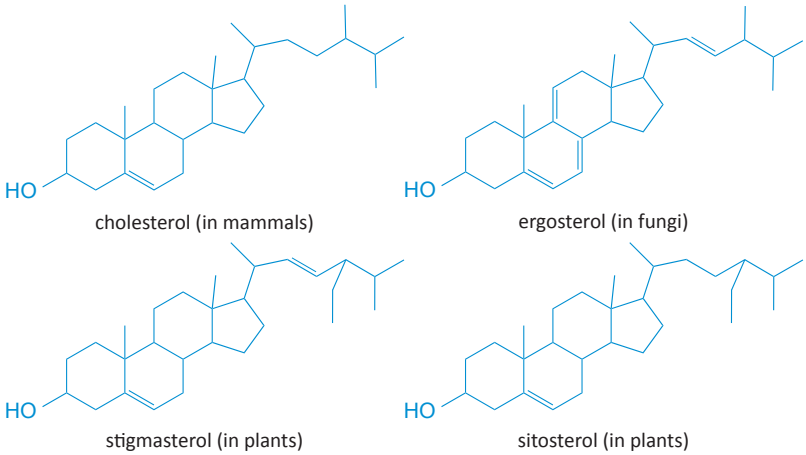

Scheme 1.1 Structural formulae of some sterols seen in membranes.

The simplest diacylglycerophospholipids contains only phosphoric acid attached to diacylglycerol and is called phosphatidic acid (PA), when additional small polar groups ('X', e.g. choline, ethanolamine, serine, inositol and glycerol) are esterified to the phosphate moiety, the lipids are called phosphatidyl−X. Thus, all the other diacylglycerophospholipids can be thought of as derivatives of PA and named after the polar moiety [20−22]. The major types of diacylglycerophospholipids are shown in *Table 1.1*, the relevant comments about their distribution and charge at neutral pH (pH=7) are listed [7].

X	Name of Phospholipid	Source	Charges (pH=7)
H	Phosphatidic acid	Animals, higher plants, micro-organisms.	-2
$OH{\cdot}CH_2CH_2N^+(CH_3)_3$ *Choline*	Phosphatidylcholine (lecithin)	Animals, higher plants, first isolated from egg yolks rare in micro-organisms.	0 (zwitterions)
$OH{\cdot}CH_2CH_2NH_3^+$ *Ethanolamine*	Phosphatidyl-ethanolamine	Animals, higher plants, micro-organism.	0 (zwitterions)
$OH{\cdot}CH_2{\cdot}CH(COO^-){\cdot}NH_3^+$ *Serine*	Phosphatidylserine	Animals, higher plants, micro-organism.	-1
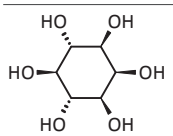 *Myo−inositol*	Phosphatidylinositol	Animals, higher plants, micro-organisms.	-1
$CH_2OH{\cdot}CHOH{\cdot}CH_2OH$ *Glycerol*	Phosphatidylglycerol	Mainly higher plants, and micro-organism.	-1

Table 1.1 Structural varieties of different diacylglycerophospholipids.

1.1.2 Lipid Distribution

The relative amounts of membrane lipids differ even in the same type of cell in different organisms, as shown in *Table 1.2* on the lipid composition of red blood cell membranes from different mammalian species [23]. The major lipid composition of plasma membrane is sterols, sphingolipids and saturated glycerolipids (*Table 1.2*), this non-random distribution contributes to the high packing densities of the bilayer, which promotes impermeability and rigidity [24].

Table 1.2 Plasma membrane lipid compositions of mammalian red blood cells (wt.%).

Lipid	Pig	Human	Cat	Rabbit	Rat
Phosphatidylcholine (PC)	13.9	17.5	18.7	22.3	31.8
Phosphatidylethanolamine (PE)	17.7	16.6	13.6	21.0	14.4
Phosphatidylserine (PS)	10.6	7.9	8.1	8.0	7.2
Phosphatidylinositol (PI)	1.1	1.2	4.5	1.0	2.3
Phosphatidic acid (PA)	< 0.2	0.6	0.5	1.0	< 0.2
Sphingomyelin (SM)	15.8	16.0	16.0	12.5	8.6
Cholesterol	26.8	26.0	26.8	28.9	24.7
Glycosphingolipids	13.4	11.0	11.9	5.3	8.3

Even in a single cell, the lipid compositions of the plasma membrane and the membranes of the various organelles within the cell are different [25–28]. For example, organelle (e.g. the microsomes, mitochondria, and nucleus) membrane lipid compositions of rat liver cells are shown in *Table 1.3* [23].

Table 1.3 Organelle membrane lipid compositions of rat liver cells (wt.%).

Lipid	Plasma membrane	Microsome	Inner mitochondria	Outer mitochondria	Nuclear membrane
PC	31.0	55.2	37.9	42.7	58.3
PE	14.3	24	38.3	28.6	21.5
PS	2.7	—	< 1.0	< 1.0	3.4
PI	4.7	7.7	2.0	7.9	8.2
PA & Cardiolipin	1.4	1.5	20.4	8.9	< 1.0
SM	16.6	3.7	0.8	4.1	3.0
Cholesterol	28.0	6.0	< 1.0	6.0	5.1
Lyso–PC	1.3	1.9	0.6	1.7	1.4

Phosphatidylcholine (PC) is usually the most abundant phospholipid in animals and plants, often amounting to almost 50% of the total as found in the microsome and nuclear membrane of rat liver cells listed in *Table 1.3* (also seen Ref. [29]). In particular, it makes up a very high proportion of the outer leaflet of the plasma membrane [6,30]. Phosphatidylethanolamine (PE) is usually the second most

component of microbial membranes, e.g. in *E. coli*, PE constitutes the majority of the total phospholipids [31]. Although phosphatidylserine (PS) is distributed widely among animals, plants and microorganisms, it is usually less than 10% of the total phospholipids in eukaryotic cell membranes [25,32], the greatest concentration is found in myelin from brain tissue, particularly in molecular species that contain a docosahexaenoic acid (22:6ω−3) polyunsaturated fatty acid [33−35]. In yeasts, such as *S. cerevisiae*, PS is the major phospholipid in the plasma membrane, can amount to ∼34% of the total lipids [36]. Furthermore, Phosphatidylglycerol (PG) is mainly present in plants [37] and microorganism (prokaryotes) [38], but rare in mammalian cellular lipids, except in lungs tissue, where the percentage of PG in the total phospholipids is about 10% [39]. Phosphatidylinositol (PI) is an important membrane constituent of eukaryotes [40−42], PI and its metabolites regulate a diverse set of cellular processes such as glycolipid anchoring of proteins [43], signal transduction [44,45]. In addition, it may be noted that only a small amount of cardiolipin (diphosphatidylglycerols) is found in plasma membrane, but mainly in the inner mitochondrial membrane [46]. In contrast to cardiolipin, sphingomyelin (SM) is mainly found in plasma membrane [25,47]. Cholesterol is another major lipid component of the plasma membrane, and estimates of its abundance is in the range of 30−50% of the phospholipids on a molar basis, while the mitochondria and the endoplasmic reticulum have very low cholesterol contents, and the Golgi contains an intermediate amount [48].

1.1.3 Transbilayer Lipid Asymmetry

The asymmetrical distribution/arrangement of the lipid composition in the inner and outer leaflets of the biological membrane is also recognized [30,32,49−51]. In plasma membrane, the aminophospholipids, PE and PS preferentially reside in the inner leaflet (cytoplasmic), while the choline phospholipids, PC and sphingomyelin (SM) are predominantly localized in the outer (cytosolic) leaflet [52,53]. The human erythrocyte membrane, the first natural membrane to be examined for the lipid asymmetry since the erythrocytes can be easily purified in large quantities and contain only a single membrane. In *Figure 1.2*, the lipid distribution of such membrane is shown, where, PC and SM are highly concentrated in the external leaflet of the plasma membrane (∼80%), PE and PI are the secondary constituents, which amounts to ∼20%, and PS is mainly on the opposite side [6]. The importance of the asymmetrical distribution of the cell membrane is seen in normal cell function, e.g. the translocation of PS in activated platelets is vital in clotting mechanisms [54], and exocytosis in mast cells (RBL−2H3) [55]. The preservation of the lipid asymmetry in lipid depends on a very low frequency of exchange from

one surface to another or a controlled reciprocal exchange, such movement of lipids between the two membrane leaflets (known as 'flip-flop', *Figure 1.3*) is not energetically favourable since the lipid's hydrophilic head would have to cross the hydrophobic core of the lipid bilayer. However, the asymmetry is sensitive to the transmembrane pH gradients [56]. In addition, the asymmetry lipid may be induced by cell activation or apoptosis [57].

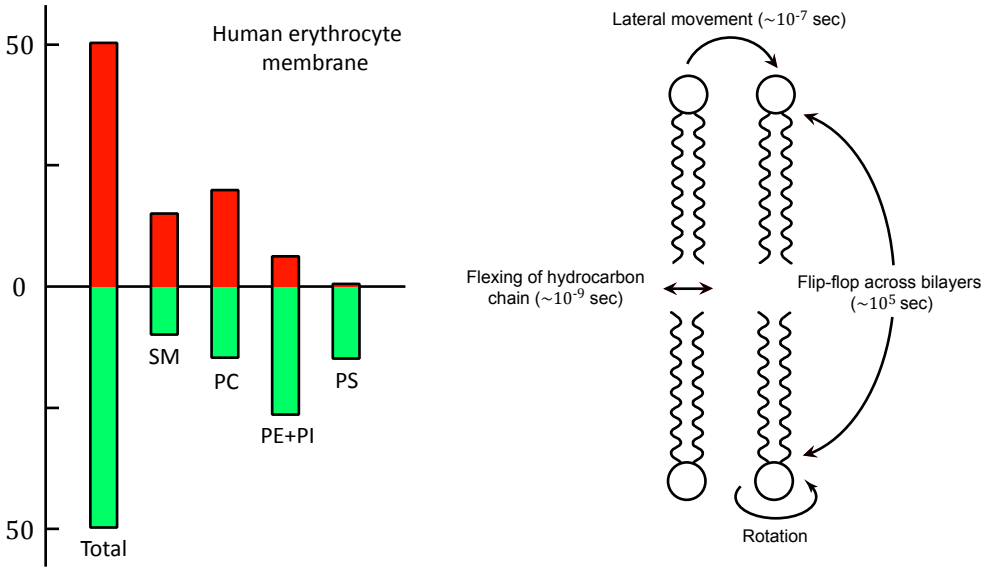

(*Left*) *Figure 1.2* Asymmetry of lipid distribution in human erythrocyte membrane.
(*Right*) *Figure 1.3* Lipid movements in an artificial membrane.

1.1.4 Phospholipid Structure

Phospholipids are major components of the cell membrane. They are similar to reformulated fats, but have only two fatty acids rather than three. The third hydroxyl group of glycerol is joined to a phosphate group, which is negative in electrical charge. Additional small molecules, usually charged or polar, can be linked to the phosphate group to form a variety of phospholipids. An example of a phospholipid is shown in *Figure 1.4*. The top region is a polar group (*in red bracket*), which is attached to the phosphate at the position **3** (*sn*-3) of glycerol backbone (*in blue bracket*), and two fatty acid tails (*in green bracket*) are esterified at positions **1** (*sn*-1) and **2** (*sn*-2), respectively.

One of the tails is a straight chain fatty acid (saturated); the other has a *cis* carbon-carbon double bond (unsaturated), see *Figure 1.4*. Moreover, saturated fatty acid is usually connected with the *sn*-1 position of glycerol backbone; on the other

hand, the *sn*-2 position is usually connected with unsaturated fatty acids. The chain length can vary between 14 and 24 carbons (most natural fatty acids are even-numbered) [58,59], and can have up to six *cis* carbon-carbon double bonds at defined locations along the hydrocarbon chain, e.g. phospholipids with docosahexaenoic acid moiety (commonly known as DHA, 22:6ω-3), which are mainly found in brain tissues [60,61].

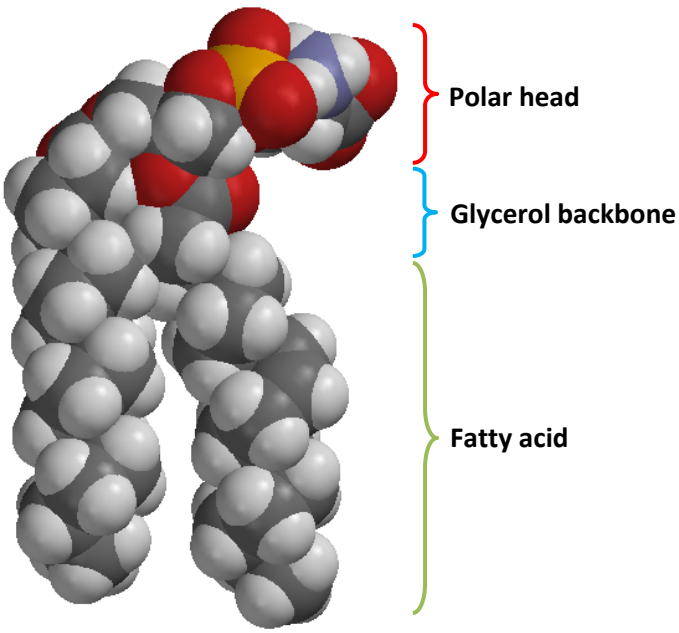

Figure 1.4 Self-filling model of a membrane phospholipid (POPS) with a 16:0 palmitic acid (R_1) in *sn*-1 position and an 18:1 (*n*-9) oleic acid (R_2) in the *sn*-2 position, an additional small molecules, usually charged or polar, are esterified to the phosphate moiety to form a variety of phospholipids.

Furthermore, according to the variability and diversity of the possible acyl or alkyl chain composition, the phospholipids comprise a very widespread and diverse group of structures. A good example is in eukaryotic cell membrane, a sum of over 1,000 molecular species of all classes of phospholipids [62].

1.1.5 Lipid Polymorphism

The ability of many membrane lipids to form the basic bilayer structure is caused by a number of properties, the most important of which is their amphiphilic character. The lipids having both the hydrophilic region and hydrophobic region cause amphiphilicity. In contact with water, they self-assemble into aggregates so that the phosphate heads make contact with the water and the hydrophobic

hydrocarbon tails are packed together by *Van der Waals* and hydrophobic interactions and restricted to water-free areas, such as the bilayer and micelle [63–65]. However, it is also true that many lipid components of membranes form hexagonal II (inverted micelles) phase and other nonlamellar structures under physiological or near-physiological condition [66–68]. In aqueous systems, e.g. in biological membranes, which contains a very high proportion of the lipids adopting the hexagonal II phase rather than bilayers [65,69], which promoted by high temperature and *cis*-unsaturated fatty acids and induced by cholesterol owing to its cone shape [70–72]. Determination of the topology of a lipid system is possible by a number of methods, the most reliable of which are X–ray diffraction and freeze-fracture electron microscopy [73–75]. In addition, ^{31}P NMR is a useful indicator of the polymorphic alteration of phospholipid dispersions [76–78] (see *Section 1.1.12.2*). In *Figure 1.5*, some of the packing characteristics of different lipids and the structures they formed are shown [6].

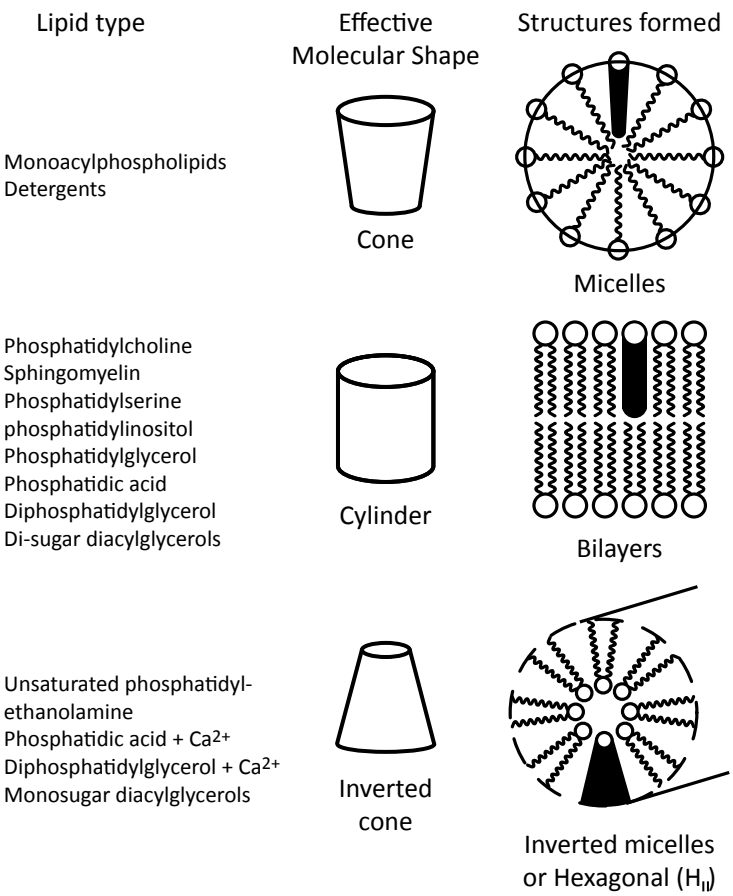

Figure 1.5 Lipids shapes and their packing characteristics.

These different structural phases of the aggregation are influenced by many external factors, e.g. the lipids present, temperature, hydration, solvent pH, pressure and ionic strength and type of ions [79–81]. On the other hand, the intrinsic factors regulating the phase behavior are the lipid architecture itself, for example, an increase in the length of the hydrocarbon tails brings about transitions from lamellar to inverted hexagonal phases [82], whereas an increase in the volume of the headgroup brings about the reverse [83]. Moreover, the spontaneous (intrinsic) surface curvature of the lipid system is considered to play a central role in determining both the system's equilibrium organization and its phase stability [84], which depends on the composition of the monolayer and headgroup–solution interactions [85]. For some monoacylphospholipids (lysophospholipids) form spherical micelles (or cylindrical micelles) in solution have *positive* spontaneous curvature [85]. Other lipids, such as unsaturated PE, form monolayers of *negative* intrinsic curvature in inverted hexagonal phases [85]. Different lipids spontaneously form monolayers of different intrinsic curvature, within which each molecule, averaged over time, occupies a different effective shape, e.g. sphingomyelin (SM) occupies a cylindrical volume (*Figure 1.5*), and hence it tends to self-assemble into bilayer [85]. For spherical vesicles, it may be composed of two monolayers having opposite intrinsic monolayer curvatures, for the reason of symmetry, the net bilayer intrinsic curvature will be zero for both membranes (having opposite intrinsic curvature), such as a mixture of unsaturated PE (*negative* intrinsic curvature) and detergents (*positive* intrinsic curvature) will adopt bilayer phases, that is, the detergents 'stabilize' the bilayer structure for unsaturated PE [86]. It is crucially important for non-bilayer phases to be present in membranes, such as inverted micelles or related structures, for example, in membrane fusion processes or in the budding of vesicles and in mitochondrial structures [69,87]. The role of non-bilayer lipids in protein insertion and translation processes was proposed to be important [88].

1.1.6 Membrane Fluidity

Membranes are not static sheets of molecules locked rigidly in place, but a fluid collection of amphiphilic molecules. A membrane is held together primarily by hydrophobic interactions (and *van der Waals*), which are much weaker than covalent bonds. The membrane fluidity depends on its lipid composition and temperature. As discussed in *Section 1.1.2*, plasma membrane is rich of the lipid species with high packing densities (e.g. cholesterol and saturated glycerolipids), which will promote bilayer rigidity and impermeability [24]. The saturated hydrocarbon tails can pack tightly together resulting in bilayer rigidity (and high

phase transition temperature [89]) due to the close packing of the molecule in the bilayer structure, on the other hand, an unsaturated hydrocarbon tail has generally one to three (even six) *cis* carbon-carbon double bonds at defined locations along the hydrocarbon chain. The unsaturated fatty acid will have a more disordered structure with looser packing (and lower phase transition temperature [89]). This feature plays an important role in the fluidity of the cell membrane [7].

Most lipids are randomly mobile in the plane of the bilayer with an average migration rate of 22 μm per second. Lipid can rotate, bob up and down in the plane of the bilayer, flexing of the hydrocarbon chains and flip-flop (*Figure 1.3*). Rotation of the molecules is fast (about 10^{-7} s in the artificial systems), and flexing is even faster than rotation, the fastest occurring with the methyl end of the acyl chain, but the flip-flop of lipids is a rare event (much slower), which preserves the bilayer asymmetry of natural membranes [6].

Temperature affects the fluidity of the membrane, other factors like hydration level, pH and electric field gradient [90]. *Figure 1.6* shows the influence of temperature on the packing of the hydrocarbons. At low temperatures, the bilayer (e.g. consisting of PE) is in a gel state and tightly packed, where the lipid's long all-*trans* acyl chains run parallel to the bilayer normal. At higher temperatures, the bilayer actually "melts' (disordering of the hydrocarbon chains) and the interior is fluid allowing the lipid molecules to move around [91–95].

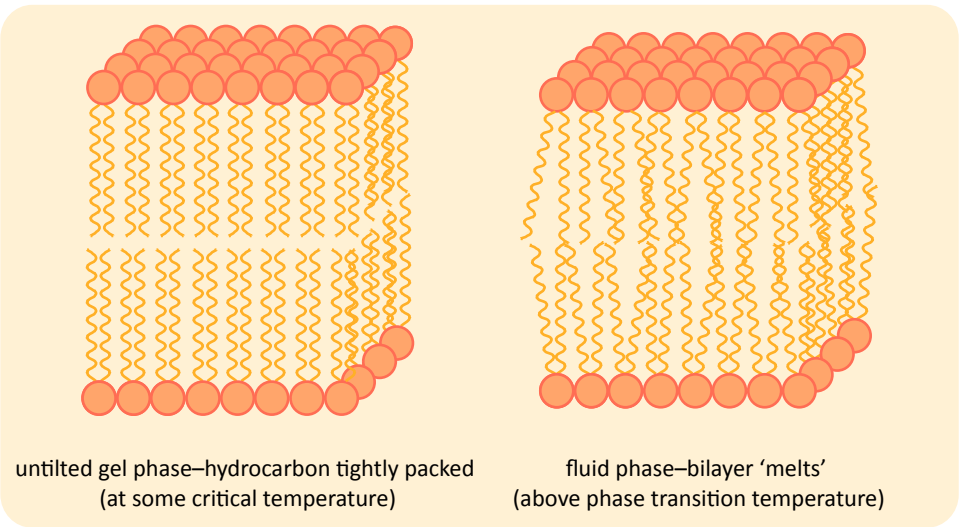

Figure 1.6 Temperature effect on the fluidity of the membrane.

A membrane rich in phospholipids with unsaturated hydrocarbon will remain fluid at a lower temperature (lower phase transition temperature, T_m). However, a cell can alter the lipid composition of its membranes to some extent as an adjustment to changing temperature [96]. For instance, in many plants that tolerate extreme cold, such as winter wheat, the percentage of unsaturated phospholipids increases in autumn, an adaptation that keeps the membranes from solidifying during winter [97]. The steroid cholesterol, which is wedged between phospholipid molecules in the plasma membranes of animals, helps stabilize the membrane by decreasing the movement of membrane phospholipids [98,99]. The fluid structure plays an extremely important role for many cell functions, e.g. rapid cell growth [100], lipid fluidity regulates cholesterol acyltransferase activity [101], reduced fluidity in the membranes of red blood cells may be related to psoriasis outbreaks [102], and the toxity of the heavy metals (e.g. chromium, cadmium, mercury and lead) may relate to their influences on the membrane fluidity [103,104].

1.1.7 The Gel-to-Liquid-Crystalline Phase Transition in Bilayers

The isolated (one-component) lipid samples show a sharp gel-to-liquid-crystalline phase transition, referring to the overall phase transition [89,105], while naturally occurring lipids show broad non-cooperative transitions due to the heterogeneity of the acyl chains. In addition, the gel-to-liquid-crystalline phase transition is accompanied by several structural changes in the lipid molecules.

As shown in *Figure 1.7*, In the $L_{\beta'}$ phase, the tilted acyl chains of the lipid adopt an all-*trans* conformation (for DPPC, a tilt angle of $32°$ relative to the bilayer normal), all the tilted all-*trans* acyl chains are packed together closely due to the lateral chain−chain contact distance is most favorable in terms of *van der Waals* attractive interactions. As the temperature is gradually raised to the transition temperature (T_m), the tilted acyl chains are progressively energized, the tight packing is released abruptly at T_m. The principal change in accompanying the transition is the *trans*→*gauche* rotational isomerization of methylene groups about the single C−C bonds along the lipid acyl chain, which results in an increased cross-sectional area of the acyl chains [89]. Moreover, the average number of *gauche* conformers can be related to bilayer thickness [89,106].

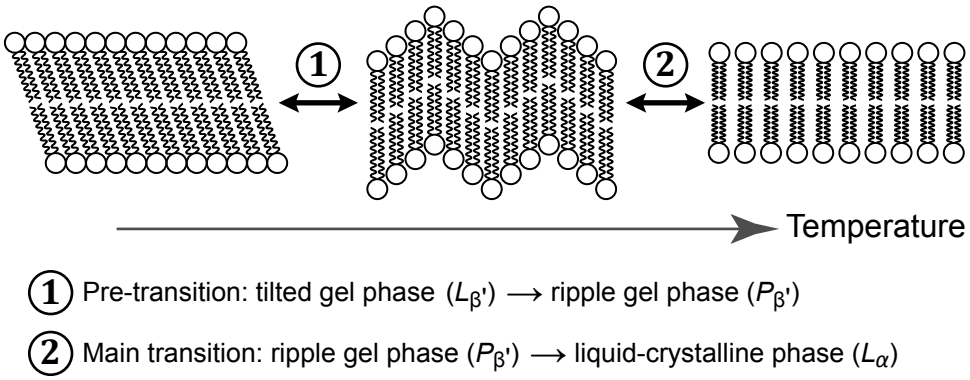

Figure 1.7 Phase transition in lipid bilayer.

The main phase transition behaviors of the isolated lipid bilayers can be influenced by many factors, both external and internal. The external factors refer to pressure, pH value and so on, and the internal factors mainly include the chain length, chain length difference between two acyl chains, chain unsaturation and headgroup structures [89]. Each lipid has a specific transition temperature (T_m), which is one of the two thermodynamic parameters closely associated with the gel-to-liquid-crystalline phase transition. The accurate T_m data can be directly obtained from DSC measurements [107], phase transition temperatures for some representative PC, PS and PE with two equal length acyl chains shown in *Figure 1.8* [89,108–113].

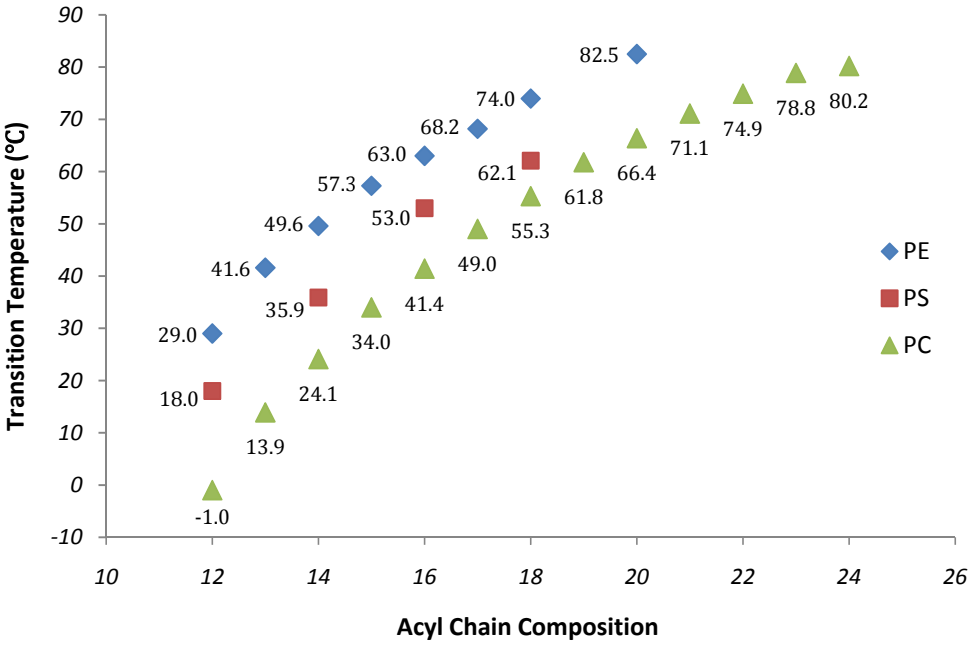

Figure 1.8 Phase transition temperatures (T_m, °C) for saturated diacylphospholipids with two equal length acyl chains (ranging from 12 to 24 carbons).

From *Figure 1.8*, it is clear that the main transition temperature T_m depends on the headgroup structures, and for a given phospholipid species with two acyl chains at equal length, T_m mainly depends on acyl chain length. Moreover, for the species with two unequal length acyl chains, T_m is influenced by the effective chain length difference between *sn*-1 and *sn*-2 acyl chains [114] (*Table 1.4*).

Table 1.4 Effect of the effective chain difference between two acyl chains on the T_m of PC species. ΔC, structural parameter denoting the effective chain length difference between the *sn*-1 and *sn*-2 acyl chains, in C–C bonds, for lipids packed in the gel state bilayer.

Molecular species of PC	T_m	ΔC
C(15:0):C(17:0) PC	41.7	0.5
C(14:0):C(18:0) PC	39.2	2.5
C(13:0):C(19:0) PC	32.6	4.5
C(12:0):C(20:0) PC	25.6	6.5

As mentioned in *Section 1.1.6*, the presence of even a single *cis*-double bond in the *sn*-2 acyl chain of phospholipid molecule will result in a more disordered structure of the bilayer with looser packing, and thus dramatically decrease T_m [89,115]. In *Table 1.5*, the T_m–profiles of C(20):C(18) PE and its unsaturated species with 1–4 *cis* Δ-bonds in the *sn*-2 acyl chains are shown. The T_m decreases regularly with successively adding of *cis* Δ-bonds into the *sn*-2 acyl chain.

Table 1.5 The T_m–diagram for *sn*-1 (saturated)/*sn*-2 (unsaturated) PEs derived from a common precursor, the C(20):C(18) PE (ω3-family).

$$\underset{\{75.8^{\circ}C\}}{C(20:0):C(18:\mathbf{0})\ PE} \Rightarrow \underset{\{54.8^{\circ}C\}}{C(20:0):C(18:\mathbf{1}\Delta^{15})\ PE} \Rightarrow \underset{\{31.6^{\circ}C\}}{C(20:0):C(18:\mathbf{2}\Delta^{12,15})\ PE} \Rightarrow$$
$$\Rightarrow \underset{\{10.4^{\circ}C\}}{C(20:0):C(18:\mathbf{3}\Delta^{9,12,15})\ PE} \Rightarrow \underset{\{3.9^{\circ}C\}}{C(20:0):C(18:\mathbf{4}\Delta^{6,9,12,15})\ PE}$$

The phase transition may be detected by various techniques such as high-resolution DSC [107–109,116–118], X–ray diffraction [106,116,119], NMR [76,120,121], dilatometry [122], ESR [123], fluorescent and Fourier transform infrared spectroscopies [124,125]. In addition, many properties of membranes, such as transport [126,127], enzyme function [128,129], drug susceptibility [130], and interaction with anesthetics [131,132] are affected by the transition.

1.1.8 Lipid Domains

In 1972, S. J. Singer and G. Nicolson developed a model to conceptualize the cells plasma membrane, known as the fluid mosaic model [133], which is still generally accepted today as the most correct model for membrane structure (*Figure 1.9*), supported by freeze-etching technique [134]. It essentially consists of a structurally and functionally asymmetric bilayer of phospholipid molecules, studded with

embedded proteins and other constituents (e.g. carbohydrate and steroids). The proteins may pass through the bilayer (as transmembrane proteins), or may be inserted at the cytoplasmic face, as well as the peripheral membrane proteins adsorbed to the surface of the membrane. The interactions of membrane proteins with lipid bilayers are principally hydrophobic and electrostatic in nature. The model also states that the molecules can move laterally and freely within the membrane (also seen in Refs. [135]).

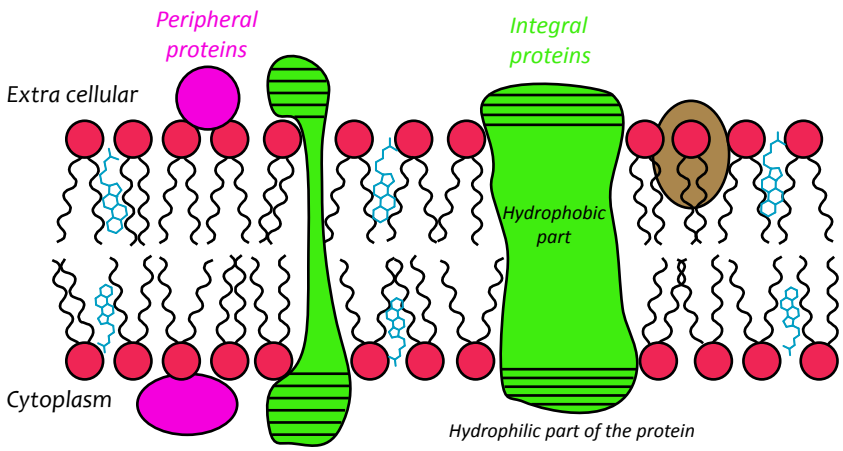

Figure 1.9 Schematic illustration of the fluid mosaic model of membrane (cross section).

Currently, membranes are viewed as a mosaic of different compartments or domains maintained by an active cytoskeleton network [136,137]. The formation of microdomains (with different characteristics and functions) in a multi-component lipid membrane was proposed to be mainly driven by hydrophobic mismatch [138], which caused by the difference in thickness of the various phospholipids species in the bilayer system [139]. Lipids are likely to play an important role in the formation of so-called lipid-enriched microdomains or lipid rafts, adding another order of complexity to the membrane model [137,140]. Rafts (*Figure 1.10*) are specialised membrane domains enriched in certain lipids, cholesterol and proteins and generally believed to exist in a liquid-ordered phase characterized by tight packing of lipid acyl chains and lateral diffusion properties similar to those of a fluid phase [141]. The original concept of rafts was used as an explanation for the transport of cholesterol from the *trans*-Golgi to the plasma membrane, furthermore, the idea was more formally developed by Simons and Ikonen in 1997 [136]. Rafts within the plasma membrane of eukaryotic cells have been implicated in many important cellular processes, such as polarized sorting of apical membrane proteins in epithelial cells [141], dendritic proteins in neurons [142] and signal transduction [143,144]. In addition, domain formation has been shown to be relevant in

enzymatic activity of phospholipase A_2 (PLA_2) [145], activity of protein kinase C (PKC) and diglucosyldiacylglycerol (DiGlcDAG) synthase [146,147], and vesicle budding and membrane trafficking [148,149]. In addition, phospholipid lateral microdomains may also be involved in membrane fusion events, intracellular, and the modulation of membrane permeability [150].

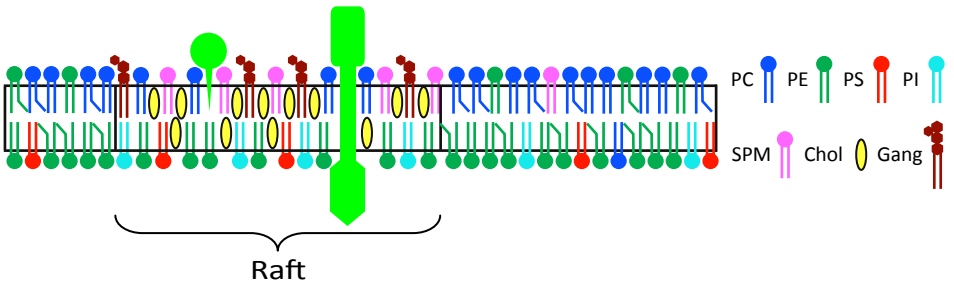

Figure 1.10 Schematic illustration of a membrane raft. The fatty-acid chains of lipids within the rafts tend to be extended and so more tightly packed, thus creating domains with higher order. It is believed that rafts exist in a separate ordered phase that floats in a sea of poorly ordered lipids.

In recent years, it has become evident that the lateral organization of the lipid bilayer is far from random or homogeneous, but rather structured in terms of lipid domains. The range of length scales over which these domains persist varies from nanometres up to the size of the whole cell [151–153], and the shape of the lipid domains can be correlated to the composition of the bilayer mixture [153,154]. Experimental evidence of lipid microdomain formation in lipid bilayers has been presented from various techniques [155–161]. In an early study, Cullis and Hope [155] detected a bilayer stabilizing effect of cholesterol on an SM–PE lipid mixture by employing ^{31}P NMR. ^{13}C NMR has been used to study cholesterol and DPPC mixtures where cholesterol is found to induce fluid-phase immiscibility in this kind of bilayer [156]. More recently, ^{2}H NMR experiments have determined that ceramide in PC bilayers cause microdomain formation of different composition and phase state in POPC/ceramide bilayers at physiological temperature [157]. However, the existence of the lipid raft remains controversial *in vivo* [162–166].

Several investigators studying the role of phospholipid acyl chain unsaturation and stability of lipid rafts composed of SM and cholesterol [158,160] support the notion that such lipid rafts are promoted by polyunsaturated acyl chains. The DHA acyl chain is found to enhance lipid raft formation by lipid phase separation [167–169], for example, in model membranes, DHA, tend to segregate from regions of cholesterol and forming membrane microdomains [170–173]. In addition, the microdomain-inducing effects of DHA probably depend on the phospholipid class in which it occurs [174]. In paper II of the current study, the existence of

microdomains of the two-component bilayer system DPPC/SDPS (60:40, molar ratio) was detected by ^{13}C MASNMR, the polyunsaturated DHA is confirmed to be important in promoting the domain formation by phase separation.

1.1.9 Polyunsaturated Fatty Acid

Cellular membranes like those of retinal rod outer segments [175–177], mitochondria [178], spermatozoa [179] and cerebral grey matter [180] have a high percentage of phospholipids with polyunsaturated acyl chains, i.e. the ω-3 and ω-6 polyunsaturated fatty acids (PUFAs) [181], which are structurally classified as ω-3 fatty acids, having three carbons between the methyl terminus and the last double bond. The PUFAs cannot be manufactured *de novo* by the mammalian body [182]. These can be supplied by the diet, as in breast milk [183] or sea food [184], or may be manufactured by synthesis within the body from dietary linoleic and *α*-linolenic acids, respectively, by sequential desaturation and elongation [185]. Reduced levels of these polyunsaturated fatty acids are associated with increased lipid peroxidation products in plasma [186], related to a variety of pathological conditions like cancer [187], visual disorder [188], schizophrenia [189] and cardiovascular disease [190–194]. On the other hand, elevated levels of the polyunsaturated PC has been observed in Crohn's disease [195]. Thus, these apparently unrelated diseases, indicate a fundamental role played by the polyunsaturated fatty acids in the cells. The ω-3 fatty acid, docosahexaenoic acid (DHA, $22{:}6\Delta^{4,7,10,13,16,19}$) and the ω-6 fatty acid, arachidonic acid (AA, $20{:}4\Delta^{5,8,11,14}$) differ in that the latter serves as a precursor for prostaglandins [196] in platelet function, whereas the former does not appear to be metabolized [175].

DHA has a function as ligand for retinoid X receptor [197], influences the Cl^- channels [198] (cystic fibrosis) and the neuronal K^+ channels [199], is released in response to serotonin [200], has an essential role in brain maturation and neuronal function and is here found in bilayer phospholipids at a 30–50% level. Bilayers with high DHA levels have distinct properties, probably related to the functioning of integral membrane proteins. When compared with less unsaturated phospholipid acyl chains, DHA–containing bilayers have reduced thickness in the fluid state and consequently an increased area occupied per phospholipid at the aqueous interface of the bilayer [201] and an increased steric bulk in the hydrophobic portion of the molecule [202,203]. As a component of cell membranes, DHA influences a variety of membrane functions including the activity of membrane bound enzymes [204,205], cell recognition phenomena [206], membrane molecular order [207], the expression of membrane-bound growth factors [208], membrane

permeability to both electrolytes and non-electrolytes [209,210], and it promotes membrane fusion [211] and exfoliation. DHA has also proven to be an effective anti-cancer agent [212,213], preventing breast and lung cancer [214,215]. It lowers the rate of tumor cell proliferation [216–218], and prolongs life in tumor-bearing animals [213]. In addition, DHA (and AA) appear to be important in the treatment of schizophrenia [219] and dementia [220].

1.1.10 Membrane Lipids in Cell Signalling

The cell membranes do not simply serve as barriers to separate the inside of the cell from the outside or to delineate different intracellular compartments. These membranes also serve as a platform for cell signalling by allowing specific sets of proteins to interact [24]. Many membrane lipids have an essential role in regulating biophysical properties, where they can control diverse aspects of cellular activity such as hormone action, cell differentiation and apoptosis [44]. For example, several PIs play a central role in the control of the spatial organization of the vital signalling pathways leading to cell growth or survival, intracellular membrane trafficking, the rearrangement of actin cytoskeleton or metabolism in response to extracellular messengers [221]. And, in particular, the catabolism of phosphatidylinositol 4,5-*bis*phosphate (PIP_2) was found to be stimulated by a whole series of important agonists. These agonists cause activation of a selective phospholipase C (PLC), which catalyzes the formation of diacylglycerol (DAG) and inositol 1,4,5-*tri*phosphate (IP_3) [222]. DAG is involved in the activation of protein kinases C (PKC), it can be hydrolyzed to yield significant quantities of arachidonate, which is a precursor of eicosanoids [223–225]. The activity of the various protein kinases regulates a host of cellular functions from metabolic regulation to differentiation [226]. Furthermore, the presence in lipid rafts of many proteins implicated in cell signalling has been proven to be important in signal transduction [227], for example, the plasma membrane, that is rich in sphingomyelin, is also rich in cholesterol. Cholesterol and sphingomyelin may coexist in microdomains such as rafts or caveolae that are known to be focal points in cell signalling [228].

In eukaryotic cells, most intracellular proteins activated by a ligand/receptor interaction possess an enzymatic activity. The receptor stimulated-enzymes lead to the production of second messengers inside the cell, including cyclic nucleotides, such as the cyclic adenosine monophosphate (cAMP), which is the initial second messenger to be identified, and cyclic guanosine monophosphate (cGMP). Other examples of second messengers include NO (nitric oxide), lysophosphatidylcholine, ceramide (viewed as the sphingolipid counterpart of DAG), PA, arachidonic acid,

and some PI derivatives, such as phosphatidylinositol 3,4,5-*tri*phosphate (PIP_3), DAG and IP_3 [229]. One of these enzymes is phospholipase D (PLD), a phosphodiesterase that cleaves the distal phosphodiester bond of phospholipids (e.g. PC) to produce PA [230–232]. As the main lipid mediator produced by PLD, PA can regulate membrane traffic events by direct regulation of target proteins involved in vesicle targeting, docking and fusion [230], and modulate the activity of numerous enzymes and proteins *in vitro* [233–239]. In addition, the formation of PA may bring out changes in lipid bilayer that can facilitate vesicle budding and fusion events in the course of intracellular membrane traffic.

1.1.11 Lipid Specificity for Membrane-Bound Proteins

Lipid bilayers are largely impermeable to most solutes, including small ions and polar molecules [4,240]. The permeability of membranes is relying on specific proteins that determine the nature of energy conduction across the system. Membrane proteins can be integral or peripheral, nearly all known integral proteins traverse the lipid bilayer (*Figure 1.11*). The primary sequence of proteins determines the ability of a protein to insert into membrane [241].

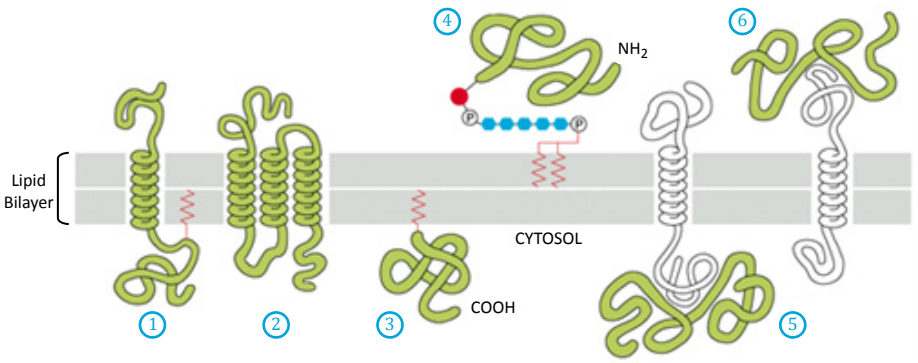

Figure 1.11 Arrangement of proteins in membranes.

The interactions between proteins and lipids are essential for membrane function and structure. Hydrophobic matching, i.e., the matching between the hydrophobic length of an integral membrane protein and the hydrophobic thickness of the lipid bilayer can be an important factor in protein-lipid interactions [139,242]. Sackmann suggested that the function of integral membrane proteins may be triggered by the lipid-bilayer properties e.g., in terms of varying molecular composition, curvature, or hydrophobic thickness [243].

The activity of membrane-bound proteins, such as receptors, channels, and enzymes, is often dependent membrane composition and membrane structure.

For example, the activity of phospholipase A_2 (PLA_2) is highly dependent on the structure of its membrane substrate [244,245], the nicotinic acetylcholine receptor (AChR) requires the presence of cholesterol for exerting the entire function [246,247]. Moreover, the acyl composition has been reported to determine the membrane partition and the activity of cytochrome b_5 [248], protein kinase C (PKC) [249], also shown in *P*-glycoprotein [250] and opioid receptor [251]. The activity of diacylglycerol kinase (DGK) of *E. coli*, is also dependent on bilayer composition, it has the highest activity in DOPC and lower activity in bilayers with shorter or longer fatty acyl chains [252]. Lipid composition also has significant effects on the interaction between metarhodopsin II (M_{II}) and the G-protein transducin [253,254]. The association constant between M_{II} and transducin is higher in bilayers of SDPC than in bilayers of SOPC, and is lower with the addition of cholesterol [254]. Interactions between lipids and Ca^{2+}−ATPase show structural specificity [255,256], binding with PC is much stronger than binding of PE [257]. Activities of a number of other membrane proteins have also been shown to be dependent on lipid composition, including rhodopsin [258−260], the glucose transporter from red blood cells [261−262], and cytochrome oxidase [263]. For the reconstitution of dopaminergic receptor (D_2), PS is particularly important, a mixture of PC, PE and PS seems to almost fully restore the receptor binding, which is about six-fold compared to the mixture in the absence of PS species, that is to say, the depletion of PS from dopamine D_2-receptor weaken the ligand affinity [264]. Thus, lipid membrane composition appears to be important for the biological function of both inserted and peripheral membrane proteins.

1.1.12 ^{13}C and ^{31}P Solid-State NMR Spectroscopy of Phospholipids

1.1.12.1 Carbon−13 Solid-State NMR

Carbon−31 NMR spectroscopy gives some information about the mobility both in the polar headgroups region and in the fatty-acid chain region of phospholipids in biomembranes. The spectra provide two kinds of information: the chemical shift of each signal and their relative intensities, these ^{13}C spectral features can be analyzed qualitatively [265]. Moreover, the ^{13}C spin-lattice relaxation (T_1) measurements can provide the detailed structural and dynamical information of the bilayer systems [266]. *Figures 1.12* shows a typical spectrum of fully hydrated PC/PS sample with the molar ratio of 60:40, carbonyl (C=O) and serine carboxyl are found downfield in the spectrum, and the *sn*-1 and *sn*-2 carbonyl resonances were resolved individually into two peaks [267]. The molar composition (PC/PS ratio) makes the theoretical ratio between the carbonyl and carboxyl resonances

to be five. In the spectral region of 128−132 ppm, the C=C resonances of the oleic acyl chain (18:1, C=C double bond at carbons 9 and 10) of sample DPPC/POPS are found. The acyl chain region (in the spectral region of 12−38 ppm, spectrum c) is dominated by the palmitic (16:0) molecular species, the molar composition of the samples cause the palmitic (16:0) acyl chain resonances to give ∼80% of the peak intensities in the spectral region, whereas the contribution from the oleic acyl chain is ∼20%. Thus, only the palmitic carbon resonances are assigned and labelled (2−16). In the 54−74 ppm region, the phospholipid choline (labelled as G, H and I, from the DPPC species) and serine (labelled as D and E, from the POPS species) carbons as well as the glycerol moiety resonances (labelled as A, B and C, from the two phospholipids species) appear.

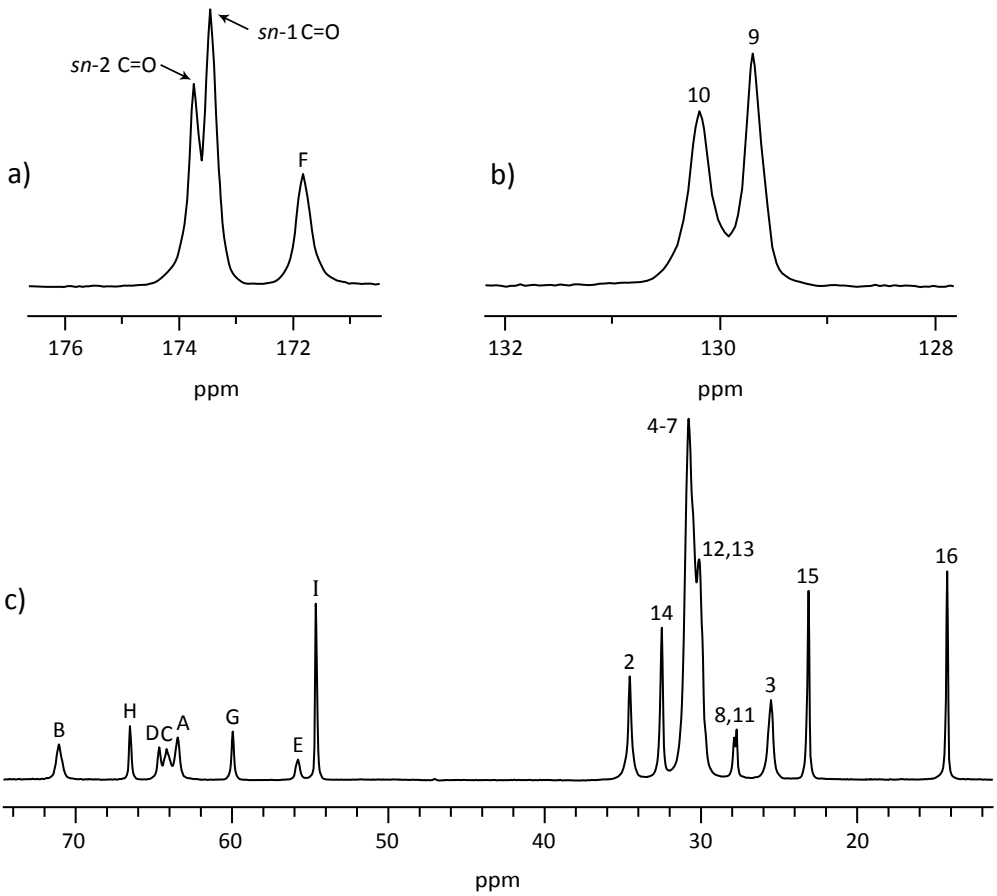

Figure 1.12 The assigned ^{13}C MASNMR spectrum of DPPC/POPS bilayer with the molar ratio of 60:40 at a sample temperature of 316 K (43°C, above the phase transition temperature T_m). Spectral region a) the carbonyl and serine headgroup carboxyl region, b) the C=C region (128−132 ppm), and c) displaying spectral region of phospholipid headgroup, glycerol and saturated acyl chain carbons (12–74 ppm). For the details of the assignment, see the text of paper IV.

1.1.12.2 Phosphorous−31 Solid-State NMR

Phosphorus is an unusual element, because it has only a single isotope, phosphorous−31, and this isotope is NMR-active with a spin number $I = 1/2$. The sensitivity of ^{31}P is relatively high, so that measurements do not require a big sample volume and it is not necessary to collect a rather large number of transients (scans). ^{31}P NMR is a suitable probe to reveal conformation and dynamics of biopolymer systems containing phosphorus, e.g. the polar region of phospholipids in biomembranes. Furthermore, ^{31}P NMR is quantitative, and which detects the single phosphorus atom present in each phospholipid molecule. The two peaks in isotropic ^{31}P NMR spectrum of DPPC/POPS bilayer system obtained with Magic-angle spinning (MAS) indicate the distinct phosphate environments of PS and PC, and can be assigned by the molar composition of DPPC and POPS species (60:40) in the NMR analysis, giving a theoretical PC/PS components' ratio of ~1.5. In *Figure 1.13*, the PC component is found slightly upfield from the PS component [268]. The ^{31}P chemical shifts are referenced to 85% phosphoric acid (H_3PO_4, 0 ppm).

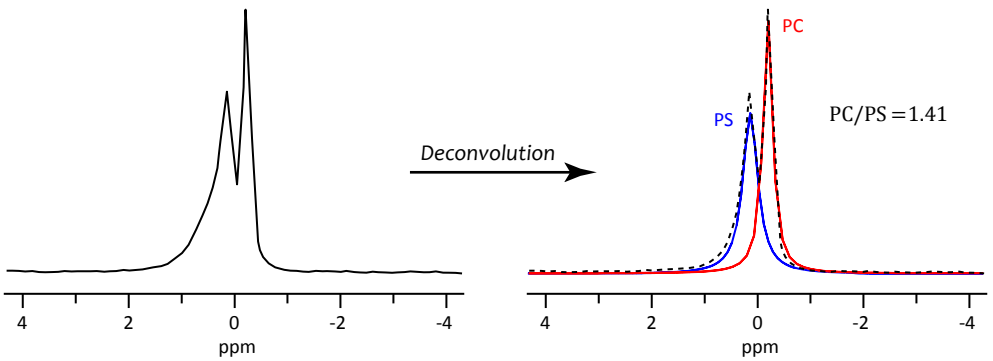

Figure 1.13 (*left*) ^{31}P MASNMR spectrum of DPPC (60%)/POPS (40%) bilayer system obtained at T=316 K (43°C); (*right*) The deconvolution curve generated by mixed *Lorentzian*/*Gaussian* shape, the integral ratio of PC (red curve) and PS (blue curve) is 1.41, which is very close to the theoretical ratio of ~1.5 given by the molar compositions of DPPC and POPS species (60:40).

The ^{31}P chemical shift of phospholipids in biomembranes depends on the orientation and dynamics of the headgroups with respect to the applied magnetic field. A general feature of phospholipid ^{31}P static NMR spectra is the large chemical shielding anisotropy (CSA), a rigid phosphodiester moiety yields the ^{31}P powder pattern with the three principle components, δ_{11}, δ_{22} and δ_{33}, which spans 190 ppm [269] as shown in *Figure 1.14−top*. Such a phosphodiester moiety in membrane is not always rigid but undergoes several types of motions with an averaging of the components of the chemical shift tensor [76,269], such as in a fully

hydrated environment, which is more relevant to biological membranes as illustrated in *Figure 1.14–middle and bottom*. Where, the chemical shift $\delta_{\parallel}$ defines the field parallel to the unique motional axis; whereas, the chemical shift $\delta_{\perp}$ ($\delta_{\perp} = (\delta_{22} + \delta_{33})/2$, the chemical shift tensor is axially symmetric) defines the field perpendicular to this axis, the resultant pattern due to rapid motions is also shown in *Figure 1.14–middle and bottom*. In the bottom spectrum, the effective tensor still has axial symmetry, but the reduced CSA ($\Delta\delta = \delta'_{\parallel} - \delta'_{\perp}$) value can be determined by the edges of the experimental spectrum. Such a distinctive lineshape change of top and middle spectra is also seen when the bilayer system undergoes the sub-transition ($L_C \rightarrow L_{\beta'}$), where the top spectrum indicates that the lipid molecules are still packed in a three-dimensional rigid lattice. When temperature is above the sub-transition temperature, the pseudoaxially symmetric pattern (middle spectrum) is found, and the lipid headgroups are undergoing axially rotation [120]. The lipid bilayer in biological membranes is generally in the liquid-crystalline phase where the axis of symmetry of the acyl chain motion is perpendicular to the plane formed by the polar headgroup. The molecular interpretation of CSA ($\Delta\delta$) is complicated, but CSA ($\Delta\delta$) can still be used as a convenient measure of headgroup motion in different bilayers.

The CSA ($\Delta\delta$) is generally larger for serine headgroup than for choline and ethanolamine headgroups [76,270], and it appears to be influenced by the chemical nature of the fatty acyl chains [271]. Furthermore, the similarities of the static shielding tensor of phosphatidylserine and phosphatidylcholine taken together with the somewhat larger CSA ($\Delta\delta$) for phosphatidylserines, suggest that the phosphatidylserine phosphate moiety differs conformationally or motionally from the phosphatidylcholine phosphate moiety [112,272]. This can be accounted for by greater rigidity of the phosphatidylserine headgroup than the phosphatidylcholine headgroup. This rigidity supposedly results from electrostatic interactions and/or hydrogen bonding between or within the phosphatidylserine headgroups. Thus, dilution of negatively charged PBPS (Pig Brain PS) with neutral DPPC removes some of this interaction and will allow greater freedom of motion of the phosphatidylserine headgroup. The gel-to-liquid-crystalline phase transition of a phospholipid bilayer upon increase in temperature can be monitored by CSA ($\Delta\delta$) changes.

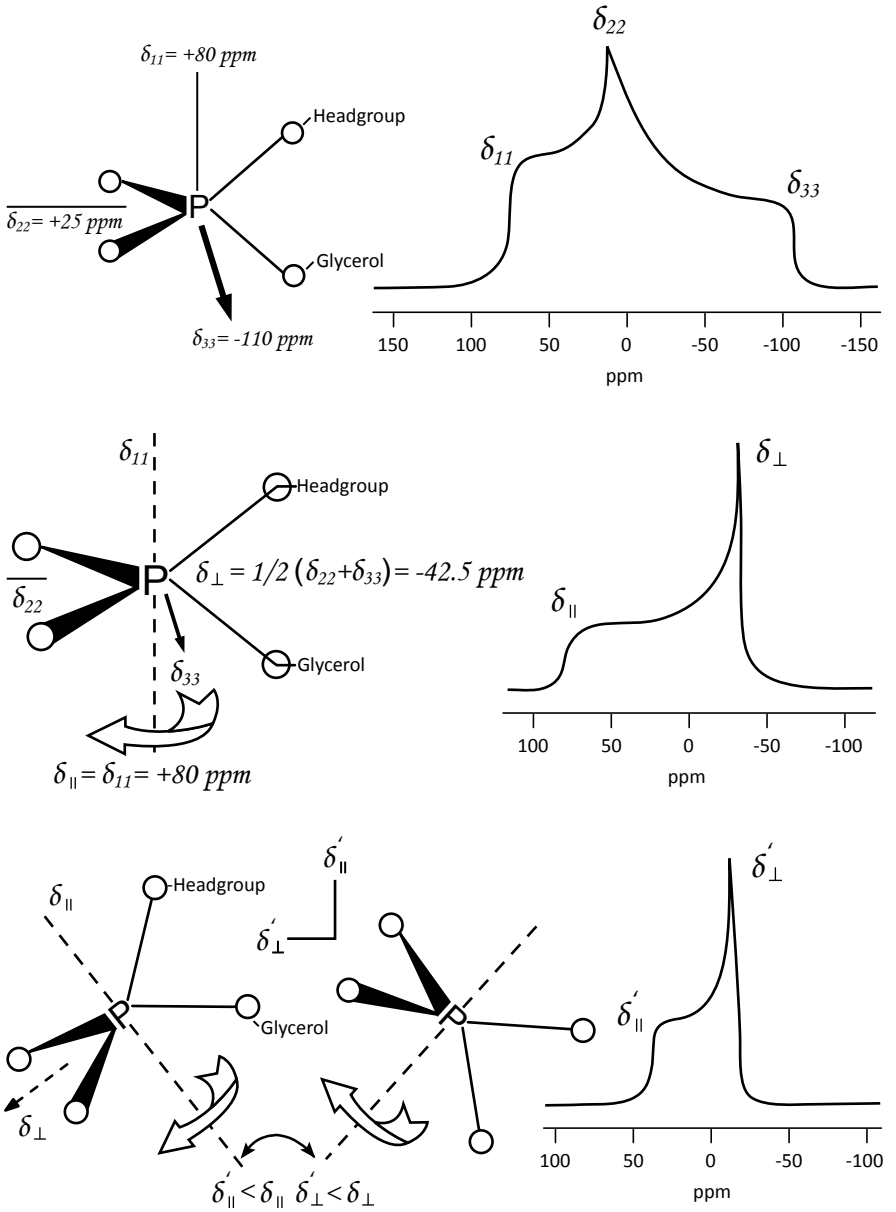

Figure 1.14 Various possible motional states of the phosphodiester moiety of a membrane lipid and the expected ^{31}P NMR spectra: (*top*) static phosphodiester; (*middle*) ordered phosphodiester, rapid axial rotation; (*bottom*) disordered phosphodiester, rapid axial rotation.

Another interesting property of ^{31}P static NMR spectroscopy is its sensitivity to lipid polymorphism: if the geometry of the lipid phase changes from lamellar (*Figure 1.15–left*) to hexagonal (*Figure 1.15–right*), ^{31}P CSA ($\Delta\delta$) changes its sign and is reduced by exactly a factor of two [76–78].

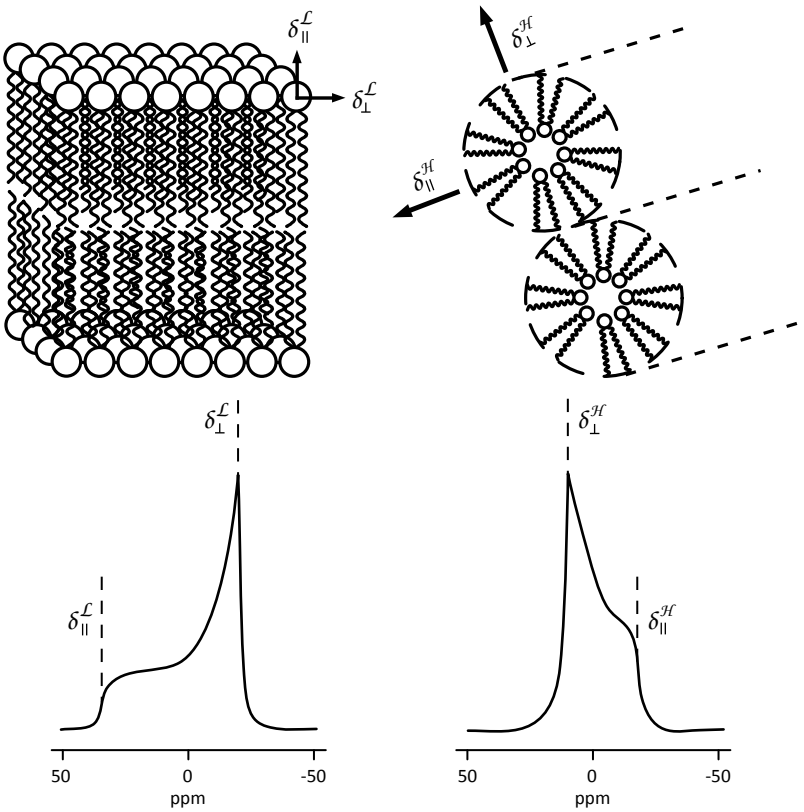

Figure 1.15 Representation of the (*left*) bilayer and (*right*) hexagonal phases form by membrane lipids and their expected ^{31}P NMR spectra [269].

1.2 Antipsychotic Drugs (CPZ, OLZ) and Local Anaesthetic (Articaine)

1.2.1 Antipsychotic Drugs

Antipsychotic drugs, also referred to as major tranquillizers, neuroleptic drugs, or simply neuroleptics, are a group of medicines used to treat conditions such as schizophrenia, agitation, anxiety, mania and aggression. There are currently two main types of antipsychotic drugs in use, classified by their structure (*Figure 1.16*) as the typical (conventional) or first-generation antipsychotic drugs and the atypical or second-generation antipsychotic drugs, they can also be distinguished by their pharmacology, their clinical properties, and by their action at receptors [273,274]. The typical antipsychotic drugs act primarily at dopamine receptors [275], while atypical antipsychotic drugs act on other receptors (e.g. the 5-HT_2 antagonist effect) as well as dopamine [276], and are less likely than typical antipsychotics to cause movement disorders as a side effect [277]. In addition, there is a new class of antipsychotic drugs has recently been discovered, known as dopamine partial

agonists, e.g. aripiprazole [278] and norclozapine (ACP-104, under clinical development) [279].

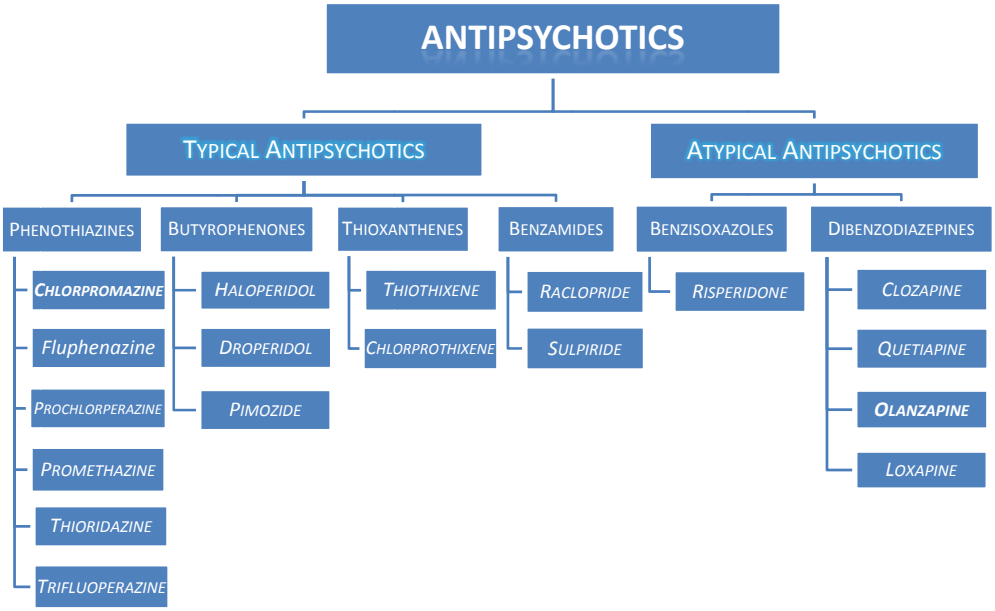

Figure 1.16 Classification of antipsychotic drugs according to their chemical structures.

1.2.2 Schizophrenia

Symptoms of schizophrenia are often divided into two groups: positive symptoms (also referred to as 'psychotic' or 'active' symptoms) and negative symptoms (also referred to as 'deficit' symptoms), other components of schizophrenia including cognitive deficits and mood symptom [280]. The positive symptoms of schizophrenia reflect an excess or distortion of normal functioning and include the following: delusions, hallucinations, disorganized thinking/behaviours and catatonia. The negative symptoms of schizophrenia reflect a loss of normal functioning and include the following: avolition (withdrawal, loss of motivation and ambivalence), anhedonia (loss of feeling or an inability to experience pleasure), alogia (poverty of speech), and affective flattening. The presence of negative symptoms early in the illness is associated with a more adverse course, including more psychotic episodes [281] and greater impairment in adaptive life skills [282]. Although not the part of diagnostic criteria, cognitive dysfunction is often present in people with schizophrenia, which shares many features with negative symptoms [283]. In addition, the mood symptom is normally containing the dysphoria, suicidality, depression and helplessness.

The causes of schizophrenia are linked to several aspects such as the genetic [284] and environmental [285–288] factors, which are the two prominent factors that may induce or trigger mental illness. No single cause of schizophrenia has been identified to date. There are most likely several contributing factors, evidence suggests that genetic vulnerability and environmental stressors can act in combination to result in diagnosis of schizophrenia. In a recent study, seven different genetic variations were found to be associated with schizophrenia and which all lie within a gene FXYD6 [289].

1.2.3 Chlorpromazine (CPZ)

Chlorpromazine (*Scheme 1.2*), the first neuroleptic agent was discovered in 1952 (in France), which is a cationic, amphiphilic phenothiazine derivative, consisting of a three-ring structure in which two benzene rings are linked by a sulphur and a nitrogen atom. The nitrogen atom carries an aliphatic side chain of three carbon atoms, terminated by a tertiary amine. This terminal nitrogen atom is protonated, which causes CPZ to have a net positive charge at physiological pH. In addition, the length of the aliphatic side chain has shown close relationship with the psychiatry effect [290].

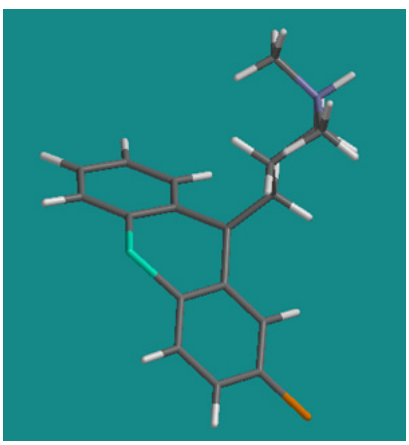

Scheme 1.2 Chemical structure of chlorpromazine, blue color represents the nitrogen, orange red color is for chlorine, and green color for the sulphur nucleus.

In therapeutic concentrations (in the magnitude of micro molar, bulk phase), CPZ affects numerous cellular responses, such as causing damage in a series of native nucleic acids by originated from its interaction with biological membranes [291]. The membrane stabilizing effect of CPZ on hypertonic hemolysis of red cells is well known, which clearly reflects CPZ–plasma membrane interactions, and depends on the membrane content of linoleate [292]. The phenothiazines, including CPZ, are

also known as CaM antagonists when exposed to red blood cell membrane ghosts [293]. Furthermore, CPZ also increases the polyphosphoinositide metabolism in platelets, and shows the strong impacts on the signal transduction [294–297]. CPZ's effects are also detected on voltage-dependent sodium currents [298] and on ATP-sensitive K^+ channels in ventricular myocytes of rats [299,300].

CPZ is thought to act by binding to and blocking the various receptors, and it is unlikely that CPZ possesses of the single mechanism of action. Furthermore, according to its amphiphilic nature, it also seems unlikely for molecules like CPZ with a low molecular weight and lipid-solublility would remain exclusively outside the cell and react only with specific receptors. Indeed, many studies have demonstrated the direct interaction of CPZ with the plasma membrane [295,301–303]. Some studies showed that CPZ increases the fluidity of biomembranes [304–306], and other studies reported that CPZ decreases membrane fluidity [307–310]. The discrepancy of these reports regarding the decrease or increase of membrane fluidity by CPZ mainly depend on the membrane system investigated, such as the cholesterol/phospholipid ratio of the membrane [311], the concentration of CPZ and temperature [306] and the discrepancy between *in vivo* and *in vitro* studies [309,310,312]. From Luxnat and Galla [15], we know that the partition coefficients, k*p*, of CPZ between the aqueous phase and lipid bilayer vesicles were determined as function of drug concentration, lipid acyl chain length and so on, and they also indicated that the membrane structure will not be disturbed at less than 30 μM (bulk phase) CPZ. Suwalsky and Neira [313] elucidated that CPZ altered the bilayer structure according to the nature of the phospholipid headgroup. The significance of the headgroup has been demonstrated by Agasøster et al. on phospholipid monolayers, where CPZ dramatically influenced the molecular area of the acidic glycerophospholipids, such as PS, PA, and PG, but no or low effects on the zwitterionic monolayers, such as PC, and PE at low concentration of 1 μM (bulk phase) [314]. Similar results were also found in other studies [315,316]. Furthermore, the nature of the phospholipid acyl chains is another important factor regulating the CPZ–membrane interaction [317]. Investigation of the significance of hydration for the interdigitation of CPZ on the plasma membrane was carried out in our laboratory by Nerdal et al. [317]. The data of ^{13}C magic-angle spinning (MAS) solid-state NMR on bilayer samples with partial hydration (~12 H_2O molecules per phospholipid) showed that CPZ had low or no interaction in the acyl packing of liposomes made of phospholipids with neutral charge and saturated acyl chains (DPPC and DMPC). Conversely, CPZ

caused a large shift (5−15 ppm) to higher ppm values of ~30% of the acyl chain carbon resonances in liposomes composed of porcine brain PBPS and DPPC.

Moreover, the observations described in *Section 1.1.11* indicate that the activity of membrane-bound proteins can be influenced by the changes in the organization and dynamics of the membrane. Therefore, one should expect that perturbation of the lipid organization by amphiphilic CPZ molecules (from CPZ−membrane interaction) would subsequently influence the activity or catalyzed processes of membrane−bound proteins, even without direct interaction between the protein and the amphiphile. It is thus possible that CPZ's effect on the dopaminergic receptor is partially due to perturbation by CPZ of the membrane that contains the receptor.

1.2.4 Olanzapine (OLZ)

Olanzapine (OLZ, *Scheme 1.3*), a relatively new thienobenzodiazepine derivative, is widely used as an antipsychotic agent and has become one of the most commonly used atypical antipsychotics [318]. It shows relatively high affinities for various neurotransmitter receptors, for example, $D_{1\text{-}5}$ dopaminergic, 5-$HT_{2A\text{-}2C}$ and 5-$HT_{3,\,6,\,7}$ serotonergic, α_1-adrenoceptors and histamine H_1 [318−324], and a moderate affinity for the five muscarinic receptor subtypes, M_{1-5} [325]. The functional blockade of these various receptors may contribute to its broad efficacy in the treatment of schizophrenia and related psychoses [326−329]. Generally speaking, atypical antipsychotics are associated with fewer extrapyramidal side effects [330] and less propensity for the development of tardive dyskinesia than the typical antipsychotics [277,331,332].

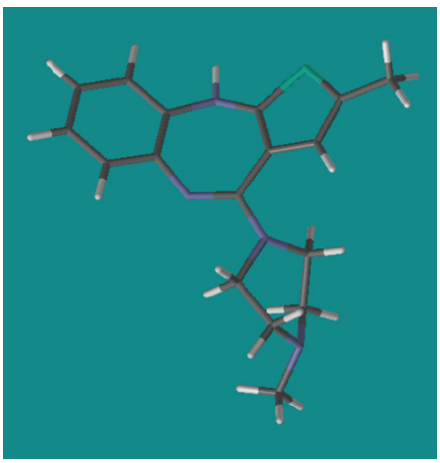

Scheme 1.3 Chemical structure of olanzapine, blue color represents the nitrogen, and green color for the sulphur nucleus.

However, the side effects of OLZ related to the antagonism at those receptors are also reported (*Table 1.5*). The mechanism of action of atypical antipsychotic drugs is unknown. The most prevailing mechanism hypothesis suggests synergism between inhibition of dopamine receptors and serotonin 5-HT receptors [333], which is responsible for the "atypicality" of atypical antipsychotics. Another hypothesis suggests that the major contribution to the atypical antipsychotic action is due to a fast dissociation constant (K_{off}) from the D_2 receptor, allowing for better transmission of normal physiological dopamine surges, and thus a lower overall affinity for dopamine D_2 receptor [334]. In addition, OLZ has a higher affinity for 5-HT_2 serotonin receptors than D_2 dopamine receptors.

Table 1.5 Side effects of OLZ coupled with its receptor antagonism.

Receptor	Side effects	References
muscarinic	anticholinergic symptoms	[335–337]
histamine H_1	somenolence, weight gain	[338,339]
α_1-adrenergic	orthostatic hypotension	[340]

In therapeutic concentrations, OLZ affects numerous other cellular responses, such as the chronical inhibition of the membrane phospholipase D (PLD) activity. PLD is the integral membrane protein that acts specifically on phosphatidylcholine [341], and causes elevation of serum creatine kinase (CK) level [342], which may cause or induce the cell membrane damage. In addition, the effect of OLZ on the elevation of apolipoprotein-D (apoD, an atypical apolipoprotein) levels has been found [343], apoD has been assumed to play an important role in phospholipid metabolism, based on its binding of arachidonic acid (AA) and cholesterol [344–346]. Recently, Parikh et al. [347] found that OLZ prevented loss of antioxidant enzymes in rat brain, and Evans et al. [348] indicated that reduced levels of antioxidant enzymes were associated with increased plasma lipid peroxides and reduced membrane EPUFAs (essential polyunsaturated fatty acids), particularly ω-3 fatty acids. Studies in rats have shown that atypicals (olanzapine, clozapine, and risperidone) have antioxidant effects and reduce lipid peroxidation [349,350], this has been shown to affect receptor affinity in membranes, for example, 5-HT_2 receptors [351]. Furthermore, OLZ and other atypical antipsychotics (clozapine, risperidone) were found to improve the levels of erythrocyte EPUFAs [352], which may be a mechanism contributing to the therapeutic effects of schizophrenia treatment [186,353]. The effects of OLZ on processes taking place in biological membranes are scarcely investigated; a recent surface plasmon resonance (SPR) study by Gjerde et al. [354] suggested a lower binding profile on bilayer membranes, compared with another three selected typical and atypical antipsychotic drugs (chlropromazine,

haloperidol, and clozapine). This is contrasted by the older typical antipsychotic drug CPZ, which has prompted many physiochemical studies of the interaction with the glycerophospholipids by various techniques, such as ESR [15], EPR [355], X-ray [313], positron autoradiography [356], fluorescence spectroscopy [357], DSC [317] and NMR [271,317].

1.2.5 Local Anaesthetics (Articaine)

1.2.5.1 Local Anaesthetics

Local anaesthetics have fundamental structural features in common that are relevant for their biological function. The first feature is a lipophilic moiety, which is joined by an amide or ester linkage to a carbon chain. The carbon chain is then joined to a hydrophilic moiety (amine) with pK_a values around physiological pH [358,359] (for structural classification and individual pK_a value of local anaesthetics, see *Table 1.6*). Local anaesthetics are weak bases that can exist as either charged (ionized) or uncharged (non-ionized) molecules. They are only slightly soluble in the base form and are therefore usually formulated as a water-soluble hydrochloride salt.

Table 1.6 Classification of local anaesthetics. The pK_a values of the drugs are referenced upon Malamed et al. [365], otherwise stated in square brackets.

Amides (**pK_a**)	Esters (**pK_a**)
Articaine (**7.8**)	Benzocaine (**2.5**) [362,363]
Bupivacaine (**8.1**)	Cocaine (**8.5**) [364]
Lidocaine (**7.8**)	Procaine (**9.1**)
Mepivacaine (**7.6**) [360]	Tetracaine (**8.2**)
Etidocaine (**8.95**) [361]	
Dibucaine (**8.8**)	
Prilocaine (**7.9**)	

The molecular mechanism of local anaesthetics connects with ion channels, nerve and depolarization of the cell membrane [366]. Local anaesthetics prevent conduction in peripheral nerves by their binding to the voltage-gated sodium channel and blocking the inward sodium transport that creates the action potential of axons and thereby causing anaesthesia [366–369]. Although it is commonly accepted that local anesthetics exert their pharmacological action by interacting with the cell membranes, but the molecular nature of the site of their action remains unclear and been extensively investigated [16,370–372]. The receptor theory proposes that the local anesthetics bind to specific receptors sites

on or within the sodium channels [373,374], while the membrane fluidization (expansion) hypothesis suggests that local anesthetics interdigitate in the membrane, changing the membrane's organization [375–377]. Both mechanisms involve the membrane, providing the clue to study the effects of local anesthetic on the membrane bilayer system by investigating the physical and chemical parameters in relation to the interaction between the local anesthetics and the model membrane [16,378–380].

As the local anaesthetic must enter the cell in order to have its effect, it must pass through the lipid cell membrane. Uncharged species will do this more readily than a charged drug [16,381]. Therefore, the drug, which is more uncharged at physiological pH, will reach its target site more quickly than the drug [382]. This explains why articaine (pK_a=7.8) has a faster onset of action than bupivacaine (pK_a=8.1) [365]. Furthermore, the pK_a of a local anaesthetic determines the amount, which exists in a charged form (or in an uncharged form) at any given pH. At physiological pH 7.4, most local anaesthetics are more charged than uncharged (as the most pK_a values are greater than 7.4, *Table 1.6*). However, the proportions vary between the drugs: articaine has a pK_a of 7.8 and is approximately 20% uncharged at pH 7.4. Bupivacaine has a pK_a of 8.1 and hence less of the drug is uncharged at pH 7.4 (~15%), according to the *Henderson–Hasselbalch* equation:

$$pK_a - \mathrm{pH} = \log^{[\text{uncharged species}]}/_{[\text{charged species}]}$$

1.2.5.2 Articaine

Articaine hydrochloride (*Scheme 1.4*), 4-methyl-3(2-[propylamino]propionamido)-2-thiophenecarboxylic acid, methyl ester hydrochloride, was initially prepared by Rusching and colleagues in 1969 and first mentioned in the literature by Muschaweck and Rippel (in 1974) [383], and the present generic name changed from carticaine in 1976, when introduced into the clinical practice in Germany [384]. Articaine is widely believed to be an effective and safe local anaesthetic agent in dentistry [365,385].

Articaine is classified as an amide local anaesthetic (*Table 1.6*), however, unlike other amide (and ester) local anaesthetics, articaine possesses a thiophene group instead of the benzene ring, which increases its liposolubility [386], and has therefore a better ability to penetrate the nerve sheath. Moreover, the other basic molecular difference is articaine containing an extra ester linkage that causes articaine to be hydrolyzed by plasma esterase [387,388] to articainic acid. In

addition, articaine is a secondary amine, while the other common local anaesthetics in clinical use are tertiary amine compounds.

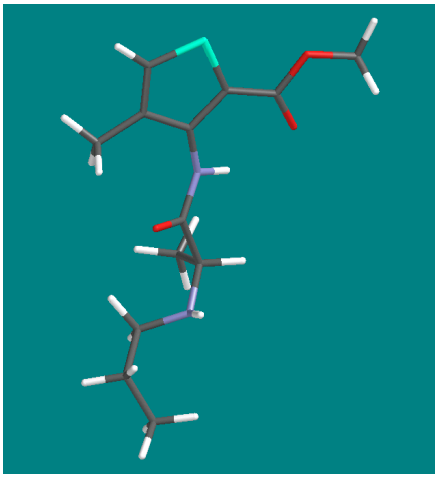

Scheme 1.4 Chemical structure of articaine, blue color represents the nitrogen, red color is for oxygen, and green color for the sulphur nucleus.

An amphiphilic compound like articaine will have an ionic or non-ionic polar moiety and a hydrophobic part, depending on pH. In an aqueous medium, amphiphilic molecules are able to organize themselves as micelles, bilayers, monolayers, hexagonal or cubic phases (*Section 1.1.5*). Thus, it is likely that at certain conditions, e.g. concentration, an amphiphile like articaine can form self-aggregated structures. This has been observed for other local anesthetics like dibucaine and tetracaine where the critical micelle concentrations (CMC) were found to be 0.066 and 0.130 M, respectively [389]. In addition, the hydrophobicity of articaine, and thereby its potential for interaction with the hydrophobic part of the phospholipid bilayer can be evaluated by the corresponding octanol/water partition coefficient (K_{eff}). The octanol/water partition coefficient for articaine is 257 [390], and this high articaine preference for octanol over water was furthermore found to correlate well with articaine binding to (isolated) guinea pig atria tissue [390].

1.2.5.3 Articaine–Membrane Interaction

Investigations of the actions of local anesthetics upon model membrane systems were engaged by several spectroscopic methods, such as fluorescence [371], infrared [371,377], X–ray diffraction [377,391,392], ESR [371,393,394], ultraviolet light absorption [378] and NMR [16,370–372,380,381]. In a previous study of Lygre et al. (unpublished data), DSC technique on disaturated membrane lipids was employed,

the findings indicated the interaction occurred between articaine and bilayer system from thermotropic point of view. In paper III, we used the high-resolution solid-state ^{13}C and ^{31}P NMR to study the uncharged articaine species in DSPC model membranes, PC is the major phospholipid in mammalian membranes, which can modulate membrane structure (*Section 1.1.2*).

The DSPC articaine−containing samples performed NMR experiments were adjusted to pH 10.0, where more than 99% articaine molecules in the unchanged form (pK_a=7.8). It is more hydrophobic [367,394] and more receptive [395,396] for DSPC bilayer interaction than charged species. The DSPC phospholipid bilayer studied with the addition articaine at four different molar ratios (10, 25, 40, and 55 mol%), which are several orders higher than the clinically used concentrations (in clinical, a 4% articaine solution is used) [386]. The design of the experiments will also provide the information about the saturation limit and crystallization of uncharged articaine in the bilayer [397,398], in addition to the structural and molecular-level mobility information of the DSPC bilayer system induced by uncharged articaine.

Another purpose of the study in paper III was to monitor the phase transition patterns of the model membrane systems at different amounts of articaine. The depression of bilayer gel-to-liquid-crystalline phase-transition temperature by local anesthetics has been found to correlate with the anesthetic hydrophobicity [399].

2. METHODS

2.1 Solid-State Nuclear Magnetic Resonance

Nuclear magnetic resonance (NMR) [400–403] is a physical phenomenon based upon the quantum mechanical magnetic properties of an atom's nucleus, which occurs when the nuclei are immersed in a static magnetic field and exposed to a second oscillating magnetic field. The principle behind NMR is that many nuclei have spin and all nuclei are electrically charged. When an external magnetic field is applied, an energy transfer is possible between the base energy level (E_α) to a higher energy level (E_β), if the energy absorption taking place at a specific radio frequency ($v_0 = -\gamma B^0/2\pi$) and when the spin returns to its base level, energy is emitted at the same frequency (*Figure 2.1*).

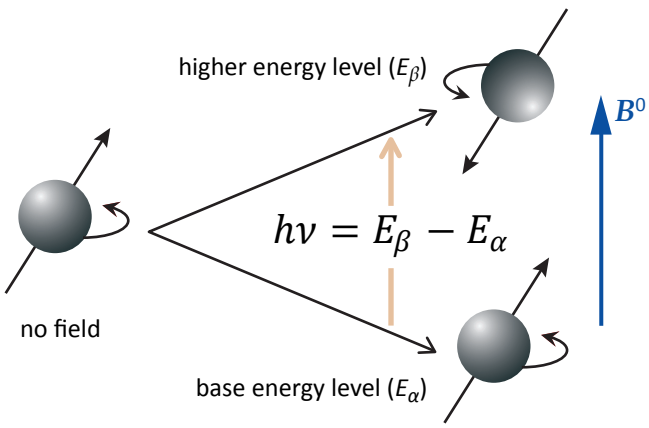

Figure 2.1 The basic description of spectroscopy in terms of energy levels (the case spin ½ nuclei).

The signal that matches this transfer is measured and processed in order to yield an NMR spectrum for the nucleus concerned. When a nuclear spin interacting with a magnetic field, spatial proximity and/or a chemical bond between two atoms can give rise to interactions between nuclei. In general, these interactions are orientation dependent. In media with no or little mobility (e.g. crystal powders, large membrane vesicles), anisotropic interactions have a substantial influence on the behaviour of a system of nuclear spins. Solid-state NMR spectroscopy [404–409] is characterized by the presence of anisotropic (directionally dependent) interactions, which is simplified in solution NMR due to time-averaging caused by rapid motional fluctuations (*Brownian* motion). Furthermore, in solids, the chemical shift interaction is not the only anisotropic interaction that determines

the spectrum. The dipolar interaction [410] between spins usually affects the resonance frequency more than the chemical shift interaction.

For spin ½ nuclei such as ^{13}C or ^{15}N, solid-state NMR spectra of biopolymers, including biomembranes, membrane proteins, polysaccharides, etc. yield enormously broadened signals that arise from nuclear interactions such as dipolar interactions and chemical shift anisotropy (CSA) [407–409], which are in the order of 10^2–10^4 Hz and 10^3–10^4 Hz, respectively. Such broadened signals are usually not easy to interpret in terms of chemical or biological significance, unless an attempt is made to narrow linewidths to give rise to high-resolution solid-state NMR, as encountered in solution NMR, by specific manipulations of spin system.

2.1.1 Dipolar Decoupling

Nuclear spins exhibit a dipole moment, which interacts with the dipole moment of other nuclei (dipolar coupling). The magnitude of the interaction is dependent on the spin species, the internuclear distance (*r*), and the orientation (θ) of the vector connecting the two nuclear spins with respect to the external magnetic field B^0 (*Figure 2.2*), expressed using quantum mechanical formalism as:

$$\mathcal{H}_D = -\gamma_I \gamma_S \hbar^2 r^{-3} (3\cos^2\theta - 1) \boldsymbol{I}_z \boldsymbol{S}_z,$$

where $\boldsymbol{I}$ and $\boldsymbol{S}$ are nuclear spin numbers for nuclei I and S, and γ_I and γ_S are gyromagnetic ratios for I and S spin, respectively, and $\hbar$ is Plank's constant h divided by 2π. In a crystal powder or amorphous solid, $\cos^2\theta$ could not be averaged to zero (all orientations occur), which is a non-zero dipolar coupling, will produce a broad line.

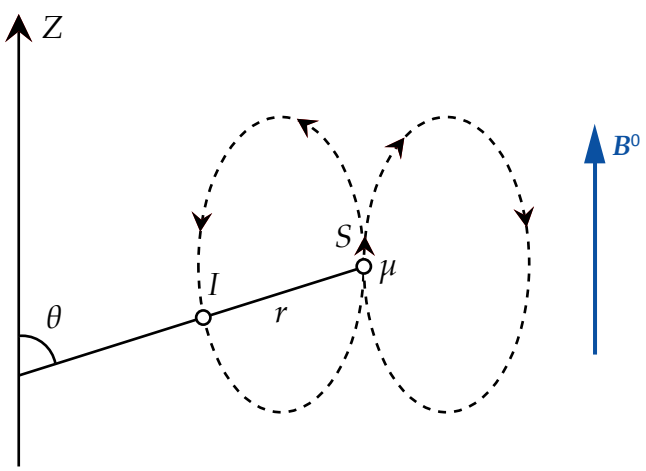

Figure 2.2 Dipolar field at the spin I caused by the neighboring spin S.

NMR signals of rare spins ($I = 1/2$) such as ^{13}C or ^{15}N are mainly broadened by dipolar interactions with neighboring proton nuclei, because of the weak homonuclear (e.g. ^{13}C–^{13}C, ^{15}N–^{15}N) dipolar interactions under the condition of natural abundance, and hence negligible in most cases. Therefore, such heteronuclear (e.g. ^{13}C–^{1}H, ^{15}N–^{1}H) dipolar couplings can be effectively removed by irradiation of strong radio-frequency (rf) at proton resonance frequency to result in time-averaged magnetic dipolar field to zero, as in a similar manner to proton decoupling in solution NMR to remove scalar ^{13}C–^{1}H spin couplings. In solids, high-power proton decoupling is required to reduce the stronger dipolar couplings of 20 KHz (in solution NMR, the scalar ^{13}C–^{1}H spin couplings ranging from 0–200 Hz). In practice, the continuous wave (CW) proton decoupling scheme [411,412,417,418] is widely used to eliminate heteronuclear couplings in solid-state NMR spectroscopy (see Appendix for the corresponding pulse programs **hpdec.av** and **hpdec.rel** used in the current study and their graphical displays). On the other hand, in solution NMR spectroscopy, CW decoupling is used much less often as it has been superseded by a number of different multiple-pulse techniques [413,414].

2.1.2 Chemical Shift Anisotropy (CSA)

The peak narrowing by the dipolar decoupling is not always sufficient to achieve high-resolution signals as found in solution NMR, because of a unique spectral pattern arising from CSA, the orientation-dependent part of the chemical shift, which spreads 10^3–10^4 Hz (for magnetic field of 5–10 T) is persistent [407]. Much larger anisotropies (up to 1000s ppm) can be found for some heavier nuclei [404]. In general, this inhomogeneous broadening factor arises from asymmetry in the electron density surrounding a given nucleus in a molecule (*Figure 2.3*), which means that the nucleus experiences a different shielding, and hence has a different chemical shift (*Figure 2.4–left*). The degree to which the electron density affects the resonance frequency of a nucleus depends on the orientation of the electron cloud (and hence the orientation of the molecule) with respect to B^0.

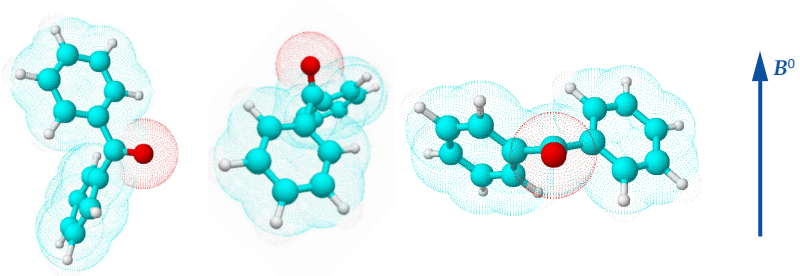

Figure 2.3 Molecules could have different orientations in a magnetic field, as demonstrated of crystalline benzophenone. These orientations cannot be averaged in a solid.

In liquids, an average chemical shift is observed due to averaging over all orientations by the fast isotropic molecular tumbling on a timescale shorter in comparison with the NMR measurement time. In most solids, on the other hand, molecular motion is restricted, such as in a powder, which consists of many crystals, all with different orientations. And the chemical shift of each crystallite (shows a sharp peak) is different which gives rise to a broad shape with sharp corners, called powder pattern. The powder pattern is the superposition of many sharp peaks with different frequencies (*Figure 2.4–right*).

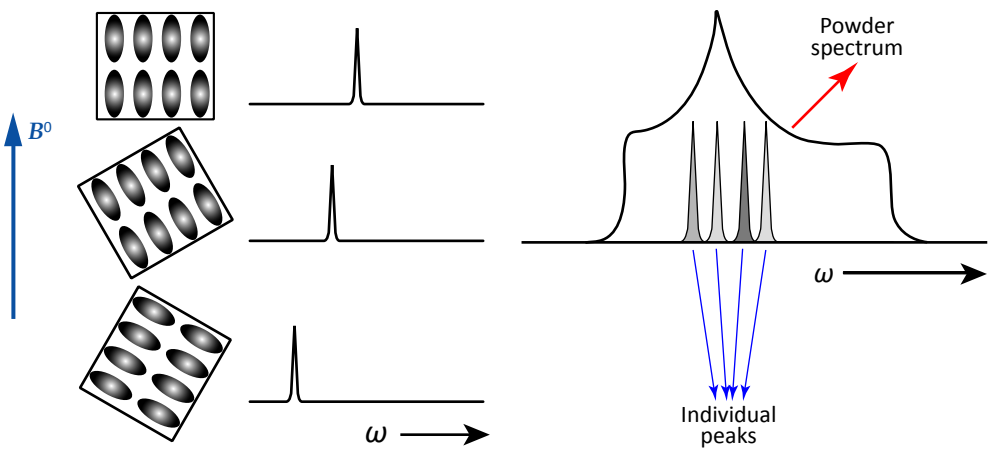

Figure 2.4 (*left*) In a crystal, e.g. crystalline benzophenone, the chemical shift depends on the orientation of the solid with respect to the magnetic field; (*right*) Formation of a powder pattern.

The mathematical entity that describes the orientation dependence of the chemical shift is called a tensor and can be represented by a 3×3 matrix,

$$\begin{pmatrix} \delta_{xx} & \delta_{xy} & \delta_{yz} \\ \delta_{yx} & \delta_{yy} & \delta_{yz} \\ \delta_{zx} & \delta_{zy} & \delta_{zz} \end{pmatrix} \xrightarrow{diagonalize} \begin{pmatrix} \delta_{11} & 0 & 0 \\ 0 & \delta_{22} & 0 \\ 0 & 0 & \delta_{33} \end{pmatrix},$$

where, δ_{11}, δ_{22}, and δ_{33} are called the components of the chemical shift tensor. Each component δ_{ii} can be represented by a vector with length that depends on the value of δ_{ii} [417]. In the case of crystalline benzophenone, the carbonyl ^{13}C chemical shifts can differ by more than 170 ppm, depending on the orientation of the C=O moiety with respect to the external field B^0, as shown in *Figure 2.5* [415]. The largest chemical shift in the resonance frequency of the (carbonyl) ^{13}C nucleus occurs when the narrowest part of the electron cloud is oriented along the B^0 axis (*Figure 2.5–a*), whereas the smallest shift occurs when the widest part of the electron cloud is oriented along B^0 (*Figure 2.5–c*). These two chemical shifts,

referred to as δ_{11} and δ_{33}, respectively. The third value δ_{22} is the shift produced by the molecular orientation perpendicular to the axes of δ_{11} and δ_{33} (*Figure 2.5–b*). These three principal values specified by three Euler angles [416] provide all the information necessary to describe the CSA of a nuclear spin [417,418].

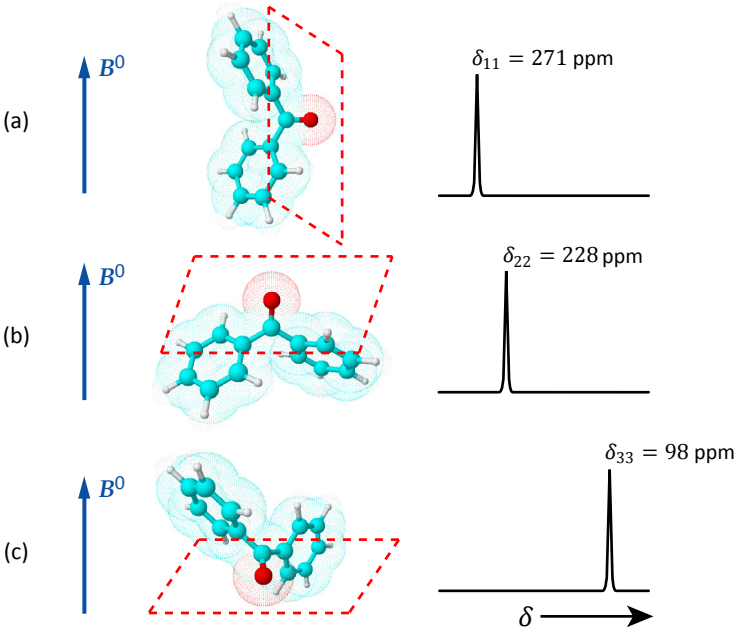

Figure 2.5 Carbonyl ^{13}C chemical shift anisotropy (CSA) of crystalline benzophenone.

Principal values of the chemical shif tensors (δ_{11}, δ_{22} and δ_{33}) are very important parameters to characterize solid-state NMR spectral feature, molecular orientation, and dynamics, which can be directly obtained from the powder anisotropy pattern (*Figure 2.6*). Such CSA dispersions are averaged to give their isotropic values, $\delta_{iso} = 1/3\,(\delta_{11} + \delta_{22} + \delta_{33})$ [419–421], by means of the combination of dipolar decoupling [412] and magic-angle spinning (MAS) technique [419–423] with spin rates at 2–10 KHz, which is a powerful and widely-used method in solid-state NMR [417,418,424–426].

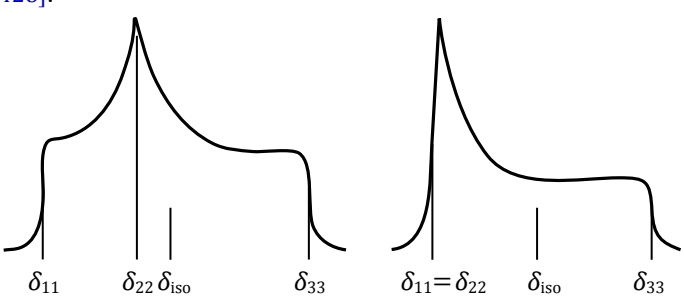

Figure 2.6 Powder pattern spectra for spin ½ nuclei: (*left*) axially asymmetric ($\delta_{11} \neq \delta_{22} \neq \delta_{33}$), (*right*) axially symmetric ($\delta_{11} \neq \delta_{22} = \delta_{33}$). $\delta_{iso} = 1/3\ (\delta_{11} + \delta_{22} + \delta_{33})$

2.1.3 Magic-Angle Spinning (MAS)

The chemical shift *Hamitonian* depends on the tensor component δ_{zz},

$$\mathcal{H}_{CS} = \gamma\hbar B^0 \delta_{zz} I_z,$$

the symbol δ_{zz} represents the component of the induced field in the z−diretion, when the external field B^0 is also in the z−direction ($B^0 \parallel z$−axis), and thus expressed as follows:

$$\delta_{zz} = \lambda_1^2\delta_{11} + \lambda_2^2\delta_{22} + \lambda_3^2\delta_{33},$$

$$\lambda_1 = \cos\alpha \sin\beta\,, \lambda_2 = \sin\alpha \sin\beta\,, \lambda_3 = \cos\beta,$$

where α and β are Euler angles which relate principal axis system ($\mathcal{X}$, $\mathcal{Y}$, and $\mathcal{Z}$) in a molecule to laboratory frames (x, y, and z, in whch z−axis is taken along the direction of applied magnetic field B^0), see *Figure 2.7–left*.

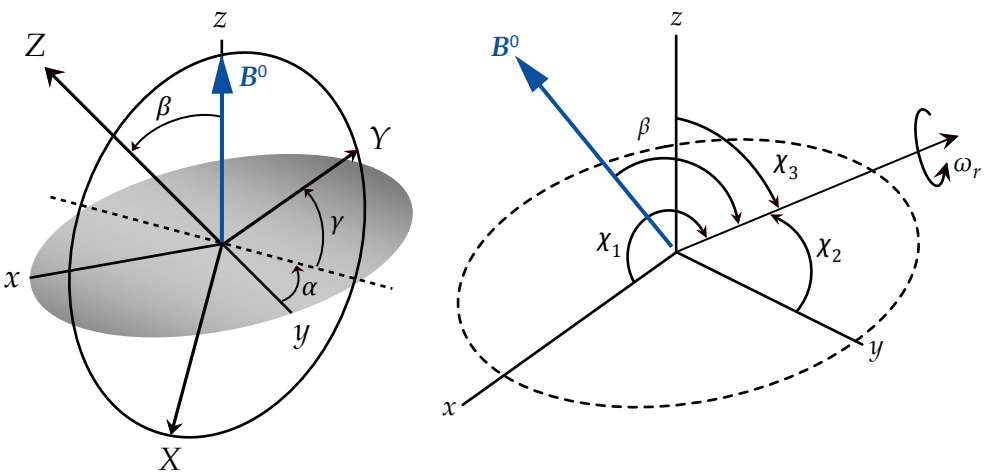

Figure 2.7 (*left*) Euler angles (α and *β*). $\mathcal{Z}$−axis of the laboratory frame is taken along the direction of applied field (B^0); (*right*) The mechanical rotation of the solid sample with the angular velocity of $\boldsymbol{\omega_r}$ about an axis inclined at a selected angle *β* (= $\mathbf{54°44'}$) to the applied field (B^0), and at the angles $\boldsymbol{\chi_i}$ to the principle axes.

In liquid state, the isotropic averages of each λ_i^2 being reduced to ⅓, the chemical shift tensor component δ_{zz} by the isotropic tumbling motions as follows [427]:

$$\delta_{zz} = 1/3\ Tr(\boldsymbol{\delta}) = 1/3\,(\delta_{11} + \delta_{22} + \delta_{33})$$

So, this chemical shift is equal to the isotropic chemical shift, and does not depend on the orientation of the sample with respect to the magnatic field. In solid state, when the rigid array of nuclei in a solid is rotated with angular velocity of ω_r about an axis inclined at an angle of β (*Figure 2.7–right*) to the applied field B^0, and we have,

$$\lambda_p = \cos\beta\cos\chi_p + \sin\beta\sin\chi_p\cos(\omega_r t + \varphi_P).$$

Substituting to $\delta_{zz} = \lambda_1^2\delta_{11} + \lambda_2^2\delta_{22} + \lambda_3^2\delta_{33}$ and taking the time-average,

$$\delta_{zz} = 1/2\ \sin^2\beta\, Tr(\boldsymbol{\delta})_{\{1\}} + 1/2\,(3\cos^2\beta - 1)_{\{2\}}\sum \delta_{pp}\cos^2\chi_p\ _{\{3\}}$$

The first term {1} is the isotropic part of the chemical shift, and the thrid term {3} is the orientation dependence of spin interaction, which could not be removed, but simply made time-dependent, the second term {2} is the part that can be removed by physical rotation, when $\beta = \sec\left(1/\sqrt{3}\right) \cong \mathbf{54°44'}$, called the magic angle. And the left term, term {1}, of the chemical shift δ_{zz} is as same as for a liquid. So, it is possible to mimic the effect of isotropic molecular motion by using magic-angle spinning (MAS) (*Figure 2.8–left*). In this treatment, the mechanical rotation of the whole solid sample should be carried out at the spinning rate $\omega_r \gg |\delta_{11} - \delta_{33}|$, which is the linewidth of the CSA dispersion (*Figure 2.6*). Normally, the rotation at 2–10 kHz is sufficient to get the single narrow resonance, otherwise the spinning sidebands remained, spaced at the rotation frequency and centered on the isotropic chemical shift (*Figure 2.8–right*). To suppress the sideband lines, one can increase the spinning frequency of MAS, speed of up to 50 kHz with rotors of 2 mm diameter was demonstrated in 1999 in an academic laboratory [428].

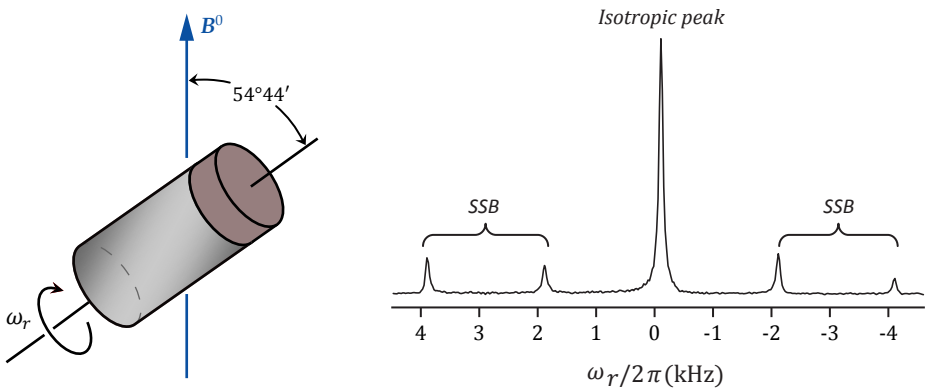

Figure 2.8 (*left*) Schematic diagram of a sample spinning at the magic-angle ($\mathbf{54°44'}$) in an applied magnetic field (B^0), the sample tube is spun around its long axis, at spinning rate $\omega_r \gg |\delta_{11} - \delta_{33}|$; (*right*) Solid-state ^{31}P spectrum of fully hydrated DMPC/40 mol% articaine, in a magnetic field of 9.4 T. The spectrum was taken using 2 kHz magic-angle spinning, the spectrum shows a central isotropic flanked by several narrow spinning sidebands (*SSB*) spaced by rotating frequency.

Magic-angle spinning is a powerful and widely-used method in solid-state NMR, in practical circumstances, high-resolution solid-state NMR spectra can be obtained by using a combination of dipolar decoupling and magic-angle spinning, which is very effective for detecting ^{13}C NMR signals from rather flexible areas of fully hydrated biopolymers such as phospholipid membrane and swollen polypeptides. On the other hand, cross polarization technique [417,418] is the very useful means to record signals from rigid portion of samples (*Figure 2.9*).

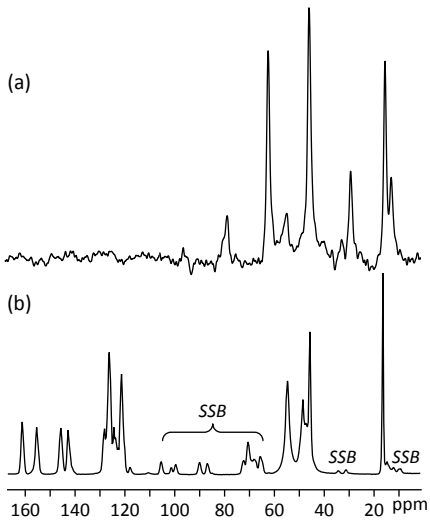

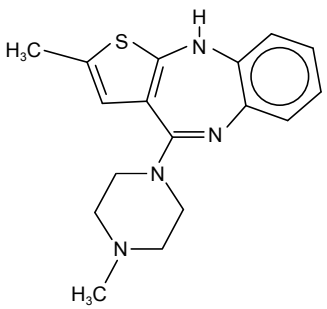

Olanzapine (OLZ)

Figure 2.9 The ^{13}C MASNMR spectra of olanzapine (OLZ) powder (with 15 wt.% D_2O) with 7 kHz magic-angle spinning by using: (*a*) high-power proton decoupling pulse program (**hpdec.rel**); (*b*) cross- polarization pulse program (**cp.av**). Spinning sidebands labelled as '*SSB*'. For the details of the pulse programs, see Appendix.

2.1.4 Cross Polarization (CP)

The majority of solid-state NMR experiments detect the magnetization of other nuclei such as ^{13}C, ^{31}P, and ^{15}N. The drawbacks of directly detecting low-γ nuclei such as ^{13}C and ^{15}N are low isotopic abundances, low spin polarization, and low signal intensity. To observe rare spins ^{13}C in solids, there are no significant homonuclear couplings; on the other hand, the heteronuclear couplings between rare spins (^{13}C) and abundant spins (^{1}H) are dominant. By using abundant I spins to enhance the rare spin S signals under appropriate condition is known as polarization transfer or cross-polarization (CP) [429,430]. In liquids, the polarization transfer was originally achieved by experiment INEPT [433]. In solids, the polarization transfer could be achieved by spin lock under *Hartmann-Hahn* condition [418,437,438], shown in following equation,

$$\gamma_I B_{1I} = \omega_I = \omega_S = \gamma_S B_{1S},$$

where, γ_I and γ_S are the gyromagnetic ratios, and ω_I and ω_S are ratio frequencies, B_{1I} and B_{1S} are the frequency strength for abundant I and rare S nuclei, respectively. This procedure starts with a $90°$ rf pulse B_{1I} about the x−axis, brings the magnetization along y−axis, then, the I magnetization $\boldsymbol{M_I}$, at the y−axis is spin-locked along with B_{1I} when the phase of the rf field is shifted by $90°$ from x−axis to y−axis. And μ_{zI} (the z−component of $\boldsymbol{M_I}$) oscillates as: $\mu_{zI} \propto \cos \omega_I t$. In the presence of B_{1I}, the rare spins S are naturally dipolar decoupled and their applied rf field B_{1S} in the y−axis, while individual S spins precess around it, thus, the z−component of $\boldsymbol{M_S}$, also oscillates as: $\mu_{zS} \propto \cos \omega_S t$, which makes the I and S nuclei precess at the same frequency, and the *Hartmann-Hahn* condition is satisfied. The abundant I spins transfer polarization to rare S spins through cross relaxation by dipolar coupling between I and S spins during the contact time or spin-locked time, then the spin lock field on the S spins is turned off. Thus, the S signal is acquired (*Figure 2.10*). The transfer process has been described using thermodynamic [430,431] as well as quantum-mechanical treatments [432–435]. In addition, the experimental implementation of this concept to obtain high-resolution NMR spectra of rare or dilute *S* spins is shown in *Figure 2.11*.

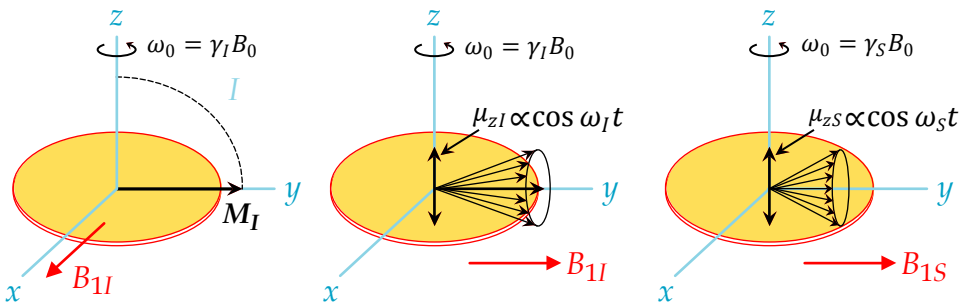

Figure 2.10 Spin-lock in the rotating frame and cross polarization between I and S spins when the condition of $\omega_I = \omega_S$ is satisfied.

Resonance enhancement of the rare spin like carbons is achieved by CP-MAS NMR [439], the optimum magnetization for carbons is $\gamma_{proton}/\gamma_{carbon} = 4$ [407,418], thus four times larger than the magnetization that would be found in the direct observation. And the experimental repetition rates depend on the shorter spin-lattice relaxation times (T_1) of abundant spin, such as proton (normally in milliseconds) rather than carbons or nitrogens. This is another advantage of CP-MAS technique, which greatly shortens the experimental time, compared with the signal acuqisition in the direct observation. In fully relaxed Fourier transform experiments, the repetition time should be ideally taken longer than $5 * T_1$ for 90° pulse to achieve the maximum S/N ratio [440], but the T_1 of the carbon nuclei in

rigid solid can even be in the order of tens of seconds or minutes [441–443], which makes the acquisition unacceptably time-consuming.

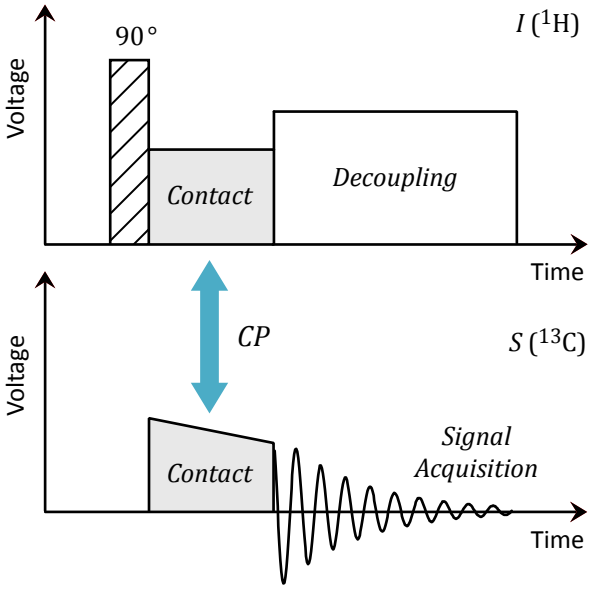

Figure 2.11 Pulse sequence for cross polarization of ^{13}C (*S*) nuclei by protons (*I*) with detection of the ^{13}C magnetization, typical contact times range from 100 μs to 10 ms. The advantage of ramped-amplitude of one of the RF fields during the mixing time was described in Refs. [444–447].

2.1.5 Relaxation Parameters (T_1 and T_2)

The constant T_1 (the spin-lattice relaxation constant, or the longitudinal relaxation time constant) determines the rate of return to thermal equilibrium (*Figure 2.12*).

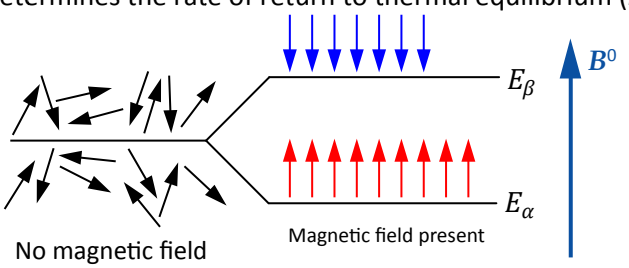

Figure 2.12 The populations of α (↑) and β (↓) spins at thermal equilibrium will be governed by *Boltzmann's* distribution law.

When perturbing nuclear spins by electromagnetic radiation (e.g. a π_x–pulse) as shown in *Figure 2.13*, the longitudinal magnetization in terms of z–component of the magnetization vector M_z decays back to its equilibrium value M_0 (represented by a unit magnetization vector along the z–axis), the motion of the longitudinal component of the magnetization vector M_z is described as: $M_z = M_0\big(1 - \exp(-t/T_1)\big)$. The return to the thermal euqilibrium is not instantaneous, it may

take from milliseconds to minutes. The spin-lattice relaxation involves an exchange of energy between the spin system and the molecular surroundings. In effect, spin-lattice relaxation is a cooling process; an even population distribution implies an infinite temperature and as cooling occurs, after the pulse, the temperature falls, allowing the excess population to return to its equilibrium state [448].

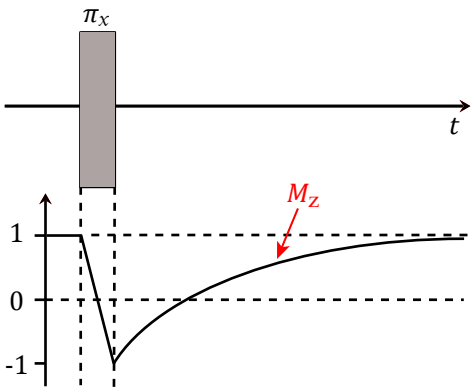

Figure 2.13 The trajectory of magnetization vector M_z during and after a π_x–pulse.

The nuclear spin-lattice relaxation time T_1 is a fundamental NMR parameter that requires special procedures where spectral intensities are obtained as a function of a time delay parameter. Usually, the *Inversion Recovery* pulse sequence is used for T_1 measurements: $[180° \rightarrow \tau \rightarrow 90° \rightarrow Aquisiton \rightarrow Recycling\ delay] \times (\#\ scans)$. The nuclear magnetization (partially) recovers from inversion by the $180°$ pulse through spin-lattice relaxation during the variable delay τ (*Figure 2.14*).

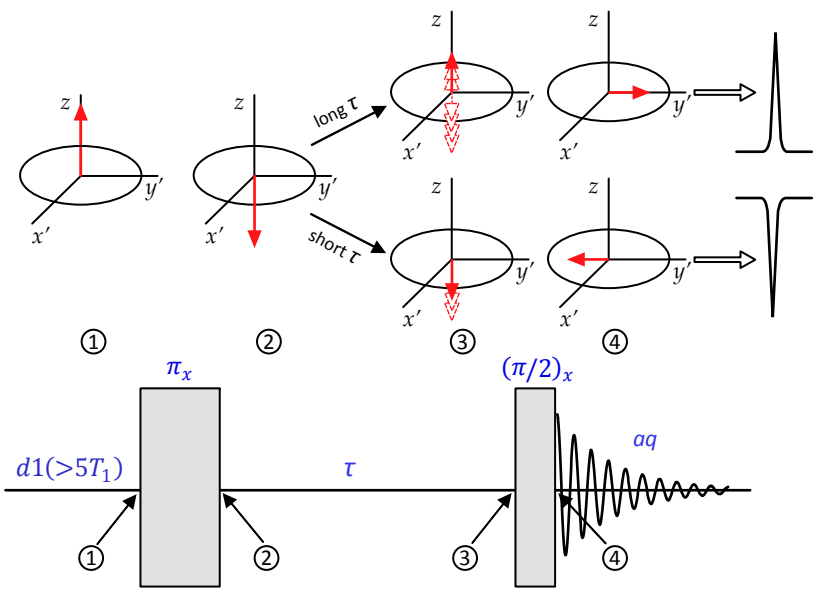

Figure 2.14 Inversion-recovery pulse sequence used to measure the spin-lattice relaxation times (T_1), note the shrinkage in the magnetization vector.

The pulse sequence consists of radiofrequency (RF) pulses separated by an variable interval τ, the first pulse in the sequence is a π_x–pulse and generates an inverted magnetization vector from z–direction to -z–direction. Then the magnetization vector relaxes exponentially back towords the equilibrium during the interval interval τ: this progress is subsequently monitored by the second RF pulse $(\pi/2)_x$, which shifts the magnetization vector 90° for the signal detection.

In practice, we will use a modified *Inversion Recovery* pulse sequence utilizing a composite 180° pulse, i.e. a $90^\circ_0 360^\circ_{120} 90^\circ_0$ pulse (the subscripts are pulse phases) [449], to counteract the problems associated with non-uniform excitation across the large range of ^{13}C chemical shifts. For the details of the pulse sequences (**t1irc360dc**, **t1irpg**, and **cpxt1ir**) used in this study, see the Appendix.

The individual relaxation time T_1 depending on the delay signals may be negative, positive, or have zero intensity. In addition, calculation of the T_1 values and plotting of the T_1 curves are executed by spectrometer software (*Figure 2.15*).

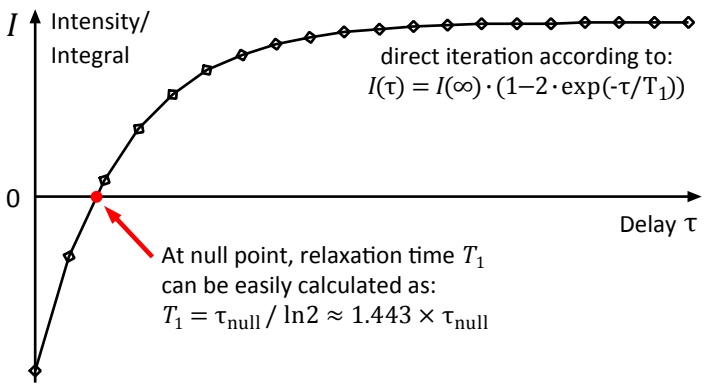

Figure 2.15 Plot of signal intensity against delay for the T_1 determination, generated by spectrometer software.

The spin-lattice relaxation time constant T_1 displays the usual minimum as a function of the correlation time (τ_c), as illustrated in *Figure 2.16*, where the correlation time (τ_c) is temperature-dependent. Warming the sample makes the fluctuations faster, reducing the correlation time (τ_c). In addition, two motional regimes can be distinguished as fast motion and slow motion. For the system (typically small molecules in non-viscous solutions) with fast motion, warming increases the spin-lattice relaxation time constant T_1 ($\omega_0\tau_c \ll 1$), and on the other hand, for the system (typically viscous solutions) with slow molecular motion ($\omega_0\tau_c \gg 1$) found to the right of the T_1 minimum ($\omega_0\tau_c = 1$), heating the sample decreases T_1 [406,450].

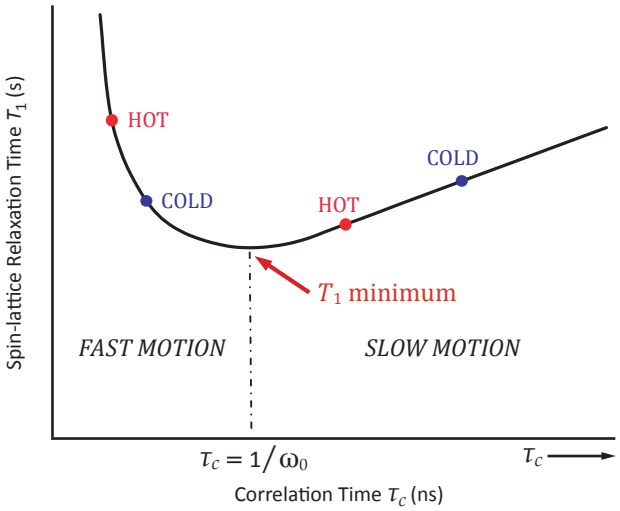

Figure 2.16 Two motional regimes. For fast molecular motion, which is mathematically defined as $\boldsymbol{\omega_0\tau_c} \ll \mathbf{1}$, where warming the sample increasing T_1, and for slow molecular motion ($\boldsymbol{\omega_0\tau_c} \gg \mathbf{1}$), where warming the sample reducing T_1.

Spin-relaxation times are also very important parameters in the solid-state, not only for recording spectra under the optimum conditions but also for gaining insight into dynamic feature of biopolymers in the solid, gels or membrane environment. In this thesis work, we measured the ^{13}C and ^{31}P T_1 values of the model membrane systems, without and with and atypical antipsychotic drugs, chlorpromazine (in paper I and II) and olanzapine (in paper IV).

The time constant T_2 (the spin-spin lattice relaxation constant, or the transverse relaxation time constant) determines the rate of loss of 'phase coherence' (*Figure 2.17*). For the transverse components of the magnetization vector M_x and M_y, decay back to zero, after the perturbation of a radiofrequency pulse (e.g. a π_x–pulse), are described as: $M_x = M_z = M_0\exp(-t/T_2)$. In addition, this decay is related to the linewidth (width at half height of the signal) as $\nu_{1/2} = 1/\pi T_2$ and crude T_2 estimates are readily obtained from ordinary NMR spectra. In addition, the linewidth (and the lineshape) is influenced by inhomogeneities (*Section 2.1.7*).

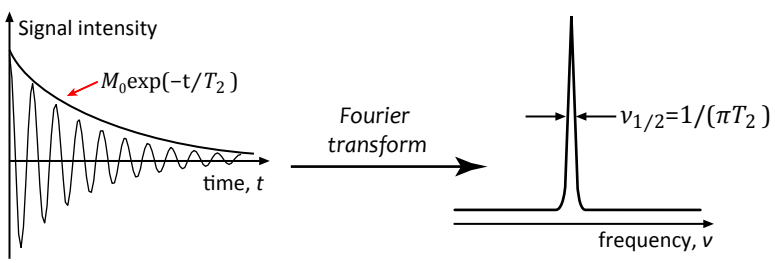

Figure 2.17 The exponential decay envelope of an FID shows the transverse relaxation or T_2 relaxation. Relationship between linewidth ($\nu_{1/2}$) and T_2 is: $\nu_{1/2} = 1/\pi T_2$.

In general, it is found that T_2 is less than, or equal to, T_1, that is: $T_2 \leq T_1$ [448].

2.1.6 Magnetic Field Dependence

In this study, two Bruker NMR spectrometers are used with different magnetic fields B^0, in paper I and II and the the static ^{31}P spectra of the paper III, the experiments were carried out at on a AVANCE DMX 400 instrument (9.4 T), the MAS ^{31}P and ^{13}C experiments of the paper III and paper IV were carried out at on a 500 MHz Ultrashield Plus instrument (11.74 T). Naturally, this causes resolution and sensitivity enhancement as the magnetic field is increased, one of the factors of the sensitivity enhancement is the *Boltzmann* distribution that causes a larger magnetization at the higher magnetic fields. Actually, the *S/N* ratio can be expressed as [451]:

$$S/N = N_s V_s \frac{(h\nu_0)^2}{(4kT)^{3/2}} \frac{\upsilon_0}{B^0} \frac{1}{\Delta\nu} \sqrt{\frac{\mu_0 \pi}{V_c}},$$

where, N_s is the number of spins, V_s is the sample volume, $\Delta\nu$ is the intrinsic linewidth, and V_c is coil volume, the size of the coil is dramatically decreased for a circuit design in the high field and hence an increased *S/N* ratio can be acquired by using ultra-high field magnet. However, when the linewidth dominates in the inhomogeneous distribution of conformations such as amorphous samples, resolution enhancement is not as efficient as that found at a high field on liquid samples.

The dipolar interaction and spin-spin interactions do not increase as the magnetic field is increased, while the chemical shift is proportional to the magnetic field strength [452]. Furthermore, T_1 increases with field strength since spin-lattie relaxation requires spectral density at the Larmor frequency ω_0. Spin-lattice relaxation is less effective at high field, since the spectral density function decays with respect to frequency, and the Larmor frequency ω_0 is higher at high field. Transverse relaxation, on the other hand, involvles spectral densities at a selection of frequencies, including zero. The zero-frequency contribution to the transverse relaxation is field-dependent. As a result, the transverse relaxation time constant is relatively insensitive to field (*Figure 2.18*). In practice, T_1 values are generally larger in the high field and vary drastically from signal to signal with the spectrometer magnetic field [406].

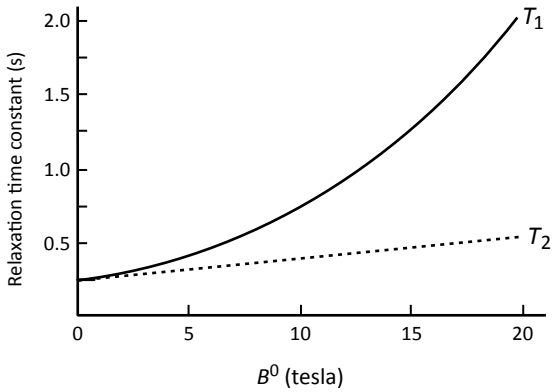

Figure 2.18 The plots of T_1 and T_2 (in second) against field B^0 (in tesla). Assume that the relaxation is exclusively caused by intramolecular dipole-dipole couplings.

2.1.7 Describing Inhomogeneous Broadening: T_2^*

The transverse relaxation time T_2^* gives the overall decay rate, due to both homogeneous and inhomogeneous contributions. In other words, the overall linewidth is the sum of a homogeneous and an inhomogeneous contribution, the inhomogeneous contribution of the decay lineshape is not due to relaxation, but due to the magnetic field inhomogeneities. To obtain the true or natural spin-spin relaxation time T_2, the contribution of the field inhomogeneities to the half-height width must be subtracted, which is possible by using the following equation [448],

$$\frac{1}{T_2} = \frac{1}{T_2^*} - \frac{\gamma \Delta B^0}{2}$$

2.2 Samples Preparation of Lipid Bilayers

In general, the whole procedure for lipid bilayer preparation should be kept under an argon atmosphere and not exposed to light, especially for phospholipids with unsaturated acyl chains.

The desired amount of phospholipids are weighted and dissolved in spectroscopic grade chloroform (or *t*-butanol) and then lyophilized to dryness (with Para-film on the top of the vial and well-proportioned perforation). Then, the sample of dry powder is suspended in degassed distilled water and left on the rotawapor for about one hour (above the sample's gel-to-liquid-crystalline phase-transition temperatures, T_m). Such suspensions contain multilamellar liposomes and unilamellar systems will be obtained by freeze–thawing cycles from 77 K (−196℃, in the liquid nitrogen) to 295 K (22℃, at the room temperature) for at least nine

times. This sample preparation procedure gives large unilamellar liposomes of unequal size. However, in the final samples, bulk water is eliminated and this bilayer procedure is found to be both stable and without artefacts, for example, without different bilayer structures such as high curvature liposomes (small diameter liposomes). In our experience, employing an additional step in the sample preparation procedure of extrusion through a carbonate filter (1000 nm) does not change or improve the subsequent NMR spectrum, i.e. the sample at the time of data acquisition [271,317]. In fact, some phospholipids (phosphatidylserines) tend towards adhering to the carbonate filter and do not pass the filter quantitatively [271].

At the freeze−thawing stage, lipid samples are adjusted to the physiochemical pH value of 7.4 by adding a small amount of 0.05 M NaOH. On the step following, the samples are subjected to 24 hours of lyophilization giving partially hydrated liposomes with a hydration level of ∼12 water molecules per lipid molecule (determined by ^{1}H MASNMR). Subsequently, the appropriate amount of degassed distilled water is added to the sample to obtain fully hydrated bilayers (∼30 water molecules per lipid molecule) [453,454]. Then, the sample is equilibrated on an oil bath for 48 hours at a temperature above T_m and packed into NMR rotors. If the lipid sample has a creamy consistency, one must centrifuge the lipid sample several times as the NMR rotors are packed with sample in order to get a homogeneous distribution.

3. General Discussion

The hypothesis that the antipsychotic effect of conventional antipsychotic drugs is induced by blockade of the D_2–like dopamine receptors has been supported by several studies. Many studies have demonstrated direct interaction of antipsychotic drugs with the plasma membrane [295,301–303,317], for example, phenothiazine antipsychotic drugs have been found to interact directly with the plasma membrane to induce shape changes in erythrocytes [301,455,456]. The two most important determinants in amphiphilic drug–membrane interactions are the nature of the functional groups of the drug and the lipid composition in the membrane [292,457], other influencing factors consist of the net charge of the drug, pH value and ionic strength [389,458], temperature [131,132] and hydration [317].

3.1 Interaction of Chlorpromazine (CPZ) with Model Membranes

3.1.1 Role of Lipid Headgroup in CPZ Interdigitation

The amphiphilic CPZ shows selectivity for anionic phospholipids (e.g. PS, PA, and PG), but no or low effects on the zwitterionic monolayers (e.g. PC and PE) [314], demonstrating an important electrostatic component in the interaction. Similar results were also found in previous work of this laboratory by Nerdal et al. [317] and Gjerde et al. [271] when using ^{13}C and ^{31}P MAS solid-state NMR. In addition, the spin-lattice relaxation time (T_1) constants have been measured in the papers (I, II, and IV) of this thesis with the aim to investigate motion of the phospholipid molecules.

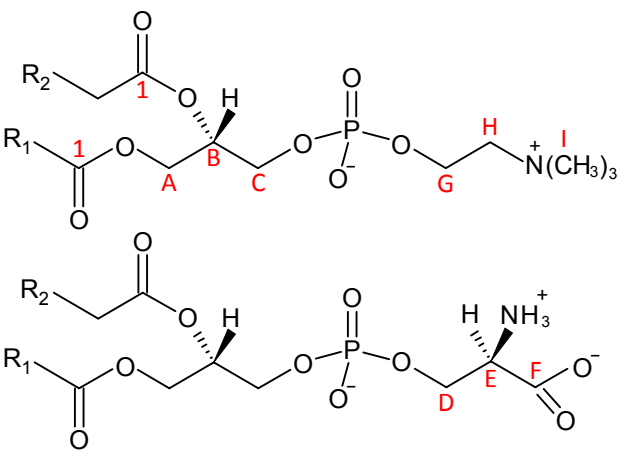

Scheme 3.1 Structural formulae of phosphatidylcholine (PC) and phosphatidylserine (PS), the acyl chains in the *sn*-1 and *sn*-2 position are shortened into R_1 and R_2, respectively.

In paper I, the ^{13}C relaxation measurements show that the choline headgroup carbon resonances (G, H, and I), two of the glycerol carbons (*sn*-2 and *sn*-3 carbons) and the carbonyl resonance (labelled as 1) of the three-component bilayer system DPPC/POPS/SDPS display no changes in T_1 upon CPZ addition (see *Scheme 3.1* for the annotation). The serine headgroup carbon resonances (D, E and F) display a 2–3 times reduction in the T_1 value upon CPZ addition (*Table 3.1*), possibly due to an increased mobility of these carbons (in the slow motional regime, see *Figure 2.16*). In addition, the ^{13}C relaxation measurements demonstrated that the lipid headgroups and the upper part of the acyl chains are immobile compared with the methyl ends, in accordance with a previous electron density maps study [459]. The ^{31}P relaxation measurements show that none of three headgroup components (PC, PS and CPZ–PS complex) varies by any significant amount as function of sample temperature, only the CPZ–PS component is to some degree temperature sensitive below the main phase transition temperature. The PC and the PS components display very similar ^{31}P relaxation constants in both bilayer samples, i.e. with and without CPZ present.

Table 3.1 ^{13}C spin-lattice relaxation times T_1 (s) of DPPC/POPS/SDPS and DPPC/POPS/SDPS/CPZ (red, in parenthesis) at 310 K (37 °C, above T_m).

	Glycerol Backbone			*Serine Headgroup*			*Choline Headgroup*		
Carbons	A (*sn*-1)	B (*sn*-2)	C (*sn*-3)	D	E	F (CO_2^-)	G	H	I
T_1 (s)	0.12 (0.31)	0.28 (0.33)	0.13 (0.15)	0.27 (0.07)	1.44 (0.77)	1.51 (0.61)	0.34 (0.30)	0.28 (0.33)	0.13 (0.15)

With the addition of 10 mol% CPZ, the static ^{31}P NMR spectra of DPPC/POPS/SDPS demonstrated a reduced CSA by 10–20 ppm over a quite large temperature range covering all the mesomorphic states of the bilayer systems. Thus, the presence of CPZ causes an enhancement of the phospholipid headgroup mobility. In the previous study of DPPC/PBPS (Pig Brain PS) bilayer system [271], the choline headgroup imposes conformational restrictions [460] on the CPZ–phosphate complex and also promotes CPZ–carboxyl binding which was not observed for the 'all serine' headgroup samples and therefore seem less favored. The weak binding of PC headgroup with CPZ follows both from the lack of a charged headgroup and from the effect of the large choline volume (319 $Å^3$) [461].

3.1.2 Importance of Polyunsaturated Acyl Chains in CPZ Interdigitation

In paper I, we also investigated the effect of acyl chain unsaturation on CPZ–membrane interaction with fully hydrated bilayer sample of DPPC (60%)/POPS (29%)/SDPS (11%), both below and above the gel-to-liquid-crystalline phase transition temperature (T_m). When CPZ is added to the DPPC/POPS/SDPS bilayer system, it causes some changes to the ^{13}C spectrum, such as changes in peak intensity and linewidth, as well as the changes in chemical shift values of some carbon nuclei.

Comparison of sp^2 acyl chain carbon resonances in 122–136 ppm region for sample without and with CPZ is shown in *Figure 3.1*, makes it clear that a pronounced intensity change of some of these peaks (E, F and G) takes place upon CPZ interaction. There are no intensity changes of DHA's resonances C_{19} and C_{20} upon addition of CPZ (peaks A and H, respectively). Furthermore, peaks E and G display a marked increase in T_1 value when CPZ is present (peak F has approximately similar T_1 values without and with CPZ). Thus, the part of SDPS's DHA acyl chain that are affected by the presence of CPZ is the part close to the polar region of the bilayer, as demonstrated by the intensity and T_1 value increase of these resonances.

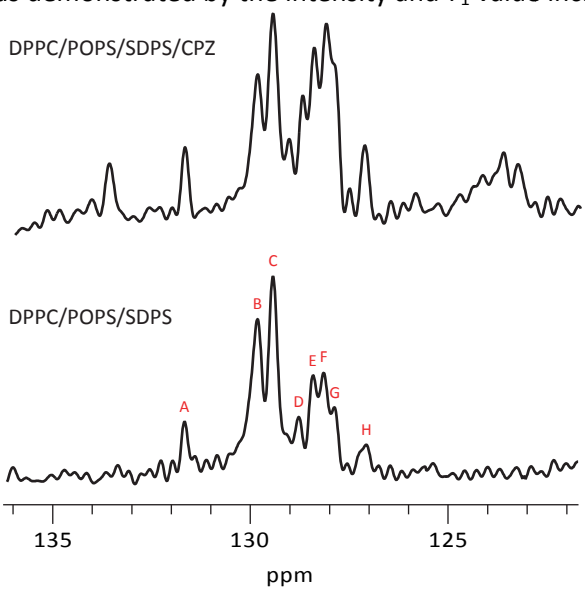

T_1 data of C=C carbons of DHA (s)

	without CPZ	with CPZ
E	0.34	1.16
F	1.04	0.99
G	0.65	2.67

Figure 3.1 (*bottom–left*) Double-bonded acyl chain carbon resonance region (122–136 ppm) of samples DPPC (60%)/POPS (29%)/SDPS (11%) and DPPC (54%)/POPS (26%)/SDPS (10%)/CPZ (10%) (*top–left*), spectra acquired at 310 K (37 °C, above T_m); (*right*) The T_1 constant(s) of some double-bonded carbons (labelled as E, F and G) in DHA (22:6$\Delta^{4,7,10,13,16,19}$) acyl chain. The C=C resonances of DHA (C_4–C_5, C_7–C_8, C_{10}–C_{11}, C_{13}–C_{14}, and C_{16}–C_{17}) are located between 127.4 and 128.4 ppm (labelled as D–H) could not be individually assigned. POPS's resonances C_9 and C_{10} are labelled as peaks C and B, respectively.

The observed increased signal intensity of SDPS's DHA acyl chain C=C carbon resonances and an increase in the corresponding ^{13}C T_1 values for two (out of three that could be measured) of the C=C peaks where the C_4 and C_5 resonances reside and, thus, the reduced mobility of C_4 and C_5 appears to be due to CPZ binding. In *Figure 3.2*, a molecular model of CPZ interaction with an SDPS molecule is presented, generated by the Titan software (Wavefunction, Irvine, CA).

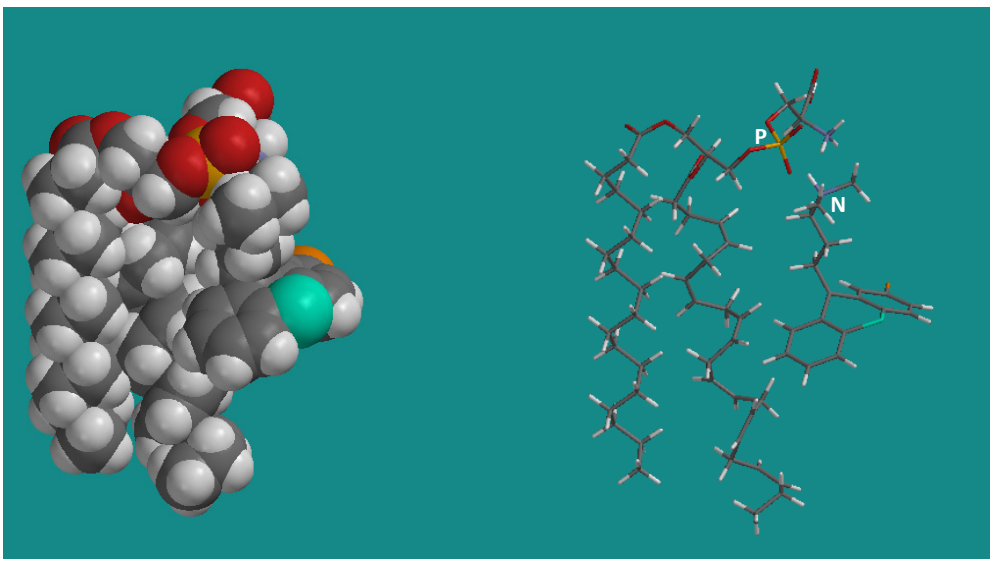

Figure 3.2 Molecular model of CPZ interaction with an SDPS molecule. The CPZ molecule is positioned with its positive charge on the nitrogen atom (labelled as **N**) on the end of CPZ's acyl chain. This positive charge is in the vicinity of the phosphate's (labelled as **P**) negative charge of the SDPS molecule. Both acyl chains of the SDPS molecule have sp^3 carbon dihedral angles of 60° (liquid-crystalline state). The molecular model suggests that an interdigitating CPZ molecule will affect carbons C_4 and C_5 of DHA (*sn*-2 position).

Even though the real conformations of the DHA's acyl chain in the *sn*-2 position may differ somewhat from the conformation displayed here, the model strongly suggests that CPZ interdigitated in such a bilayer will have an effect on both carbons C_4 and C_5 of the DHA. Additionally, T_1 relaxation measurements make it clear that the saturated acyl chains carbons (palmitic, stearic and most of the oleic chain) are not essentially affected by the presence of CPZ.

The found tendency of DHA (22:6), determined by ^2H NMR and X−ray diffraction [462], the *sn*-2 attached acyl chain in a (16:0–22:6)PC bilayer has a distribution of mass that is shifted toward the bilayer aqueous interface would imply bending of the DHA acyl chain. Polyunsaturated bilayers are relatively soft to bending, for polyunsaturated acyl chains, the rotational isomerisation of the doubly allylic ($CH=CH-CH_2-CH=CH$) groups is from skew-to-skew, unlike the *trans−gauche*

isomerizations in saturated chains, and can have many different isomers, through changing the dihedral angles. In *Figure 3.3*, three isomers are chosen to illustrate such acyl chain movement.

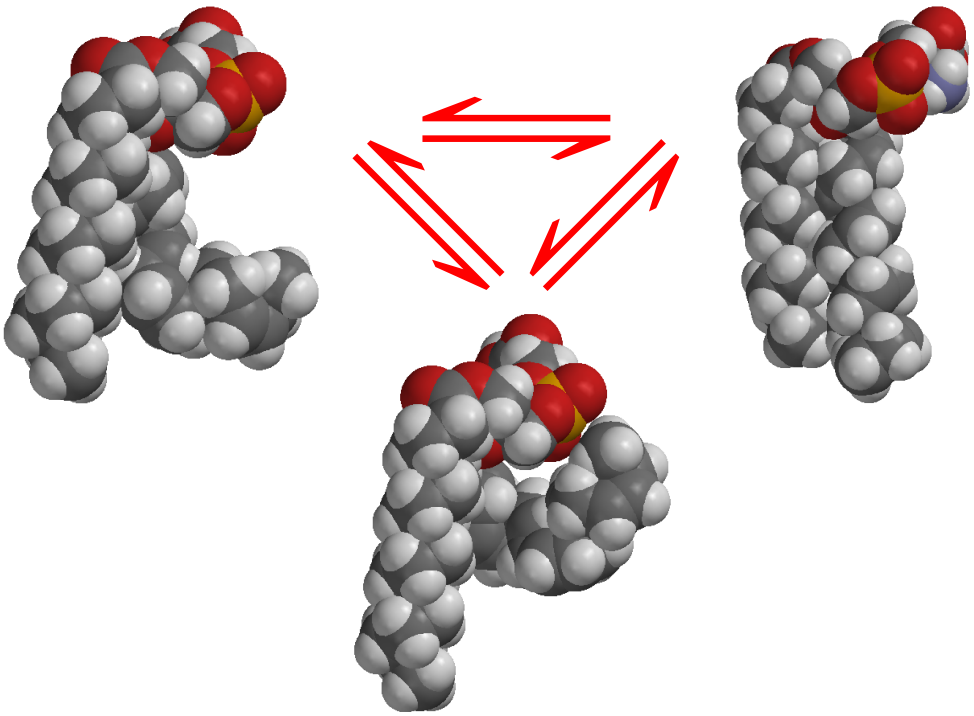

Figure 3.3 Three rotational isomers of DHA acyl chain, the model generated by the Titan software (Wavefunction, Irvine, CA).

In such a process, it is possible that the terminal methyl group can be located somewhere in the vicinity of the polar region of the bilayer. The DHA acyl chain movement will increase the area occupied by an SDPS molecule, and this will promote CPZ bilayer interdigitation (*Figure 3.4*).

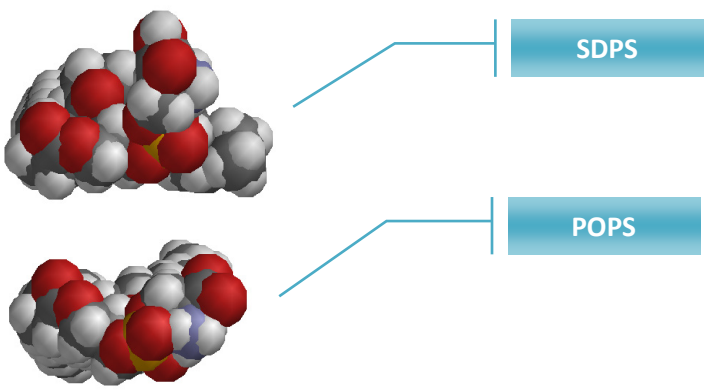

Figure 3.4 Top view of the area occupied by an SDPS molecule, compared with a POPS molecule.

The findings presented here suggest CPZ bound to the phosphate of SDPS phosphatidylserine will slow down and partially inhibit such a DHA acyl chain movement in a bilayer, as shown in *Figure 3.5*. This would affect the area occupied by an SDPS molecule (in the bilayer) and probably the thickness of the bilayer where SDPS molecules reside as well. Thus, it is quite likely that such CPZ caused changes can affect the function of proteins embedded in the bilayer.

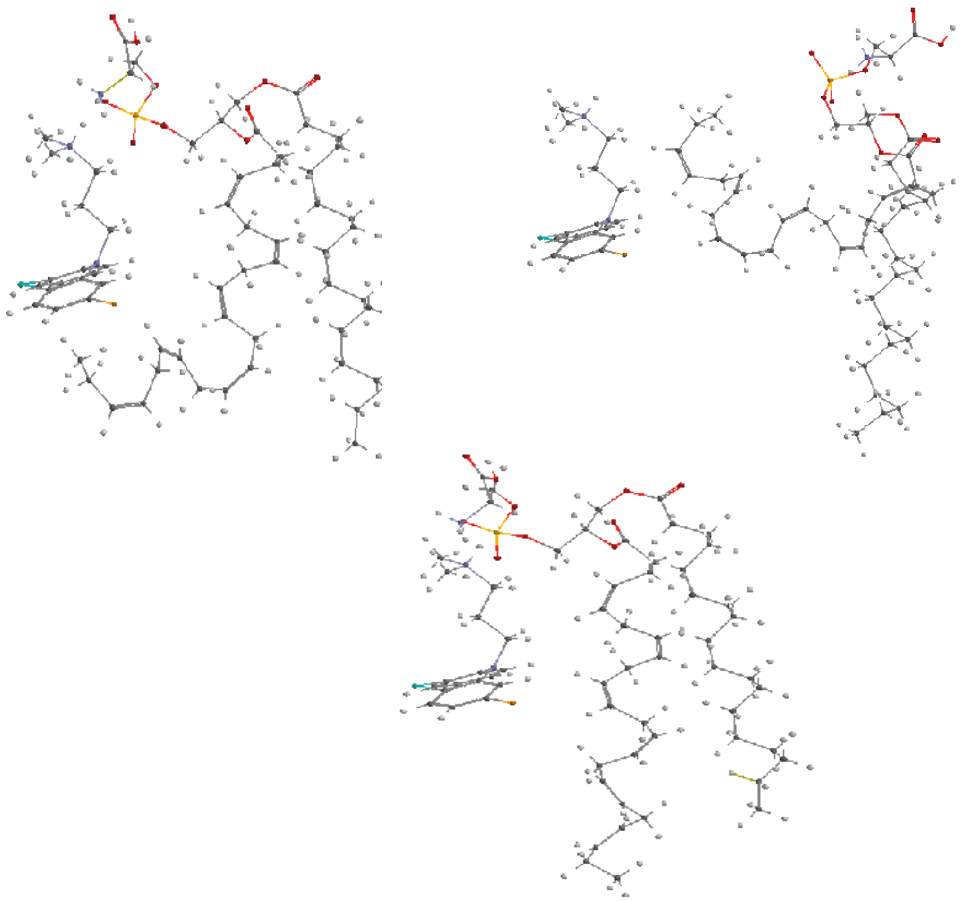

Figure 3.5 High bending/mobility of DHA acyl chain in conflict with simultaneous CPZ binding to phosphate, the model generated by the Titan software (Wavefunction, Irvine, CA).

3.1.3 Existence of Microdomains in Binary System DPPC/SDPS (60:40, Molar Ratio)

A substantial amount of work has been done on the phase behavior of binary lipid mixtures to get a better understanding of lipid interactions in cell membranes. In bilayers composed of two or more phospholipids with different gel-to-liquid-crystalline phase transition temperatures, different acyl chain lengths and different degrees of acyl chain unsaturation, it is conceivable that one can find segregation

of bilayer components in the plane of the bilayer [463]. In such a case, one important driving force would be the hydrophobic mismatch due to differences in thickness of the phospholipid species in the bilayer [139]. Effects of adding an amphiphile like chlorpromazine (CPZ) to such a bilayer could possibly provide valuable information on both the modes of action by the drug (amphiphile) and the robustness of the lipid microdomains in the bilayer. The docosahexenoyl (22:6, DHA) acyl chain is found to enhance membrane lipid raft formation by lipid phase separation [167–169].

The ^{13}C MAS solid-state NMR spectra (9–42 ppm) of DPPC (60%)/SDPC (40%) and its counterpart DPPC (54%)/SDPS (36%)/CPZ (10%) are shown in *Figure 3.6* (from paper II). Resonances that are present in the bottom spectrum of the binary sample and disappear after the addition of CPZ, most probably are due to the special environment at the interface of DPPC and SDPS microdomains, for example, the hydrophobic mismatch of DPPC domains alongside SDPS domains appears to be the origin of peaks labelled with asterisks.

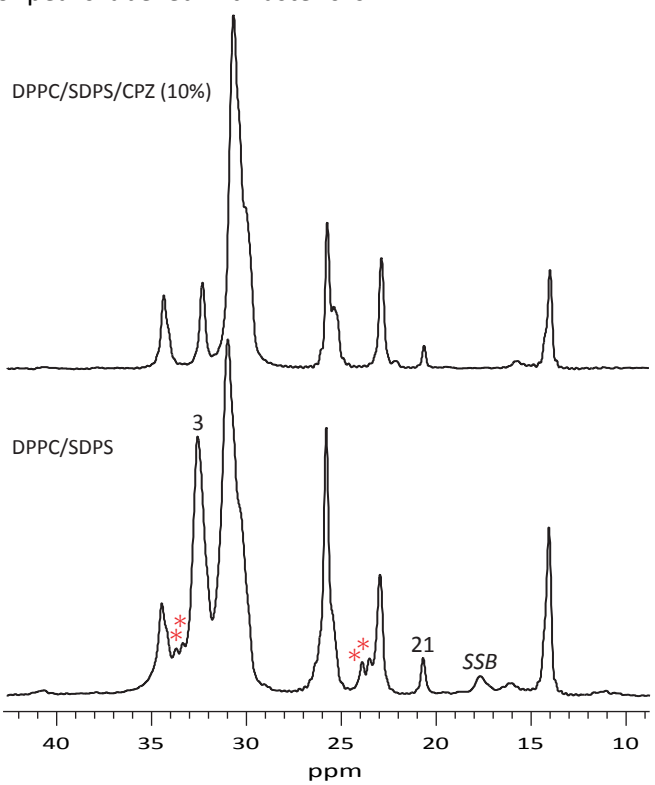

Figure 3.6 ^{13}C MASNMR spectra, acquired at 310 K, displaying spectral region of DHA acyl chain carbons (9–42 ppm), resonances labelled with '*' in the bottom spectrum, denote peaks that change chemical shifts when CPZ is present, which is mainly due to the existence of microdomains. The broad resonance at ~18 ppm is the spinning sideband (*SSB*), arising from carbon 3 of the acyl chain.

Rationalizing the effects of microdomains in the sample, it is reasonable to expect the existence of special local environments at the interface of microdomains where one predominantly consists of DPPC molecules and a neighboring domain contains SDPS molecules. Moreover, assuming the peaks at 33−34 and 23−24 ppm regions would come as a result of a methylene group (of the palmitoyl or C_3 and C_{21} of the DHA) that experience an increased local field due to a neighboring electronegative nucleus, such as oxygen, or the deshielding region of a C=C group with strong magnetic susceptibility (*Figure 3.7*).

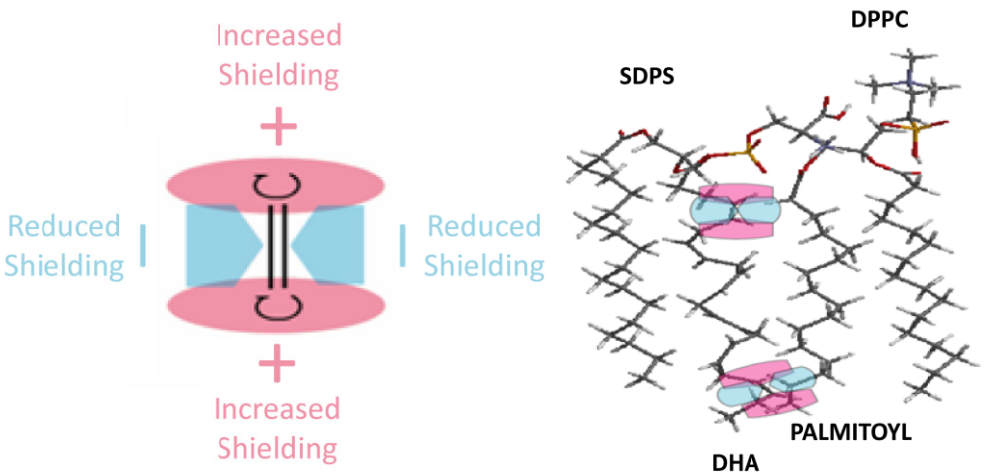

Figure 3.7 (*left*) The shielding and deshielding regions of a C=C group; (*right*) Hydrophobic mismatch of DPPC domains alongside SDPS domains.

The demonstrated disappearance of bilayer microdomain in presence of CPZ together with the found CPZ effects on DHA mobility, point at the crucial role of DHA in formation and perseverance of phospholipid microdomains in this bilayer [464].

3.2 Interaction of Local Anaesthetic (Articaine) with Model Membranes

It has been proposed that the uncharged form of local anaesthetic is the main species transported across the cell membrane, the protonated form binds to a specific site on the channel, triggering the anesthetic effect [465−467]. Thus, the higher partitioning abilities of uncharged anesthetics into the membrane play an important role in the molecular mechanism of local anesthesia [359]. In paper III, we study the uncharged articaine species (at four different molar ratios of 10 mol%, 25 mol%, 40 mol%, and 55 mol%, respectively) interacting with DSPC model membranes.

We monitored the phase transition of the DSPC model membrane at different percentages of articaine. Depression of gel-to-liquid-crystalline phase-transition temperature by local anesthetics has been found to correlate with the anesthetic hydrophobicity (potency) [399]. *Figure 3.8* shows the ^{31}P chemical shift anisotropy (CSA) as a function of sample temperature at pH 10.0. The CSA of pure DSPC displays a sudden drop at the DSPC's gel-to-liquid-crystalline phase-transition temperature of 329.1−329.2 K. CSA values of DSPC bilayers with 10 mol%, 25 mol%, 40 mol%, and 55 mol% articaine display a bilayer phase transition temperature of 325.3−325.4 K, 321.1−321.2 K, 321.3−321.4 K, and 318.6−318.7 K, respectively. Thus, the observed concentration-dependent decrease in bilayer (gel-to-liquid crystalline) phase-transition temperature demonstrates substantial uncharged articaine interaction with this bilayer. And the presence of uncharged articaine demonstrated a CSA decrease up to ~30 ppm over the large temperature range indicating enhancement of PC headgroup mobility. The most pronounced reduction of the phospholipid phosphorous CSA in presence of articaine is detected at an articaine ratio of 40 mol% (e.g. at 323 K).

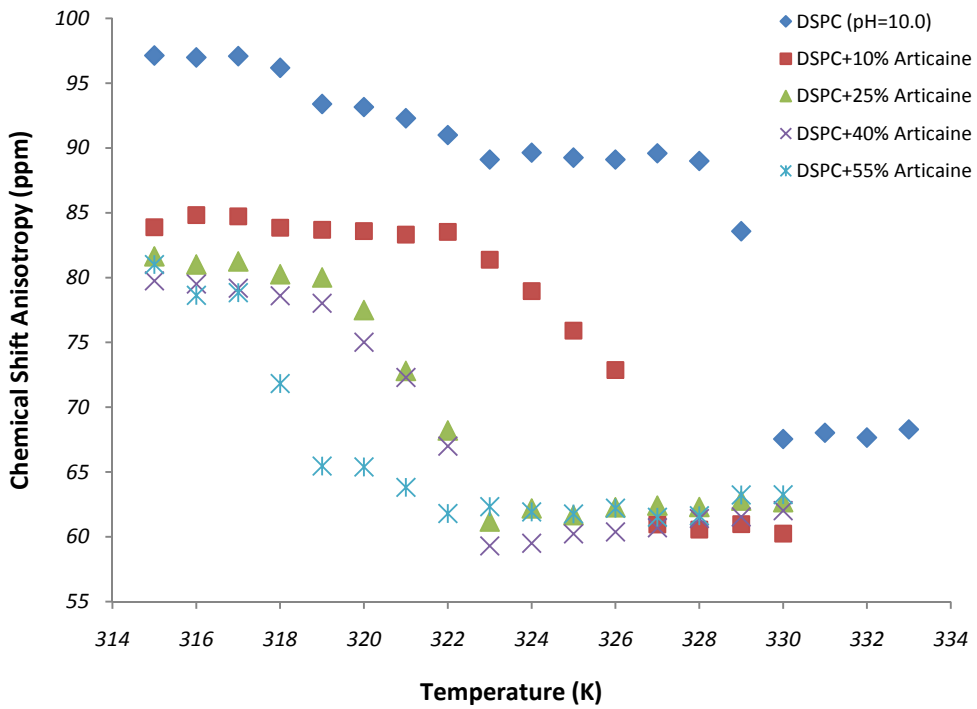

Figure 3.8 ^{31}P chemical shift anisotropy (CSA, in ppm) from 314 K−330 K/333 K (covering all the mesomorphic states of the bilayer systems) of pure DSPC and four articaine−containing samples (pH=10.0).

The influence of the phospholipid packing of the phosphate/headgroup region of the DSPC bilayer (pH=10.0) in presence of uncharged articaine was revealed by ^{13}C MASNMR spectra (the spectral region of 159−181 ppm, shown in *Figure 3.9−left*). At 40 mol% articaine (spectrum c), the influence on phospholipid packing in the phosphate/headgroup region of the DSPC bilayer appears to be severely affected in that the articaine carboxyl resonance (labeled as '†') appears at ~179.0 ppm and two other carboxyl peaks are found at ~174.7 and ~175.3 ppm. The articaine carboxyl resonance at 40 mol% articaine in the DSPC bilayer demonstrates that the articaine carboxyl group is likely to be the major articaine moiety with DSPC interaction in the polar region of this bilayer. The articaine carboxyl resonance is greatly reduced in spectrum of 55 mol% articaine (spectrum d).

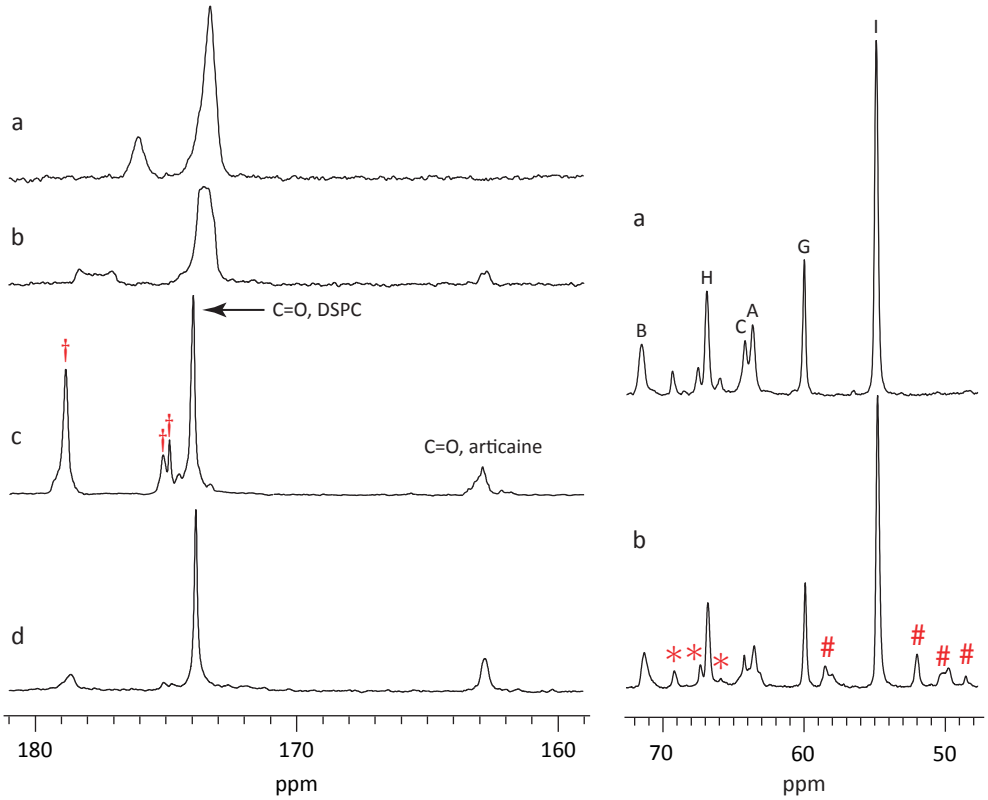

Figure 3.9 (*left*) Carbonyl carbon resonance region (159−181 ppm) of sample DSPC (a), and the spectra of DSPC with 10 mol%, 40 mol%, and 55 mol% uncharged articaine (b−d), from top to bottom. In spectrum c, the resonance labelled '†' denotes the articaine carboxyl resonance, and the articaine carbonyl resonance locating at ~162.6 ppm; (*right*) Resonance region of glycerol moiety and the choline headgroup (48−74 ppm) of a: pure DSPC sample (pH=10.0) where resonances are labelled A−C, H, G and I (see *Scheme 3.1* for the annotation), and b shows spectrum of DSPC with 55 mol% articaine. Resonances labelled with an asterisk '*' denote DSPC resonances present only at a pH of 10.0, and the resonances labelled '#' denote articaine resonances.

The carbonyl resonance of DSPC is found at ~174 ppm and an additional and smaller resonance at ~176 ppm (*Figure 3.9–left-a*). The latter corresponds with the molecular packing of a minor part of the DSPC molecules that takes place at a pH of 10.0 are visible in the glycerol/headgroup region, this disappears with addition of 10 mol% articaine (*Figure 3.9–left-b*), suggesting that the pH related disturbance of the DSPC bilayer is located mainly to the polar region. A further demonstration of articaine influence on DSPC bilayer's polar region (at pH=10.0) is found in the spectral region of glycerol and choline headgroup carbon resonances (47–73 ppm, *Figure 3.9–right*), where several smaller resonances in this spectral region are due to some perturbation of phospholipid packing at a pH of 10.0. Further evidence for articaine influence on phospholipid packing in DSPC bilayer (at pH=10.0) hydrophobic region is found when comparing ^{13}C MASNMR spectra shown in *Figure 3.10*.

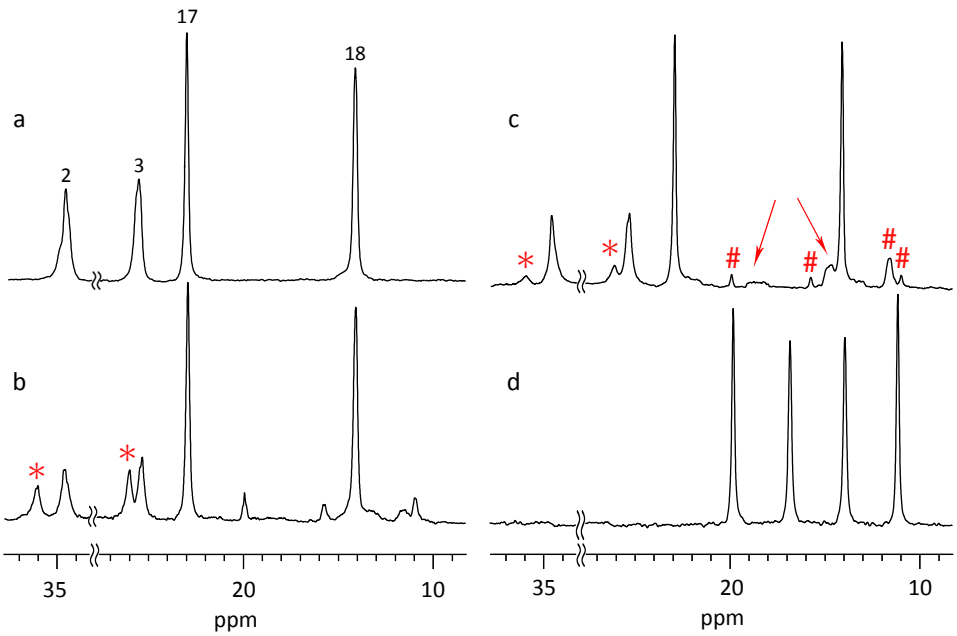

Figure 3.10 Acyl chain carbon resonance in regions of 9–27 ppm, and 34–37 ppm (main acyl chain peak not shown), of a: pure DSPC, b: DSPC with 40 mol% articaine, c: with 55 mol%, d: pure articaine (with 15 wt.% D_2O). Resonances labelled with '*' denote new DSPC resonances when articaine is present, and resonances labelled with '#' denote articaine resonances. Arrows point at broad articaine resonances that appear at high articaine ratios (55 mol%), these resonances could be due to presence of articaine aggregates.

Major spectral changes are evident for acyl chain carbon resonances 2 and 3, in *Figure 3.10–b and c*, where the two resonances that can be assigned to carbon 2 of the stearoyl acyl chain, and similarly the two resonances assigned to carbon 3, suggest conversion between two mesomorphic lipid states at a rate slower than

the NMR timescale. As demonstrated in *Figure 3.10–c*, the large molecular packing effect on the phospholipids by 40 mol% articaine (*Figure 3.10–b*) is reduced in the 55 mol% articaine sample. The arrows in *Figure 3.10–c* point at broad resonances that are not present in spectrum 40 mol% articaine–containing sample. Accompanying these spectral changes is a marked reduction in articaine resonances (marked with '#' in *Figure 3.10–c*) even though the total articaine mol% increases from 40 to 55. The broad resonances only present in spectrum of the 55 mol% DSPC sample could very well come from self-aggregated articaine molecules, such an interpretation is supported by the observed reduction in signal intensity of articaine resonances as articaine mol% is increased from 40 to 55.

The observed ^{13}C NMR spectral changes when articaine is increased from 40 mol% to 55 mol%, suggest formation of articaine aggregates and decrease in DSPC bilayer perturbation at the latter articaine level, which is also supported by ^{31}P MASNMR spectra (*Figure 3.11*).

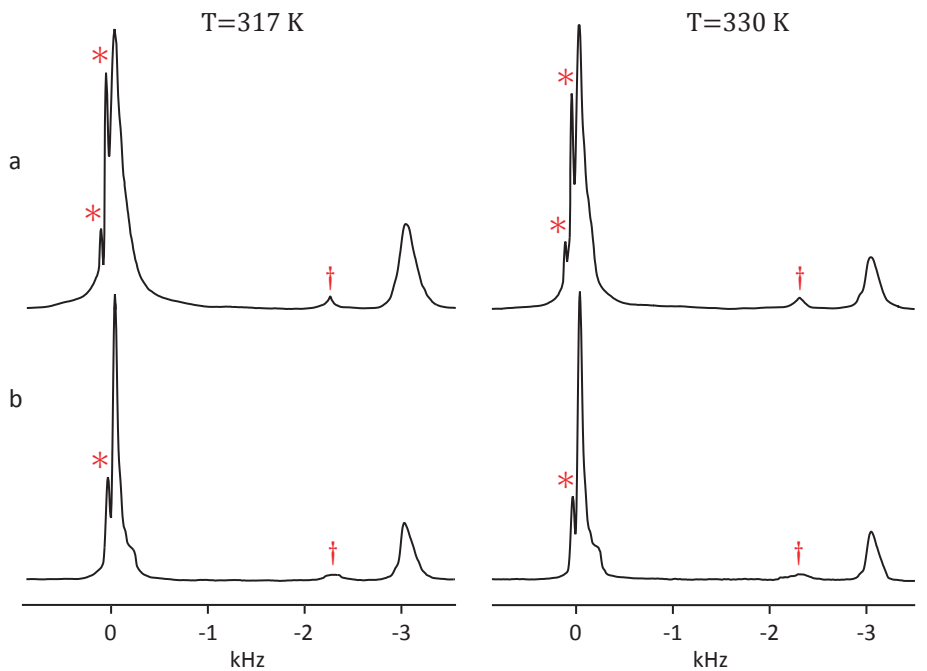

Figure 3.11 ^{31}P MASNMR spectra of DSPC with 40 mol % (a) and 55 mol % (b), at temperatures below (317 K, left column) and above (330 K, right column) the phase transition temperature (T_m) of DSPC with/without uncharged articaine. All spectra were obtained with 3 kHz MAS spinning rate. The symbol '*' in spectra shown marks isotropic phase resonances. In general, the central band peaks caused by the presence of articaine demonstrate chemical environments for the phospholipid phosphate-group that are due to interaction with local anesthetics. The change in spectra when articaine content is increased from 40 mol% to 55 mol% shows a reduction from three central band peaks to two. This could indicate articaine self-association/phase separation in DSPC bilayer at high (55 mol%) articaine levels. The symbol '†' in spectra marks unidentified resonances.

A DSPC bilayer contains a large hydrophobic core and the NMR spectra of the 40 mol% articaine−containing sample demonstrate a maximum disturbance in the molecular packing of the polar bilayer region that extends into the hydrophobic region, evidenced by carbon 2 and 3 of the acyl chains (*Figure 3.10−b*). In addition, articaine carboxyl group interaction with the DSPC bilayer appears to be substantial at a sample pH of 10.0, with uncharged articaine, and non-existent/minor at a sample pH of 7.4. As mentioned above, this positioning affects atoms at the choline (G, H and I), glycerol backbone (A, B and C), carbonyl and the first portion of the acyl chain (carbons 2 and 3). In a previous EPR and NMR study on lidocaine−egg phosphatidylcholine (EPC), the amino-ester local anaesthetic lidocaine was found to insert into a similar location in acyl chain region of the lipid membrane compared with the positioning of articaine when interdigitating into the DSPC bilayer [371].

Moreover, interaction with the membrane is not solely governed by the hydrophobicity of the local anesthetic, polar interactions or steric parameters in the local anesthetic−phospholipid interaction will determine the preferential positioning of the anesthetic in the bilayer [372]. The van der Waals volume of articaine is 289.7 $Å^3$, which is somewhat larger than lidocaine (228.5 $Å^3$) [371] and tetracaine (251.4 $Å^3$) [359], which suggests the spacing created by articaine would be greater than that of lidocaine and tetracaine. The steric hindrance of articaine can be related to its lesser biological activity due to the difficulty in fitting in a specific site in the sodium channel [468], which subsequently plays a crucial role in the mechanism of anesthesia [381].

3.3 Interaction of Atypical Antipsychotic Drug (Olanzapine) with Model Membranes

3.3.1 Role of Hydration on the Bilayer Structure

We ever addressed the NMR studies on the interaction of CPZ with the model membranes at two different hydrations, with ~36 wt.% H_2O [271] and even a lower water content with ~15 wt.% H_2O (~12 H_2O per phospholipid) [317], the water content was found to heavily influence the interdigitation of CPZ molecules into the acyl chain regions, which suggested that the structural and dynamic properties of the membrane change drastically with hydration. A straightforward interpretation of the role of hydration on the structure of bilayers remains unclear, and we thus studied DPPC/POPS bilayers with two different hydration schedules, i) full hydration, i.e. in excess water (~42 H_2O per phospholipid, i.e. ~50 wt.% H_2O),

and ii) partial hydration (~30 H_2O per phospholipid, i.e. ~36 wt.% H_2O), by means of high-field ^{13}C and ^{31}P MASNMR spectroscopy. The membrane measured at full hydration will correlate the results to the biologically relevant state more tightly, which is a better model for the study of OLZ−model membrane system interaction.

The comparison of the carbonyl resonance and the serine headgroup carboxyl resonance of the two bilayer samples at two different hydration levels can be carried out in spectra shown in *Figure 3.12*. Surprisingly, the *sn*-1 and *sn*-2 carbonyl resonances were resolved individually into two peaks (spectrum b), these can be assigned [469]. In spectrum a (the partially hydrated sample), an additional peak is resolved at 174.05 ppm (labelled with the dagger '†'), which could be assigned as the *sn*-2 carbonyl resonance, for example, linked with the monounsaturated oleic acyl chain from POPS species. The mean lifetime of this *sn*-2 carbonyl resonance should be longer than 31 ms, corresponding to the observed 0.26 ppm separation (with the resonance 1^b). For the fully hydrated sample (spectrum b), where is a more mobile environment for the acyl chains, the interconversion between *sn*-2 carbonyls (in the palmitic acyl chains of DPPC and the oleic acyl chains of POPS) takes place at rates that are faster on the NMR time scale, *sn*-2 carbonyls resonances were motionally averaged and not always resolved. The *sn*-1 group appears to be further away from the lipid−water interface and more deeply buried in the hydrocarbon layer, this makes it less affected by increasing the hydration of the system.

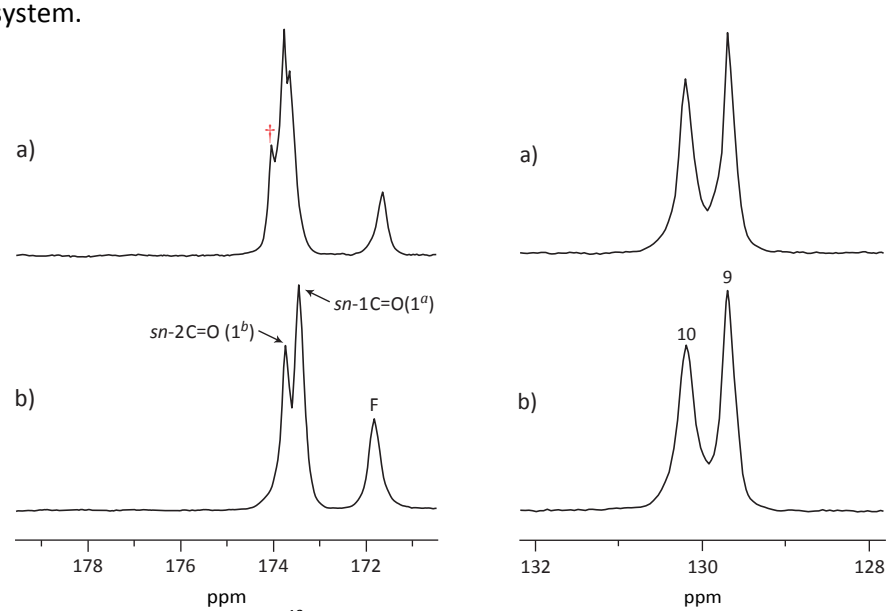

(*left*) *Figure 3.12* Proton-decoupled ^{13}C MASNMR spectra acquired at 316 K (43°C, above T_m): carbonyl and carboxyl carbon resonance region (171−179 ppm) of samples DPPC (60%)/POPS (40%) with ~36 wt.% H_2O (a) and ~50 wt.% H_2O (b); (*right*) *Figure 3.13* C=C resonance region (128−132 ppm).

Figure 3.13 shows the spectral region of 128−132 ppm, where C=C resonances of the oleic acyl chain (18:1, C=C double bond at carbons 9 and 10) of samples DPPC/POPS are found. Comparison of the C=C resonances from the DPPC/POPS samples with different hydrations (spectra a and b), display almost no concomitant variations in intensities or chemical shift changes.

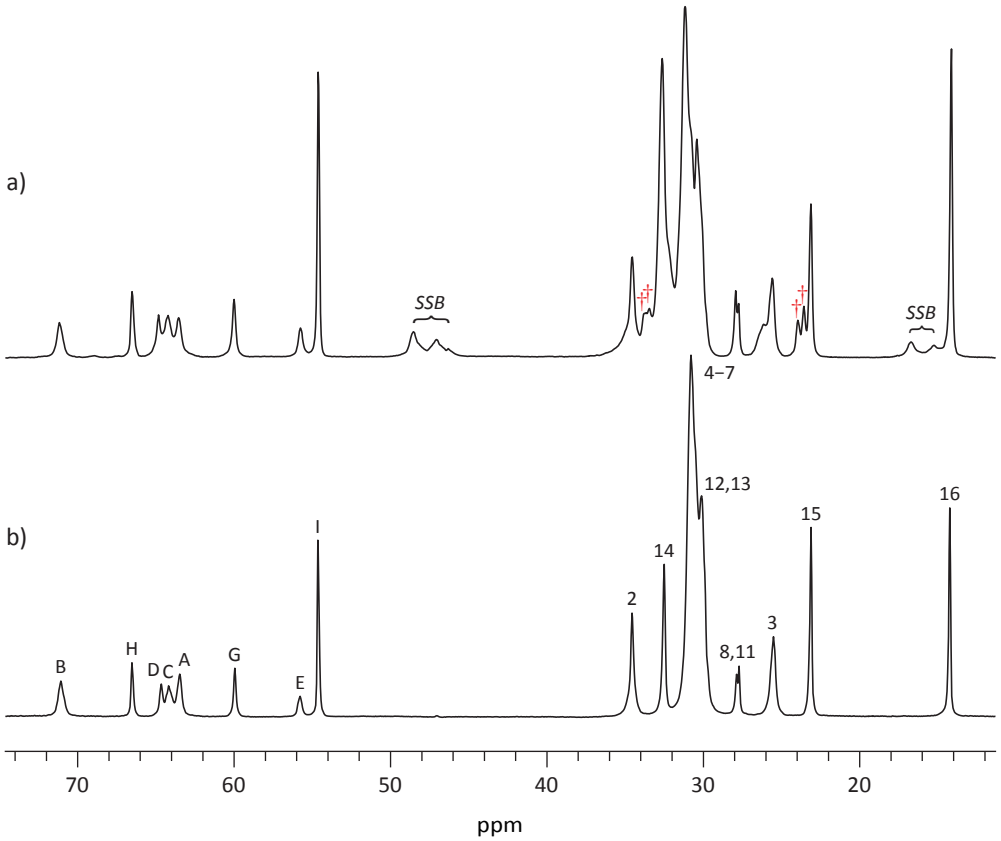

Figure 3.14 Proton-decoupled ^{13}C MASNMR spectra acquired at 316 K (43°C, above T_m), displaying spectral region of phospholipid headgroups, glycerol and saturated acyl chain carbons (12−74 ppm) of samples DPPC (60%)/POPS (40%) with ~36 wt.% H_2O (a) and with ~50 wt.% H_2O (b). Glycerol and phospholipid headgroup resonances are labelled A−I in spectrum b (see *Scheme 3.1* for the annotation). The spectral region of 12−38 ppm is labelled with the palmitic (16:0) acyl chain resonances of DPPC.

By comparison of the DPPC and POPS acyl chain sp^3 carbon resonances (in 12−38 ppm) as well as the resonances of phospholipid headgroups (choline and serine), and the glycerol moiety resonances (in the 52−74 ppm spectral region) displayed in *Figure 3.14*. It is clear that the spinning sidebands (labelled as '*SSB*') in the acyl chain region vanished, which is mainly due to the higher mobility of the phospholipids in fully hydrated bilayer, and also evident from the narrower

lineshapes of some resonances of the fully hydrated bilayer, such as the internal methylene $(CH_2)_n$. For the partially hydrated sample (spectrum a), some resonances in the acyl chain region (labelled with the dagger '†') emerged, these are probably due to the special environment of DPPC domains alongside POPS domains, similar to the existence of microdomain composed of DPPC and brain phosphatidylserine binary, detected by Jutlia et al. [470]. With increasing hydration of the bilayer system (from ~36 wt.% H_2O to ~50 wt.% H_2O), these microdomains disappear and come as singlets (spectrum b). Phospholipids in bilayers with lower hydration (spectrum a) will have to share the few available water molecules among the polar groups distributed in the polar region of the bilayer. This promotes dense packing of the phospholipids and consequently makes some acyl chain carbons in DPPC come close to acyl chain carbons in POPS. In such a case, the peaks at 23.58 and 24.01 ppm appears as a result of a methylene group (carbon 3) that experience an increased local field due to a neighboring electronegative nucleus, such as oxygen. The peaks at 33.62 and 33.78 ppm, on the other hand, where the methylene group (carbon 2) spends most of its time in the shielding region of methylene groups, this resonance is shifted to a lower ppm value by the environment of the microdomain interface. Rationalizing the effects of hydration levels on the bilayer system of DPPC/POPS is shown in *Figures 3.12–3.14*, it is apparent that the main changes occur in the acyl chain region, and this finding is consistent with the work of Meidan et al. [471]. Furthermore, in the study of a DPPC (60%)/SDPS (40%) bilayer using ~36 wt.% H_2O (paper II), certain spinning sideband resonances were mis-assigned to be due to phospholipid domain formation, we clarify this by comparing a DPPC/POPS bilayer system at two different hydrations.

A comparison of ^{31}P T_1 values of these two DPPC/POPS samples with different hydrations shows that higher mobilities is observed for both phosphatidylserine and phosphatidylcholine at higher hydration. The static ^{31}P spectra of these two samples are in agreement with the observed T_1 measurements, i.e. a higher mobility of the phosphates with increasing hydration (a prominent CSA reduction, from 87 to 64 ppm). In addition, it is the PS phosphorous chemical shift that shows sensitivity on increasing hydration from ~36 wt.% to ~50 wt.% H_2O (*Figure 3.19*).

3.3.2 Olanzapine Interacting with Binary Mixture of DPPC/DPPS (60:40, molar ratio)

The ^{13}C MASNMR spectra of partially hydrated (~36 wt.% H_2O) bilayer samples DPPC (60%)/DPPS (40%) and DPPC (54%)/DPPS (36%)/OLZ (10%) were recorded at a temperature of 316 K (43°C) and are presented as spectral regions (12–74 ppm,

and 170−180 ppm) in *Figure 3.15*, where the left spectrum is the binary mixture of DPPC/DPPS and the right spectrum shows the corresponding sample with 10 mol% OLZ. In the left spectrum, the acyl chain sp^3 carbon resonances (in the 12−38 ppm region) as well as the phospholipid choline (labelled G, H and I), serine (numbering D and E) headgroup carbons and the glycerol moiety (labelled A, B and C) resonances in the 52−74 ppm spectral region are displayed [472,473], together with the carbonyl resonance (labelled 1, 173.82 ppm) and the serine headgroup carboxyl (labelled F, 171.69 ppm) [474]. With addition of OLZ (the right spectrum), two new resonances are observed (at 178.57 and 174.48 ppm, marked with the double dagger '‡'), these can be identified as the serine headgroup carboxyl resonances, in light of the molar composition of the DPPC/DPPS sample giving a theoretical peak ratio of 5 between the carbonyl and carboxyl resonances. This strongly indicates influence of OLZ on the serine carboxyl groups, moreover, an effect of OLZ on the chemical shift of DPPS carboxyl carbon F is also present (downfield by 0.38 ppm). In the spectral region of 52−74 ppm, the dramatic signal reductions were found for the serine carbons D and E with the addition of 10 mol% OLZ, and the choline headgroup resonances G, H and I were experiencing a moderate perturbation by the presence of OLZ. The above findings reveal that the serine headgroup is directly affected by incorporation of OLZ, and probably the interdigitation of OLZ is driven by electrostatic attraction of the serine headgroup.

For the DPPC and DPPS acyl chain sp^3 carbon resonances (in 12−38 ppm), several small resonances at unusual chemical shift values observed at the left spectrum (such as at 26.11 and 23.78 ppm, labelled with the dagger '†'), these are primarily associated with an order-disorder exchange of the palmitic acyl chains of the bilayer system DPPC/DPPS at the experimental temperature of 316 K (43°C). DPPS ($T_m \approx 57$°C) is in the gel state, and the palmitic acyl chains are in an all-*trans* conformation, whereas DPPC ($T_m \approx 41.3$°C) is in the liquid-crystalline phase with a significant population of *gauche* isomers in the palmitic acyl chains. These small resonances in the acyl chain region are perturbed by the presence of 10 mol% OLZ in the DPPC (54%)/DPPS (36%)/OLZ (10%) sample, see right spectrum, where the above-mentioned resonances at 26.11 and 23.78 ppm are 'neighboring' two new resonances (labelled with the asterisk '*'). Furthermore, when OLZ is incorporated into the bilayer, more narrow resonances are found, such as the carbonyl resonance 1 and the internal methylene resonance (carbons 4−13), these may reflect fewer intermolecular restrictions or interactions between the hydrocarbon chains of DPPC/DPPS phospholipids, and also demonstrates the presence of 10 mol% OLZ decreasing the phase transition temperature of the bilayer to some

extent [475,476]. In addition, the abolishment of the spinning sidebands (labelled as '*SSB*') locating at 46.82 and 48.39 ppm (the origins are carbons 4−13 and carbon 14 of the acyl chains, respectively) provides coherent evidence for increased mobility of the rigid carbons by the addition of OLZ, especially carbon 14. Comparison of the right spectrum of *Figure 3.15* and ^{13}C MASNMR spectrum of the pure OLZ powder with 15 wt.% D_2O (see Appendix, *Page 120*), shows that the resonances within the spectral region of 42−52 ppm and the resonance at 16.79 ppm can be assigned as the OLZ resonances [477].

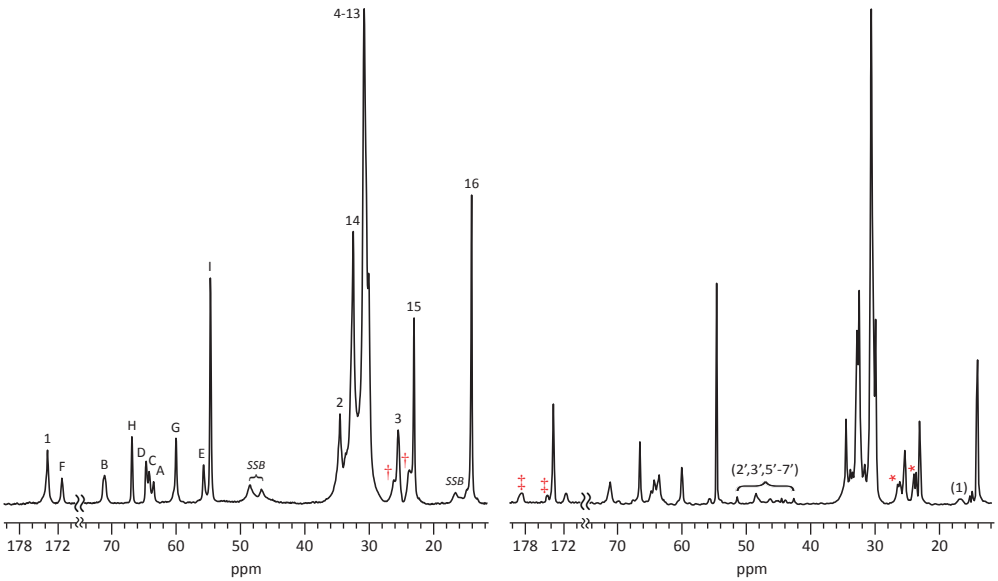

Figure 3.15 Proton-decoupled ^{13}C MASNMR spectra of partially hydrated bilayers at 316 K (43°C) with left spectrum: DPPC (60%)/DPPS (40%), and the right spectrum: DPPC (54%)/DPPS (36%)/OLZ (10%), displaying spectral regions from 12−74 ppm, and 170−180 ppm.

3.3.3 Influence of Acyl Chain Unsaturation on OLZ Interaction with PC/PS Bilayer

A further investigation of OLZ perturbation on the PC/PS binary system, and its dependence on the acyl chain unsaturation (which determines physical features of bilayers [478]), we employed POPS phospholipids instead of DPPS, where one of the saturated (palmitoyl) acyl chains is substituted by a monounsaturated (oleoyl) acyl chain. Spectra of the fully hydrated bilayer sample DPPC (60%)/POPS (40%) (with ~50 wt.% H_2O), and the bilayer with an OLZ content of 10 mol% were recorded above the bilayer's T_m at 316 K (43°C, from the previous endothermic measurements of DPPC multilamellar vesicles, the T_m of pure DPPC is about 41.3°C, and the addition of brain PS species will decrease and broaden the phase transition temperature of the binary system [470]), and presented as spectral

regions in *Figures 3.16–3.18*, where spectrum a shows the fully hydrated sample, and spectrum b is of the corresponding fully hydrated sample with 10 mol% OLZ.

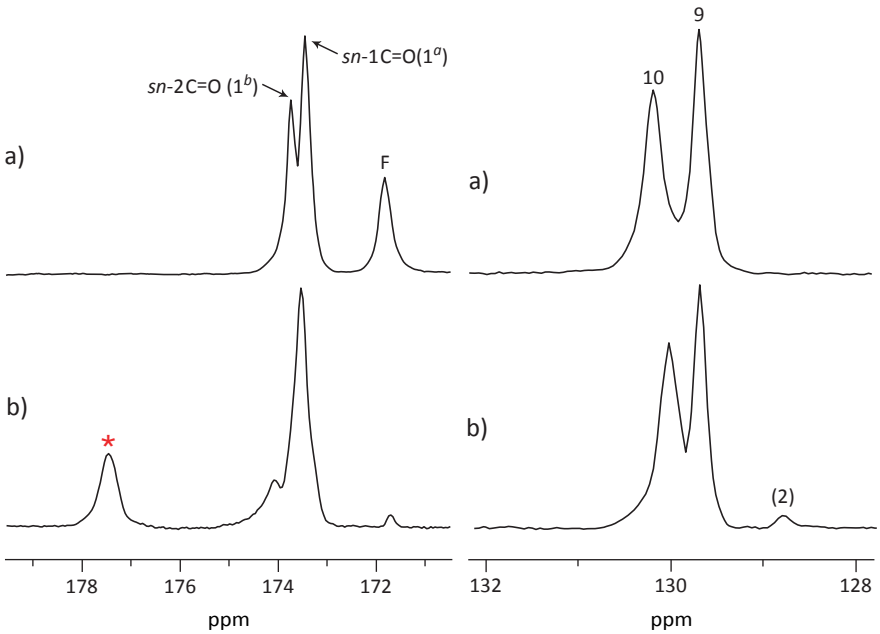

(*left*) *Figure 3.16* Proton-decoupled ^{13}C MASNMR spectra acquired at 316 K (43°C, above T_m): carbonyl and carboxyl carbon resonance region (171–179 ppm) of fully hydrated sample DPPC (60%)/POPS (40%) with ~50 wt.% H_2O (a) and DPPC (54%)/POPS (36%) /OLZ (10%) with 10 mol% OLZ (b); (*right*) *Figure 3.17* C=C resonance region (128–132 ppm) of the two samples with/without OLZ.

For the fully hydrated sample with 10 mol% OLZ (*Figure 3.16–b*), the carbonyl signals are broadened and asymmetric compared with its counterpart in *Figure 3.16–a*. It is apparent that the carbonyl resonances are affected by the addition of OLZ, especially the *sn*-2 carbonyls. The corresponding ^{13}C T_1 changes for both carbonyl resonances by adding OLZ into the system suggest a reduced molecular mobility. Furthermore, the chemical shifts of both *sn*-1 and *sn*-2 carbonyls were affected by the incorporation of OLZ, the chemical shift difference ($\Delta\delta$) of *sn*-1 and *sn*-2 carbonyls is increased (~0.28 ppm) upon incorporation of 10 mol% OLZ. Moreover, the changes in the *sn*-2 carbonyl chemical shift and T_1 value strongly suggest local conformational changes and a unique chemical environment brought by OLZ [476]. A comparison of the serine carboxyl headgroup F in the spectra a and b, makes it evident that a main portion of the carboxyl resonance is downfield shifted about 5.80 ppm (to 177.51 ppm, labelled with an asterisk '*') by the addition of 10 mol% OLZ. A similar observation is found for DPPC/DPPS and its counterpart DPPC/DPPS/OLZ (10%) (*Figure 3.15*). The T_1 value of the carboxyl group 'residue' (at 171.71 ppm, spectrum c) increased by 51% with the addition of

OLZ (from 1.66 s to 2.51 s), the T_1 value of the new carboxyl resonance (labelled with the asterisk '*') at 177.51 ppm is 3.24 s.

The influence of OLZ on the C=C resonances of the oleic acyl chain (18:1, C=C double bond at carbons 9 and 10) of samples DPPC/POPS is found in the spectral region of 128−132 ppm (*Figure 3.17*). In spectrum b, the chemical shift difference ($\Delta\delta$) of carbons 9 and 10 is reduced by 0.16 ppm (∼30%) upon incorporation of 10 mol% OLZ, and T_1 values for these two C=C resonances increase in the same way with presence of OLZ (carbon 9, ∼14%, from 0.71 s to 0.81 s; carbon 10, ∼33%, from 0.60 s to 0.80 s).

In *Figure 3.15*, the spectral regions (in 52−74 ppm) display a dramatic effect of OLZ on the serine carbons D and E, and a smaller effect on the choline headgroup resonances (G, H and I). Similar observations for serine and choline headgroups are found in the DPPC/POPS bilayer sample with the addition of OLZ, this confirms the crucially important role of the serine headgroup in the interdigitation of OLZ (*Figure 3.18*). Similar findings are illustrated by the T_1 data, where the choline headgroup is not severely affected (∼25% increment in T_1) by the addition of OLZ, whereas the serine headgroup T_1 values show increases of ∼214% (for carbon D) and ∼133% (for carbon E) in the presence of OLZ. The peak intensities of the glycerol carbons A (*sn*-1) and B (*sn*-2) are heavily reduced, the glycerol carbon C (*sn*-3) resonance shows only slight reduction in intensity. The glycerol carbon T_1 values, on the other hand, demonstrate a diverse effect of OLZ. The T_1 value of the *sn*-1 glycerol carbon is unaffected, while the *sn*-2 glycerol carbon (where the POPS monounsaturated acyl chain is attached) displays an increased T_1 value (∼74%, reflecting increased motion) due to OLZ in contrast to the *sn*-3 glycerol carbon's (where the phosphate and headgroup attached), that is reduced by ∼60% (reflecting reduced motion). The existence of resonances marked with an asterisk '*' in the glycerol/headgroups region (in 52−74 ppm, *Figure 3.18−b*) is the evidence of a changed packing pattern of the phospholipids in the polar region, i.e. the molecular packing of a minor part of the DPPC/POPS molecules that takes place in the presence of OLZ is visible in the glycerol/headgroups region of the spectrum. Furthermore, the large disturbance in the molecular packing of the polar bilayer region of the OLZ−containing sample extends into the hydrophobic region, evidenced by the carbon 2 and 3 of the acyl chain, where two additional resonances are found at 35.41 ppm and 25.88 ppm, labelled with the asterisk '*' (*Figure 3.18−b*). The OLZ influence in the hydrophobic region, by interdigitation of OLZ molecules, is further revealed as changes of the internal acyl chain methylene resonance 4−7, these are partially resolved into two peaks. The T_1 relaxation

measurements make it clear that most of the acyl chain carbons (especially carbons 2, 3 and 4−7) change in mobilities upon OLZ addition.

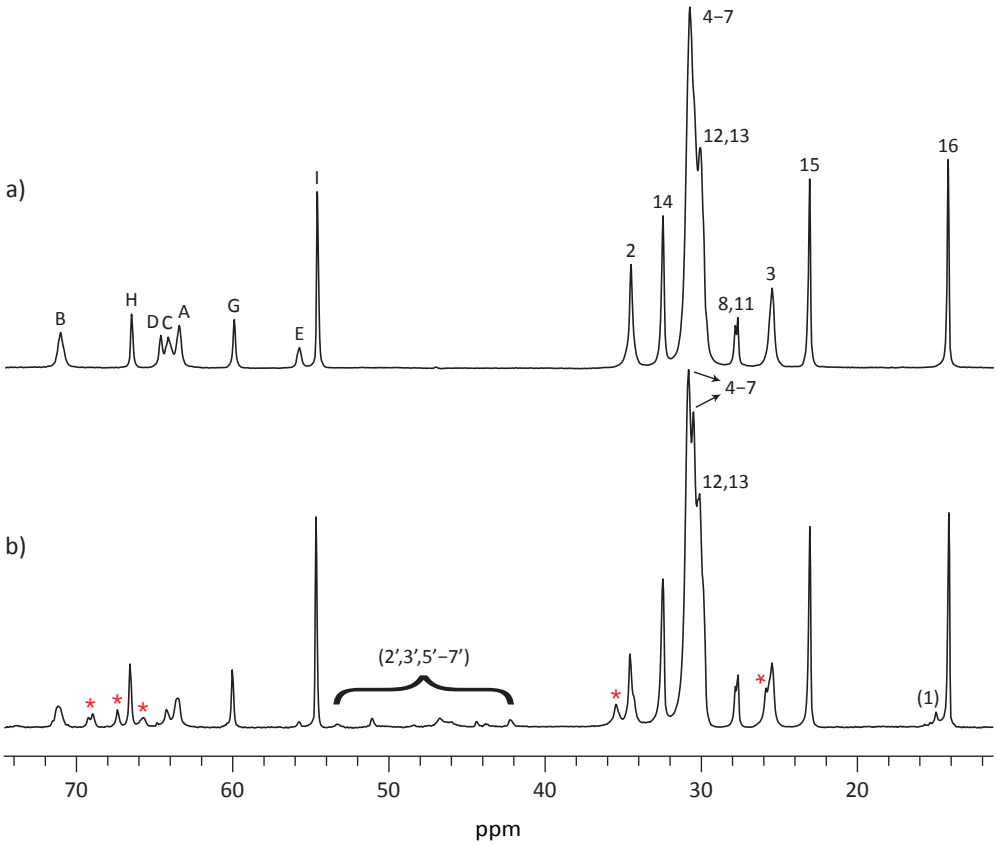

Figure 3.18 Proton-decoupled ^{13}C MASNMR spectra acquired at 316 K (43°C, above T_m), displaying spectral region of phospholipid headgroups, glycerol and saturated acyl chain carbons (12−74 ppm) of samples DPPC (60%)/POPS (40%) with ~50 wt.% H_2O (a) and the corresponding sample with 10 mol% OLZ (b). Glycerol and phospholipid headgroup resonances are labelled A−I in spectrum b (see *Scheme 3.1* for the annotation). The spectral region of 12−38 ppm is labelled with the palmitic (16:0) acyl chain resonances of DPPC.

3.3.4 Role of Lipid Headgroup in OLZ Interdigitation

The DPPC/DPPS bilayer (*Figure 3.15*) displays substantial effects of OLZ on the serine headgroup carbon resonances (D and E). Furthermore, a smaller effect is found for the DPPC/POPS bilayer (*Figure 3.18*) on the choline headgroup resonances (G, H and I). The above observations on the PC/PS headgroups upon the interdigitation of OLZ are further supported by the ^{31}P NMR experiments.

Existence of several lipid packing conformations is demonstrated in the ^{31}P MASNMR spectra of *Figure 3.19*, middle column and bottom row, in the somewhat broad appearance of the PS and PC resonances, even at 316 K (43°C) where the bilayer is in the liquid-crystalline state. This tendency of several lipid packing conformations is becoming more pronounced at lower temperature where the bilayer is in the gel state (middle column and top row). At a sample temperature of 296 K (23°C), a new resonance appears in between the PS and PC resonances, and is just a residue in the liquid-crystalline bilayer state (43°C, middle column and bottom row). The co-existence of several molecular packing arrangements in the DPPC/POPS bilayer at 23°C is further supported by the molecular composition of the bilayer that is a 1.5 PC/PS ratio of ^{31}P resonances. Thus, the resonance in between the PS and PC resonances of *Figure 3.19*, middle column and top row, at a sample temperature of 23°C, must have PS as well as PC phosphorous resonances contributing to the peak intensity.

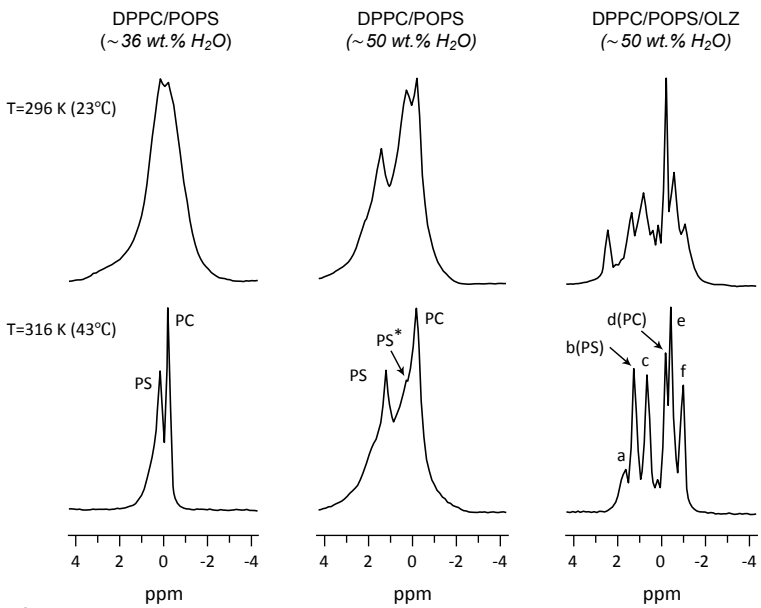

Figure 3.19 ^{31}P MASNMR spectra of samples DPPC (60%)/POPS (40%) with ~36 wt.% H_2O (left column) and DPPC (60%)/POPS (40%) with ~50 wt.% H_2O (middle column), and DPPC (54%)/POPS (36%)/OLZ (10%) with ~50 wt.% H_2O (right column) at sample temperatures 296 K (23°C) and 316 K (43°C), the experimental temperature is labelled with the corresponding spectrum. All spectra were obtained with a 2 kHz MAS spinning rate. The phosphatidylcholine and phosphatidylcholine components are assigned in the spectra at the temperature of 316 K (43 °C).

In the left column of *Figure 3.19*, the partially hydrated DPPC/POPS bilayer sample (~36 wt.% H_2O) demonstrate two not fully resolved peaks separated by 0.48 ppm, and the phosphatidylcholine component (labelled as 'PC') is found slightly upfield from the phosphatidylserine component (labelled as 'PS') [268,271]. In spectra of

~50 wt.% H_2O DPPC/POPS sample displayed in middle column, the corresponding chemical shift difference between PS and PC is 1.21 ppm. Comparing spectrum of DPPC/POPS/OLZ sample (right column and bottom row) with corresponding spectrum of sample without OLZ (middle column and bottom row), resonances labelled a−c and d−f (*Figure 3.19*, right column and bottom row) are PS and PC ^{31}P resonances, respectively. Of the three ^{31}P resonances attributed to PS, resonances a−c, the resonance labelled b is at the same chemical shift as the PS resonance in spectrum without OLZ (middle column and bottom row). Similarly, the resonance labelled d (right column and bottom row) is at the same chemical shift as the resonance labelled PC in spectrum without OLZ (middle column and bottom row). Thus, presence of OLZ in the bilayer gives rise to chemical environments in the bilayer polar region that affects both PS and PC headgroups. Furthermore, lowering sample temperature from 43 to 23 ℃ (right column and top row) broadens all PS resonances (a−c) and two PC resonances (e and f) without affecting the PC resonance labelled d (right column and bottom row). The OLZ affected ^{31}P resonances a−c of PS as well as e and f of PC are presumably broadened in spectra at lower temperatures due to chemical exchange caused by presence of OLZ. According to the difference of the resonance positions for resonances a and c (a difference of 207 Hz), one can estimate the exchange rate of the two complexes to be about 4.8 ms or longer (a lifetime much shorter would lead to coalescence and only one observed chemical shift for these two resonances). For the phosphatidylcholine components (the isotropic peaks e and f), the mean lifetime of this exchange can be estimated to $\geq$ 9.0 ms.

^{31}P T_1 values of the central band peaks displayed in *Figure 3.19* show that both PS and PC phosphorous mobilities are sensitive to sample temperature. The ^{31}P T_1 values for all of the phosphatidylserine resonances decrease with increasing temperature, indicating an increase in phosphorous mobility (slow motional regime, *Figure 2.16*). For the phosphatidylcholine components of the sample with OLZ, on the other hand, the T_1 values demonstrate a diverse change with increasing temperature, resonances d and e display the increased T_1 values, whereas the peak f shows the reduced T_1 values. Thus, peaks d and peak e are charactered with shorter correlation time (fast motional regime, *Figure 2.16*). Notably, the T_1 values of the PC peak of the fully hydrated sample (in the middle column) decrease quickly down to 0.59 s (35℃) from 1.04 s (23℃), and then increase to 0.74 s at 39℃, and finally remains approximately constant (0.78 s, at 43 ℃). This intriguing result can be due to partition of perchlorate anions into the looser liquid-crystalline phase of DPPC and bound to the phosphatidylcholine

group, which is triggered as the fully hydrated DPPC dispersion undergoes the gel-to-liquid-crystalline phase transition at the temperature region of 38 ℃ to 41 ℃ [479]. Comparison of the T_1 value of PS in the fully hydrated sample (0.61 s, 43℃) and peak b (PS), in the sample with OLZ (0.54 s, 43℃), shows reduced T_1 values of the phosphatidylserine phosphate region in the liquid-crystalline phase with OLZ and presumably this is caused by an increased mobility. The conclusion on the PS phosphate made from the ^{31}P T_1 data is in good agreement with the ^{13}C T_1 data of the serine headgroups (carbon D and E). From the T_1 values of the PC peak of the fully hydrated sample (in the middle column) and peak d (PC) in the sample with OLZ (at the right column), shows that these two components have distinctly different correlation times (τ_c).

Phospholipid headgroup (and phosphate) motion and an altered motion caused by an interacting amphiphile (like OLZ) in a bilayer will give static ^{31}P NMR spectra that differ in chemical shift anisotropy ($\Delta\delta$). The static ^{31}P NMR spectra demonstrate a substantial decrease in CSA of the OLZ−containing bilayer. The corresponding increased phospholipid headgroup mobilities producing such a CSA reduction in presence of OLZ could very well lead to a changed lateral phospholipid organization of the bilayer [469]. In fact, the ^{31}P MASNMR spectra presented in *Figure 3.19* indicate that imperfections in DPPC and POPS mixing (middle column and top row) are reduced in presence of OLZ (right column and top row).

The experiments of this study were carried out at a sample pH of 7.4 where two approximately equimolar OLZ species present in a positively charged and the neutral form of OLZ (OLZ has a pK_a value of 7.37). The ^{31}P MASNMR experiments presented in *Figure 3.19* show two (major) new ^{31}P resonances for both the PS and the PC phosphorous in presence of OLZ. In addition, OLZ is found to form dimers in the solid-state and such dimer formation is possible through intermolecular interactions, such as hydrogen bonding and electrostatic forces where stabilization appears to be achieved by interactions between *N*-methylpiperazine moiety and the phenyl/thiophene systems [480]. Furthermore, OLZ displays polymorphism and can form both dehydrated and hydrated dimers in the solid-state [477]. Thus, in light of such a tendency to dimer-formation, it cannot be ruled out that some of the bilayer interaction of OLZ is carried out by OLZ−dimers.

In general, the results of this study reveal that the serine headgroup is directly affected by OLZ interdigitation of the bilayer, and that the OLZ interaction with PS is to a great extent caused by electrostatic attraction to the serine headgroup. The molecular model of the OLZ interaction with a POPS molecule is presented in *Figure 3.20*, generated by the Titan software (Wavefunction, Irvine, CA).

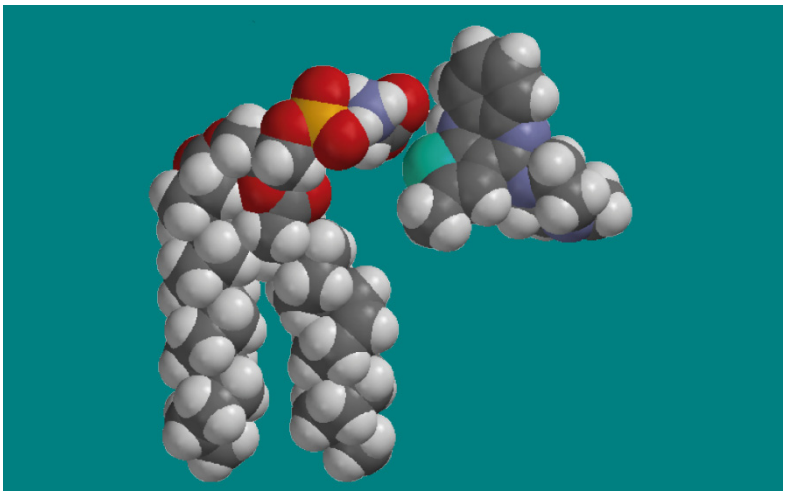

Figure 3.20 Molecular model of CPZ interaction with a POPS molecule. The OLZ molecule is positioned with its positive charge on the nitrogen atoms of the *N*-methylpiperazine moiety.

Even though conformations of the POPS acyl chain in the *sn*-2 position may differ somewhat from the conformation displayed here, the model suggests that OLZ interdigitated in such a bilayer will have an effect on carbons at the serine headgroup (*Figures 3.15*, *3.18, 3.19*), glycerol (*Figures 3.15, 3.18*), carbonyl (*Figure 3.16*) and the upper portion of the acyl chains (C=C double bonds, *Figure 3.17*; the rest saturated acyl chain carbons, *Figure 3.18*). Such an OLZ positioning is further supported by the ^{13}C and ^{31}P T_1 data.

4. CONCLUSIONS

Phenothiazine antipsychotic drugs (like CPZ) have an amphiphilic nature [295,301,302] and their interdigitation into a lipid bilayer can affect the bilayer´s fluidity [304−310]. An interdigitated phenothiazine occupies space in the bilayer´s polar region with effects on the packing of the acyl chains, and consequently on acyl chain mobility and bilayer fluidity. The presence of phospholipids with the DHA acyl chain in the *sn*-2 position is of great importance for CPZ interaction with the bilayer, whereas saturated acyl chains (palmitoyl and stearoyl) do not promote CPZ bilayer interdigitation. Thus, CPZ bilayer interdigitation depends on the lipid composition of the bilayer. Furthermore, the disappearance of bilayer microdomains in presence of 10 mol% CPZ points at a crucial role of DHA in formation and perseverance of phospholipid microdomains in the DPPC (60%)/SDPS (40%) bilayer. The NMR data of this study have demonstrated that the neutral PC phospholipid with a choline headgroup does not favour CPZ bilayer interdigitation, in contrast to the negatively charged PS with a serine headgroup that favour CPZ bilayer interdigitation (paper I and paper II).

The atypical antipsychotic drug OLZ shows a different bilayer interdigitation profile compared to a conventional antipsychotic drug like CPZ. In paper IV, the NMR data revealed that the serine headgroup of PS interacts with interdigitated OLZ by electrostatic attraction to the serine headgroup, in contrast to the minor effects of OLZ found on the choline headgroup resonances. Furthermore, OLZ dimers may contribute to some of the OLZ−bilayer interaction.

Interdigitation of the uncharged amide local anaesthetic articaine in the DSPC bilayer demonstrated a disturbance of the molecular packing in the polar region of the bilayer. This disturbance extends into the hydrophobic region. In addition, the observed ^{31}P and ^{13}C NMR spectral changes when articaine is increased from 40 to 55 mol%, suggest formation of amphiphilic articaine aggregates and decrease in DSPC bilayer perturbation at the latter articaine level (paper III).

In general, perturbation of lipid organization in a bilayer by amphiphilic molecules can be conceived to have consequences for the activity of membrane-bound proteins in cellular membranes, even without direct interaction between protein and amphiphile. Thus, it is possible that effects of antipsychotic drugs on the receptors are partially due to the drug perturbation of the membranes that contain these receptors.

5. Future Perspectives

The present study found perturbation of lipid bilayer organization by antipsychotic drugs and established that the phospholipid serine headgroup interacts with OLZ/CPZ. Further studies should be carried out to investigate high-resolution structural information obtainable by isotope enhancements i.e. OLZ/phospholipid (and CPZ/phospholipid) enriched with ^{13}C and/or ^{15}N. A starting point can be the ^{31}P nucleus of the phospholipids and $^{13}C/^{15}N$ of the drug. Such spin ½ nuclei can yield accurate interatomic distances from dipolar interactions that are normally sacrificed under the condition of high-power decoupling and MAS techniques [424–426]. Reintroduction of the dipolar coupling by use of the Rotational Echo Double Resonance (REDOR) experiment will provide interatomic distances of the drug-phospholipid interaction in the bilayer [480–483].

Furthermore, a study of bilayer perturbation of the local anaesthetic drug articaine on negatively charged species of PS as well as the dependence on acyl chain unsaturation will promote better understanding of the anaesthetic effect.

REFERENCES

[1] S.J. Singer, G.L. Nicolson, The fluid mosaic model of the structure of cell membranes. *Science* **175**(4023) (1972) 720−731.

[2] T. Hianik, V.I. Passečnik, *Bilayer Lipid Membranes: Structure and Mechanical Properties*. Springer−Verlag, New York, 1995.

[3] M.K. Jain, *Introduction to Biological Membranes*. Wiley, New York, 1988.

[4] J.F. Danielli, H. Davson, A contribution to the theory of permeability of thin films. *Cell. Comp. Physiol.* **5**(4) (1935) 495−508.

[5] H. Davson, J.F. Danielli, *The Permeability of Natural Membranes*. Cambridge University Press, Cambridge, 1952.

[6] M.I. Gurr, J.L. Harwood, K.N. Frayn, *Lipid Biochemistry: An Introduction* (5^{th} Edition), Blackwell publishing, Oxford, 2002.

[7] G. Cevc (ed.), *Phospholipids Handbook*. Marcel Dekker, New York, 1993.

[8] D.J. Morré, J. Kartenbeck, W.W. Franke, Membrane flow and interconversions among endomembranes. *Biochim. Biophys. Acta* **559**(1) (1979) 71−152.

[9] A.-H. Etemadi, Membrane asymmetry A survey and critical appraisal of the methodology II. Methods for assessing the unequal distribution of lipids. *Biochim. Biophys. Acta* **604**(3−4) (1980) 423−475.

[10] P.J. Quinn, The fluidity of cell membranes and its regulation. *Prog. Biophys. Mol. Biol.* **38** (1981) 1−104.

[11] D. Papahadjopoulos, D.J. Hanahan, Observations on the interaction of phospholipids and certain clotting factors in prothrombin activator formation. *Biochim. Biophys. Acta* **90**(2) (1964) 436−439.

[12] P.G. Barton, C.M. Jackson, D.J. Hanahan, Relationship between factor V and activated factor X in generation of prothrombinase. *Nature* **214**(5091) (1967) 923−924.

[13] C.T. Esmon, W.G. Owen, C.M. Jackson, A plausible mechanism for prothrombin activation by factor X_a, factor V_a, phospholipid and calcium ions. *J. Biol. Chem.* **249**(24) (1974) 8045−8047.

[14] R.A. Harris, P. Bruno, Membrane disordering by anesthetic drugs: relationship to synaptosomal sodium and calcium fluxes. *J. Neurochem.* **44**(4) (1985) 1274−1281.

[15] M. Luxnat, H.-J. Galla, Partition of chlorpromazine into lipid bilayer membranes: the effect of membrane structure and composition. *Biochim. Biophys. Acta* **856**(2) (1986) 274−282.

[16] Y. Boulanger, S. Schreier, I.C.P. Smith, Molecular details of anesthetic-lipid interaction as seen by deuterium and phosphorus-31 nuclear magnetic resonance. *Biochemistry* **20**(24) (1981) 6824−6830.

[17] R.B. Gennis, J.L. Strominger, Activation of C_{55}-isoprenoid alcohol phosphokinase from *Staphylococcus aureus*: I. Activation by phospholipids and fatty acids*. J. Biol. Chem.* **251**(5) (1976) 1264–1282.

[18] M. Morillas, W. Swietnicki, P. Gambetti, W.E. Surewicz, Membrane environment alters the conformational structure of the recombinant human prion protein. *J. Biol. Chem.* **274**(52) (1999) 36859–36865.

[19] W. van Klompenburg, I. Nilsson, G. von Heijne, B. de Kruijff, Anionic phospholipids are determinants of membrane protein topology. *EMBO J.* **16**(14) (1997) 4261–4266.

[20] IUPAC–IUB Commission on Biochemical Nomenclature, The nomenclature of lipids. *J. Lipid Res.* **8**(5) (1976) 523–528.

[21] IUPAC–IUB Commission on Biochemical Nomenclature, The nomenclature of lipids (Recommendations 1976). *J. Lipid Res.* **19**(1) (1978)114–128.

[22] IUPAC–IUB Joint Commission on Biochemical Nomenclature (JCBN), Nomenclature of Glycolipids (Recommendations 1997). *J. Mol. Biol.* **286**(3) (1999) 963–970.

[23] T.E. Andreoli, D.D. Fanestil, J.F. Hoffman, S.G. Schultz (Eds.), *Membrane Physiology* (2nd Edition). Springer, New York (1987) Chapter 27.

[24] J.C. Holthuis, T.P. Levine, Lipid traffic: Floppy drives and a superhighway. *Nat. Rev. Mol. Cell Biol.* **6**(3) (2005) 209–220.

[25] T.W. Keenan, D.J. Morré, Phospholipid class and fatty acid composition of Golgi apparatus isolated from rat liver and comparison with other cell functions. *Biochemistry* **9**(1) (1970) 19–25.

[26] B. Fleischer, F. Zambrano, S. Fleischer, Biochemical characterization of the golgi complex of mammalian cells. *J. Supermol. Struct.* **2**(5–6) (1974) 737–750.

[27] A. Zachowski, Phospholipids in animal eukaryotic membranes: transverse asymmetry and movement. *Biochem. J.* **294** (1993) 1–14.

[28] R. Schneiter, B. Brügger, R. Sandhoff, G. Zellnig, A. Leber, M. Lampl, K. Athenstaedt, C. Hrastnik, S. Eder, G. Daum, F. Paltauf, F.T. Wieland, S.D. Kohlwein, Electrospray ionization tandem mass spectroscopy (ESI-MS/MS) analysis of the lipid molecular species composition of yeast subcellular membranes reveals acyl chain-based sorting/remodeling of distinct molecular species en route to the plasma membrane. *J. Cell Biol.* **146**(4) (1999) 741–754.

[29] T. Neitcheva, D. Peeva, Phospholipid composition, phospholipase A_2 and spingomyelinase activities in rat liver nuclear membrane and matrix. *Int. J. Biochem. Cell Biol.* **27**(10) (1995) 995–1001.

[30] J.E. Rothman, J. Lenard, Membrane asymmetry. *Science* **195**(4280) (1977) 743–753.

[31] C.R.H. Raetz, W. Dowhan, Biosynthesis and function of phospholipids in *Escherichia coli*. *J. Biol. Chem.* **265**(3) (1990) 1235–1238.

[32] J.A. Higgins, R.M.C. Dawson, Asymmetry of the phospholipid bilayer of rat liver endoplasmic reticulum. *Biochim. Biophys. Acta* **470**(3) (1977) 342–356.

[33] M.C. Garcia, G. Ward, Y.-C. Ma, N. Salem, Jr., H.-Y. Kim, Effect of docosahexaenoic acid on the synthesis of phosphatidylserine in rat brain in microsomes and C6 glioma cells. *J. Neurochem.***70**(1) (1998) 24–30.

[34] J. Hamilton, R. Greiner, N. Salem, Jr., H.Y. Kim, n-3 fatty acid deficiency decreases phosphatidylserine accumulation selectively in neuronal tissues. *Lipids* **35**(8) (2000) 863–869.

[35] H.-Y. Kim, J. Bigelow, J.H. Kevala, Substrate preference in phosphatidylserine biosynthesis for docosahexaenoic acid containing species. *Biochemistry* **43**(4) (2004) 1030–1036.

[36] E. Zinser, C.D.M. Sperka-Gottlieb, E.-V. Fasch, S.D. Kohlwein, F. Paltauf, G. Daum, Phospholipid synthesis and lipid composition of subcellular membranes in the unicellular eukaryote *Saccharomyces cerevisiae*. *J. Bacteriol*. **173**(6) (1991) 2026–2034.

[37] D.E. Vance, "*Phospholipid biosynthesis in eukaryotes*," in *Biochemistry of Lipids, Lipoproteins and Membranes* (4th Edition). D.E. Vance, J.E. Vance (Eds.), Elsevier Science, Amsterdam (2002) 205−232.

[38] K. Matsumoto, Dispensable nature of phosphatidylglycerol in *Escherichia coli*: dual roles of anionic phospholipids. *Mol. Microbiol.* **39**(6) (2001) 1427−1433.

[39] M. Hallman, L. Gluck, Phosphatidylglycerol in lung surfactant II. Subcellular distribution and mechanism of biosynthesis in vitro. *Biochim. Biophys. Acta* **409**(2) (1975) 172−191.

[40] B. Antonsson, Phosphatidylinositol synthase from mammalian tissues. *Biochim. Biophys. Acta* **1348**(1−2) (1997) 179–186.

[41] M. Jackson, D.C. Crick, P.J. Brennan, Phosphatidylinositol is an essential phospholipid of mycobacteria. *J. Biol. Chem.* **275**(39) (2000) 30092–30099.

[42] J.-i. Nikawa, S. Yamashita, Phosphatidylinositol synthase from yeast. *Biochim. Biophys. Acta* **1348**(1−2) (1997) 173–178.

[43] D. Shields, P. Arvan, Disease models provide insights into post-Golgi protein trafficking, localization and processing. *Curr. Opin. Cell Biol.* **11**(4) (1999) 489–494.

[44] N. Divecha, R.F. Irvine, Phospholipid signaling. *Cell* **80**(2) (1995) 269–278.

[45] J. Ohanian, V. Ohanian, Sphingolipids in mammalian cell signalling. *Cell. Mol. Life Sci.* **58**(14) (2001) 2053–2068.

[46] F.L. Hoch, Cardiolipins and biomembrane function. *Biochim. Biophys. Acta* **1113**(1) (1992) 71–133.

[47] A.H. Merrill, Jr., K. Sandhoff, "*Sphingolipids: metabolism and cell signaling*," in *Biochemistry of Lipids, Lipoproteins and Membranes* (4th Edition). D.E. Vance, J.E. Vance (Eds.), Elsevier Science, Amsterdam (2002) 373−407.

[48] L. Liscum, "*Cholesterol biosynthesis*," in *Biochemistry of Lipids, Lipoproteins and Membranes* (4th Edition). D.E. Vance, J.E. Vance (Eds.), Elsevier Science, Amsterdam (2002) 409−431.

[49] J.A.F. Op den Kamp, Lipid asymmetry in membranes. *Annu. Rev. Biochem.* **48** (1979) 47−71.

[50] C.-T. Wang, Y.-J. Shiao, J.-C. Chen, W.-J. Tsai, C.-C. Yang, Estimation of the phospholipid distribution in the human platelet plasma membrane based on the effect of phospholipase A_2 from *Naja nigricollis*. *Biochim. Biophys. Acta* **856**(2) (1986) 244–258.

[51] J.A. Post, G.A. Langer, J.A.F. Op den Kamp, A.J. Verkleij, Phospholipid asymmetry in cardiac sarcolemma. Analysis of intact cells and 'gas-dissected' membranes. *Biochim. Biophys. Acta* **943**(2) (1988) 256–266.

[52] A.J. Verkleij, R.F.A. Zwaal, B. Roelofsen, P. Comfurius, D. Kastelijn, L.L.M. van Deenen, The asymmetric distribution of phospholipids in the human red cell

membrane. A combined study using phospholipases and freeze-etch electron microscopy. *Biochim. Biophys. Acta* **323**(2) (1973) 178−193.

[53] S.E. Gordesky, G.V. Marinetti, R. Love, The reaction of chemical probes with the erythrocyte membrane. *J. Membrane Biol.* **20** (1975) 111−132.

[54] E.M. Bevers, P. Comfurius, J.L.M.L. van Rijn, H.C. Hemker, R.F.A. Zwaal, Generation of prothrombin-converting activity and the exposure of phosphatidylserine at the outer surface of platelets. *Eur. J. Biochem.* **122**(2) (1982) 429−436.

[55] N. Kato, M. Nakanishi, N. Hirashima, Transbilayer asymmetry of phospholipids in the plasma membrane regulates exocytotic release in mast cells. *Biochemistry* **41**(25) (2002) 8068−8074.

[56] M.J. Hope, P.R. Cullis, Lipid asymmetry induced by transmembrane pH gradients in large unilamellar vesicles. *J. Biol. Chem.* **262**(9) (1987) 4360−4366.

[57] R.F.A. Zwaal, P. Comfurius, E.M. Bevers, Surface exposure of phosphatidylserine in pathological cells. *Cell Mol. Life Sci.* **62**(9) (2005) 971−988.

[58] N.H. Tattrie, J.R. Bennett, Jr., R. Cyr, Maximum and minimum values for lecithin classes from various biological sources. *Can. J. Biochem.* **46**(8) (1968) 819−824.

[59] W.E.M. Lands, P. Hart, The control of fatty acid composition in glycerolipids. *J. Am. Oil Chem. Soc.* **43** (1966) 290−295.

[60] C.W. Cotman, M.L. Blank, A. Moehl, F. Snyder, Lipid composition of synaptic plasma membranes isolated from rat brain by zonal centrifugation. *Biochemistry* **8**(11) (1969) 4606−4612.

[61] A.J. Fliesler, R.E. Anderson, Chemistry and metabolism of lipids in the vertebrate retina. *Prog. Lipid Res.* **22**(2) (1983) 79−131.

[62] C.R.H. Raetz, Molecular genetics of membrane phospholipid synthesis. *Annu. Rev. Genet.* **20** (1986) 253−291.

[63] J.N. Israelachvili, S. Marcelja, R.G. Horn, Physical principles of membrane organization. *Q. Rev. Biophys.* **13**(2) (1980) 121−200.

[64] J.N. Israelachvili, D.J. Mitchell, B.W. Ninham, Theory of self-assembly of hydrocarbon amphiphiles into micelles and bilayers. *J. Chem. Soc., Faraday Trans. 2* **72** (1976) 1525−1586.

[65] P.R. Cullis, M.J. Hope, "*Physical properties and functional roles of lipids in membranes*, " in *Biochemistry of Lipids, Lipoproteins and Membranes* (Revised Edition). D.E. Vance, J.E. Vance (Eds.), Elsevier Science, Amsterdam (2002) 1−41.

[66] P.R. Cullis, B. de Kruijff, Lipid polymorphism and the functional roles of lipids in biological membranes. *Biochim. Biophys. Acta* **559**(4) (1979) 399−420.

[67] K. Gounaris, A. Sen, A.P.R. Brain, P.J. Quinn, W.P. Williams, The formation of non-bilayer structures in total polar lipid extracts of chloroplast membranes. *Biochim. Biophys. Acta* **728**(1) (1983) 129−139.

[68] A.D. Albert, A. Sen, P.L. Yeagle, The effect of calcium on the bilayer stability of lipids from bovine rod outer segment disk membranes. *Biochim. Biophys. Acta* **771**(1) (1984) 28−34.

[69] I.M. Hafez, P.R. Cullis, Roles of lipid polymorphism in intracellular delivery. *Adv. Drug. Deliv. Rev.* **47**(2−3) (2001) 139−148.

[70] R.N.A.H. Lewis, D.A. Mannock, R.N. McElhaney, D.C. Turner, S.M. Gruner, Effect of fatty acyl chain length and structure on the lamellar gel to liquid-crystalline and

lamellar to reversed hexagonal phase transitions of aqueous phosphatidylethanolamine dispersions. *Biochemistry* **28**(2) (1989) 541−548.

[71] Å. Wieslander, A. Christiansson, L. Rilfors, A. Khan, L.B.-Å. Johansson, G. Lindblom. Lipid phase structure governs the regulation of lipid composition in membranes of *Acholeplasma laidlawii*. *FEBS Lett.* **124**(2) (1981) 273−278.

[72] Å. Wieslander, A. Christiansson, L. Rilfors, G. Lindblom, Lipid bilayer stability in membranes. Regulation of lipid composition in *Acholeplasma laidlawii* as governed by molecular shape. *Biochemistry* **19**(16) (1981) 3650−3655.

[73] V. Luzzati, F. Husson, The structure of the liquid-crystalline phases of lipid-water systems. *J. Cell Biol.* **12**(2) (1962) 207–219.

[74] J.M. Seddon, G. Cevc, R.D. Kaye, D. Marsh, X-ray diffraction study of the polymorphism of hydrated diacyl- and dialkylphosphatidylethanolamines. *Biochemistry* **23**(12) (1984) 2634–2644.

[75] Y.S. Tarahovsky, A.L. Arsenault, R.C. MacDonald, T.J. McIntosh, R.M. Epand, Electrostatic control of phospholipid polymorphism. *Biophys. J.* **79**(6) (2000) 3193−3200.

[76] J. Seelig, ^{31}P nuclear magnetic resonance and the head group structure of phospholipids in membranes. *Biochim. Biophys. Acta* **515**(2) (1978) 105−140.

[77] P.R. Cullis, B. de Kruijff, Polymorphic phase behaviour of lipid mixtures as detected by ^{31}P NMR. Evidence that cholesterol may destabilize bilayer structure in membrane systems containing phosphatidylethanolamine. *Biochim. Biophys. Acta* **507**(2) (1978) 207−218.

[78] H.U. Gally, G. Pluschke, P. Overath, J. Seelig, Structure of *Escherichia coli* membranes. Fatty acyl chain order parameters of inner and outer membranes and derived liposomes. *Biochemistry* **19**(8) (1980) 1638−1643.

[79] X-j. Li, M. Schnick, Theory of lipid polymorphism: application to phosphatidylethanolamine and phosphatidylserine. *Biophys. J.* **78**(1) (2000) 34−46.

[80] J.M. Seddon, G. Cevc, D. Marsh, Calorimetric studies of the gel-fluid (L_β–L_α) and lamellar-inverted hexagonal (L_α–H_{II}) phase transitions in dialkyl- and diacylphosphatidylethanolamines. *Biochemistry* **22**(5) (1983) 1280–1289.

[81] S.M. Bezrukov, R.P. Rand, I. Vodyanoy, V.A. Parsegian, Lipid packing stress and polypeptide aggregation: alamethicin channel probed by proton titration of lipid charge. *Faraday Discuss.* **111** (1999) 173–183.

[82] J.M. Seddon, Structure of the inverted hexagonal (H_{II}) phase, and non-lamellar phase transitions of lipids. *Biochim. Biophys. Acta* **1031**(1) (1990) 1–69.

[83] S.M. Gruner, Stability of lyotropic phases with curved interfaces. *J. Phys. Chem.* **93**(22) (1989) 7562–7570.

[84] R. Leventis, N. Fuller, R.P. Rand, P.L. Yeagle, A. Sen, M.J. Zuckermann, J.R. Silvius, Molecular organization and stability of hydrated dispersions of headgroup-modified phosphatidylethanolamine analogues. *Biochemistry* **30**(29) (1991) 7212−7219.

[85] J. Zimmerberg, Are the curves in all the right places? *Traffic* **1**(4) (2000) 366−368.

[86] T.D. Madden, P.R. Cullis, Stabilization of bilayer structure for unsaturated phosphatidylethanolamines by detergents. *Biochim. Biophys. Acta* **684**(1) (1982) 149–153.

[87] Y. Deng, M. Marko, K.F. Buttle, A. Leith, M. Mieczkowski, C.A. Mannella, Cubic membrane structure in amoeba (*Chaos carolinensis*) mitochondria determined by electron microscopic tomography. *J. Struct. Biol.* **127**(3) (1999) 231−239.

[88] J.A. Killian, A.M. de Jong, J. Bijvelt, A.J. Verkleij, B. de Kruijff, Induction of non-bilayer lipid structures by functional signal peptides. *EMBO J.* **9**(3) (1990) 815−819.

[89] C.-h. Huang, S. Li, Calorimetric and molecular mechanics studies of the thermotropic phase behavior of membrane phospholipids. *Biochim. Biophy. Acta* **1422**(3) (1999) 273−307.

[90] O.G. Mouritsen, K. Jørgensen, Dynamical order and disorder in lipid bilayers. *Chem. Phys. Lipids* **73**(1−2) (1994) 3−25.

[91] B.D. Ladbrooke, D. Chapman, Thermal analysis of lipids, proteins and biological membranes a review and summary of some recent studies. *Chem. Phys. Lipids* **3**(4) (1969) 304−356.

[92] D.M. Engelman, X-ray diffraction studies of phase transitions in membrane of *Mycoplasma laidlawii*. *J. Mol. Biol.* **47**(1) (1970) 115−116.

[93] W.L. Hubbell, H.M. McConnell, Molecular motion in spin-labeled phospholipids and membranes. *J. Am. Chem. Soc*. **93**(2) (1971) 314−326.

[94] D. Marsh, Statistical mechanics of the fluidity of phospholipid bilayers and membranes. *J. Membr. Biol.* **18**(1) (1974) 145−162.

[95] H. Träuble, H. Eibl, Electrostatic effects on lipid phase transitions: membrane structure and ionic environment. *Proc. Natl. Acad. Sci. USA* **71**(1) (1974) 214−219.

[96] N. Murata, H. Wada, Acyl lipid desaturases and their importance in the tolerance and acclimatization to cold of cyanobacteria. *Biochemical J.* **308** (1995) 1−8.

[97] N. Murata, O. Ishizaki-Nishizawa, S. Higashi, H. Hayashi, Y, Tasaka, I. Nishida, Genetically engineered alteration in the chilling sensitivity of plants. *Nature* **356**(6371) (1992) 710−713.

[98] T.H. Haines, Do sterols reduce proton and sodium leaks through lipid bilayers? *Prog. Lipid Res.* **40**(4) (2001) 299−324.

[99] Y. Barenholz, Cholesterol and other membrane active sterols: from membrane evolution to "raft". *Prog. Lipid Res.* **41**(1) (2002) 1−5.

[100] R. Zeisig, T. Koklič, B. Wiesner, I. Fichtner, M. Sentjurč, Increase in fluidity in the membrane of MT3 breast cancer cells correlates with enhanced cell adhesion *in vitro* and increased lung metastasis in NOD/SCID mice. *Arch. Biochem. Biophy.* **459**(1) (2007) 98−106.

[101] J.S. Parks, K.W. Huggins, A.K. Gebre, E.R. Burleson, Phosphatidylcholine fluidity and structure affect lecithin: cholesterol acyltransferase activity. *J. Lipid Res.* **41**(4) (2000) 546−553.

[102] P.V. Sergeev, T.V. Ukhina, M.M. Shegai, G.Zh. Kalmagambetova, Lipid spectrum of the skin in psoriasis. *Bull. Exp. Biol. Med.* **116**(9) (1993) 1102−1104.

[103] J. Belagyi, M. Pas, P. Raspor, M. Pesti, T. Páli, Effect of hexavalent chromium on eukaryotic plasma membrane studied by EPR spectroscopy. *Biochim. Biophys. Acta* **1421**(1) (1999) 175–182.

[104] J.J. García, E. Martínez-Ballarín, S. Millán-Plano, J.L. Allué, C. Albendea, L. Fuentes, J.F. Escanero, Effects of trace elements on membrane fluidity. *J. Trace Elem. in Med. Biol.* **19**(1) (2005) 19–22.

[105] G. Wang, S. Li, H. Lin, E.E. Brumbaugh, C.-h. Huang, Effects of various numbers and positions of *cis* double bonds in the *sn*-2 acyl chain of phosphatidylethanolamine on the chain-melting temperature. *J. Biol. Chem.* **274**(18) (1999) 12289−12299.

[106] J.F. Nagle, R. Zhang, S. Tristram-Nagle, W. Sun, H.I. Petrache, R.M. Suter, X-ray structure determination of fully hydrated L_α phase dipalmitoylphosphatidylcholine bilayers. *Biophys. J.* **70**(3) (1996) 1419−1431.

[107] S. Mabrey, J.M. Sturtevant, Investigation of phase transitions of lipids and lipid mixtures by high sensitivity differential scanning calorimetry. *Proc. Natl. Acad. Sci. USA* **73**(11) (1976) 3862−3866.

[108] H. Xu, C.-h. Huang, Scanning calorimetric study of fully hydrated asymmetric phosphatidylcholines with one acyl chain twice as long as the other. *Biochemistry* **26**(4) (1986) 1036−1043.

[109] R.H.A.H. Lewis, N. Mak, R.N. McElhaney, A differential calorimetric study of the thermotropic phase behavior of model membranes composed of phosphatidylcholines containing linear saturated fatty acyl chains. *Biochemistry* **26**(19) (1987) 6118−6126.

[110] H.-n. Lin, Z.-q. Wang, C.-h. Huang, The influence of acyl chain-length asymmetry on the phase transition parameters of phosphatidylcholine dispersions. *Biochim. Biophys. Acta* **1067**(1) (1991) 17−28.

[111] J.B. Massey, H.S. She, H.J. Pownall, Interaction of vitamin E with saturated phospholipid bilayers. *Biochem. Biophys. Res. Commun.* **106**(3) (1982) 842−847.

[112] J.L. Browning, J. Seelig, Bilayers of phosphatidylserine: a deuterium and phosphorus nuclear magnetic resonance study. *Biochemistry* **19**(6) (1980) 1262−1270.

[113] T.P.W. McMullen, R.N. McElhaney, Differential scanning calorimetric studies of the interaction of cholesterol with distearoyl and dielaidoyl molecular species of phosphatidylcholine, phosphatidylethanolamine, and phosphatidylserine. *Biochemistry* **36**(16) (1997) 4979−4986.

[114] T. Bultmann, H.-n. Lin, Z.-q. Wang, C.-h. Huang, Thermotropic and mixing behavior of mixed-chain phosphatidylcholines with molecular weights identical with that of L-*α*-dipalmitoylphosphatidylcholine. *Biochemistry* **30**(29) (1991) 7194−7202.

[115] C. Huang, Z.-q. Wang, H.-n. Lin, E.E. Brumbaugh, S. Li, Interconversion of bilayer phase transition temperatures between phosphatidylethanolamines and phosphatidylcholines. *Biochim. Biophys. Acta* **1189**(1) (1994) 7−12.

[116] J. Katsaras, D.S.-C. Yang, R.M. Epand, Fatty-acid chain tilt angles and directions in dipalmitoyl phosphatidylcholine bilayers. *Biophys. J.* **63**(4) (1992) 1170−1175.

[117] Z.-q. Wang, H.-n. Lin, C.-h. Huang, Differential scanning calorimetric study of a homologous series of fully hydrated saturated mixed-chain C(*X*):C(*X*+6) phosphatidylcholine. *Biochemistry* **29**(30) (1990) 7072−7076.

[118] H. Ichimori, T. Hata, H. Matsuki, S. Kaneshina, Barotropic phase transitions and pressure-induced interdigitation on bilayer membranes of phospholipids with varying acyl chain lengths. *Biochim. Biophys. Acta* **1414**(1−2) (1998) 165−174.

[119] A. Tardieu, V. Luzzati, F.C. Reman, Structure and polymorphism of the hydrocarbon chains of lipids: A study of lecithin-water phases. *J. Mol. Biol.* **75**(4) (1973) 711−733.

[120] H.H. Füldner, Characterization of a third phase transition in multilamellar dipalmitoyllecithin liposomes. *Biochemistry* **20**(20) (1981) 5707−5710.

[121] J. Frye, A.D. Arlene, B.S. Selinsky, P.L. Yeagle, Cross polarization P-31 nuclear magnetic resonance of phospholipids. *Biophys. J.* **48**(4) (1985) 547−552.

[122] J.F. Nagle, D.A. Wilkinson, Lecithin bilayers. Density measurement and molecular interactions. *Biophys. J.* **23**(2) (1978) 159−175.

[123] I.C.P. Smith, G.W. Stockton, A.P. Tulloch, C.F. Polnaszek, K.G. Johnson, Deuterium NMR and spin label ESR as probes of membrane organization. *J. Col. Interface Sci.* **58**(3) (1977) 439−451.

[124] G. Smutzer, A fluorescent sterol probe study of cholesterol/phospholipid membranes. *Biochim. Biophys. Acta* **946**(2) (1988) 270−280.

[125] H.L. Casal, D.G. Cameron, H.C. Jarrell, I.C.P. Smith, H.H. Mantsch, Lipid phase transitions in fatty acid-homogeneous membranes of *Acholeplasma laidlawii B*. *Chem. Phys. Lipids* **30**(1) (1982) 17−26.

[126] P. Overath, H.U. Schairer, W. Stoffel, Correlation of *in vivo* and *in vitro* phase transitions of membrane lipids in *Escherichia coli*. *Proc. Natl. Acad. Sci. USA* **67**(2) (1970) 606−612.

[127] G. Wilson, S.P. Rose, C.F. Fox, The effect of membrane lipid unsaturation on glycoside transport. *Biochem. Biophys. Res. Commun.* **38**(4) (1970) 617−623.

[128] D. Chapman, J. Urbina, Phase transitions and bilayer structure of *Mycoplasma laidlawii* **B**. *FEBS Lett.* **12**(3) (1970) 169−172.

[129] D. Papahadjopoulos, M. Moscarello, E.H. Eylar, T. Isac, Effects of proteins on the thermotropic phase transitions of phospholipid membranes. *Biochim. Biophys. Acta* **401**(3) (1975) 317−335.

[130] M.K. Jain, N.Y.-M. Wu, L.V. Wray, Drug-induced phase change in bilayer as possible mode of action of membrane expanding drugs. *Nature* **255**(5508) (1975) 494−496.

[131] A. Makriyannis, D.J. Siminovitch, K. Sunil, D. Gupta, R.G. Griffin, Studies on the interaction of anesthetic steroids with phosphatidylcholine using ^{2}H and ^{13}C solid state NMR. *Biochim. Biophys. Acta* **859**(1) (1986) 49−55.

[132] J.R. Trudell, D.G. Payan, J.H. Chin, E.N. Cohen, The antagonistic effects of an inhalation anesthetic and high pressure on the phase diagram of mixed dipalmitoyl-dimyristoylphosphatidylcholine bilayers. *Proc. Natl. Acad. Sci. USA* **72**(1) (1975) 210−213.

[133] S.J. Singer, G.L. Nicolson, The fluid mosaic model of the structure of cell membranes. *Science* **175**(4023) (1972) 720−731.

[134] S. Bullivant, Freeze-etching techniques applied to biological membranes. *Phil. Trans. R. Soc. Lond. B. Biol. Sci.* **268**(891) (1974) 5−14.

[135] G.L. Nicolson, R. Yanagimachi, Mobility and the restriction of mobility of plasma membrane lectin-binding components. *Science* **184**(4143) (1974) 1294−1296.

[136] K. Simons, E. Ikonen, Functional rafts in cell membranes. *Nature* **387**(6633) (1997) 569**–**572.

[137] K. Jacobson, C. Dietrich, Looking at lipid rafts? *Trends in Cell Biol.* **9**(3) (1999) 87**–**91.

[138] J.Y.A. Lehtonen, J.M. Holopainen, P.K.J. Kinnunen, Evidence for the formation of microdomains in liquid crystalline large unilamellar vesicles caused by

hydrophobic mismatch of the constituent phospholipids. *Biophys. J.* **70**(4) (1996) 1753−1760.

[139] M.Ø. Jensen, O.G. Mouritsen, Lipids do influence protein function−the hydrophobic matching hypothesis revisited. *Biochim. Biophys. Acta* **1666**(1−2) (2004) 205−226.

[140] T.E. Thompson, T.W. Tillack, Organization of glycosphingolipids in bilayers and plasma membranes of mammalian cells. *Annu. Rev. Biophys. & Biophys. Chem.* **14** (1985) 361–386.

[141] K. Simons, G. van Meer, Lipid sorting in epithelial cells. *Biochemistry* **27**(17) (1988) 6197−6202.

[142] C.G. Dotti, R.G. Parton, K. Simons, Polarized sorting of glypiated proteins in hippocampal neurons. *Nature* **349**(6305) (1991) 158–161.

[143] T. Stauffer, T. Meyer, Compartmentalized IgE receptor-mediated signal transduction in living cells. *J. Cell Biol.* **139**(6) (1997) 1447–1454.

[144] T.V. Kurzchalia, R.G. Parton, Membrane microdomains and caveolae. *Curr. Opin. Cell Biol.* **11**(4) (1999) 424–431.

[145] T. Hønger, K. Jørgensen, R.L. Biltonen, O.G. Mouritsen, Systematic relationship between phospholipase A_2 activity and dynamic lipid bilayer microheterogeneity. *Biochemistry* **35**(28) (1996) 9003–9006.

[146] A.R.G. Dibble, A.K. Hinderliter, J.J. Sando, R.L. Biltonen, Lipid lateral heterogeneity in phosphatidylcholine/phosphatidylserine/diacylglycerol vesicles and its influence on protein kinase C activation. *Biophys. J.* **71**(4) (1996) 1877–1890.

[147] O.P. Karlsson, M. Rytömaa, A. Dahlqvist, P.K.J. Kinnunen, Å. Wieslander, Correlation between bilayer lipid dynamics and activity of the diglucosyldiacylglycerol synthase from *Acholeplasma laidlawii* membranes. *Biochemistry* **35**(31) (1996) 10094–10102.

[148] P. Verkade, K. Simons, Lipid microdomains and membrane trafficking in mammalian cells. *Histochem. Cell Biol.* **108**(3) (1997) 211–220.

[149] S. Mukherjee, T.T. Soe, F.R. Maxfield, Endocytic sorting of lipid analogues differing solely in the chemistry of their hydrophobic tails. *J. Cell Biol.* **144**(6) (1999) 1271–1284.

[150] E.E. Williams, Membrane lipids: What membrane physical properties are conserved during physiochemically-induced membrane restructuring? *Amer. Zool.* **38**(2) (1998) 280−290.

[151] J. Hwang, L.A. Gheber, L. Margolis, M. Edidin, Domains in cell plasma membranes investigated by near-field scanning optical microscopy. *Biophys. J.* **74**(5) (1998) 2184–2190.

[152] L.A. Bagatolli, E. Gratton, Two-photon fluorescence microscopy of coexisting lipid domains in giant unilamellar vesicles of binary phospholipid mixtures. *Biophys. J.* **78**(1) (2000) 290–305.

[153] L.A. Bagatolli, E. Gratton, A correlation between lipid domain shape and binary phospholipid mixture composition in free standing bilayers: A two-photon fluorescence microscopy study. *Biophys. J.* **79**(1) (2000) 434–447.

[154] C.W. McConlogue, T.K. Vanderlick, A close look at domain formation in DPPC monolayers. *Langmuir* **13**(26) (1997) 7158−7164.

[155] P.R. Cullis, M.J. Hope, The bilayer stabilizing role of sphingomyelin in the presence of cholesterol. A ^{31}P NMR study. *Biochim. Biophys. Acta* **597**(3) (1980) 533–542.

[156] M.B. Sankaram, T.E. Thompson, Cholesterol-induced fluid-phase immiscibility in membranes. *Proc. Natl. Acad. Sci. USA* **88**(19) (1991) 8686–8690.

[157] Y.-W. Hsueh, R. Giles, N. Kitson, J. Thewalt, The effect of ceramide on phosphatidylcholine membranes: a deuterium NMR study. *Biophys. J.* **82**(6) (2002) 3089–3095.

[158] S.R. Shaikh, M.R. Brzustowicz, N. Gustafson, W. Stillwell, S.R. Wassall, Monounsaturated PE does not phase-separate from the lipid raft molecules sphingomyelin and cholesterol: Role for polyunsaturation? *Biochemistry* **41**(34) (2002) 10593–10602.

[159] M.R. Brzustowicz, V. Cherezov, M. Caffrey, W. Stillwell, S.R. Wassall, Molecular organization of cholesterol in polyunsaturated membranes: microdomain formation. *Biophys. J.* **82**(1) (2002) 285–298.

[160] S.R. Shaikh, A.C. Dumaual, D. LoCascio, R.A. Siddiqui, W. Stillwell, Acyl chain unsaturation in PEs modulates phase separation from lipid raft molecules. *Biochem. Biophys. Res. Commun.* **311**(3) (2003) 793–796.

[161] S. Moffett, D.A. Brown, M.E. Linder, Lipid-dependent targeting of G proteins into rafts. *J. Biol. Chem.* **275**(3) (2000) 2191–2198.

[162] S. Munro, Lipid rafts: elusive or illusive? *Cell* **115**(4) (2003) 377−388.

[163] H.M. McConnell, M. Vrljic, Liquid-liquid immiscibility in membranes. *Annu. Rev. Biophys. Biomol. Struct.* **32** (2003) 469−492.

[164] S. Mayor, M. Rao, Rafts: scale-dependent, active lipid organization at the cell surface. *Traffic* **5**(4) (2004) 231−240.

[165] M. Edidin, The state of lipid rafts: from model membranes to cells. *Annu. Rev. Biophys. Biomol. Struct.* **32** (2003) 257−283.

[166] K. Simons, W.L.C. Vaz, Model system, lipid rafts, and cell membranes. *Annu. Rev. Biophys. Biomol. Struct.* **33** (2004) 269−295.

[167] D. Huster, K. Arnold, K. Gawrisch, Influence of docosahexaenoic acid and cholesterol on lateral lipid organization in phospholipid mixtures. *Biochemistry* **37**(49) (1998) 17299–17308.

[168] M.R. Brzustowicz, V. Cherezov, M. Zerouga, M. Caffrey, W. Stillwell, S.R. Wassall, Controlling membrane cholesterol content. A role for polyunsaturated (docosahexaenoate) phospholipids. *Biochemistry* **41**(41) (2002) 12509–12519.

[169] S.R. Shaikh, A.C. Dumaual, A. Castillo, D. LoCascio, R.A. Siddiqui, W. Stillwell, S.R. Wassall, Oleic and docosahexaenoic acid differentially phase separate from lipid raft molecules: a comparative NMR, DSC, AFM, and detergent extraction study. *Biophys. J.* **87**(3) (2004) 1752–1766.

[170] R.A. Demel, W.S.M. Geurtz van Kessel, L.L.M. van Deenen, The properties of polyunsaturated lecithins in monolayers and liposomes and the interactions of these lecithins with cholesterol. *Biochim. Biophys. Acta* **266**(1) (1972) 26–40.

[171] M. Pasenkiewicz-Gierula, W.K. Subczynski, A. Kusumi, Rotational diffusion of a steroid molecule in phosphatidylcholine-cholesterol membranes: fluid-phase microimmiscibility in unsaturated phosphatidylcholine-cholesterol membranes. *Biochemistry* **29**(17) (1990) 4059–4069.

[172] W. Stillwell, S.R. Wassall, A.C. Dumaual, W.D. Ehringer, C.W. Browning, L.J. Jenski, Use of merocyanine (MC540) in quantifying lipid domains and packing in phospholipid vesicles and tumor cells. *Biochim. Biophys. Acta* **1146**(1) (1993) 136–144.

[173] W. Stillwell, T. Dallman, A.C. Dumaual, F.T. Crump, L.J. Jenski, Cholesterol versus α-Tocopherol: effects on properties of bilayers made from heteroacid phosphatidylcholines. *Biochemistry* **35**(41) (1996) 13353–13362.

[174] Y. Bayon, M. Croset, D. Daveloose, F. Guerbette, V. Chirouze, J. Viret, J.-C. Kader, M. Lagarde, Effect of specific phospholipid molecular species incorporated in human platelet membranes on thromboxane A_2/prostaglandin H_2 receptors. *J. Lipid Res.* **36**(1) (1995) 47−56.

[175] D.B. Jump, The biochemistry of *n*-3 polyunsaturated fatty acids. *J. Biol. Chem.* **277**(11) (2002) 8755–8758.

[176] P.S. Sastry, Lipids of nervous tissues: Composition and metabolism. *Prog. Lipid Res.* **24**(2) (1985) 69−176.

[177] N.M. Giusto, S.J. Pasquaré, G.A. Salvador, P.I. Castagnet, M.E. Roque, M.G.I. de Boschero, Lipid metabolism in vertebrate retinal rod outer segments. *Prog. Lipid Res.* **39**(4) (2000) 315−391.

[178] L.A. Witting, C.C. Harvey, B. Century, M.K. Horwitt, Dietary alterations of fatty acids of erythrocytes and mitochondria of brain and liver. *J. Lipid Res.* **2**(4) (1961) 412–418.

[179] A. Lenzi, L. Gandini, V. Maresca, R. Rago, P. Sgrò, F. Dondero, M. Picardo, Fatty acid composition of spermatozoa and immature germ cells. *Mol. Hum. Reprod.* **6**(3) (2000) 226–231.

[180] J.S. O'Brien, E.L. Sampson, Fatty acid and fatty aldehyde composition of the major brain lipids in normal human gray matter, white matter, and myelin. *J. Lipid Res.* **6**(4) (1965) 545–551.

[181] W. Stillwell, S.R. Wassall, Docosahexaenoic acid: membrane properties of a unique fatty acid. *Chem. Phys. Lipids* **126**(1) (2003) 1–27.

[182] D.F. Horrobin, Nutritional and medical importance of gamma-linolenic acid. *Prog. Lipid Res.* **31**(2) (1992)163−194.

[183] R.A. Gibson, G.M. Kneebone, Fatty acid composition of human colostrum and mature breast milk. *Am. J. Clin. Nutr.* **34**(2) (1981) 252−257.

[184] N. Salem, Jr., H.-Y. Kim, J.A. Yergey, *Docosahexaenoic acid: membrane function and metabolism.* in *Health Effects of Polyunsaturated Fatty Acids in Seafoods*, A.P. Simopoulos, R.R. Kifer, R.E. Martin (Eds.), Academic Press, Orlando (1986) 263–317.

[185] H. Sprecher, D.L. Luthria, B.S. Mohammed, S.P. Baykousheva, Reevaluation of the pathways for the biosynthesis of polyunsaturated fatty acids. *J. Lipid Res.* **36**(12) (1995) 2471–2477.

[186] M.M. Khan, D.R. Evans, V. Gunna, R.E. Scheffer, V.V. Parikh, S.P. Mahadik, Reduced erythrocyte membrane essential fatty acids and increased lipid peroxides in schizophrenia at the never-medicated first-episode of psychosis and after years of treatment with antipsychotics. *Schizophr. Res.* **58**(1) (2002) 1−10.

[187] C.E. Borgeson, L. Pardini, R.S. Pardini, R.C. Reitz, Effects of dietary fish oil on human mammary carcinoma and on lipid-metabolizing enzymes. *Lipids* **24**(4) (1989) 290–295.

[188] M. Neuringer, W.E. Connor, D.S. Lin, L. Barstad, S. Luck, Biochemical and functional effects of prenatal and postnatal ω3 fatty acid deficiency on retina and brain in rhesus monkeys. *Proc. Natl. Acad. Sci. USA* **83**(11) (1986) 4021– 4025.

[189] W.S. Fenton, J. Hibblen, M. Knable, Essential fatty acids, lipid membrane abnormalities, and the diagnosis and treatment of schizophrenia. *Biol. Psychiat.* **47**(1) (2000) 8−21.

[190] J.A. Glomset, Fish, fatty acids, and human health. *N. Engl. J. Med.* **312**(19) (1985) 1253–1254.

[191] J. Dyerberg, H.O. Bang, N. Hjørne, Fatty acid composition of the plasma lipids in Greenland Eskimos. *Am. Clin. Nutr.* **28**(9) (1975) 958–966.

[192] A. Hirai, T. Hamasaki, T. Terano, T. Nishikawa, Y. Tamura, A. Kumagai, J. Sajiki, Eicosapentaenoic acid and platelet function in tapanese. *Lancet* **316**(8204) (1980) 1132–1133.

[193] D. Kromhout, E.B. Bosschieter, C. de-Lezenne-Coulander, The inverse relation between fish consumption an 20-year mortality from coronary heart disease. *N. Engl. J. Med.* **312**(19) (1985)1205–1209.

[194] S.E. Norell, A. Ahlbom, M. Feychting, N.L. Pedersen, Fish consumption and mortality from coronary heart disease. *Br. Med. J.* (*Clin. Res. Ed.)* **293**(6544) (1986) 426.

[195] S.P. Pereira, T.B. Cassell, J.L. Engelman, G.E. Sladen, G.M. Murphy, R.H. Dowling, Plasma arachidonic acid-rich phospholipids in Crohn's disease: response to treatment. *Clin. Sci.* **91**(4)(1996) 509−512.

[196] M. Lagarde, N. Gualde, M. Rigaud, Metabolic interactions between eicosanoids in blood and vascular cells. *Biochem. J.* **257** (1989) 313–320.

[197] A.M. de Urquiza, S. Liu, M. Sjöberg, R.H. Zetterström, W. Griffiths, J. Sjövall, T. Perlmann, Docosahexaenoic acid, a ligand for the retinoid X receptor in mouse brain. *Science* **290**(5499) (2000) 2140–2144.

[198] S.D. Freedman, H.M. Katz, E.M. Parker, M. Laposata, M.Y. Urman, J.G. Alvarez, A membrane lipid imbalance plays a role in the phenotypic expression of cystic fibrosis in *cftr*$^{-/-}$ mice. *Proc. Natl. Acad. Sci. USA* **96**(24) (1999) 13995–14000.

[199] J.S. Poling, S. Vicini, M.A. Rogawski, N. Salem, Jr., Docosahexaenoic acid block of neuronal voltage-gated K^+ channels: subunit selective antagonism by zinc. *Neuropharmacol.* **35**(7) (1996) 969–982.

[200] M.C. Garcia, H.-Y. Kim, Mobilization of arachidonate and docosahexaenoate by stimulation of the 5-HT_{2A} receptor in rat C6 glioma cells. *Brain Res.* **768**(1−2) (1997) 43–48.

[201] A. Salmon, S.W. Dodd, G.D. Williams, J.M. Beach, M.F. Brown, Configurational statistics of acyl chains in polyunsaturated lipid bilayers from ^{2}H NMR. *J. Am. Chem. Soc.* **109**(9) (1987) 2600–2609.

[202] X. Han, R.W. Gross, Plasmenylcholine and phosphatidylcholine membrane bilayers possess distinct conformational motifs. *Biochemistry* **29**(20) (1990) 4992−4996.

[203] J.M. Smaby, A. Hermetter, P.C. Schmid, F. Paltauf, H.L. Brockman, Packing of ether and ester phospholipids in monolayers. Evidence for hydrogen-bonded water at

the *sn*-1 acyl group of phosphatidylcholines. *Biochemistry* **22**(25) (1983) 5808−5813.

[204] S. Hexeberg, N. Willumsen, R.K. Berge, Docosahexaenoic acid induces lipid accumulation in myocardial cells of rats. *Scand. J. Clin. Lab. Invest.* **54**(8) (1994) 665−671.

[205] O. Holian, R. Nelson, Action of long-chain fatty acids on protein kinase C activity : comparison of omega-6 and omega-3 fatty acids. *Anticancer Res.* **12**(3) (1992) 975−980.

[206] A.W. Pascale, W.D. Ehringer, W. Stillwell, L.K. Sturdevant, L.J. Jenski, Omega-3 fatty acid modification of membrane structure and function. II. Alteration by docosahexaenoic acid of tumor cell sensitivity to immune cytolysis. *Nutr. Cancer* **19**(2) (1993) 147−157.

[207] J.A. Barry, T.P. Trouard, A. Salmon, M.F. Brown, Low-temperature ^{2}H NMR spectroscopy of phospholipid bilayers containing docosahexaenoyl (22:6 ω3) chains. *Biochemistry* **30**(34) (1991) 8386−8394.

[208] V. Dolo, P. Pizzurro, A. Ginestra, M.L. Vittorelli, Inhibitory effects of vesicles shed by human breast carcinoma cells on lymphocyte ^{3}H-thymidine incorporation, are neutralised by anti TGF-β antibodies. *J. Submicrosc. Cytol. Pathol.* **27**(4) (1995) 535−541.

[209] L.J. Jenski, L.K. Sturdevant, W.D. Ehringer, W. Stillwell, Omega-3 fatty acid modification of membrane structure and function. I. Dietary manipulation of tumor cell susceptibility to cell- and complement-mediated lysis. *Nutr. Cancer* **19**(2) (1993) 135−146.

[210] Th. Hendriks, A.A. Klompmakers, F.J.M. Daemen, S.L. Bonting, Biochemical aspects of the visual process XXXII. Movement of sodium ions through bilayers composed of retinal and rod outer segment lipids. *Biochim. Biophys. Acta* **433**(2) (1976) 271−281.

[211] W. Ehringer, D. Belcher, S.R. Wassall, W. Stillwell, A comparison of the effects of linolenic (18:3Ω3) and docosahexaenoic (22:6Ω3) acids on phospholipid bilayers. *Chem. Phys. Lipids* **54**(2) (1990) 79−88.

[212] M.M. Guffy, J.A. Rosenberger, I. Simon, C.P. Burns, Effect of cellular fatty acid alteration on hyperthermic sensitivity in cultured L1210 murine leukemia cells. *Cancer Res.* **42**(9) (1982) 3625−3630.

[213] L.J. Jenski, M. Zerouga, W. Stillwell, Omega-3 fatty acid-containing liposomes in cancer therapy. *Proc. Soc. Exp. Biol. Med.* **210**(3) (1995) 227−233.

[214] C.B. Ambrosone, J.L. Freudenheim, R. Sinha. S. Graham, J.R. Marshall, J.E. Vena, R. Laughlin, T. Nemoto, P.G. Shields. Breast cancer risk, meat consumption and *N*-acetyltransferase (*NAT2*) genetic polymorphorisms. *Int. J. Cancer* **75**(6) (1998) 825−830.

[215] M.B. Veierod, P. Laake, D.S. Thelle, Dietary fat intake and risk of lung cancer: a prospective study of 51,452 Norwegian men and women. *Eur. J. Cancer Prev.* **6**(6) (1997) 540−549.

[216] C.W. Hendrickse, M.R.B. Keighley, J.P. Neoptolemos, Dietary ω-3 fats reduce proliferation and tumor yields at colorectal anastomosis in rats. *Gastroenterology* **109**(2) (1995) 431−439.

[217] N.W. Istfan, J. Wan, Z.-Y. Chen, Fish oil and cell proliferation kinetics in a mammary carcinoma tumor model. *Adv. Exp. Med. Biol.* **375** (1995) 149−156.

[218] M. Zerouga, W. Stillwell, J. Stone, A. Powner, A.C. Dumaual, L.J. Jenski, Phospholipid class as a determinant in docosahexaenoic acid's effect on tumor cell viability. *Anticancer Res.* **16**(5A) (1996) 2863−2868.

[219] M. Peet, Nutrition and schizophrenia: beyond omega-3 fatty acids. *Prostaglandins. Leukotr. Essent. Fatty Acids* **70**(4) (2004) 417−422.

[220] J.A. Astin, Why patients use alternative medicine: results of a national study. *JAMA* **279**(19) (1998) 1548−1553.

[221] B. Payrastre, K. Missy, S. Giuriato, S. Bodin, M. Plantavid, M.-P. Gratacap, Phosphoinositides: key players in cell signalling, in time and space. *Cell. Signal.* **13**(6) (2001) 377–387.

[222] M.J. Beridge, P. Lipp, M.D. Bootman, The versatility and universality of calcium signalling. *Nat. Rev. Mol. Cell Biol.* **1**(1) (2000) 11−21.

[223] W.L. Smith, R.M. Garavito, D.L. DeWitt, Prostaglandin endoperoxide H synthases (cyclooxygenases)−1 and −2. *J. Biol. Chem.* **271**(52) (1996) 33157−33160.

[224] C.D. Funk, Prostaglandins and leukotrienes: Advances in eicosanoids biology. *Science* **294**(5548) (2001) 1871−1875.

[225] A.R. Brash, Lipoxygenases: occurrence, functions, catalysis, and acquisition of substrate. *J. Biol. Chem.* **274**(34) (1999) 23679−23682.

[226] A.A. Farooqui, L.A. Horrocks, Signalling and interplay mediated by phospholipases A_2, C and D in LA-N-1 cell nuclei. *Reprod. Nutr. Dev.* **45**(5) (2005) 613−631.

[227] L.J. Pike, Lipid rafts: bringing order to chaos. *J. Lipid Res.* **44**(4) (2003) 655–667.

[228] R.N. Kolesnick, F.M. Goñi, A. Alonso, Compartmentalization of ceramide signaling: physical foundations and biological effects. *J. Cell Physiol.* **184**(3) (2000) 285–300.

[229] M. Liscovitch, L.C. Cantley, Lipid second messengers. *Cell* **77**(3) (1994) 329−334.

[230] M. Liscovitch, Phospholipase D: role in signal transduction and membrane traffic. *J. Lipid Mediators Cell Signalling* **14**(1−3) (1996) 215−221.

[231] K. Fukami, T. Takenawa, Phosphatidic acid that accumulates in platelet-derived growth factor-stimulated Balb/c 3T3 cells is a potential mitogenic signal. *J. Biol. Chem.* **267**(16) (1992) 10988−10993.

[232] J.-K. Pai, M.I. Siegel, R.W. Egan, M.M. Billah, Phospholipase D catalyzes phospholipid metabolism in chemotactic peptide-stimulated HL-60 granulocytes. *J. Biol. Chem.* **263**(25) (1988) 12472−12477.

[233] P. Bellavite, F. Corso, S. Dusi, M. Grzeskowiak, V. Della-Bianca, F. Rossi, Activation of NADPH-dependent superoxide production in plasma membrane extracts of pig neutrophils by phosphatidic acid. *J. Biol. Chem.* **263**(17) (1988) 8210−8214.

[234] M.H. Tsai, C.L. Yu, F.S. Wei, D.W. Stacey, The effect of GTPase activating protein upon Ras is inhibited by mitogenically responsive lipids. *Science* **243**(4890) (1989) 522−526.

[235] S. Ahmed, J. Lee, R. Kozma, A. Best, C. Monfries, L. Lim, A novel functional target for tumor-promoting phorbol esters and lysophosphatidic acid. The p21*rac*-GTPase activating protein *n*-chimaerin. *J. Biol. Chem.* **268**(15) (1993) 10709−10712.

[236] Z. Zhao, S.-H. Shen, E.H. Fischer, Stimulation by phospholipids of a protein-tyrosine-phosphatase containing two *src* homology 2 domains. *Proc. Natl. Acad. Sci. USA* **90**(9) (1993) 4251−4255.

[237] G.A. Jones, G. Carpenter, The regulation of phospholipase C-*γ*1 by phosphatidic acid. Assessment of kinetic parameters. *J. Biol. Chem.* **268**(28) (1993) 20845−20850.

[238] G.H. Jenkins, P.L. Fisette, R.A. Anderson, Type I phosphatidylinositol 4-phosphate 5-kinase isoforms are specifically stimulated by phosphatidic acid. *J. Biol. Chem.* **269**(15) (1994) 11547−11554.

[239] P.A. Randazzo, R.A. Kahn, GTP hydrolysis by ADP-ribosylation factor is dependent on both an ADP-ribosylation factor GTPase-activating protein and acid phospholipids. *J. Biol. Chem.* **269**(14) (1994) 10758−10763.

[240] S.J. Singer, The molecular organization of membrane. *Annu. Rev. Biochem.* **43** (1974) 805−833.

[241] J.A. Killian, G. von Heijne, How proteins adapt to a membrane−water interface. *TIBS* **25**(9) (2000) 429−434.

[242] O.G. Mouritsen, M. Bloom, Models of lipid-protein interactions in membranes. *Annu. Rev. Biophys. Biomol. Struct.* **22** (1993) 145–171.

[243] E. Sackmann, "*Physical basis for trigger processes and membrane structures*," in *Biological Membranes*. O. Chapman (Ed.), Academic Press, London (1980) 105–143.

[244] D.W. Grainger, A. Reichert, H. Ringsdorf, S. Salesse, Hydrolytic action of phospholipase A_2 in monolayers in the phase transition region: direct observation of enzyme domain formation using fluorescence microscopy. *Biochim. Biophys. Acta* **1023**(3) (1990) 365−379.

[245] W.R. Burack, R.L. Biltonen, Lipid bilayer heterogeneities and modulation of phospholipase A_2 activity. *Chem. Phys. Lipids* **73**(1−2) (1994) 209−222.

[246] C. Sunshine, M.G. McNamee, Lipid modulation of nicotinic acetylcholine receptor function: the role of membrane lipid composition and fluidity. *Biochim. Biophys. Acta* **1191**(1) (1994) 59–64.

[247] S.E. Rankin, G.H. Addona, M.A. Kloczewiak, B. Bugge, K.W. Miller, The cholesterol dependence of activation and fast desensitization of the nicotinic acetylcholine receptor. *Biophys. J.* **73**(5) (1997) 2446–2455.

[248] K.M.P. Taylor, M.A. Roseman, Effect of cholesterol, fatty acyl chain composition, and bilayer curvature on the interaction of cytochrome b_5 with liposomes of phosphatidylcholines. *Biochemistry* **34**(11) (1995) 3841–3850.

[249] E.J. Bolen, J.J. Sando, Effect of phospholipid unsaturation on protein kinase C activation. *Biochemistry* **31**(25) (1992) 5945−5951.

[250] Y. Romsicki, F.J. Sharom, The membrane lipid environment modulates drug interactions with the *P*-glycoprotein multidrug transporter. *Biochemistry* **38**(21) (1999) 6887−6896.

[251] D.F. Lazar, F. Medzihradsky, Altered microviscosity at brain membrane surface induces distinct and reversible inhibition of opioid receptor binding. *J. Neurochem.* **59**(4) (1992) 1233−1240.

[252] J.D. Pilot, J.M. East, A.G. Lee, Effects of bilayer thickness on the activity of diacylglycerol kinase of *Escherichia coli*. *Biochemistry* **40**(28) (2001) 8188–8195.

[253] D.C. Mitchell, S.-L. Niu, B.J. Litman, Optimization of receptor-G protein coupling by bilayer lipid composition I. Kinetics of rhodopsin-transducin binding. *J. Biol. Chem.* **276**(46) (2001) 42801–42806.

[254] S.-L. Niu, D.C. Mitchell, B.J. Litman, Optimization of receptor-G protein coupling by bilayer lipid composition II. Formation of metarhodopsin II-transducin complex. *J. Biol. Chem.* **276**(46) (2001) 42807–42811.

[255] J.M. East, A.G. Lee, Lipid selectivity of the calcium and magnesium ion dependent adenosinetriphosphatase, studied with fluorescence quenching by a brominated phospholipid. Fluorescence quenching in model membranes. 2. Determination of the local lipid environment of the calcium adenosinetriphosphatase from sarcoplasmic reticulum. *Biochemistry* **21**(17) (1982) 4144–4151.

[256] E. London, G.W. Feigenson, Fluorescence quenching in model membranes. 2. Determination of the local lipid environment of the calcium adenosinetriphosphatase from sarcoplasmic reticulum. *Biochemistry* **20**(7) (1981) 1939–1948.

[257] A.P. Starling, K.A. Dalton, J.M. East, S. Oliver, A.G. Lee, Effects of phosphatidylethanolamines on the activity of the Ca^{2+}-ATPase of sarcoplasmic reticulum. *Biochem. J.* **320** (1996) 309–314.

[258] P.A. Baldwin, W.L. Hubbell, Effects of lipid environment on the light-induced conformational changes of rhodopsin. 1. Absence of metarhodopsin II production in dimyristoylphosphatidylcholine recombinant membranes. *Biochemistry* **24**(11) (1985) 2624–2632.

[259] P.A. Baldwin, W.L. Hubbell, Effects of lipid environment on the light-induced conformational changes of rhodopsin. 2. Roles of lipid chain length, unsaturation, and phase state. *Biochemistry* **24**(11) (1985) 2633–2639.

[260] T.S. Wiedmann, R.D. Pates, J.M. Beach, A. Salmon, M.F. Brown, Lipid-protein interactions mediate the photochemical function of rhodopsin. *Biochemistry* **27**(17) (1988) 6469–6474.

[261] A. Carruthers, D.L. Melchior, Human erythrocyte hexose transporter activity is governed by bilayer lipid composition in reconstituted vesicles. *Biochemistry* **23**(26) (1984) 6901–6911.

[262] R.E. Tefft, Jr., A. Carruthers, D.L. Melchior, Reconstituted human erythrocyte sugar transporter activity is determined by bilayer lipid head groups. *Biochemistry* **25**(12) (1986) 3709–3718.

[263] C. Montecucco, G.A. Smith, F. Dabenni-sala, A. Johansson, Y.M. Galante, R. Bisson, Bilayer thickness and enzymatic activity in the mitochondrial cytochrome *c* oxidase and ATPase complex. *FEBS Lett.* **144**(1) (1982) 145–148.

[264] L.K. Srivastava, S.M.I. Kazmi, A.J. Blume, R.K. Mishra, Reconstitution of affinity-purified dopamine D_2 receptor binding activities by specific lipids. *Biochim. Biophys. Acta* **900**(2) (1987) 175−182.

[265] W.-g. Wu, L.-M. Chi, Comparisons of lipid dynamics and packing in fully interdigitated monoarachidoylphosphatidylcholine and non-interdigitated dipalmitoylphosphatidylcholine bilayers: cross polarization/magic angle spinning ^{13}C-NMR studies. *Biochim. Biophys. Acta* **1026**(2) (1990) 225−235.

[266] P.E. Godici, F.R. Landsberger, Dynamic structure of lipid membranes. A ^{13}C nuclear magnetic resonance study using spin labels. *Biochemistry* **13**(2) (1974) 362−368.

[267] S.O. Smith, I. Kustanovich, S. Bhamidipati, A. Salmon, J.A. Hamilton, Interfacial conformation of dipalmitoylglycerol and dipalmitoylphosphatidylcholine in phospholipid bilayers. *Biochemistry* **31**(46) (1992) 11660−11664.

[268] T.J.T. Pinheiro, A. Watts, Resolution of individual lipids in mixed phospholipid membranes and specific lipid-cytochrome *c* interactions by magic-angle spinning solid-state phosphorus-31 NMR. *Biochemistry* **33**(9) (1994) 2459–2467.

[269] I.C.P. Smith, I.H. Ekiel, "*Phosphorus-31 NMR of phospholipids in membranes*," in *Phosphorous-31 NMR, Principles and Applications*. D.G. Gorenstein (Ed.), Academic Press, New York (1984) 447−475.

[270] J. Seelig, H-U. Gally, Investigation of phosphatidylethanolamine bilayers by deuterium and phosphorus-31 nuclear magnetic resonance. *Biochemistry* **15**(24) 5199−5204.

[271] A.U. Gjerde, H. Holmsen, W. Nerdal, Chlorpromazine interaction with phosphatidylserines: A ^{13}C and ^{31}P solid-state NMR study. *Biochim. Biophys. Acta* **1682**(1−3) (2004) 28−37.

[272] S.J. Kohler, M.P. Klein, Orientation and dynamics of phospholipid head groups in bilayers and membranes determined from ^{31}P nuclear magnetic resonance chemical shielding tensors. *Biochemistry* **16**(3) (1977) 519–526.

[273] B.H.C. Westerink, Y. Kawahara, P. De Boer, C. Geels, J.B. De Vries, H.V. Wikström, A. Van Kalkeren, B. Van Vliet, C.G. Kruse, S.K. Long, Antipsychotic drugs classified by their effects on the release of dopamine and noradrenaline in the prefrontal cortex and striatum. *Eur. J. Pharmacol.* **412**(2) (2001) 127–138.

[274] H.Y. Meltzer, S. Matsubara, J.-C. Lee, Classification of typical and atypical antipsychotic drugs on the basis of dopamine D-1, D-2 and serotonin$_2$ pK_i values. *J. Pharmacol. Exp. Ther.* **251**(1) (1989) 238−246.

[275] P. Seeman, The membrane actions of anesthetics and tranquilizers. *Pharmacol. Rev.* **24**(4) (1972) 583–655.

[276] F.P. Bymaster, D.L. Nelson, N.W. DeLapp, J.F. Falcone, K. Eckols, L.L. Truex, M.M. Foreman, V.L. Lucaites, D.O. Calligaro, Antagonism by olanzapine of dopamine D1, serotonin$_2$, muscarinic, histamine H_1 and α_1-adrenergic receptors in vitro. *Schizophr. Res.* **37**(1) (1999) 107−122.

[277] C.M. Beasley, M.A. Dellva, R.N. Tamura, H. Morgenstern, W.M. Glazer, K. Ferguson, G.D. Tollefson, Randomised double-blind comparison of the incidence of tardive dyskinesia in patients with schizophrenia during long-term treatment with olanzapine or haloperidol. *Br. J. Psychiatry* **174** (1999) 23–30.

[278] M.A Davies, D.J. Sheffler, B.L. Roth, Aripiprazole: a novel atypical antipsychotic drug with a uniquely robust pharmacology. *CNS Drug Reviews* **10**(4) (2004) 317–336.

[279] E. Spina, A. Avenoso, G. Facciolà, M. G. Scordo, M. Ancione, A. G. Madia, A. Ventimiglia, E. Perucca, Relationship between plasma concentrations of clozapine and norclozapine and therapeutic response in patients with schizophrenia resistant to conventional neuroleptics. *Psychopharmacol.* **148**(1) (2000) 83–89.

[280] P.F. Liddle, The symptoms of chronic schizophrenia. A re-examination of the positive-negative dichotomy. *Br. J. Psychiatry* **151** (1987) 145–151.

[281] A. Breier, J.L. Schreiber, J. Dyer, D. Pickar, National institute of mental health longitudinal study of chronic schizophrenia. Prognosis and predictors of outcome. *Arch. Gen. Psychiatry.* **48**(3) (1991) 239–246.

[282] W.S. Fenton, T.H. McGlashan, Natural history of schizophrenia subtypes. II. Positive and negative symptoms and long-term course. *Arch. Gen. Psychiatry.* **48**(11) (1991) 978–986.

[283] P.D. Harvey, D. Koren, A. Reichenberg, C.R. Bowie, Negative symptoms and cognitive deficits: what is the nature of their relationship? *Schizophr. Bull.* **32**(2) (2006) 250–258.

[284] M.J. Owen, N. Craddock, M.C. O'Donovan, Schizophrenia: genes at last? *Trends in Genetics* **21**(9) (2005) 518–525.

[285] R. Day, J.A. Nielsen, A. Korten, G. Ernberg, K.C. Dube, J. Gebhart, A. Jablensky, C. Leon, A. Marsella, M. Olatawura, N. Sartorius, E. Strmögen, R. Takahshi, N. Wig, L.C. Wynne, Stressful life events preceding the acute onset of schizophrenia: a cross-national study from the World Health Organization. *Cult. Med. Psychiatr.* **11**(2) (1987) 123–205.

[286] H.L. MacMillan, J.E. Fleming, D.L. Streiner, E. Lin, M.H. Boyle, E. Jamieson, E.K. Duku, C.A. Walsh, M.Y.-Y. Wong, W.R. Beardslee, Childhood abuse and lifetime psychopathology in a community sample. *Am. J. Psychiat.* **158**(11) (2001) 1878–1883.

[287] L.S. Schenkel, W.D. Spaulding, D. DiLillo, S.M. Silverstein, Histories of childhood maltreatment in schizophrenia: Relationships with premorbid functioning, symptomatology, and cognitive deficits. *Schizophr. Res.* **76**(2−3) (2005) 273−286.

[288] I. Janssen, L. Krabbendam, M. Bak, M. Hanssen, W. Vollebergh, R. De Graaf, J. van Os, Childhood abuse as a risk factor for psychotic experiences. *Acta Psychiatr. Scand.* **109**(1) (2004) 38–45.

[289] P.J. Harrison, M.J. Owen, Genes for schizophrenia? Recent findings and their pathophysiological implications. *Lancet* **361**(9355) (2003) 417–419.

[290] J.M. Ford, W.C. Prozialeck, W.N. Hait, Structural features determining activity of phenothiazines and related drugs for inhibition of cell growth and reversal of multidrug resistance. *Mol. Pharmacol.* **35**(1) (1989) 105−115.

[291] T. Lialiaris, A. Pantazaki, E. Sivridis, D. Mourelatos, Chlorpromazine-induced damage on nucleic acids: a combined cytogenetic and biochemical study. *Mutat. Res.* **265**(2) (1992) 155−163.

[292] G. Housley, G. V. Born, D. M. Conroy, J. Berlin, A. D. Smith, Influence of dietary lipids on the effect of chlorpromazine on membrane properties of rabbit red cells. *Proc. R. Soc. Lond. B. Biol. Sci.* **227**(1246) (1986) 43−51.

[293] M. A. Yacko, D. A. Butterfield, Spin-labeling studies of the conformation of the Ca^{2+}-regulatory protein calmodulin in solution and bound to the membrane skeleton in erythrocyte ghosts: Implications to transmembrane signaling. *Biophys. J.* **63**(2) (1992) 317−322.

[294] K.W. Frølich, G. M. Aarbakke, H. Holmsen, Chlorpromazine increases the turnover of metabolically active phosphoinositides and elevates the steady-state level of phosphatidylinositol-4-phosphate in human platelets. *Biochem. Pharmacol.* **44**(10) (1992) 2013−2020.

[295] P. Tharmapathy, M.H. Fukami, H. Holmsen, The stimulatory effects of cationic amphiphilic drugs on human platelets treated with thrombin. *Biochem. Pharmacol.* **60**(9) (2000) 1267−1277.

[296] O.-B. Tysnes, V.M. Steen, K.W. Frølich, H. Holmsen, Evidence that chlorpromazine and prostaglandin E_1 but not neomycin interfere with the inositol phospholipid metabolism in intact human platelets. *FEBS Lett.* **264**(1) (1990) 33−36.

[297] K.O. Daasvatn, H. Holmsen, Chlorpromazine and human platelet glycerolipid metabolism: precursor specificity and significance of drug-platelet interaction time. *Biochem. Pharmacol.* **57**(10) (1999) 1113−1123.

[298] M. Wakamori, M. Kaneda, Y. Oyama, N. Akaike, Effects of chlordiazepoxide, chlorpromazine, diazepam, diphenylhydantoin, flunitrazepam and haloperidol on the voltage-dependent sodium current of isolated mammalian brain neurons. *Brain Res.* **494**(2) (1989) 374–378.

[299] M. Müller, J.R. De Weille, M. Lazdunski, Chlorpromazine and related phenothiazines inhibit the ATP-sensitive K^+ channel. *Eur. J. Pharmacol.* **198**(1) (1991) 101–104.

[300] K. Kon, E. Krause, H. Gögelein, Inhibition of K^+ channels by chlorpromazine in rat ventricular myocytes. J. *Pharmacol. Exp. Ther.* **271**(2) (1994) 632–637.

[301] M.P. Sheetz, S.J. Singer. Biological membranes as bilayer couples. A molecular mechanism of drug–erythrocyte interactions. *Proc. Natl. Acad. Sci. USA* **71**(11) (1974) 4457–4461.

[302] H. Holmsen, T. Rygh, Chlorpromazine makes the platelet plasma membrane permeable for low-molecular weight substances and reduces ATP production. *Biochem. Pharmacol*. **40**(2) (1990) 373–376.

[303] Y. Kuroda, K. Kitamura, Intra- and intermolecular ^1H-^1H nuclear Overhauser effect studies on the interactions of chlorpromazine with lecithin vesicles. *J. Am. Chem. Soc.* **106**(1) (1984) 1−6.

[304] S. Noji, T. Takahashi, H. Kon, A spin-label study of the correlation between stomatocyte formation and membrane fluidization of erythrocytes. *Biochem Pharmacol*. **31**(20) (1982) 3173–3180.

[305] I. Scuntaro, U. Kientsch, U.N. Wiesmann, U.E. Honegger, Inhibition by vitamin E of drug accumulation and of phospholipidosis induced by desipramine and other cationic amphiphilic drugs in human cultured cells. *Br. J. Pharmacol.* **119**(5) (1996) 829–834.

[306] R. Salesse, J. Garnier, F. Leterrier, D. Daveloose, J. Viret, Modulation of adenylate cyclase activity by the physical state of pigeon erythrocyte membrane: 1. Parallel drug-induced changes in the bilayer fluidity and adenylate cyclase activity. *Biochemistry* **21**(7) (1982) 1581–1586.

[307] K.-W. Ahn, C.-H. Choi, I.-S. Kim, I.-K. Chung, G.-J. Cho, H.-O. Jang, I. You, Transbilayer effects of chlorpromazine·HCl on rotational mobility of synaptosomal plasma membrane vesicles isolated from bovine brain. *J. Biochem. Mol. Biol.* **33**(6) (2000) 541–547.

[308] H.-O. Jang, D.-K. Jeong, S.-H. Ahn, C.-D. Yoon, S.-C. Jeong, S.-D. Jin, I. You, Effects of chlorpromazine·HCl on the structural parameters of bovine brain membranes. *J. Biochem. Mol. Biol*. **37**(5) (2004) 603–611.

[309] G.S. Zubenko, B.M. Cohen, Effects of phenothiazine treatment on the physical properties of platelet membranes from psychiatric patients. *Biol. Psychiat.* **20**(4) (1985) 384–396.

[310] G.S. Zubenko, B.M. Cohen, A cell membrane correlate of tardive dyskinesia in patients treated with phenothiazines. *Psychopharmacol.* **88**(2) (1986) 230–236.

[311] D.B. Goldstein, The effects of drugs on membrane fluidity. *Annu. Rev. Pharmacol. Toxicol*. **24** (1984) 43–64.

[312] H. Tanii, J. Huang, T. Ohyashiki, K. Hashimoto, Physical–chemical–activity relationship of organic solvents: effects on Na^+-K^+-ATPase activity and membrane fluidity in mouse synaptosomes. *Neurotoxicol. Teratol.* **16**(6) (1994) 575–582.

[313] M. Suwalsky, L. Gimenez, V. Saenger, F. Neira, X-ray studies on phospholipid bilayers. VIII. Interactions with chlorpromazine.HCl. *Z. Naturforsch[c].* **43**(9−10) (1988) 742−748.

[314] A.V. Agasøster, L.M. Tungodden, D. Čejka, E. Bakstad, L.K. Sydnes, H. Holmsen, Chlorpromazine-induced increase in dipalmitoylphosphatidylserine surface area in monolayers at room temperature. *Biochemical Pharmacol*. **61**(7) (2001) 817−825.

[315] J. Dachary-Prigent, J. Dufourcq, C. Lussan, and M. Boisseau, Propranolol, chlorpromazine and platelet membrane: A fluorescence study of the drug-membrane interaction. *Thromb. Res.* **14**(1) (1979) 15−22.

[316] R.A. Schwendener, Incorporation of chlorpromazine into bilayer liposomes for protection against microsomal metabolism and liver absorption. *Eur. J. Drug Metab. Pharmacokinet* **13**(2) (1988) 135−141.

[317] W. Nerdal, S.A. Gundersen, V. Thorsen, H. Høiland, H. Holmsen, Chlorpromazine interaction with glycerophospholipid liposomes studied by magic angle spinning solid-state ^{13}C-NMR and differential scanning calorimetry. *Biochim. Biophys. Acta* **1464**(1) (2000) 165−175.

[318] N.A. Moore, N.C. Tye, M.S. Axton, F.C. Risius, The behavioral pharmacology of olanzapine, a novel “atypical” antipsychotic agent. *J. Pharmacol. Exp. Ther.* **262**(2) (1992) 545–551.

[319] F.P. Bymaster, D.L. Nelson, N.W. DeLapp, J.F. Falcone, K. Eckols, L.L. Truex, M.M. Foreman, V.L. Lucaites, D.O. Calligaro, Antagonism by olanzapine of dopamine D1, serotonin$_2$, muscarinic, histamine H_1 and α_1-adrenergic receptors in vitro. *Schizophr. Res.* **37**(1) (1999) 107−122.

[320] A. Fuller, H.D. Snoddy, Neuroendocrine evidence for antagonism of serotonin and dopamine receptors by olanzapine (LY170053), an antipsychotic drug candidate, *Res. Commun. Chem. Pathol. Pharmacol.* **77**(1) (1992) 87−93.

[321] F.P. Bymaster, D.O. Calligaro, J.F. Falcone, R.D. Marsh, N.A. Moore, N.C. Tye, P. Seeman, D.T. Wong, Radioreceptor binding profile of the atypical antipsychotic olanzapine, *Neuropsychopharmacol.* **14**(2) (1996) 87−96.

[322] F.P. Bymaster, K.W. Perry, D.L. Nelson, D.T. Wong, K. Rasmussen, N.A. Moore, D.O. Calligaro, Olanzapine: a basic science update. *Br. J. Psychiatry Suppl.* **(37)** (1999) s36−40.

[323] B.L. Roth, S.C. Craigo, M.S. Choudhary, A. Uluer, F.J. Monsma, Jr., Y. Shen, H.Y. Meltzer, D.R. Sibley, Binding of typical and atypical antipsychotic agents to 5-hydroxytryptamine-6 and 5-hydroxytryptamine-7 receptors. *J. Pharmacol. Exp. Ther.* **268**(3) (1994) 1403−1410.

[324] F.P. Bymaster, J.F. Falcone, D. Bauzon, J.S. Kennedy, K. Schenck, N.W. DeLapp, M.L. Cohen, Potent antagonism of 5-HT_3 and 5-HT_6 receptors by olanzapine. *Eur. J. Pharmacol.* **430**(2−3) (2001) 341−349.

[325] F.P. Bymaster, J.F. Falcone, Decreased binding affinity of olanzapine and clozapine for human muscarinic receptors in intact clonal cells in physiological medium. *Eur. J. Pharmacol.* **390**(3) (2000) 245−248.

[326] B. Fulton, K.L. Goa, Olanzapine. A review of its pharmacological properties and therapeutic efficacy in the management of schizophrenia and related psychoses. *Drugs* **53**(2) (1997) 281−298.

[327] G.D. Tollefson, C.M. Beasley, Jr., P.V. Tran, J.S. Street, J.A. Krueger, R.N. Tamura, K.A. Graffeo, M.E. Thieme, Olanzapine versus haloperidol in the treatment of schizophrenia and schizoaffective and schizophreniform disorders: results of an international collaborative trial. *Am. J. Psychiatry* **154**(4) (1997) 457−465.

[328] M. Tohen, T.M. Sanger, S.L. McElroy, G.D. Tollefson, K.N.R. Chengappa, D.G. Daniel, F. Petty, F. Centorrino, R. Wang, S.L. Grundy, M.G. Greaney, T.G. Jacobs, S.R. David, V. Toma, and The Olanzapine HGEH study group, Olanzapine versus placebo in the treatment of acute mania. *Am. J. Psychiatry* **156**(5) (1999) 702−709.

[329] C.M. Beasley, Jr., G. Tollefson, P. Tran, W. Satterlee, T. Sanger, S. Hamilton, and The Olanzapine HGAD study group, Olanzapine versus placebo and haloperidol: acute phase results of the North American double-blind olanzapine trial. *Neuropsychopharmacol.* **14**(2) (1996) 111−123.

[330] H.Y. Meltzer, Pre-clinical pharmacology of atypical antipsychotic drugs: a selective review. *Br. J. Psychiatry Suppl.* **29** (1996) s23−31.

[331] J.M. Kane, M.G. Woerner, S. Pollack, A.Z. Safferman, J.A. Lieberman, Does clozapine cause tardive dyskinesia? *J. Clin. Psychiatry* **54**(9) (1993) 327**–**330.

[332] D.V. Jeste, J.P. Lacro, A. Bailey, E. Rockwell, M.J. Harris, M.P. Caligiuri, Lower incidence of tardive dyskinesia with risperidone compared with haloperidol in older patients. *J. Am. Geriatr. Soc.* **47**(6) (1999) 716**–**719.

[333] H.Y. Meltzer, Role of serotonin in the action of atypical antipsychotic drugs. *Clin. Neurosci.* **3**(2) (1995) 64**–**75.

[334] S. Kapur, P. Seeman, Does fast dissociation from the dopamine D_2 receptor explain the action of atypical antipsychotics?: A new hypothesis. *Am. J. Psychiat.* **158**(3) (2001) 360−369.

[335] J. Lavalaye, J. Booij, D.H. Linszen, L. Reneman, E.A. van Royen, Higher occupancy of muscarinic receptors by olanzapine than risperidone in patients with schizophrenia A [^{123}I]-IDEX SPECT study. *Psychopharmacol.* **156**(1) (2001) 53**–**57.

[336] T. Hori, K. Makabe, K. Nemoto, T. Asada, Hypersalivation induced by olanzapine with fluvoxamine. *Prog. Neuro-Psychopharmacol. Biol. Psychiatry* **30**(4) (2006) 758−760.

[337] D.O. Perkins, R.K. McClure, Hypersalivation coincident with olanzapine treatment. *Am. J. Psychiatry* **155**(7) (1998) 993**–**994.

[338] E. Richelson, Receptor pharmacology of neuroleptics: relation to clinical effects. *J. Clin. Psychiatry* **60**(Suppl. 10) (1999) 5−14.

[339] N. Bhana, C.M. Perry, Olanzapine: a review of its use in the treatment of bipolar I disorder. *CNS Drugs* **15**(11) (2001) 871−904.

[340] F.A. Wiesel, Ziprasidone: from receptor profile to patient outcomes−a review of short-term efficacy studies. *Euro. Psychiat.* **13** (Suppl. 4) (1998) 225s.

[341] M. Krzystanek, H.I. Trzeciak, I. Krupka-Matuszczyk, E. Krzystanek, Antidepressant-like influence of olanzapine on membrane phospholipase D activity in rat brain. *Eur. Neuropsychopharmacol.* **12** (Suppl. 3) (2002) 297–298.

[342] K. Melkersson, Serum creatine kinase levels in chronic psychosis patients–a comparison between atypical and conventional antipsychotics. *Prog. Neuro-Psychopharmacol. Biol. Psychiatry* **30**(7) (2006) 1277–1282.

[343] M.M. Khan, V.V. Parikh, S.P. Mahadik, Antipsychotic drugs differentially modulate apolipoprotein D in rat brain. *J. Neurochem.* **86**(5) (2003) 1089–1100.

[344] J.K. Boyles, L.M. Notterpek, M.R. Wardell, S.C. Rall, Jr., Identification, characterization and tissue distribution of apolipoprotein D in the rat. *J. Lipid Res.* **31**(12) (1990) 2243–2256.

[345] P.P. Desai, C.H. Bunker, F.A.M. Ukoli, M.I. Kamboh, Genetic variation in the apolipoprotein D gene among African blacks and its significance in lipid metabolism. *Atherosclerosis* **163**(2) (2002) 329–338.

[346] W.Y. Ong, C.P. Lau, S.K. Leong, U. Kumar, S. Suresh, S.C. Patel, Apolipoprotein D gene expression in the rat brain and light and electron microscopic immunocytochemistry of apolipoprotein D expression in the cerebellum of neonatal, immature and adult rats. *Neuroscience* **90**(3) (1999) 913–922.

[347] V.V. Parikh, M.M. Khan, S.P. Mahadik, Differential effects of antipsychotics on expression of antioxidant enzymes and membrane lipid peroxidation in rat brain. *J. Psychiatric Res.* **37**(1) (2003) 43–51.

[348] D.R. Evans, V.V. Parikh, M.M. Khan, C. Coussons, P.F. Buckley, S.P. Mahadik, Red blood cell membrane essential fatty acid metabolism in early psychotic patients following antipsychotic drug treatment. *Prostag. Leukotr. Essential Fatty Acids* **69**(6) (2003) 393–399.

[349] S.P. Mahadik, D.R. Evans, H. Lal, Oxidative stress and role of antioxidant and ω-3 essential fatty acid supplementation in schizophrenia. *Prog. Neuro-Psychopharmacol. Biol. Psychiatry* **25**(3) (2001) 463–493.

[350] S.P. Mahadik, D.R. Evans, A. Terry, W. Hill, Neuroprotective actions of atypical antipsychotics in schizophrenia: improved cognitive performance and underlying mechanisms of action. *Schizophr. Res.* **49**(2) (*Suppl. 1*) (2001) 94.

[351] A.C. Rego, C.R. Oliveira, Influence of lipid peroxidation on [^{3}H]ketanserin binding to 5-HT$_2$ prefrontal cortex receptors. *Neurochem. Int.* **27**(6) (1995) 489–496.

[352] D.R. Evans, S.P. Mahadik, J. Akin, W. Evans, D. Jain, Cell membrane essential fatty acid status in drug-naive first-episode psychotic patients and its relation to outcome. *Schizophr. Res.* **49**(2) (*Suppl. 1*) (2001) 83.

[353] D.F. Horrobin, The membrane phospholipid hypothesis as a biochemical basis for the neurodevelopmental concept of schizophrenia. *Schizophr. Res.* **30**(3) (1998) 193–208.

[354] A.U. Gjerde, W. Nerdal, H. Holmsen, Typical versus atypical antipsychotic drugs in biomembrane interaction–A surface plasmon resonance study. *Manuscript in preparation*, 2005.

[355] K. Ondrias, A. Staško, V. Mišik, J. Reguli, E. Švajdlenka, Comparison of perturbation effect of propranolol, verapamil, chlorpromazine and carbisocaine on lecithin liposomes and brain total lipid liposomes. An EPR spectroscopy study. *Chem.-Biol. Interact.* **79**(2) (1991) 197–206.

[356] N. Maruoka, T. Murata, N. Omata, Y. Takashima, H. Tanii, Y. Yonekura, Y. Fujibayashi, Y. Wada, Effects of chlorpromazine on plasma membrane permeability and fluidity in the rat brain: A dynamic positron autoradiography and fluorescence polarization study. *Prog. Neuro-Psychopharmacol. Biol. Psychiatry* **31**(1) (2007) 178–186.

[357] A.U. Gjerde, H. Holmsen, Chlorpromazine interaction with phospholipid membranes: A fluorescence spectroscopy study. *Manuscript in preparation*, 2006.

[358] J.M. Ritchie, B. Ritchie, P. Greengard, The active structure of local anesthetics. *J. Pharmacol. Exp. Ther.* **150**(1) (1965) 152–159.

[359] S.P. Gupta, Quantitative structure–activity relationship studies on local anesthetics. *Chem. Rev.* **91**(6) (1991) 1109–1119.

[360] P. Chiap, B. Boulange, L. Fotsing, P. Hubert, J. Crommen, Liquid chromatographic analysis of local anesthetics in human plasma after sample preparation by on-line dialysis. Optimization by use of experimental design. *Chromatographia* **53**(11−12) (2001) 678−686.

[361] G. Vanderkooi, Dibucaine fluorescence and lifetime in aqueous media as a function of pH. *Photochem. Photobiol.* **39**(6) (1984) 755−762.

[362] J. Schmidtmayer, W. Ulbricht, Interaction of lidocaine and benzocaine in blocking sodium channels. *Pflügers Arch.* **387**(1) (1980) 47−54.

[363] N. Chidambaram, D. J. Burgess, Effect of nonionic surfactant on transport of surface-active and non-surface-active model drugs and emulsion stability in triphasic systems. *AAPS PharmSci.* **2**(3) (2000) (article 30).

[364] M.M. Francis, E.Y. Cheng, G.A. Weiland, R.E. Oswald, Specific activation of the α7 nicotinic acetylcholine receptor by a quaternary analog of cocaine. *Mol. Pharmacol.* **60**(1) (2001) 71–79.

[365] S.F. Malamed, S. Gagnon, D. Leblanc, Efficacy of articaine: a new amide local anesthetic. *J. Am. Dent. Assoc.* **131**(5) (2000) 635−642.

[366] A.M. Shanes, W.H. Freygang, H. Grundfest, E. Amatniek, Anesthetic and calcium action in the voltage-clamped squid giant axon. *J. Gen. Physiol.* **42**(4) (1959) 793−802.

[367] J.F. Butterworth, G.R. Strichartz, Molecular mechanisms of local anesthesia: a review. *Anesthesiology* **72**(4) (1990) 711−734.

[368] G.B. Weiss, R.E. Coalson, L. Hurwitz, K transport and mechanical responses of isolated longitudinal smooth muscle from guinea pig ileum. *Am. J. Physiol.* **200**(4) (1962) 789–793.

[369] L. Hurwitz, F. Battle, G.B. Weiss, Action of the calcium antagonists cocaine and ethanol on contraction and potassium efflux of smooth muscle. *J. Gen. Physiol.* **46**(2) (1962) 315–332.

[370] A. Yoshino, T. Yoshida, H. Okabayashi, H. Kamaya, I. Ueda, ^{19}F and ^{1}H NMR and NOE study on halothane-micelle interaction: residence location of anesthetic molecules. *J. Colloid. Interface Sci.* **198**(2) (1998) 319−322.

[371] L.F. Fraceto, L. de. M.A. Pinto, L. Franzoni, A.A.C. Braga, A. Spisni, S. Schreier, E. de Paula, Spectroscopic evidence for a preferential location of lidocaine inside phospholipid bilayers. *Biophys. Chem.* **99**(3) (2002) 229−243.

[372] L.F. Fraceto, A. Spisni, S. Schreier, E. de Paula, Differential effects of uncharged aminoamide local anesthetics on phospholipid bilayers, as monitored by ^{1}H-NMR measurements. *Biophys. Chem.* **115**(1) (2005) 11−18.

[373] S.W. Postma, W.A. Catterall, Inhibition of binding of [^{3}H]batrachotoxinin A 20-α-benzoate to sodium channels by local anesthetics. *Mol. Pharmacol.* **25**(2) (1984) 219−227.

[374] G.K. Wang, Binding affinity and stereoselectivity of local anesthetics in single batrachotoxin−activated Na^{+} channels. *J. Gen. Physiol.* **96**(5) (1990) 1105−1127.

[375] S.V. Balasubramanian, R.B. Campbell, R.M. Straubinger, Propofol, a general anesthetic, promotes the formation of fluid phase domains in model membranes. *Chem. Phys. Lipids* **114**(1) (2002) 35−44.

[376] J. R. Trudell, A unitary theory of anesthesia based on lateral phase separation in nerve membranes. *Anesthesiology* **46**(1) (1977) 5−10.

[377] M. Suwalsky, C. Schneider, F. Villena, B. Norris, H. Cárdenas, F. Cuevas, C.P. Sotomayor, Structural effects of the local anesthetic bupivacaine hydrochloride on the human erythrocyte membrane and molecular models. *Blood Cells Mol. Dis.* **29**(1) (2002) 14–23.

[378] J. Westman, Y. Boulanger, A. Ehrenberg, I.C.P. Smith, Charge and pH dependent drug binding to model membranes. A ^{2}H-NMR and light absorption study. *Biochim. Biophys. Acta* **685**(3) (1982) 315−328.

[379] J. Cerbón, NMR evidence for the hydrophobic interaction of local anesthetics: Possible relation to their potency. *Biochim. Biophys. Acta* **290** (1972) 51−57.

[380] E.C. Kelusky, I.C.P. Smith, The influence of local anesthetics on molecular organization in phosphatidylethanolamine membranes. *Mol. Pharmacol.* **26**(2) (1984) 314−321.

[381] E. de Paula, S. Schreier, Use of a novel method for determination of partition coefficients to compare the effect of local anesthetic on membrane structure. *Biochim. Biophys. Acta* **1240**(1) (1995) 25−33.

[382] S. Schreier, W.A. Frezzatti, Jr., P.S. Araujo, H. Chaimovich, I.M. Cuccovia, Effect of lipid membranes on the apparent p*K* of the local anesthetic tetracaine spin label and titration studies. *Biochim. Biophys. Acta* **769**(1) (1984) 231–237.

[383] R. Muschaweck, R. Rippel, A new local anesthetic (carticaine) from the thiophene-series (author's translation). *Prakt. Anaesth.* **9**(3) (1974) 135–146.

[384] S.F. Malamed, *Handbook of Local Anesthesia.* Mosby-Year Book, St. Louis, 1997.

[385] S.F. Malamed, S. Gagnon, D. Leblanc, Articaine hydrochloride: a study of the safety of a new amide local anesthetic. *J. Am. Dent. Assoc.* **132** (2) (2001) 177−185.

[386] S.F. Malamed, S. Gagnon, D. Leblanc, A comparison between articaine HCl and lidocaine HCl in pediatric dental patients. *Ped. Dent.* **22**(4) (2000) 307–311.

[387] T.B. Vree, A.M. Baars, G.E.C.J.M. van Oss, L.H.D.J. Booij, High-performance liquid chromatography and preliminary pharmacokinetics of articaine and its 2-carboxy metabolite in human serum and urine. *J. Chromatogr. B Biomed. Sci. Appl.* **424**(2) (1988) 440−444.

[388] M. Grossmann, G. Sattler, H. Pistner, R. Oertel, K. Richter, S. Schinzel, L. D. Jacobs, Pharmacokinetics of articaine hydrochloride in tumescent local anesthesia for liposuction. *J. Clin. Pharmacol.* **44**(11) (2004) 1282−1289.

[389] S. Schreier, S.V.P. Malheiros, E. de Paula, Surface active drugs: self-association and interaction with membranes and surfactants. Physicochemical and biological aspects. *Biochim. Biophys. Acta* **1508**(1−2) (2000) 210−234.

[390] H. Lüllman, P.B.W.M. Timmermans, G.M. Weikert, A. Ziegler, Accumulation of drugs by guinea pig isolated atria. Quantitative correlations. *J. Med. Chem.* **23**(5) (1980) 560−565.

[391] M. Suwalsky, C. Schneider, F. Villena, B. Norris, H. Cárdenas, F. Cuevas, C.P. Sotomayor, A study of the perturbation effects of the local anesthetic procaine on human erythrocyte and model membranes and of modifications of the sodium transport in toad skin. *Biophys. Chem.* **116**(3) (2005) 227−235.

[392] H.G.L. Coster, V.J. James, C. Berthet, A. Miller, Location and effect of procaine on lecithin/cholesterol membranes using X-ray diffraction methods. *Biochim. Biophys. Acta* **641**(1) (1981) 281−285.

[393] M.J. Neal, K.W. Butler, C.F. Polnaszek, I.C.P. Smith, The influence of anesthetics and cholesterol on the degree of molecular organization and mobility of ox brain white matter. Lipids in multibilayer membranes: a spin probe study using spectral simulation by the stochastic method. *Mol. Pharmacol.* **12**(1) (1976) 144−155.

[394] L. de M.A. Pinto, D.K. Yokaichiya, L.F. Fraceto, E. de Paula, Interaction of benzocaine with model membranes. *Biophys. Chem*. **87**(2−3) (2000) 213−223.

[395] S. Kaneshina, H. Satake, T. Yamamoto, Y. Kume. H. Matsuki, Partitioning of local anesthetic dibucaine into bilayer membranes of dimyristoylphosphatidylcholine. *Colloids Surf. B* **10**(1) (1997) 51−57.

[396] T. Hata, T. Sakamato, H. Matsuki, S. Kaneshina, Partition coefficients of charged and uncharged local anesthetics into dipalmitoylphosphatidylcholine bilayer membrane: estimation from pH dependence on the depression of phase transition temperatures. *Colloids Surf. B* **22**(1) (2000) 77−84.

[397] M.S. Fernández, E. Calderón, Formation of micelles and membrane action of the local anesthetic tetracaine hydrochloride. *Biochim. Biophys. Acta* **597**(1) (1980) 83−91.

[398] F. de Verteuil, D.A. Pink, E.B. Vadas, M.J. Zuckermann, Phase diagrams for impure lipid systems: Application to lipid/anaesthetic mixtures. *Biochim. Biophys. Acta* **640**(1) (1981) 207−222.

[399] S.V.P. Malheiros, L.M.A. Pinto, L. Gottardo, D.K. Yokaichiya, L.F. Fraceto, N.C. Meirelles, E. de Paula, A new look at the hemolytic effect of local anesthetics, considering their real membrane/water partitioning at pH 7.4. *Biophys. Chem.* **110**(3) (2004) 213–221.

[400] I.I. Rabi, J.R. Zacharias, S. Millman, P. Kusch, A new method of measuring nuclear magnetic moment. *Phys. Rev.* **53**(4) (1938) 318.

[401] F. Bloch, Nuclear induction. *Phys. Rev.* **70**(7−8) (1946) 460−474.

[402] N. Bloembergen, E.M. Purcell, R.V. Pound, Relaxation effects in nuclear magnetic resonance absorption. *Phys. Rev.* **73**(7) (1948) 679−712.

[403] *Nobel Lecture for Felix Bloch and Edward Mills Purcell* (1952).

[404] D.D. Laws, H.-M.L. Bitter, A. Jerschow, Solid-state NMR spectroscopic methods in chemistry. *Angew. Chem. Int. Ed. Engl.* **41**(17) (2002) 3096−3129.

[405] M.J. Duer, *Introduction to Solid State NMR Spectroscopy*. Blackwell publishing, Oxford, 2004.

[406] M.H. Levitt, *Spin dynamics: Basics of Nuclear Magnetic Resonance*. Wiley, Chichester, 2003.

[407] H. Saitô, I. Ando, A. Naito, *Solid State NMR Spectroscopy for Biopolymers: Principles and Applications*. Springer, Dordrecht, 2006.

[408] M. Mehring, *Principles of High Resolution NMR in Solids* (2nd Edition). Springer−Verlag, Berlin, 1983.

[409] C.A. Fyfe, *Solid State NMR for Chemists*. CFC Press, Guelph, 1983.

[410] A. Abragam, *The Principles of Nuclear Magnetism*. Clarendon Press, Oxford, 1961.

[411] F. Bloch, Dynamical theory of nuclear induction. II. *Phys. Rev.* **102**(1) (1956) 104−135.

[412] F. Bloch, Theory of line narrowing by double-frequency irradiation. *Phys. Rev.* **111**(3) (1958) 841−853.

[413] A. J. Shaka, J. Keeler, Broadband spin decoupling in isotropic-liquids. *Prog. Nucl. Magn. Reson. Spectrosc.* **19**(1) (1987) 47−129.

[414] M.H. Levitt, Composite pulses. *Prog. Nucl. Magn. Reson. Spectrosc.* **18**(2) (1986) 61−122.

[415] J. Kempf, H.W. Spiess, U. Haeberlen, H. Zimmermann, ^{13}C Anisotropic chemical shift in a single of benzophenone. *Chem. Phys. Lett.* **17**(1) (1972) 39−42.

[416] A.R. Edmonds, *Angular Momentum in Quantum Mechanics (Investigations in Physics)* (Reissue Edition). Princeton University Press, New Jersey, 1996.

[417] U. Haeberlen, "*High Resolution NMR in Solids: Selective Averaging*," in *Advances in Magnetic Resonance, Supplement 1*. Academic Press, New York, 1976.

[418] M. Mehring, *High Resolution NMR in Solids*. Springer, New York, 1983.

[419] J. Schaefer, E.O. Stejskal, Carbon-13 nuclear magnetic resonance of polymers spinning at the magic angle. *J. Am. Chem. Soc.* **98**(4) (1976) 1031−1032.

[420] E.R. Andrew, A. Bradbury, R.G. Eades, Nuclear magnetic resonance spectra from a crystal rotated at high speed. *Nature* **182**(4650) (1958) 1659.

[421] E.R. Andrew, The narrowing of NMR spectra of solids by high-speed specimen rotation and the resolution of chemical shift and spin multiplet structures for solids. *Prog. Nucl. Magn. Reson. Spectrosc.* **8**(1) (1971) 1−39.

[422] E.R. Andrew, Magic angle spinning in solid state n.m.r. spectroscopy. *Phil. Trans. R. Soc. Lond. A* **299** (1452) (1981) 505−520.

[423] I.J. Lowe, Free induction decays of rotating solids. *Phys. Rev. Lett.* **2**(7) (1959) 285−287.

[424] A.E. Bennett, C.M. Rienstra, M. Auger, K.V. Lakshmi, R.G. Griffin, Heteronuclear decoupling in rotating solids. *J. Chem. Phys.* **103**(16) (1995) 6951−6958.

[425] A. Detken, E.H. Hardy, M. Ernst, B.H. Meier, Simple and efficient decoupling in magic-angle spinning solid-state NMR: the XiX scheme. *Chem. Phys. Lett.* **356**(3−4) (2002) 298−304.

[426] M. Ernst, Heteronuclear spin decoupling in solid-state NMR under magic-angle sample spinning. *J. Magn. Reson.* **162**(1) (2003) 1−34.

[427] W.S. Veeman, D.J. Greenslade, ^{13}C chemical shift tensors in organic single crystals [and discussion]. *Phil. Trans. R. Soc. Lond. A* **299** (1452) (1981) 629−641.

[428] A. Samoson, T. Tuherm, J. Past, Ramped-speed cross polarization MAS NMR. *J. Magn. Reson.* **149**(2) (2001) 264−267.

[429] A. Pines, M.G. Gibby, J.S. Waugh, Proton-enhanced nuclear induction spectroscopy. A method for high resolution NMR of dilute spins in solids. *J. Chem. Phys.* **56**(4) (1972) 1776−1777.

[430] A. Pines, M.G. Gibby, J.S. Waugh, Proton-enhanced NMR of dilute spins in solids. *J. Chem. Phys.* **59**(2) (1973) 569−590.

[431] M.H. Levitt, D. Suter, R.R. Ernst, Spin dynamics and thermodynamics in solid-state NMR cross polarization. *J. Chem. Phys.* **84**(8) (1986) 4243–4255.

[432] D.E. Demco, J. Tegenfeldt, J.S. Waugh, Dynamics of cross relaxation in nuclear magnetic double resonance. *Phys. Rev. B* **11**(11) (1975) 4133–4151.

[433] D. Marks, S. Vega, A theory for cross-polarization NMR of nonspinning and spinning samples. *J. Magn. Reson. A* **118**(2) (1996) 157–172.

[434] S.C. Shekar, A. Ramamoorthy, The unitary evolution operator for cross-polarization schemes in NMR. *Chem. Phys. Lett.* **342**(1−2) (2001) 127–134.

[435] S.C. Shekar, A. Ramamoorthy, R.J. Wittebort, Determination of the chemical shielding tensor orientation from two or one of the three conventional rotations of a single crystal. *J. Magn. Reson.* **155**(2) (2002) 257–262.

[436] A.E. Derome, *Modern NMR Techniques for Chemistry Research*. Pergamon, Oxford, 1987.

[437] S.R. Hartmann, E.L. Hahn, Nuclear double resonance in the rotating frame. *Phys. Rev.* **128**(5) (1962) 2042−2053.

[438] L. Müller, A. Kumar, T. Baumann, R.R. Ernst, Transient oscillations in NMR cross-polarization experiments in solids. *Phys. Rev. Lett.* **32**(25) (1974) 1402−1406.

[439] E.O. Stejskal, J. Schaefer, J.S. Waugh, Magic-angle spinning and polarization transfer in proton-enhanced NMR. *J. Magn. Reson. (1969)* **28**(1) (1977) 105−112.

[440] R.R. Ernst, G. Bodenhausen, A. Wokaun, *Principles of Nuclear Magnetic Resonance in One and Two dimensions*. Oxford University Press, Oxford, 1987.

[441] F. Horii, A. Hirai, R. Kitamaru, CP/MAS carbon-13 NMR study of spin relaxation phenomena of cellulose containing crystalline and noncrystalline components. *J. Carbohydr. Chem.* **3**(4) (1984) 641−662.

[442] D.L. Vanderhart, Natural-abundance ^{13}C–^{13}C spin exchange in rigid crystalline organic solids. *J. Magn. Reson. (1969)* **72**(1) (1987) 13−47.

[443] R. Kitamaru, F. Horii, K. Murayama, Noncrystalline contents in linear polyethylene samples, crystallized from the melt and dilute solution as revealed by proton dipole decoupled/magic angle sample spinning ^{13}C NMR. *Polym. Bull.* **7**(11−12) (1982) 583−588.

[444] O.B. Peersen, X.L. Wu, I. Kustanovich, S.O. Smith, Variable-amplitude cross-polarization MAS NMR. *J. Magn. Reson. A* **104**(3) (1993) 334−339.

[445] G. Metz, X.L. Wu, S.O. Smith, Ramped-amplitude cross polarization in magic-angle-spinning NMR. *J. Magn. Reson. A* **110**(2) (1994) 219−227.

[446] O.B. Peersen, X.L. Wu, S.O. Smith, Enhancement of CP-MAS signals by variable-amplitude cross polarization. Compensation for inhomogeneous B_1 fields. *J. Magn. Reson. A* **106**(1) (1994) 127−131.

[447] S.M. Zhang, C.L. Czekaj, W.T. Ford, Enhancement of polarization transfer under high-speed MAS using a quasi-adiabatic cross-polarization sequence. *J. Magn. Reson. A* **111**(1) (1994) 87−92.

[448] H. Friebolin, *Basic One− and Two−Dimensional NMR Spectroscopy* (3rd Revised Edition). Wiley−VCH publisher, New York, 1998.

[449] M.H. Levitt, Symmetrical composite pulse sequences for NMR population inversion. I. Compensation of radiofrequency field inhomogeneity. *J. Magn. Reson. (1969)* **48**(2) (1982) 234–264.

[450] J. Keeler, *Understanding NMR Spectroscopy*. Wiley, Chichester, 2005.

[451] U. Haeberlen, "*Solid state NMR in high and very high magnetic fields*," in *NMR Basic Principles and Progress (Vol. 25)*. P. Diehl, E. Fluck, H. Guenther, R. Kosfeld, J. Seelig (Eds.), Springer-Verlag, Berlin (1991) 143.

[452] T.N. Mitchell, B. Costisella, *NMR−From Spectra to Structures: An Experimental Approach*. Springer-Verlag, Berlin Heidelberg, 2004.

[453] M.J. Janiak, D.M. Small, G.G. Shipley, Temperature and compositional dependence of the structure of hydrated dimyristoyl lecithin. *J. Biol. Chem.* **254**(13) (1979) 6068−6078.

[454] D.M. Small, Phase equilibria and structure of dry and hydrated egg lecithin. *J. Lipid Res.* **8**(6) (1967) 551−557.

[455] H. Hägerstrand, M. Danieluk, M. Bobrowska-Hägerstrand, A. Iglič, A. Wróbel, B. Isomaa, M. Nikinmaa, Influence of band 3 protein absence and skeletal structures on amphiphile- and Ca^{2+}-induced shape alterations in erythrocytes: a study with lamprey (*Lampetra fluviatilis*), trout (*Onchorhynchus mykiss*) and human erythrocytes. *Biochim Biophys Acta* **1466**(1−2) (2000) 125–138.

[456] M. Yabuki, N. Tani, T. Yoshioka, H. Nishibe, H. Kanamaru, H. Kaneko, Local thrombus formation in the site of intravenous injection of chlorpromazine: possible colloid-osmotic lysis of the local endothelial cells. *Biol. Pharm. Bull.* **23**(8) (2000) 957–961.

[457] A.A. Hidalgo, W. Caetano, M. Tabak, O.N. Oliveria, Jr., Interaction of two phenothiazine derivatives with phospholipid monolayers. *Biophys. Chem.* **109**(1) (2004) 85−104.

[458] A. Broniec, A.B. Ølmheim, A.U. Gjerde, H. Holmsen, Trifluoperazine causes disturbance in glycerophospholipid monolayers containing phosphatidylserine (PS): effects of pH, acyl unsaturation and proportion of PS. *Manuscript in preparation*, 2006.

[459] K.E. McAuley, P.K. Fyfe, J.P. Ridge, N.W. Isaacs, R.J. Cogdell, M.R. Jones, Structural details of an interaction between cardiolipin and an integral membrane protein. *Proc. Natl. Acad. Sci. USA* **96**(26) (1999) 14706–14711.

[460] P.R. Cullis, B. de Kruyff, R.E. Richards, Factors affecting the motion of the polar headgroup in phospholipid bilayers. A ^{31}P NMR study of unsonicated phosphatidylcholine liposomes. *Biochim. Biophys. Acta* **426**(3) (1976) 433– 446.

[461] H.I. Petrache, S.E. Feller, J.F. Nagle, Determination of component volumes of lipid bilayers from simulations. *Biophys. J.* **72**(5) (1997) 2237–2242.

[462] K. Rajamoorthi, H.I. Petrache, T.J. McIntosh, M.F. Brown, Packing and viscoelasticity of polyunsaturated ω-3 and ω-6 lipid bilayers as seen by ^{2}H NMR and X-ray diffraction. *J. Am. Chem. Soc.* **127**(5) (2005) 1576–1588.

[463] C. Leidy, K. Gousset, J. Ricker, W.F. Wolkers, N.M. Tsvetkova, F. Tablin, J.H. Crowe, Lipid phase behavior and stabilization of domains in membranes of platelets. *Cell Biochem. Biophys.* **40**(2) (2004) 123–148.

[464] L.L. Holte, F. Separovic, K. Gawrisch, Nuclear magnetic resonance investigation of hydrocarbon chain packing in bilayers of polyunsaturated phospholipids. *Lipids* **31**(1) (1996) Suppl. S199–S203.

[465] D.T. Frazier, T. Narahashi, M. Yamada, The site of action and active form of local anesthetics. II. Experiments with quaternary compounds. *J. Pharmacol. Exp. Ther.* **171**(1) (1970) 45−51.

[466] T. Narahashi, D.T. Frazier, M. Yamada, The site of action and active form of local anesthetics. I. Theory and pH experiments with tertiary compounds. *J. Pharmacol. Exp. Ther.* **171**(1) (1970) 32−44.

[467] J.M. Ritchie, P. Greengard, On the active structure of local anesthetics. *J. Pharmacol. Exp. Ther.* **133**(2) (1961) 241−245.

[468] K.R. Courtney, G.R. Strichartz, G.R. in *Local Anesthetics, Handbook of Experimental Pharmacology* (Vol. 81), G.R. Strichartz (Ed.), Springer-Verlag, Berlin (1987) 53−94.

[469] C.F. Schmidt, Y. Barenholz, C. Huang, T.E. Thompson, Phosphatidylcholine ^{13}C-labeled carbonyls as a probe of bilayer structure. *Biochemistry* **16**(18) (1977) 3948−3954.

[470] A. Jutila, T. Söderlund, A.L. Pakkanen, M. Huttunen, P.K.J. Kinnunen, Comparison of the effects of clozapine, chlorpromazine, and haloperidol on membrane lateral heterogeneity. *Chem. Phys. Lipids* **112**(2) (2001) 151−163.

[471] V.M. Meidan, J.S. Cohen, N. Amariglio, D. Hirsch-Lerner, Y. Barenholz, Interaction of oligonucleotides with cationic lipids: the relationship between electrostatics, hydration and state of aggregation. *Biochim. Biophys. Acta* **1464**(2) (2000) 251−261.

[472] L.R. Brown, K. Wüthrich, NMR and ESR studies of the interactions of cytochrome *c* with mixed cardiolipin-phosphatidylcholine vesicles. *Biochim. Biophys. Acta* **468**(3) (1977) 389−410.

[473] T. Mavromoustakos, E. Theodoropoulou, D.-P. Yang, The use of high-resolution solid-state NMR spectroscopy and differential scanning calorimetry to study interactions of anesthetic steroids with membrane. *Biochim. Biophys. Acta* **1328**(1) (1997) 65−73.

[474] D.L. Holwerda, P.D. Ellis, R.E. Wuthier, Carbon-13 and phosphorus-31 nuclear magnetic resonance studies on the interaction of calcium with phosphatidylserine. *Biochemistry* **20**(2) (1981) 418−428.

[475] E. Oldfield, F. Adebodun, J. Chung, B. Montez, K.D. Park, H.-b. Le, B. Phillips, Carbon-13 nuclear magnetic resonance spectroscopy of lipids: differential line broadening due to cross-correlation effects as a probe of membrane structure. *Biochemistry* **30**(46) (1991) 11025−11028.

[476] B.A. Cornell, M. Keniry, The effect of cholesterol and gramicidin A' on the carbonyl groups of dimyristoylphosphatidylcholine dispersions. *Biochim. Biophys. Acta* **732**(3) (1983) 705−710.

[477] S.M. Reutzel-Edens, J.K. Bush, P.A. Magee, G.A. Stephenson, S.R. Byrn, Anhydrates and hydrates of olanzapine: crystallization, solid-state characterization, and structural relationships. *Cryst. Growth Des.* **3**(6) (2003) 897−907.

[478] L.L. Holte, F. Separovic, K. Gawrisch, Nuclear magnetic resonance investigation of hydrocarbon chain packing in bilayers of polyunsaturated phospholipids. *Lipids* **31**(1) (1996) Suppl: S199−S203.

[479] I. Wawrzycka-Gorczyca, P. Borowski, J. Osypiuk-Tomasik, L. Mazur, A.E. Koziol, Crystal structure of olanzapine and its solvates. Part 3. Two and three-component solvates with water, ethanol, butan-2-ol and dichloromethane. *J. Mol. Struct.* **830**(1–3) (2007) 188–197.

[480] T. Gullion, J. Schaefer, Detection of weak heteronuclear dipolar coupling by rotational-echo double-resonance nuclear magnetic resonance. *Adv. Magn. Reson.* **13** (1989) 57–83.

[481] T. Gullion, J. Schaefer, Rotational-echo double-resonance NMR. *J. Magn. Reson. (1969)* **81**(1) (1989) 196–200.

[482] K.T. Mueller, T.P. Jarvie, D.J. Aurentz, B.W. Roberts, The REDOR transform: direct calculation of internuclear couplings of dipolar-dephasing NMR data. *Chem. Phys. Lett.* **242**(6) (1995) 535–542.

[483] T.P. Jarvie, G.T. Went, K.T. Mueller, Simultaneous multiple distance measurements in peptides via solid-state NMR. *J. Am. Chem. Soc. (Communication)* **118**(22) (1990) 6347–6364.

APPENDIX

hpdec.av

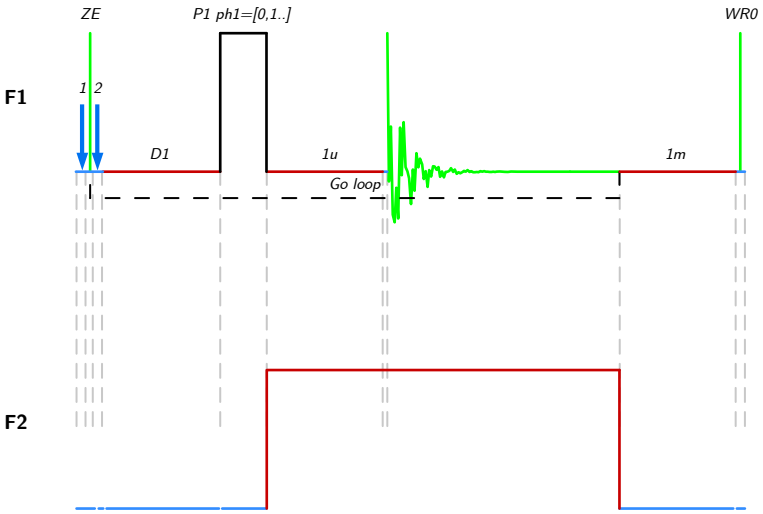


```
;hpdec.av
;acquisition on X with hp proton decoupling
;suitable for various types of decoupling
;set:
;d1 :       recycle delay
;d30 :      =1s/cnst31-p4, for pidec12 and pidec13, pi-pulse decoupling
;d31 :      =1s/cnst31, 1 rotor period
;p1 :       X 90 degree pulse
;p5 :       LG 360 degree pulse
;p6 :       =p5-0.4u
;p10 :      pulse length for phase modulated pulses (e.g. PMLG, DUMBO)
;p20 :      =p21-0.4u
;p21 :      H 90 at power level pl13 (BLEW12)
;p22 :      H 180 at power level pl13 (pidec)
;p29 :      5 - 10 us, to avoid exact rotor synchronization
;p30 :      =p31-0.4u → calculated pulse for cpd
;p31 :      pulse length in decoupling sequence
;pl1 :      X power level for excitation pulse
;pl2 :      =119 dB, not used
;pl12 :     power level for standard proton decoupling
;pl13 :     e.g. used in tppm13, pidec13, cw13, pidec13, cwlg, cwlgs
;spnam1:   lgs-1, lgs-4 or pmlg-36,
;l31 :      number of rotor cycles for XiX (=3)
;cnst20 :   proton RF field to calculate LG parameters
;cnst21 :   =0, proton offset
;cnst22 :   +ve Lee-Goldburg offset
;cnst23 :   -ve Lee-Goldburg offset
;cnst24 :   additional Lee-Goldburg offset
```

```
;cnst31 :    spinning frequency
;cpdprg2 :  sequence used for decoupling (tppm15, cw, etc.)
;ZGPTNS :  options for zg must be blew12, xix, pidec, lg, or tppm
# ifdef blew12
"p20=p21-0.4u"
# endif /* blew12 */
# ifdef xix
"p31=(1s*l31)/cnst31+p29"
# endif /* xix */
# ifdef pidec
"d30=1s/cnst31-p22"
# endif /* pidec */
# ifdef lg
#include <lgcalc.incl>
# endif
# ifdef tppm
"p30=p31-0.4u"
# endif /* tppm */
1 ze                    ;set RCU to replace mode
2 d1 do:f2              ;recycle delay
  (p1 ph1):f1           ;transmitter pulse on F1 with power level pl1
  1u cpds2:f2           ;use cpdprg2 cw or tppm at power pl12
  go=2 ph31             ;make sure the adc is finished, turn decoupling off
  1m do:f2
  wr #0                 ;save data in current data set
exit
ph0= 0                  ;constant phase for acquisition
ph1= 0 1 2 3            ;simple pulse phase list
ph31=0 1 2 3            ;signal routing corresponds to pulse phase list
```

hpdec.rel

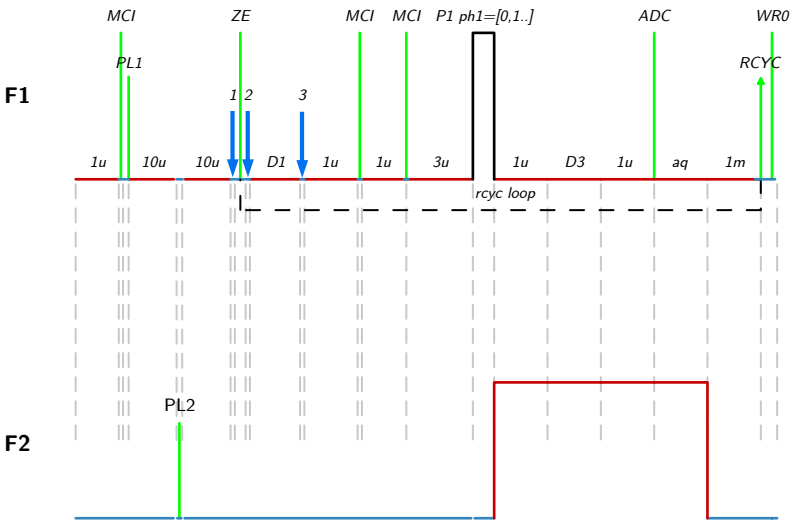


```
;hpdec.rel
;simple one-pulse acquisition using the DDS phase shifter
;with CW proton decoupling, standard method in solids NMR
;read through include files to understand what they mean
#include <preamp.incl>          ;preamp protection in HFs instrument
#include <powswi.incl>          ;enables HP transmitter gain switching
                                ;if new style 400V boards are available
#include <trigg.incl>           ;this provide a trigger output from
                                ;HP router BNC NMR5-13
                                ;this is only necessary for 3 channel
#include <observe.incl>         ;SE-451 and uxnmr versions before
                                ;vs. xwin-nmr.a.9
;the following lines are not necessary starting with xwin-nmr.a.q.
;1u senmr2|11^12^13             ;remove semicolon for X-observation on F1
;1u senmr2^11|12^13             ;remove semicolon for 1H observation on F2
;1u senmr2^11^12|13             ;remove semicolon for F3 observation
10u pl1:f1              ;set pl1 for F1 <default>
10u pl2:f2              ;set pl2 for F2 <default>
1 ze                    ;set RCU to replace mode
2 d1                    ;recycle delay
3 1u setnmr0|10         ;setnmr 0|10 all preamps
  1u setnmr5|13         ;provide a scope trigger at HP router
  3u:f1  ph1            ;this line is not necessary if phaser is set to 3u in edscon
  (p1 ph1):f1           ;transmitter pulse on F1 with power level Pl1
  1u cw:f2              ;turn on CW proton decoupling at power pl2
  d3:f1 ph0             ;reset the RF phase for detection, dead time delay
  1u adc ph31           ;trigger adc, define signal routing in ph31
  aq                    ;allow the adc to sample data
  1m do:f2              ;make sure the adc is finished, turn decoupling off
  rcyc=2                ;repeat NS times with RCU in add mode
  wr #0                 ;save data in current data set
exit
ph0=0                   ;constant phase for acquisition
ph1= 0 1 2 3            ;simple pulse phase list
ph31=0 1 2 3            ;signal routing corresponds to pulse phase list
```

zg

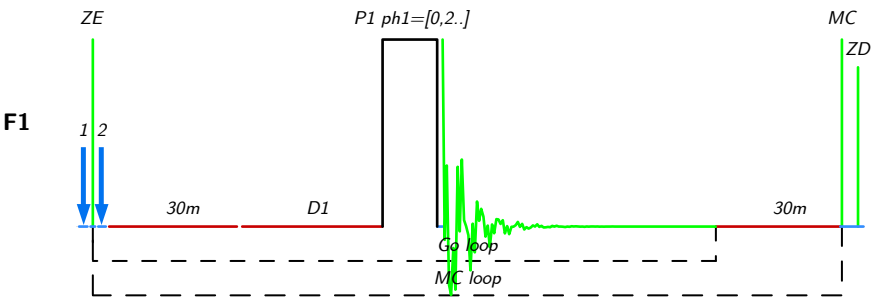


```
;zg
;avance-version (02/05/31)
;1D sequence
#include <Avance.incl>
1 ze
2 30m
  d1
  p1 ph1
  go=2 ph31
  30m mc #0 to 2 F0(zd)
exit
ph1=0 2 2 0 1 3 3 1
ph31=0 2 2 0 1 3 3 1
;pl1 :        f1 channel - power level for pulse (default)
;p1 :         f1 channel - high power pulse
;d1 :         relaxation delay; 1-5 × T1
;NS :         1 × n, total number of scans: NS × TD0
;$ Id: zg,v 1.7 2002/06/12 09:05:19 ber Exp $
```

cp.av

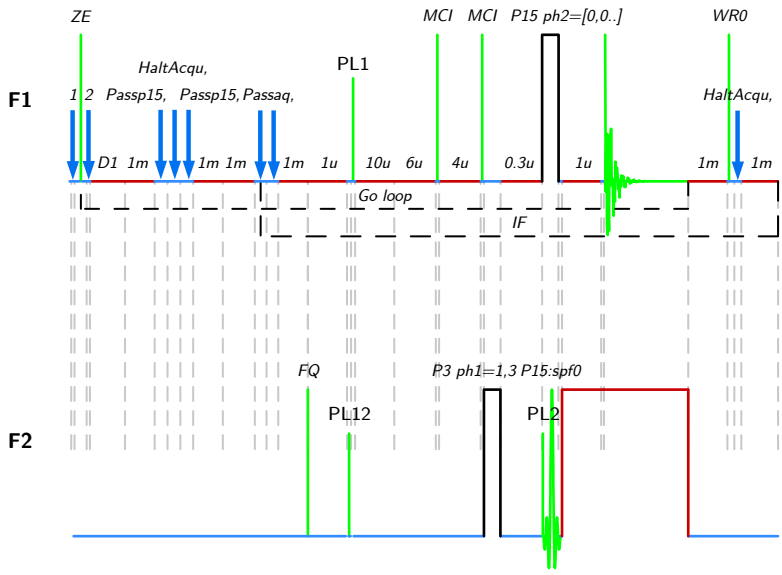


```
;cp.av basic cp experiment
;written by HF 1.3.2001
;changed by JOS 05/06/03
;set: p3 proton 90 at power level pl12
;p15 contact time at pl1 (f1) and pl2 (f2)
;cpdprg2 cw, tppm (at pl12), or lgs, cwlg. cwlgs (LG-decoupling here pl13 is used instead of pl12)
prosol relations=<solids_cp>
#include <lgcalc.incl>
;cnst20=RF field achieved at pl13
;cnst24:additional LG-offset
#include <trigg.incl>
;10 usec trigger pulse at TCU connector I cable 6
#include <tppm.incl>
1 ze                    ;accumulate into an empty memory
2 d1 do:f2              ;recycle delay, decoupler off in go-loop
#include <prp15.prot>
                        ;make sure p15 does not exceed 10 msec
                        ;let supervisor change this pulse program if more is needed
#ifndef lacq            /* disable protection file for long acquisition change decoupling power!
Or you risk probe damage */
                        /* if you set the label lacq (ZGOPTNS -Dlacq), the protection is disabled */
#include <praq.prot>
                        ;allows max. 50 msec acquisition time, supervisor may change to
;max. 1 s at less than 5% duty cycle and reduced decoupling field
#endif
  1u fq=cnst21:f2
  10u pl12:f2 pl1:f1    ;pre-select pl12 drive power for F2, pl1 for F1
   trigg                ;trigger for scope, 10 usec
   p3:f2 ph1            ;proton 90 pulse
   0.3u
   (p15 ph2):f1 (p15:spf0 pl2 ph10):f2
;contact pulse with square or ramp
```

```
  1u cpds2:f2          ;pl12 is used here with tppm, pl13 with cwlg, cwlgs
  go=2 ph31            ;select appropriate decoupling sequence, cw or
                       ;tppm, both executed at power level 12, or lgs
                       ;executed at power level pl13
  1m do:f2             ;decoupler off
  wr #0                ;save data to disk
HaltAcqu, 1m           ;jump address for protection files
exit                   ;quit
ph0= 0
ph1= 1 3
ph2= 0 0 2 2 1 1 3 3
ph10= 0
ph31= 0 2 2 0 1 3 3 1
```

cpxt1ir.kmi

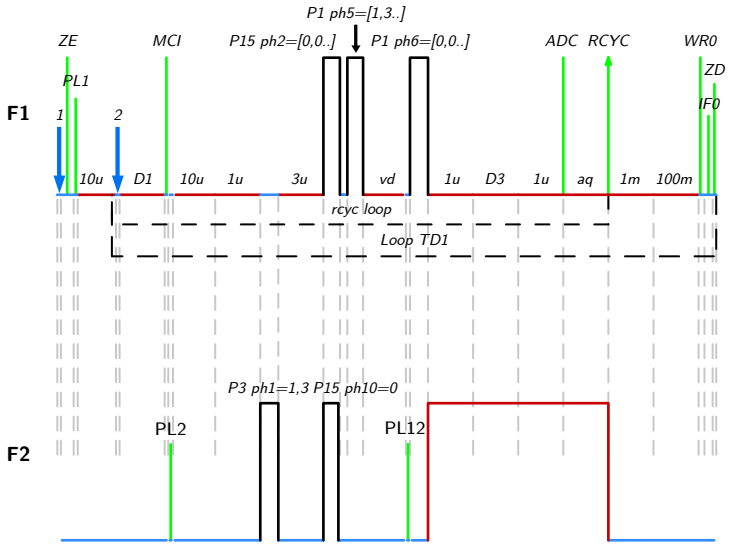


```
;cpxt1ir.kmi
;cp program with bi-level decoupling
;set pl2 to low cp power, pl12 about 1-3 dB lower for high power
;X-nucleus T1 experiment, relaxation curve to be evaluated as T1 inversion recovery
;setup like cp4c.hf but parmod=2D
#include <preamp.incl>
1 ze
  10u pl1: f1; use pl1 for F1 drive power
2 d1
  protect
  10u pl2: f2; set cp power level for F2
  1u: f1 ph2
  p3: f2 ph1
  3u
  (p15 ph2): f1 (p15 ph10): f2
  (p1 ph5): f1
  vd pl12: f2
  (p1 ph6): f1
  1u cw: f2
  d3: f1 ph0
  1u adc ph31
  aq
  rcyc=2
  1m do: f2
  100m wr #0 if #0 ivd zd
  lo to 2 times td1
exit
ph0= 0
ph10= 0
ph1= 1 3
ph2= 0 0 2 2 1 1 3 3
ph5= 1 3 3 1 2 0 0 2
ph6= 0 0 2 2 1 1 3 3
ph31= 0 0 2 2 1 1 3 3
```

t1irpg

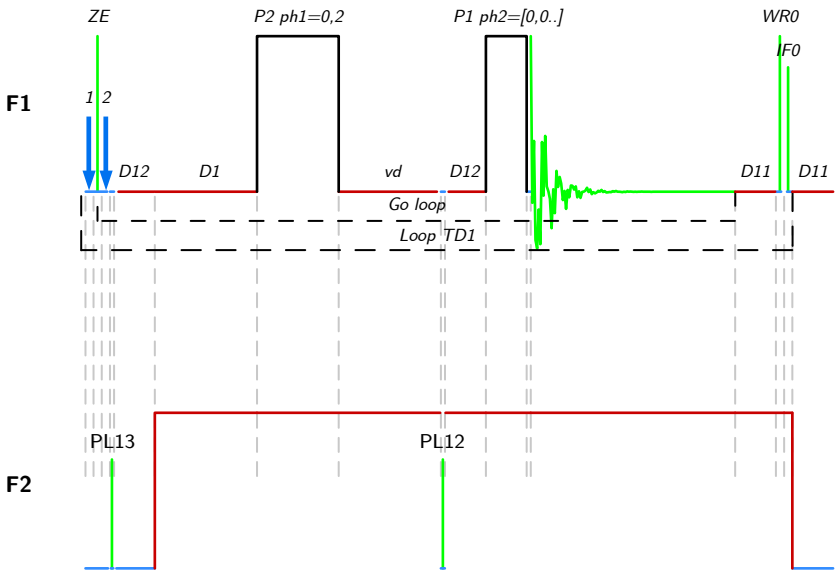


```
;t1irpg
;avance-version (04/09/06)
;T1 measurement using inversion recovery with power gated decoupling
#include <Avance.incl>
"p2=p1 × 2"
"d11=30m"
"d12=20u"
1 ze
2 d12 pl13:f2
  d1 cpd2:f2
  p2 ph1
  vd
  d12 pl12:f2
  p1 ph2
  go=2 ph31
  d11 wr #0 if #0 ivd
  lo to 1 times td1
  d11 do:f2
exit
ph1=0 2
ph2=0 0 2 2 1 1 3 3
ph31=0 0 2 2 1 1 3 3
;pl1 :      f1 channel - power level for pulse (default)
;pl12 :     f2 channel - power level for CPD/BB decoupling
;pl13 :     f2 channel - power level for second CPD/BB decoupling
;p1 :       f1 channel -  90 degree high power pulse
;p2 :       f1 channel - 180 degree high power pulse
;d1 :       relaxation delay; 1-5 × T1
;d11 :      delay for disk I/O                    [30 msec]
;d12 :      delay for power switching             [20 usec]
;vd :       variable delay, taken from vd-list
;NS :       8 × n
```

```
;DS :       4
;td1 :      number of experiments = number of delays in vd-list
;FnMODE : undefined
;cpd2 :     decoupling according to sequence defined by cpdprg2
;pcpd2 :    f2 channel - 90 degree pulse for decoupling sequence
;define VDLIST
;this pulse program produces a ser-file (PARMOD = 2D)
;$ Id: t1irpg,v 1.8.10.1 2004/11/23 15:08:14 ber Exp $
```

t1irc360dc

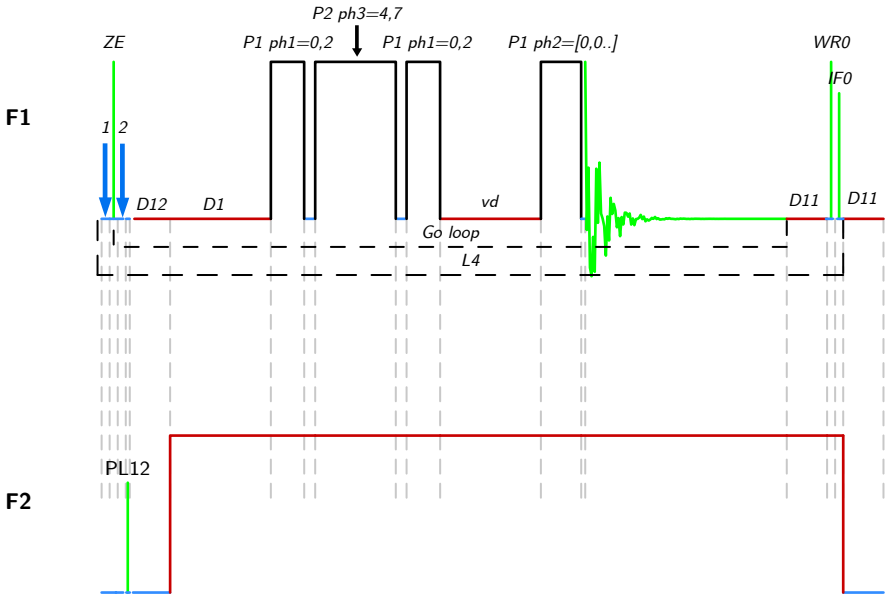


```
;t1irc360dc
;avance-version
;T1 measurement using inversion recovery with Waltz decoupling
;composite 180 degree inversion pulse (90(x)-360(120)-90(x))
;M. Levitt, J. Magn. Reson. 48 (1982) 234-264.
#include <Avance.incl>
"p2=p1 × 4"
"d11=30m"
"d12=20u"
1 ze
2 d12 pl12:f2
  d1 cpd2:f2
  p1 ph1
  p2 ph3
  p1 ph1
  vd
  p1 ph2
  go=2 ph31
  d11 wr #0 if #0 ivd
  lo to 1 times l4
  d11 do:f2
exit
ph1=0 2
ph2=0 0 2 2 1 1 3 3
ph3=(12) 4 7
ph31=0 0 2 2 1 1 3 3
;pl1 :      f1 channel - power level for pulse (default)
;pl12 :     f2 channel - power level for CPD/BB decoupling
;p1 :       f1 channel - 90 degree high power pulse
;p2 :       f1 channel - 360 degree high power pulse
;d1 :       relaxation delay; 1-5 × T1
```

```
;d11 :      delay for disk I/O                                  [30 msec]
;d12 :      delay for power switching                           [20 usec]
;vd :       variable delay, taken from vd-list
;L4 :       l4 = number of experiments = number of delays in vd-list
;NS :       8 × n
;DS :       4
;td1:       number of experiments
;cpd2 :     decoupling according to sequence defined by cpdprg2
;pcpd2 :    f2 channel - 90 degree pulse for decoupling sequence
;define VDLIST
;this pulse program produces a ser-file (PARMOD = 2D)
```

^{13}C CP-MASNMR spectrum of pure olanzapine with 15 wt.% D_2O

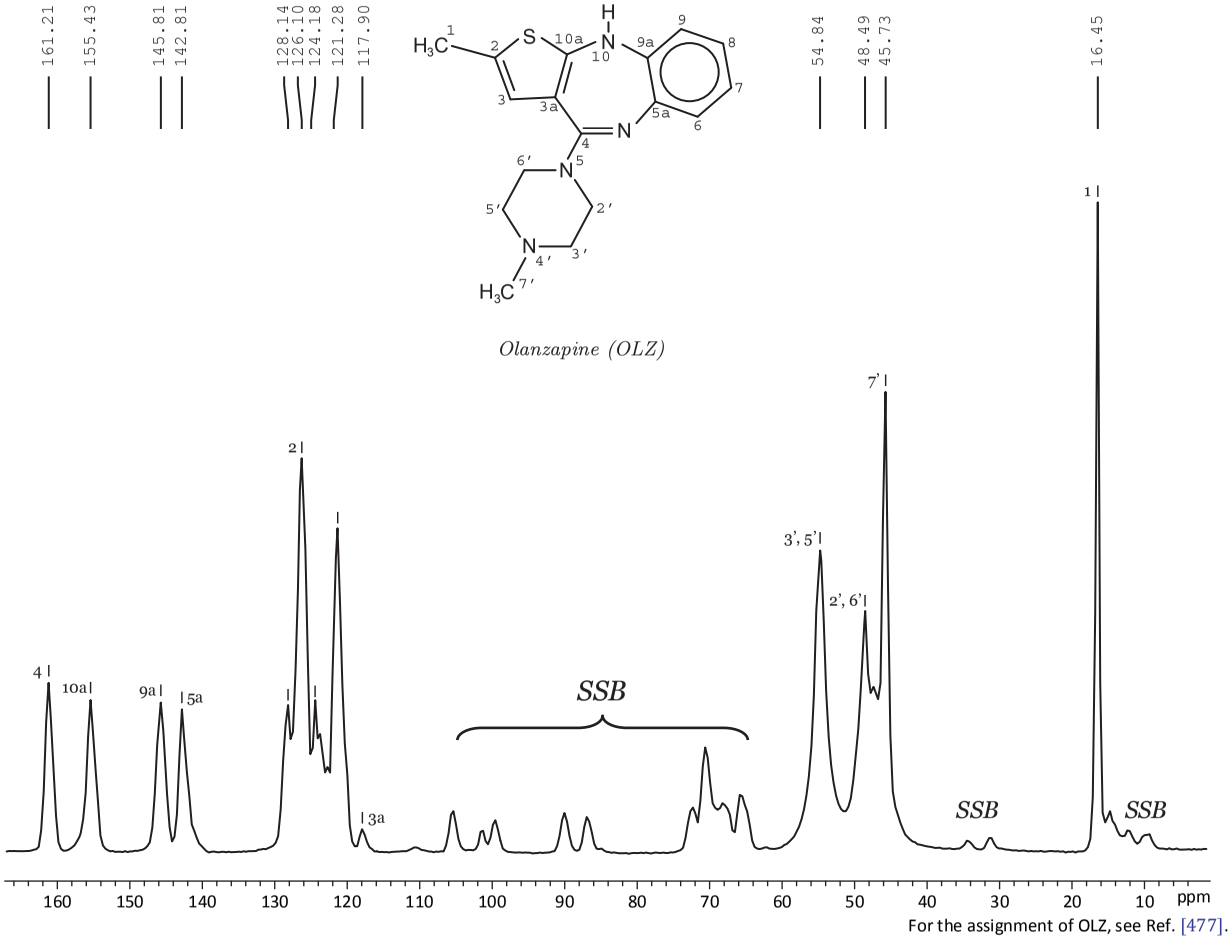

Olanzapine (OLZ)

For the assignment of OLZ, see Ref. [477].

BRUKER

```
Current Data Parameters
NAME      Olanzapine15D2013C
EXPNO                      2
PROCNO                     1

F2 - Acquisition Parameters
Date              20061010
Time                 18.20
INSTRUM              av500
PROBHD    4 mm MAS BB/1H
PULPROG              cp.av
TD                    8192
SOLVENT               None
NS                   12288
DS                       4
SWH              87719.297 Hz
FIDRES           10.707922 Hz
AQ               0.0467501 sec
RG                    4600
DW                   5.700 usec
DE                   6.00 usec
TE                   316.0 K
CNST20           1.0000000
CNST22           1.7071069
CNST23           0.2928932
CNST24           1.0000000
D1               5.00000000 sec
p5                816666.69 usec
P6                816666.31 usec
ZGOPTNS

======== CHANNEL f1 ========
NUC1                    13C
P4                     0.01 usec
P15                 2500.00 usec
PL1                    8.00 dB
PL4                  120.00 dB
SFO1          125.7703648 MHz

======== CHANNEL f2 ========
cnst21               0.000000
CPDPRG2                  cw
NUC2                     1H
P3                     4.20 usec
PL2                    6.00 dB
PL12                   6.00 dB
PL15                   8.00 dB
SFO2          500.1325007 MHz
SPNAM0    ramp80100.1000
SPOAL0               0.500
SPOFFS0              0.00 Hz

F2 - Processing parameters
SI                    8192
SF           125.7582101 MHz
WDW                     EM
SSB                      0
LB                    0.00 Hz
GB                       0
PC                    1.00
```

Paper I

ELSEVIER

Biophysical Chemistry 117 (2005) 101 – 109

Biophysical Chemistry

http://www.elsevier.com/locate/biophyschem

Importance of polyunsaturated acyl chains in chlorpromazine interaction with phosphatidylserines: A ^{13}C and ^{31}P solid-state NMR study☆

Song Chen[b], Anja Underhaug Gjerde[a], Holm Holmsen[a], Willy Nerdal[b,*]

[a]*Department of Biomedicine and Molecular Biology, University of Bergen, Norway*
[b]*Department of Chemistry, University of Bergen, Allegaten 41, N-5007 Bergen, Norway*

Received 8 April 2005; received in revised form 10 May 2005; accepted 10 May 2005
Available online 25 May 2005

Abstract

The polyunsaturated fatty acid docosahexaenoic acid (DHA, c22:6, n-3) is found at a level of about 50% in the phospholipids of neuronal tissue membranes and appears to be crucial to human health. Dipalmitoyl phosphatidylcholine (DPPC, 16:0/16:0 PC), 1-palmitoyl-2-oleoyl phosphatidylserine (POPS) and the DHA containing 1-stearaoyl-2-docosahexenoyl phosphatidylserine (SDPS) were used to make DPPC (60%)/POPS (29%)/SDPS (11%) bilayers with and without 10 mol% chlorpromazine (CPZ), a cationic, amphiphilic phenothiazine. The T_1 relaxation measurements make it clear that the saturated acyl chains carbons (palmitic, stearic and most of the oleic chain) and the choline head group are not affected by CPZ addition. The observed increased signal intensity and T_1-values of DHA indicate reduced mobility of C_4 and C_5 due to CPZ binding. ^{31}P NMR spectra confirm that CPZ binding to the phosphatidylserines in the bilayer enhances phospholipid head group mobility.

Keywords: ^{13}C NMR; ^{31}P NMR; DPPC/SDPS/POPS; DPPC/SDPS/POPS bilayers; Chlorpromazine HCl interaction

1. Introduction

The effects of phospholipid acyl chain length and degree of unsaturation on bilayer thickness is well documented [1] and so is the effect of bilayer thickness on membrane enzyme activity [2]. The polyunsaturated fatty acid docosahexaenoic acid (DHA, c22:6, n-3) is found at a level of about 50% in the phospholipids of neuronal tissue membranes and appears to be crucial to human health [3,4]. Despite this cruciality, only sparse information has been gathered on DHA's physical function(s) in the membrane. Findings on the conformational changes of rhodopsin (the MI-to-MII transition) suggest that phospholipid membranes with polyunsaturated acyl chains promote these conformational changes of rhodopsin [5]. DHA has been modelled by molecular mechanics methods and suggested to have a rigid and ordered structure [6–8]. Contrary to the results of these modelling studies, DHA with its long run of double-bonded carbons separated by a single methylene group has been found in a compressibility study [9] to have high flexibility and minimal sensitivity to temperature in that DHA showed to be the most easily compressed acyl chain, when compared with saturated (stearoyl) and monounsaturated (oleic) acyl chains in phospholipids with choline head group.

The importance of the specific phospholipid head group is illustrated by the membrane protein topology and activity-

Abbreviations: CPZ, Chlorpromazine; CSA, Chemical Shift Anisotropy; DMPC, Dimyristoyl phosphatidylcholine (14:0/14:0 PC); DMPE, Dimyristoyl phosphatidylethanolamine (16:0/16:0 PE); DPPC, Dipalmitoyl phosphatidylcholine(16:0/16:0 PC); HPLC, High pressure liquid chromatography; PA, Phosphatidic acid; PBPS, Bovine brain phosphatidylserine; POPS, 1-Palmitoyl-2-oleoyl phosphatidylserine (16:0/18:1 (n-9) PS); SDPS, 1-Stearaoyl-2-docosahexenoyl phosphatidylserine (18:0/22:6 (n-3) PS); PC, Phosphatidylcholine; PI, Phosphatidylinositol; PKC, Protein kinase C; PLA2, Phospholipase A_2; PS, Phosphatidylserine; Tc, Transition temperature.

☆ This work was supported by EU BIOMED 2 grant EC BMH4-97-2609 from the European Union (EU) (no 149115/310), grants from the Norwegian Research Council (NFR) and from the Blix foundation.

* Corresponding author. Tel.: +47 55 583353; fax: +47 55 589400.
E-mail address: Willy.Nerdal@kj.uib.no (W. Nerdal).

0301-4622/$ - see front matter © 2005 Elsevier B.V. All rights reserved.
doi:10.1016/j.bpc.2005.05.002

determining properties of glycerophospholipids with anionic head groups [10], these phospholipids alter the structure of human recombinant prion protein associated with membranes in living cells [11]. Influence of lipid composition on membrane protein activities has recently been reviewed by Lee [12].

The above observations indicate that the activity of membrane-bound proteins can be influenced by the lipid composition of the membranes. Thus, it is possible that perturbation of lipid organization in a bilayer by amphiphilic molecules will influence the activity of such proteins even without direct interaction between the protein and the amphiphile. Chlorpromazine, a cationic, amphiphilic phenothiazine, has been found to interact preferentially with bilayers containing phospholipids with a high proportion of phosphatidylserines and highly unsaturated acyl chains [13]. Furthermore, CPZ has been found to slightly increase lipid order when the bilayer is above the gel to liquid crystalline phase transition temperature, Tc, and decrease lipid order when the bilayer is below Tc [14].

Membrane perturbation with CPZ and other amphiphils induces a host of genes in both bacteria and mammalian cells (reviewed in [15]). It is, thus, possible that CPZ's reported/claimed antagonistic effect on the D_2-receptor is partially due to perturbation by CPZ of the membrane that contains the receptor. In micromolar concentration CPZ causes large increases in the mean molecular areas in monolayers of acidic phospholipids, whereas no such molecular area increase is found for the neutral glycerophospholipids in monolayers [16]. Similar findings by us [17], using magic angle spinning solid state ^{13}C NMR on bilayer samples with partial hydration (12 H_2O per phospholipid), showed that CPZ had low or no interaction on the acyl packing of liposomes made of phospholipids without a net negative head group charge and with saturated acyl chains, such as palmitoyl (DPPC) and myristoyl (DMPC), while it caused a large (5–15 ppm) shift to higher ppm values of ~30% of the acyl chain carbon resonances in liposomes composed of pig brain PS (PBPS) and DPPC. PS is a major anionic phospholipid in mammalian cell membranes like peripheral and central nervous system myelin and PBPS was subjected to CPZ interaction studies as PBPS bilayer and in a mixture with DPPC as a DPPC (60 mol%)/PBPS (40 mol%) bilayer. This pig brain PS contained molecular species of phospholipids with the following acyl chains: two major molecular species 18:0–18:1 (49%) and 18:0–22:6 (28%), and five minor molecular species each in the 3–7% range, of which two are known 16:0–22:6 (6%) and 18:0–20:4 (3%).

Recently [13], we have studied the interaction on fully hydrated (30 H_2O per phospholipid) DPPC (60%)/PBPS (40%) bilayers above the gel to liquid crystalline phase transition temperature, Tc. In this recent study on a DPPC(60%)/PBPS(40%) bilayer and with CPZ added (DPPC(54%)/PBPS(36%)/CPZ(10%)), the Tcs were found to be about the same, 303.5 and 305.8 K, respectively. With this acyl chain composition of pig brain PS (18:0–18:1 (49%), 18:0–22:6 (28%), 16:0–22:6 (6%) and 18:0–20:4 (3%)), the sample composition can be outlined as a DPPC (60%)/SOPS (20%)/SDPS (11%)/OTHER (9%). Compared with the sample of this work DPPC (60%)/POPS (29%)/SDPS (11%), the samples differ in the amounts of polyunsaturated PS (11% SDPS and 9% OTHER versus 11% SDPS of this study) and monounsaturated PS (20% SOPS versus 29% POPS of this work). (We have carried out solid-state NMR experiments on pure SOPS and pure POPS bilayers with CPZ added and found the CPZ interaction to be negligible for both of these monounsaturated phosphatidylserines.) On the basis of the amount of unsaturated acyl chains, it is reasonable to expect the Tcs of samples used in the work presented here to be comparable with the Tcs of 303.5–305.8 K of the previous study.

A general feature of the phosphatidylserine ^{31}P static NMR spectra is a large chemical shielding anisotropy (CSA) (the CSA is generally larger for serine than for choline and ehanolamine head groups). The CSA appears to be influenced by the chemical nature of the fatty acyl chains [13]. Furthermore, the similarities of the static shielding tensor of phosphatidylserine and -choline taken together with the somewhat larger CSA for phosphatidylserines, suggest that the phosphatidylserine phosphate moiety differs conformationally or motionally from the phosphatidylcholine phosphate moiety [18,19]. This can be accounted for by greater rigidity of the phosphatidylserine head group than the phosphatidylcholine head group. This rigidity supposedly results from electrostatic interactions and/or hydrogen bonding between or within the phosphatidylserine head groups. Thus, dilution of negatively charged PBPS with neutral DPPC removes some of this interaction and will allow greater freedom of motion of the phosphatidylserine head group. The gel to liquid crystalline phase transition of a phospholipid bilayer upon increase in temperature is accompanied by several structural changes in the lipid molecules. The principal change is the *trans*-gauche isomerization in the saturated carbons in the acyl chains and the average number of gauche conformers can be related to bilayer thickness.

In our previous study [13] we deduced from our analysis of the composition of molecular species in PBPS that it must have been SDPS in the PBPS that caused the main, strong interaction with CPZ since POPS and SOPS showed negligible interaction with CPZ. In the present study, we have investigated phospholipid acyl chain unsaturation effect on CPZ bilayer interaction further by employing fully hydrated (30 H_2O per phospholipid) and authentic DPPC(60%)/POPS(29%)/SDPS(11%) and DPPC(54%)/POPS(26%)/SDPS(10%)/CPZ(10%) bilayers both below and above the gel to liquid crystalline phase transition temperature, Tc. The biologically abundant phosphatidylserines, POPS and SDPS, where the POPS species has its unsaturated *sn*-2 acyl chain bond at C_9-C_{10}, and the DHA containing SDPS species, with the 6 unsaturated acyl chain

bonds at C_4-C_5, C_7-C_8, $C_{10}-C_{11}$, $C_{13}-C_{14}$, $C_{16}-C_{17}$ and at $C_{19}-C_{20}$. With this distribution of unsaturated acyl chain bonds and the chosen molar percentages, the contribution to the NMR spectra from the C=C resonances other than C_9-C_{10} of POPS will be due to the DHA acyl chain of the SDPS phospholipid. In this way specific phospholipid bilayer interaction of CPZ can be detected. This DPPC (56 mol%)/POPS (29 mol%)/SDPS (11 mol%) phospholipid bilayer was studied without and with 10 mol% of CPZ added. Samples were pH adjusted to 7.4 in order to ensure that the serine head group carboxyl group was deprotonated (pK_a of ~4.4). ^{13}C [20] and ^{31}P [19] solid-state NMR techniques were employed to obtain structural and dynamic information of this phospholipid bilayer when interacting with the CPZ amphiphile.

2. Materials and methods

2.1. Liposome preparation

Chlorpromazine HCl (CPZ) and synthetic 1, 2-dipalmitoyl phosphatidylcholine (DPPC, powder) were obtained from Sigma Chemical Co. (St. Louis, MO, USA). Synthetic 1-palmitoyl-2-oleoyl phosphatidylserine (POPS, dissolved in chloroform), and 1-stearaoyl-2-docosahexenoyl phosphatidylserine (SDPS, dissolved in chloroform) were purchased from Avanti Polar Lipids Inc. (Birmingham, Alabaster, AL, USA). Phospholipid bilayers containing choline and serine head groups were made in a molar composition of 60% PC and 40% PS (29% POPS, 11% SDPS) and dissolved in *t*-butanol and then lyophilized to dryness. The PC/PS and the PC/PS/CPZ bilayers were kept under an argon atmosphere and not exposed to air and light. Each sample of dry powder was then suspended in H_2O. These suspensions contained multilamellar liposomes and unilamellar systems were obtained by freeze-thawing 7 times. At the freeze-thawing stage all samples were adjusted to a pH of 7.4 by adding a small amount of 0.05 M NaOH. Subsequently, the lipid suspension was divided into two equal parts and to one part was added an amount of CPZ HCl (dissolved in H_2O) to obtain a 10% molar ratio. Thus a sample of 54% PC, 36% PS (26% POPS and 10% SDPS) and 10% CPZ was obtained as well as the corresponding sample without CPZ. The samples with added CPZ HCl were then incubated on a waterbath for 24 h at 317 K. Subsequently, the samples were subjected to 24 h of lyophilization giving partially hydrated liposomes with a hydration level of ~12 water molecules per lipid molecule (determined by ^1H-MAS NMR). Then, water was added to the samples to obtain fully hydrated bilayers (~30 water molecules per lipid molecule) [21,22] and the samples were equilibrated at 315 K for 48 h (above the samples gel to liquid crystalline transition temperature(s)) and packed in NMR rotors (Scheme 1).

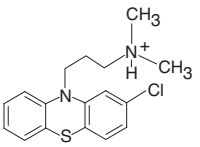

Scheme 1. Chlorpromazine (CPZ).

2.2. CP-MAS-^{13}C NMR spectroscopy

The ^{13}C-MAS NMR experiments were obtained at 100.62 MHz with the Bruker AVANCE DMX 400 instrument equipped with *magic angle spinning* (MAS) hardware and used ZrO_2 spinning rotors with a diameter of 4 mm. Experiments were done at sample temperature of 310 K with sample spinning rate of 1500 Hz. Calibration of the MAS probe temperature has been done by the manufacturer (Bruker, Germany) upon delivery of the solid state equipment. Confirmation of the MAS probe temperature calibration in the temperature range with relevance to phospholipids bilayer phase transitions was carried out on a pure DPPC sample. ^{13}C NMR spectra were recorded from 293 to 317 K, and the DPPC phase transition was found to occur between 313.6 and 315.6 K. These experiments were carried out with high-power proton decoupling during the acquisition, i.e. without Nuclear Overhauser Effect (NOE). In this study, experiments of the two DPPC/POPS/SDPS and DPPC/POPS/SDPS/CPZ bilayer systems were carried out with a relaxation delay of 5 s between transients, unless otherwise stated. Typically, a total of 16,000 transients were acquired. The spectra were multiplied with an exponential window function increasing the line-width by 2 Hz to reduce noise prior to Fourier transformation.

^{13}C spin-lattice relaxation times were obtained by a modified inversion-recovery pulse sequence using a composite 180° pulse [23] to counteract potential problems associated with non-uniform excitation across the range of ^{13}C chemical shifts. A recycling delay of 10 s between transients were used between the 256 and 512 transients accumulated a sample temperature of 310 ± 0.5 K. In order to obtain accurate relaxation data on the palmitic acyl chain methyl group, relaxation experiments using a pulse program with broadband ^1H-decoupling and a 50 s relaxation delay were also carried out with 128 transients.

2.3. ^{31}P NMR spectroscopy

Static ^{31}P spectra were acquired on these two fully hydrated bilayer samples at the various temperatures ranging from 296 to 318 K at 161.98 MHz and high-power decoupling during acquisition, i.e. without Nuclear Overhauser Effect (NOE). Typically, 512 transients were collected for each experiment with a relaxation delay of 5 s between transients. These fids were multiplied with an exponential window function increasing the line-width by 50 Hz to reduce noise prior to Fourier transformation. Magic

angle spinning ^{31}P experiments (T_1 measurements) were carried out with a rotor spinning speed of 2 KHz. These fids of 64 transients were Fourier transformed without apodization in order to keep spectral resolution. ^{31}P relaxation data were obtained with ^{1}H-cross-polarization at temperatures from 296 K to 318 K, and with rotor spinning speed of 2 kHz. Typically 512 transients were accumulated.

3. Results

The ^{13}C magic angle spinning (MAS) spectra of bilayer samples DPPC/POPS/SDPS and DPPC/POPS/SDPS/CPZ in the liquid crystalline phase were recorded at a temperature of 310 K and are presented as spectral regions in Figs. 1–4 where the top spectrum shows the phospholipid sample with 10% CPZ and the bottom spectrum the corresponding sample without CPZ. Fig. 1 shows the DPPC, POPS and SDPS acyl chain sp^3 carbon resonances in the 12–38 ppm region. The two spectra (Fig. 1, top and bottom) are dominated by the palmitic (DPPC and POPS) as well as the oleic (POPS) molecular species. The molar composition of the samples cause the palmitic (16:0) acyl chain resonances to give ~75% of the peak intensities in this spectral region, whereas the contribution from the SDPS species in this spectral region is 10% (5% from each of the 18:0 and 22:6 acyl chains). Thus, only the palmitic carbon resonances are assigned, see Fig. 1 (some of these peaks contain contribution from carbon resonances of other acyl chains than palmitoyl chains). The phospholipid choline and serine head group carbon resonances as well as the glycerol moiety resonances appear in the 52–73 ppm spectral region—see Fig. 2. Of these resonances, only the choline head group resonances come from a single molecular species, the DPPC molecule. The serine resonances come from two PS species, POPS and SDPS, and the molar composition gives a PC/PS peak ratio of 1.5. The three glycerol resonances will be composed of the three phospholipid species in the two samples, DPPC, POPS and SDPS.

From the T_1 data presented in Table 1, one finds that the carbon T_1 values of the choline head group are not affected

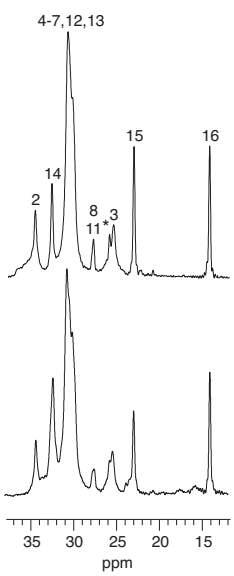

Fig. 1. Methylene and methyl carbon resonance region (12–38 ppm) of samples DPPC(60%)/POPS(29%)/SDPS(11%) (bottom spectrum) and DPPC(54%)/POPS(26%)/SDPS(10%)/CPZ(10%) (top spectrum). Spectra are acquired at 310 K (samples are in liquid crystalline phase). The samples molar composition cause the palmitic (16:0) acyl chain resonances to dominate (~ 75% of the peak intensities) in this spectral region. Thus, only the palmitic carbon resonances are assigned in the two spectra. An asterisk "*" indicate a possible DHA resonance. See the text for details.

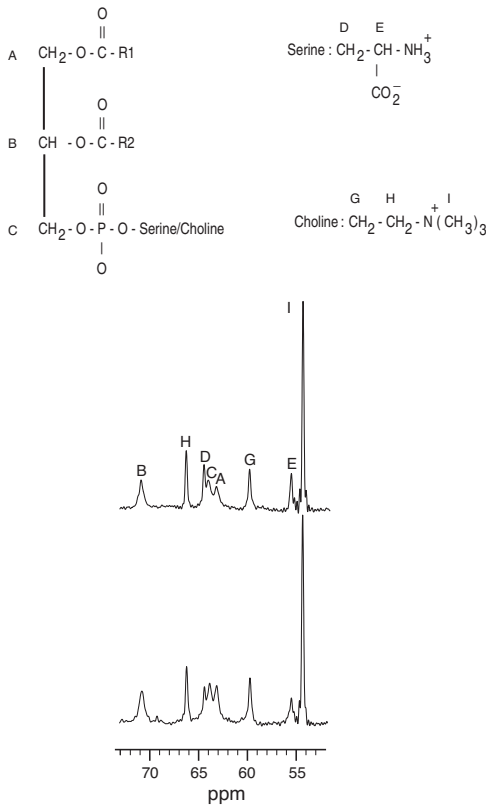

Fig. 2. Top: Structural formula of the glycerol moiety and the two phospholipids head groups, serine and choline, with the corresponding assignment letters used in the spectra. Bottom: Phospholipid head group and glycerol carbon resonance region (52–73 ppm) of samples DPPC(60%)/POPS(29%)/SDPS(11%) (bottom spectrum) and DPPC(54%)/POPS(26%)/SDPS(10%)/CPZ(10%) (top spectrum). Spectra are acquired at 310 K (samples are in liquid crystalline phase). The molar composition makes a PC/PS ratio of 1.5. See the text for details.

Table 1
^{13}C spin-lattice relaxation times T_1 (s) at 310 K DPPC/POPS/SDPS and DPPC/POPS/SDPS/CPZ bilayers

Carbon	DPPC/POPS/SDPS	DPPC/POPS/SDPS/CPZ
C=O	2.04	2.15
CO_2^-	1.51	0.61
POPS C=C:		
C9 (C^a)	0.75	1.83
C10 (B^a)	1.32	1.03
DHA C=C:		
(E^a)	0.34	1.16
(F^a)	1.04	0.99
(G^a)	0.75	2.67
Glycerol carbon:		
sn-1	0.12	0.31
sn-2	0.28	0.33
sn-3	0.13	0.15
Serine carbon:		
α	0.27	0.07
β	1.44	0.77
Choline carbon:		
α	0.34	0.30
β	0.26	0.22
CH_3	0.32	0.29
Palmitic carbon:		
2	0.55	0.36
3	0.68	0.52
4–14	0.72	0.60
15	3.51	2.12
16	5.03	5.33
Oleic carbon:		
8, 11	0.55	0.61

[a] Peaks labeled in Fig. 3.

by the addition of CPZ, whereas the serine head group T_1 values show a reduction in presence of CPZ. The glycerol carbon T_1 values, on the other hand, demonstrate a diverse effect of CPZ. The *sn*-1 glycerol carbon display an increased T_1 value due to CPZ in contrast to both the *sn*-2 and *sn*-3 glycerol carbons (where the POPS and SDPS unsaturated acyl chain and the phosphate and head group are attached, respectively) that have T_1 values unaffected by CPZ.

Fig. 3 shows the 125–135 ppm region where the C=C resonances of the acyl chains of samples DPPC/POPS/SDPS and DPPC/POPS/SDPS/CPZ are found. The molar composition of the samples makes the oleic(18:1)/DHA(22:6) acyl chain ratio 2.5. The oleic(18:1) acyl chain of POPS double bond (at C_9-C_{10}) and the six double bonds of DHA of SDPS (double bonds at C_4-C_5, C_7-C_8, $C_{10}-C_{11}$, $C_{13}-C_{14}$, $C_{16}-C_{17}$,$C_{19}-C_{20}$) makes the carbon–carbon double bond ratio between POPS and SDPS to be 1/6. Consequently, the observed sp^2 carbon resonances in the ^{13}C NMR spectra can be expected to be close to the described 1/6 ratio multiplied by the species percentages of the samples. Thus, samples with and without CPZ has a POPS/SDPS acyl chain C=C ratio of $(0.29\times1$ double bond$)/(0.11\times6$ double bonds) or approximately 0.4.

Comparison of the C=C resonances with/without CPZ (see Fig. 3) shows a pronounced intensity change of some of these, the peaks at 127–129 ppm, upon CPZ interaction.

The crowded spectral region displayed in Fig. 3 pose an obstacle to a complete resonance assignment. However, in a recent solid-state NMR where $^1H-^{13}C$ two-dimensional cross-polarization experiments were employed [24], the investigators managed to firmly assign DHA's C_{19} and C_{20} to 126.8 and 131.3 ppm, respectively. Thus, peak A is assigned to resonance C_{20} and peak H to resonance C_{19}—see Fig. 3. The remaining C=C resonances of DHA (C_4-C_5, C_7-C_8, $C_{10}-C_{11}$, $C_{13}-C_{14}$, $C_{16}-C_{17}$) are located between 127.4 and 128.4 ppm and could not be individually assigned. In an early study on C=C resonance assignment and estimation of chemical shifts Gunstone et al. [25] showed that in monoenoic acyl chains, like the oleic chain of POPS, the C_{10} resonance would come at a higher chemical shift than the C_9, they found 130.02 and 129.78 ppm, respectively. Based on our own previous work, on the signal intensities of these resonances (Fig. 3) and on POPS and the described higher chemical shift of C_{10} of the C_9=C_{10} pair, peaks B and C in Fig. 3 can be assigned to the oleic acyl chain of POPS where resonance B corresponds to C_{10} and resonance C to C_9 of POPS. These two C=C resonances from the middle of POPS's acyl chain, display almost no changes in intensity and T_1 values (Table 1) when CPZ is added (T_1 values for peaks B, C, E, F and G in Fig. 3 could be determined).

As evident in Fig. 3 there is no intensity change of DHA's resonances C_{19} and C_{20} upon addition of CPZ (peaks A and H, respectively). Furthermore, peaks E and G (Fig. 3 and Table 1) display a marked increase in T_1 value when CPZ is present (peak F has approximately similar T_1 values without and with CPZ). Thus, the part of SDPS's DHA acyl chain that are affected by the presence of CPZ is the part close to the polar region of the bilayer, as demonstrated by the intensity and T_1 value increase of these resonances.

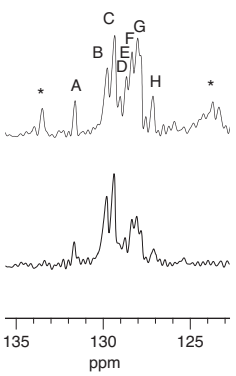

Fig. 3. Double bonded acyl chain carbon resonance region (125–135 ppm) of samples DPPC(60%)/POPS(29%)/SDPS(11%) (bottom spectrum) and DPPC(54%)/POPS(26%)/SDPS(10%)/CPZ(10%) (top spectrum). Spectra are acquired at 310 K (samples are in liquid crystalline phase). The molar composition of the samples makes the oleic(18:1)/DHA(22:6) ratio of 2.5. This causes the total oleic(C=C)/DHA(C=C) peak ratio to be 0.4. See the text for details.

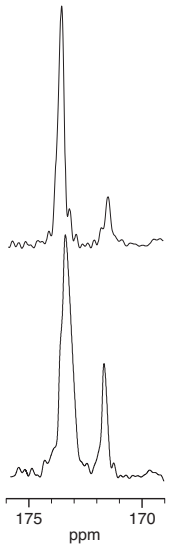

Fig. 4. Carbonyl and carboxyl carbon resonance region (170–176 ppm) of samples DPPC(60%)/POPS(29%)/SDPS(11%) (bottom spectrum) and DPPC(54%)/POPS(26%)/SDPS(10%)/CPZ(10%) (top spectrum). Spectra are acquired at 310 K (samples are in liquid crystalline phase). The molar composition (PC/PS ratio) makes the theoretical ratio between the carbonyl and carboxyl resonances to be 2.5. See the text for details.

All these assignments are further supported by the molar composition of the samples. The spectrum of the sample without CPZ demonstrates DHA double bonded carbon resonances with smaller signal intensity than necessary for a good correspondence with the molecular ratio of the sample. On the other hand, the sample containing CPZ show these resonances with larger signal intensities and some with increased T_1 values (Table 1), when compared with the sample without CPZ. The appearance of some broad peaks around 124 ppm labeled with an asterisk "*" (Fig. 3, top spectrum) when CPZ is present correspond to double bonded carbon resonances of the CPZ molecule, as does the peak at ~133.5 ppm labeled with an asterisk "*" (Fig. 3, top spectrum). Another interesting feature in the carbon T_1 data (Table 1) is the ~240% increase in the T_1 value of carbon C_9 of the unsaturated acyl in the POPS molecule and the ~28% T_1 value reduction of C_9's acyl chain neighbor, the C_{10} carbon, in presence of CPZ.

Fig. 4 shows the carbonyl resonance (~173 ppm) and the serine head group carboxyl (~171 ppm) [26] resonance of samples DPPC/POPS/SDPS (bottom spectrum) and DPPC/POPS/SDPS/CPZ (top spectrum). The molar composition (PC/PS ratio) makes the theoretical peak ratio of 2.5 between the carbonyl and carboxyl resonances. From the two spectra shown in Fig. 4, it is apparent that the carbonyl resonance (~173 ppm) of the bilayer is not affected by

Table 2
^{31}P chemical shift anisotropy (CSA, in ppm) from 296 K to 318 K DPPC/POPS/SDPS and DPPC/POPS/SDPS/CPZ bilayers

Temperature (K)	DPPC/POPS/SDPS	DPPC/POPS/SDPS/CPZ
296	108	88
297	103	87
298	104	84
299	104	83
300	101	84
301	103	86
302	99	82
303	96	79
304	96	79
305	92	80
306	94	67
307	91	67
308	88	70
309	89	69
310	87	69
311	88	67
312	82	70
313	81	71
314	79	69
315	79	67
316	77	69
317	75	73
318	76	66

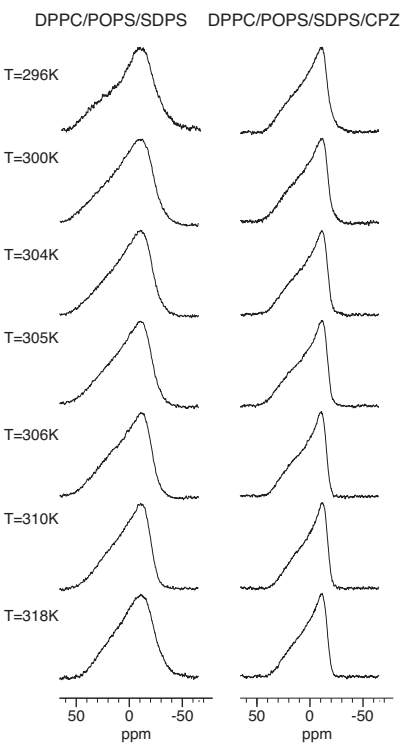

Fig. 5. Static ^{31}P NMR spectra of samples DPPC(60%)/POPS(29%)/SDPS(11%) (left column) and DPPC(54%)/POPS(26%)/SDPS(10%)/CPZ(10%) (right column). Sample temperatures from 296 K (top spectra) to 318 K (bottom spectra). See the text for details.

Table 3
^{31}P T_1 values (s) from 296 K to 318 K DPPC/POPS/SDPS and DPPC/POPS/SDPS/CPZ bilayers

Temperature (K)	DPPC/POPS/SDPS		DPPC/POPS/SDPS/CPZ		
	PC	PS	PC	PS	CPZ–PS
296	0.57	0.53	0.77	0.64	0.60
298	0.54	0.52	0.65	0.64	0.60
300	0.57	0.54	0.64	0.58	0.62
302	0.51	0.50	0.57	0.51	0.51
304	0.55	0.51	0.61	0.52	0.49
305	0.51	0.49	0.52	0.50	0.51
306	0.54	0.49	0.51	0.53	0.53
308	0.53	0.50	0.52	0.52	0.49
310	0.57	0.47	0.49	0.49	0.42
312	0.55	0.51	0.51	0.48	0.42
314	0.55	0.51	0.49	0.47	0.41
316	0.57	0.57	0.46	0.46	0.45
318	0.58	0.52	0.50	0.48	0.46

addition of CPZ. A corresponding comparison of the serine head group carboxyl resonance (~ 171 ppm), on the other hand, makes it evident that the 10% CPZ reduces the carboxyl resonance intensity by about 2/3 and the T_1 (Table 1) value by 40% (from 1.15 to 0.61 s). The corresponding T_1 values for the carbonyl resonance is about unchanged in presence of CPZ.

In general, the ^{31}P CSA data presented in Table 2 and Fig. 5 show that the sample without CPZ has a higher CSA than when CPZ is added over the whole temperature range measured (296–310 K). The CSA of the sample without CPZ (the DPPC/POPS/SDPS sample) displays a fairly steady decrease in CSA value as temperature increases. In addition to a general decrease in CSA value upon temperature increase, the CPZ containing sample (the DPPC/POPS/SDPS/CPZ sample) displays a sudden drop in CSA of 13 ppm from 305 to 306 K. Thus, the CPZ containing sample displays this sudden reduction in CSA at a sample temperature of about 305.5 K, in correspondence with the main melting (transition) temperature displayed by this kind of phospholipid sample. The ^{31}P T_1 values are measured at the central band of the MAS spectra, and presented in Table 3. In Fig. 6 the three central band peaks are displayed at several of the temperatures investigated. They can be assigned [13,27] to the three molecular species: PC, PS and CPZ–PS complex. Both the PC and the PS species show similar T_1 values with and without CPZ and the CPZ–PS complex shows a T_1 similar to the PC and the PS species—see Table 3.

4. Discussion

The observed intensity decrease of the glycerol carbon resonances of the DPPC/SDPS/CPZ sample (Fig. 2) when compared with the DPPC/SDPS sample is most pronounced for the *sn*-3 carbon, i.e. the glycerol carbon where the phosphorus and head group are attached. A similar signal intensity decrease/line broadening is observed for the serine carboxyl resonance of the DPPC/SDPS/CPZ sample when compared with the DPPC/SDPS sample. An explanation for these observations can be found in the possibility of an altered transverse relaxation of dipolar coupled spins under radiofrequency irradiation (decoupling) [28]. In such a case destructive interference effects cause line broadening due to (molecular) motion interfering with the coherent modulation from radiofrequency decoupling. Even carbons without directly attached protons (such as carbonyl and carboxyl carbons) can to some extent experience these effects when coupled to other nearby protons. Furthermore, dipolar interactions are expected to be weak for nonprotonated sp^2 carbons and the main line broadening mechanism will be the chemical shift anisotropy (CSA). (Protonated sp^2 carbons of the acyl chains' olefinic double bonds will experience both the described line broadening mechanisms [28].)

With the possibility of such effects (as described above) complicating the spectral interpretations the ^{13}C T_1 data obtained on the DDPC/POPS/SDPS and DDPC/POPS/

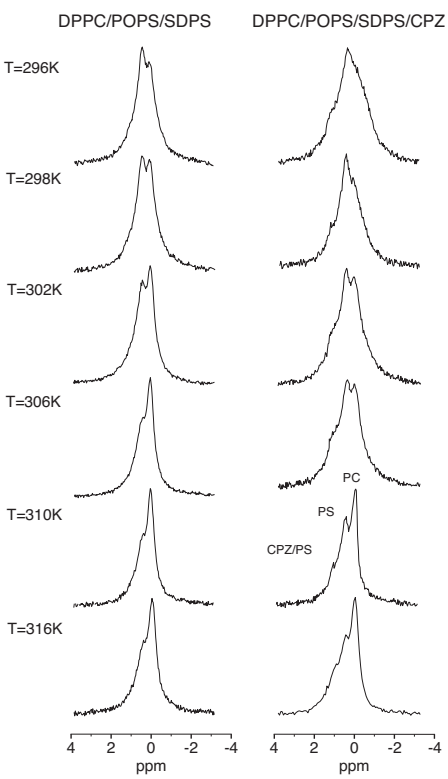

Fig. 6. ^{31}P MAS spectra of samples DPPC(60%)/POPS(29%)/SDPS(11%) (right column) and DPPC(54%)/POPS(26%)/SDPS(10%)/CPZ(10%) (left column) between sample temperatures 296 and 318 K. Note sudden decrease in CSA of CPZ containing sample at 305 K. See the text for details.

SDPS/CPZ samples (of this work) are of great value. This is even more so due to the simpler molecular species makeup of the DDPC/POPS/SDPS sample of this work when compared with the higher molecular species complexity of our previous work [13], where we employed pig brain PS (PBPS). For example, the C=C region of the ^{13}C spectra displayed in Fig. 3, the C_9 and C_{10} resonances of POPS could be assigned, so that the remaining C=C resonances are known to belong to SDPS's *sn*-2 attached DHA acyl chain. Of these latter C=C resonances, the C_{19} and C_{20} of DHA could be firmly assigned, and all the remaining unassigned C=C resonances are then known to belong to the DHA acyl chain, namely the C_4, C_5, C_7, C_8, C_{10}, C_{11}, C_{13}, C_{14}, C_{16} and C_{17} carbon resonances.

Binding of CPZ to phospholipids can be followed in the ^{13}C spectra where serine head group carbon resonances show increased intensity when CPZ is added to the DPPC/POPS/SDPS bilayer. This result is contrary to the results found in our previous work [13] on a PC/PS/CPZ sample where the PS component is an extract from pig brain and composed as follows: The PS composition of PBPS used has been determined to mainly contain these components: 18:0–18:1 (49%), 18:0–22:6 (28%), 16:0–22:6 (6%) and 18:0–20:4 (3%). Thus, this can be described as a DPPC(60%)/SOPS(20%)/SDPS(11%)/OTHER (9%) sample. Effects of an altered transverse relaxation of dipolar coupled spins under radiofrequency irradiation (decoupling) has been described earlier [28] and the possibility of such effects producing potentially confusing changes in signal intensities when CPZ is present, make the ^{13}C T_1 measurements on both DPPC/POPS/SDPS and DPPC/POPS/SDPS/CPZ samples important. (Unfortunately, we did not carry out ^{13}C T_1 experiments on the pig brain PS samples (PBPS) of our previous work, this kind of sample has a higher molecular species complexity than the samples of this work.)

In a previous study [17] addition of CPZ to partially hydrated DPPC/PBPS bilayer (~ 12 H_2O/phospholipid) ~ 30% of the main acyl chain carbon resonances in the ^{13}C NMR spectra were shifted down field by 5–15 ppm, demonstrating CPZ interdigitation among the phospholipid acyl chains. The fully hydrated DPPC/POPS/SDPS bilayer of this study showed no such down field shift of acyl chain resonances in the ^{13}C NMR spectra when CPZ was present. The lower mobility of the phospholipids in partially hydrated bilayers when compared with the fully hydrated bilayers of this study is evident from the broader line shapes in the ^{13}C NMR spectra of the partially hydrated bilayers [17]. Thus, a less dense molecular packing of the phospholipids in fully hydrated bilayers would presumably not make interdigitated CPZ molecules come in close enough contact with acyl chain carbons to perturb the p-orbitals of these carbons, and consequently, a 5–15 ppm shift to higher ppm values of these acyl chain carbon resonances is not observed in the fully hydrated bilayers of this study.

Phospholipid head group (and phosphate) motion and an altered motion caused by an interacting amphiphile like CPZ in a bilayer will give static ^{31}P NMR spectra that differ in chemical shift anisotropy (CSA). In the static ^{31}P NMR spectra of DPPC/POPS/SDPS/and DPPC/POPS/SDPS/CPZ (Fig. 5 and Table 2), the former demonstrate a CSA that is 10–17 ppm larger than the latter over a quite large temperature range covering the gel to liquid crystalline phase transition temperature. Thus, the presence of CPZ causes an enhancement of the phospholipid head group mobility. A separate (new) ^{31}P chemical shift for the CPZ-phosphate is observed when CPZ binds to the phosphate of phosphatidylserine bilayers as demonstrated in the ^{31}P NMR spectra of the DPPC/POPS/SDPS and DPPC/POPS/SDPS/CPZ bilayers. In the previous study of 60%/40% DPPC/PBPS bilayer the bulky choline head groups imposes conformational restrictions [13,29] on the CPZ-phosphate complex and also promote CPZ-carboxyl binding which was not observed for the "all serine" head group samples and therefore seem less favoured.

The T_1 relaxation measurements make it clear that the unsaturated acyl chain carbons (palmitic, stearic and most of the oleic chain) do not change in mobilities upon CPZ addition (these carbons have similar T_1 values (Table 1) without and with CPZ in the bilayer). The unsaturated carbons of the DHA acyl chain, on the other hand, display a 2–3 times increase in T_1 value with CPZ present, i.e. these unsaturated carbons experience a decreased mobility when CPZ is present in the bilayer. The choline head group carbon resonances, two of the glycerol carbons (the *sn*-2 and *sn*-3 carbons) and the carbonyl resonance display no change in T_1 upon CPZ addition. The serine head group carbon resonances (the Cα, Cβ and CO_2^-) display a 2–3 times reduction in the T_1 value upon CPZ addition, possibly due to an increased mobility of these carbons (the phospholipids are in the slow motion regime at the relaxation measurement temperature). The ^{31}P relaxation measurements show that all three head group components (PC, PS and CPZ–PS) do not

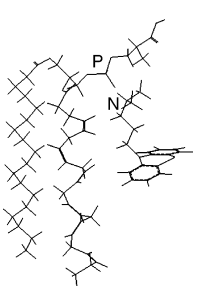

Scheme 2. Molecular model of chlorpromazine (CPZ) interaction with a 1-stearoyl-2-docosahexanoylserine (SDPS) molecule. The CPZ molecule (right) is positioned with its positive charge on the nitrogen atom (labelled N) on the end of CPS's acyl chain. This positive charge is in the vicinity of the phosphate's (labelled P) negative charge in the SDPS molecule (left). Both acyl chains of the SDPS molecule have sp^3 carbon dihedral angles of 60° (liquid crystalline state). The molecular model suggests that the carbons C_4 and C_5 of DHA (*sn*-2 position) will be affected by an interdigitating CPZ molecule.

vary by any significant amount as function of sample temperature, only the CPZ–PS component is to some degree temperature sensitive below the main phase transition temperature. The PC and the PS components display very similar ^{31}P relaxation in both bilayer samples, i.e. with and without CPZ present.

In addition to the importance of the phospholipid head group, also the degree of phospholipid acyl chain unsaturation will determine [30] part of the CPZ interaction with the bilayer. The observed increased signal intensity of C=C SDPS's DHA acyl chain carbon resonances and an increase in the corresponding T_1-values for two (out of three that could be measured) of the C=C peaks where the C_4 and C_5 resonances reside and, thus, the reduced mobility of C_4 and C_5 appear to be due to CPZ binding. A molecular model of the CPZ interaction with a 1-stearoyl-2-docosahexanoylserine (SDPS) molecule generated by the Titan software (Wavefunction, Irvine, CA) is presented in Scheme 2. In this model a CPZ is located with its positive charge (acyl chain nitrogen) in the vicinity of a SDPS's phosphate group negative charge. SDPS's acyl chains have the sp^3 carbon dihedral angles of 60° (liquid crystalline state). Even though the actual conformation(s) of the DHA's acyl chain (in the *sn*-2 position) may differ somewhat from the conformation displayed in Scheme 2, the model suggests that CPZ interdigitated in such a bilayer will have an effect on both carbons C_4 and C_5 of the DHA.

References

[1] A.M. Stinson, R.D. Wiegand, R.E. Anderson, Fatty acid and molecular species compositions of phospholipids and diacylglycerols, Exp. Eye Res. 52 (1991) 213–218.

[2] R.B. Genniss, J.L. Strominger, Activation of C55-isoprenoid alcohol phosphokinase from Staphylococcus aureus: I. Activation by phospholipids and fatty acids, J. Biol. Chem. 251 (1976) 1264–1282.

[3] E.E. Birch, D.G. Birch, D.R. Hoffman, R. Uauy, Dietary essential fatty acid supply and visual acuity development, Invest. Ophthamol. Vis. Sci. 33 (1992) 3242–3253.

[4] N. Salem Jr., Omega-3 fatty acids: molecular and biochemical aspects, in: G.A. Spiller , J. Scala (Eds.), New Protective Roles for Selected Nutrients, Alan R. Liss, New York, 1989, pp. 109–228.

[5] B.J. Litman, D.C. Mitchell, A role for phospholipid polyunsaturation in modulating protein function, Lipids 31 (1996) S193–S197 (Suppl.).

[6] K.R. Applegate, J.A. Glomset, Computer-based modeling of the conformation and packing properties of docosahexaenoic acid, J. Lipid Res. 27 (1986) 658–680.

[7] K.R. Applegate, J.A. Glomset, Effect of acyl chain unsaturation on the conformation of model diacylglycerols: a computer modeling study, J. Lipid Res. 32 (1991) 635–644.

[8] K.R. Applegate, J.A. Glomset, Effect of acyl chain unsaturation on the packing of model diacylglycerols in simulated monolayers, J. Lipid Res. 32 (1991) 645–655.

[9] B.W. Koening, H.H. Strey, K. Gawrisch, Membrane lateral compressibility determined by NMR and X-ray diffraction. Effect of acyl chain polyunsaturation, Biophys. J. 73 (1997) 1954–1966.

[10] W. van Klompenburg, I.M. Nilsson, G. von Heijne, B. de Kruijff, Anionic phospholipids are determinants of membrane protein topology, EMBO J. 16 (1997) 4261–4266.

[11] M. Morillas, W. Swietnicki, P. Gambetti, W.E. Surewicz, Membrane environment alters the conformational structure of the recombinant human prion protein, J. Biol. Chem. 274 (1999) 36859–36865.

[12] A.G. Lee, Lipid–protein interactions in biological membranes: a structural perspective, Biochim. Biophys. Acta 1612 (2003) 1–40.

[13] A.U. Gjerde, H. Holmsen, W. Nerdal, Chlorpromazine interaction with phosphatidylserines: A ^{13}C and ^{31}P solid-state NMR study, Biochim. Biophys. Acta 1682 (2004) 28–37.

[14] A. Wisniewska, A. Wolnicka-Glubisz, ESR studies on the effect of cholesterol on chlorpromazine interaction with saturated and unsaturated liposome membranes, Biophys. Chem. 111 (2004) 43–52.

[15] L. Vigh, B. Maresca, J.L. Harwood, Does the membrane's physical state control the expression of heat shock and other genes?, TIBS 23 (1998) 369–374.

[16] A.V. Agasøster, L.M. Tungodden, D. Cejka, E. Bakstad, L. Sydnes, H. Holmsen, Chlorpromazine-induced increase in dipalmitoylphosphatidylserine surface area in monolayers at room temperature, Biochem. Pharmacol. 61 (2001) 817–825.

[17] W. Nerdal, S.A. Gundersen, V. Thorsen, H. Høiland, H. Holmsen, Chlorpromazine interaction with glycerophospholipid liposomes studied by magic angle spinning solid state ^{13}C-NMR and differential scanning calorimetry, Biochim. Biophys. Acta 1464 (2000) 165–175.

[18] S.J. Kohler, M.P. Klein, Orientation and dynamics of phospholipid head groups in bilayers and membranes determined from nuclear magnetic resonance chemical shielding tensors, Biochemistry 16 (1977) 519–526.

[19] J.L. Browning, J. Seelig, Bilayers of phosphatidylserine: a deuterium and phosphorus nuclear magnetic resonance study, Biochemistry 19 (1980) 1262–1270.

[20] W.-g. Wu, L.-M. Chi, Comparisons of lipid dynamics and packing in fully interdigitated monoarachidoylphosphatidylcholine and non-interdigitated dipalmitoylphosphatidylcholine bilayers: cross polarization/magic angle spinning ^{13}C-NMR studies, Bichim. Biophys. Acta 1026 (1990) 225–235.

[21] M.J. Janiak, D.M. Small, G.G. Shipley, Temperature and compositional dependence of the structure of hydrated dimyristoyl lecithin, J. Biol. Chem. 254 (1979) 6068–6078.

[22] D.M. Small, Observations on lecithin. Phase equilibria and structure of dry and hydrated egg lecithin, J. Lipid Res. 8 (1967) 551–557.

[23] M. Levitt, Symmetrical composite pulse sequences for NMR population inversion: I. Compensation of radiofrequency field inhomogeneity, J. Magn. Reson. 48 (1982) 234–264.

[24] S. Everts, J.H. Davis, 1H and 13C NMR of multilamellar dispersions of polyunsaturated (22:6) phospholipids, Biophys. J. 79 (2000) 885–897.

[25] F.D. Gunstone, M.R. Pollard, C.M. Scrimgeour, H.S. Vedanayagam, Fatty acids: Part 50. Nuclear magnetic resonance studies of olefinic fatty acids and esters, Chem. Phys. Lipids 18 (1977) 115–129.

[26] D.L. Holwerda, P.D. Ellis, R.E. Wuthier, Carbon-13 and Phosphorus-31 nuclear magnetic resonance studies on interaction of calcium with phosphatidylserine, Biochemistry 20 (1981) 418–428.

[27] T.J.T. Pinheiro, A. Watts, Resolution of individual lipids in mixed phospholipid membranes and specific lipid–cytochrome *c* interactions by magic-angle spinning solid-state phosphorus-31 NMR, Biochemistry 33 (1994) 2459–2467.

[28] F. Adebodun, J. Chung, B. Montez, E. Oldfield, X. Shan, Spectroscopic studies of lipids and biological membranes: carbon-13 and proton magic-angle sample-spinning nuclear magnetic resonance study of glycolipid–water systems, Biochemistry 31 (1992) 4502–4509.

[29] P.R. Cullis, B. de Kruyff, R.E. Richards, Factors affecting the motion of the polar head group in phospholipid bilayers. A ^{31}P NMR study of unsonicated phosphatidylcholine liposomes, Biochim. Biophys. Acta 426 (1976) 433–446.

[30] L.L. Holte, F. Separovic, K. Gawrisch, Nuclear magnetic resonance investigation of hydrocarbon chain packing in bilayers of polyunsaturated phospholipids, Lipids 31 (1996) 199–203.

Paper II

ELSEVIER

Biophysical Chemistry 120 (2006) 178 – 187

Biophysical Chemistry

http://www.elsevier.com/locate/biophyschem

Existence of lipid microdomains in bilayer of dipalmitoyl phosphatidylcholine (DPPC) and 1-stearoyl-2-docosahexenoyl phosphatidylserine (SDPS) and their perturbation by chlorpromazine: A ^{13}C and ^{31}P solid-state NMR study☆

Chen Song [b], Holm Holmsen [a], Willy Nerdal [b,*]

[a] *Department of Biomedicine, University of Bergen, Norway*
[b] *Department of Chemistry, University of Bergen, Allegaten 41, N-5007 Bergen, Norway*

Received 7 October 2005; received in revised form 18 November 2005; accepted 22 November 2005
Available online 13 December 2005

Abstract

The polyunsaturated fatty acid docosahexaenoic acid (DHA, 22:6, n-3) is found at a level of about 50% in the phospholipids of neuronal tissue membranes and appears to be crucial to human health. Dipalmitoyl phosphatidylcholine (DPPC, 16:0/16:0 PC) and the DHA containing 1-stearoyl-2-docosahexenoyl phosphatidylserine (SDPS) were used to make DPPC (60%)/SDPS (40%) bilayers with and without 10 mol% chlorpromazine (CPZ), a cationic, amphiphilic phenothiazine.

Resonances that are present in ^{13}C NMR spectrum of the DPPC (60%)/SDPS (40%) sample and that disappear in presence of 10% CPZ most probably are due to the special interface environment, e.g. the hydrophobic mismatch, at the interface of DPPC and SDPS microdomains in the DPPC/SDPS bilayer. In itself the appearance of resonances at novel chemical shift values is a clear demonstration of a unique chemical environment in the DPPC (60%)/SDPS (40%) bilayer. The findings of the study presented here suggest CPZ bound to the phosphate of SDPS will slow down and partially inhibit such a DHA acyl chain movement in the DPPC/SDPS bilayer. This would affect the area occupied by a SDPS molecule (in the bilayer) and probably the thickness of the bilayer where SDPS molecules reside as well. It is quite likely that such CPZ caused changes can affect the function of proteins embedded in the bilayer.

Keywords: ^{13}C NMR; ^{31}P NMR; DPPC/SDPS; DPPC/SDPS; Lipid microdomains; Bilayers; ChlorpromazineHCl interaction

1. Introduction

Cellular membranes like those of retinal rod outer segments [1], mitochondria [2], spermatozoa [3] and cerebral grey matter [4] have a high percentage of phospholipids with polyunsaturated acyl chains, i.e. the ω-3 and ω-6 fatty acids [5]. Low levels of these polyunsaturated fatty acids are related to a variety of pathological conditions like cancer [6], visual disorder [7] and cardiovascular disease [8]. Thus, these apparently unrelated diseases, indicate a fundamental role played by the polyunsaturated fatty acids in the cells. The ω-3 fatty acid, docosahexaenoic acid (DHA) and the ω-6 fatty acid, arachidonic acid (AA), differ in that the latter serves as a precursor for prostaglandins [9] in platelet function, whereas the former does not appear to be metabolized [1].

Abbreviations: CPZ, Chlorpromazine; CSA, Chemical Shift Anisotropy; DMPC, Dimyristoyl phosphatidylcholine (14:0/14:0 PC); DMPE, Dimyristoyl phosphatidylethanolamine (16:0/16:0 PE); DPPC, Dipalmitoyl phosphatidylcholine (16:0/16:0 PC); HPLC, High Pressure Liquid Chromatography; PA, Phosphatidic acid; PBPS, Pig brain phosphatidylserine; POPS, 1-palmitoyl-2-oleoyl phosphatidylserine (16:0/18:1 (n-9) PS); SDPS, 1-stearoyl-2-docosahexenoyl phosphatidylserine (18:0/22:6 (n-3) PS); PC, Phosphatidylcholine; PI, Phosphatidylinositol; PKC, Protein kinase C; PLA2, Phospholipase A_2; PS, Phosphatidylserine; Tc, transition temperature.

☆ This work was supported by EU BIOMED 2 grant EC BMH4-97-2609 from the European Union (EU) (no. 149115/310), grants from the Norwegian Research Council (NFR) and from the Blix foundation.

* Corresponding author. Tel.: +47 55 583353; fax: +47 55 589400.
E-mail address: Willy.Nerdal@kj.uib.no (W. Nerdal).

0301-4622/$ - see front matter © 2005 Elsevier B.V. All rights reserved.
doi:10.1016/j.bpc.2005.11.007

DHA has a function as ligand for retinoid X receptor [10], influences the Cl^- channels [11] (cystic fibrosis) and the neuronal K^+ channels [12], is released in response to serotonin [13], has an essential role in brain maturation and neuronal function and is here found in bilayer phospholipids at a 30–50% level. Bilayers with such high DHA levels have distinct properties, probably related to the functioning of integral membrane proteins. When compared with less unsaturated phospholipid acyl chains, DHA-containing bilayers have reduced thickness in the fluid state and consequently an increased area occupied per phospholipid at the aqueous interface of the bilayer [14]. A substantial amount of work has been done on the phase behavior of binary lipid mixtures to get a better understanding of lipid interactions in cell membranes. In bilayers composed of two or more phospholipids with different gel to liquid crystalline phase transition temperatures, different acyl chain lengths and different degrees of acyl chain unsaturation, it is conceivable that one can find segregation of bilayer components in the plane of the bilayer [15]. In such a case, one important driving force would be the hydrophobic mismatch due to differences in thickness of the phospholipid species in the bilayer [16]. Effects of adding an amphiphile like chlorpromazine (see later) to such a bilayer could possibly provide valuable information on both the modes of action by the drug (amphiphile) and the robustness of the lipid microdomains in the bilayer.

Experimental evidence of lipid microdomain formation in lipid bilayers has been presented from various techniques [17–23]. In an early study, Cullis and Hope [17] detected a bilayer stabilizing effect of cholesterol on a sphingomyelin–phosphatidylethanolamine lipid mixture by employing ^{31}P NMR. ^{13}C NMR has been used to study cholesterol and DPPC mixtures where cholesterol is found to induce fluid-phase immiscibility in this kind of bilayer [18]. More recently, ^{2}H NMR experiments have determined that ceramide in phosphatidylcholine bilayers cause microdomain formation of different composition and phase state in POPC/ceramide bilayers at physiological temperature [19].

Several investigators studying the role of phospholipid acyl chain unsaturation and stability of lipid rafts composed of sphingomyelin and cholesterol [20,22] support the notion that such lipid rafts are promoted by polyunsaturated acyl chains. The docosahexenoyl (22:6, DHA) acyl chain is found to enhance membrane lipid raft formation by lipid phase separation [24–26].

Molecular mechanics modelling of DHA suggests a rigid and ordered DHA structure [27–29]. Contrasting these modelling studies, DHA has been found in a compressibility study [30] to have high flexibility and minimal sensitivity to temperature in that DHA showed to be the most easily compressed acyl chain, when compared with saturated (stearoyl) and monounsaturated (oleoyl) acyl chains in phospholipids with choline head group. Furthermore, findings in a ^{2}H NMR and X-ray diffraction study, suggest that the *sn-2* attached (22:6) acyl chain in a (16:0–22:6) PC bilayer has a distribution of mass that is shifted toward the bilayer aqueous interface. The (16:0) acyl chain, on the other hand, is found to be displaced toward the membrane center [31]. The activity of membrane-bound proteins is influenced by the lipid composition of the membranes [32]. Consequently, perturbation of lipid organization in a bilayer by amphiphilic molecules can influence the activity of such proteins even without direct interaction between the protein and the amphiphile.

We have previously investigated [33], by the use of solid-state NMR [34], chlorpromazine interaction with partially hydrated phospholipid bilayers with choline head group and saturated acyl chains (DPPC (60%)/DMPC (40%)) and mixture of choline and serine head groups (DPPC (60%)/PS (40%)). These PS phospholipids extracted from pig brain (PBPS) have the following acyl chain composition: 49% of (18:0–18:1), 28% of (18:0–22:6), and five minor molecular species where two are known: 6% of (16:0–22:6) and 3% of (18:0–20:4). This study showed that CPZ has low or no interaction with the DPPC (60%)/DMPC (40%) bilayer. Conversely, CPZ causes a 5–15 ppm low field shift of ~30% of the saturated carbon acyl chain resonances in the DPPC (54%)/PS (36%)/CPZ (10%) bilayer.

It is important to note that phosphatidylcholine and phosphatidylserine species of like acyl chain composition [35] and samples of mixed bovine brain phosphatidylserine (about 8% of the 22:6 acyl chain) and DPPC [36] have been found to be completely miscible.

Supported by these findings [33], we investigated further [37] by ^{13}C and ^{31}P NMR [38] on 1,2-dipalmitoyl phosphatidycholine (DPPC, 16:0–16:0 PC) in mixture with the previously described PS extract from pig brain: DPPC (60%)/PBPS (40%) as well as pure 1-palmitoyl-2-oleoylphosphatidylserine (POPS) and pure PBPS bilayers with and without CPZ. The data showed that CPZ prefers binding to the phosphate of phosphatidylserine and that also carboxyl binding of CPZ is present in the DPPC/PBPS/CPZ bilayer and that CPZ interaction depends on acyl chain unsaturation. Recently, we followed up these findings by a ^{13}C and ^{31}P solid-state NMR study [39] on a bilayer composed of 1,2-dipalmitoyl phosphatidycholine (DPPC, 16:0–16:0 PC), 1-palmitoyl-2-oleoylphosphatidylserine (POPS) and the DHA containing 1-stearoyl-2-docosahexenoyl phosphatidylserine (SDPS) in a DPPC (60%)/POPS (29%)/SDPS (11%) bilayer with and without 10% CPZ. The T_1 relaxation data showed that the palmitic, the stearic and most of the oleic acyl chains (as well as the choline head group) were not affected by CPZ. The data indicated reduced mobility of DHA's c4 and c5 carbons upon CPZ binding as well as a clear increase in serine head group mobility. This recent study [39] showed that chlorpromazine interacts preferentially with bilayers containing phospholipids with a high proportion of phosphatidylserines with highly unsaturated acyl chains.

A general feature of the phosphatidylserine ^{31}P static NMR spectra is a large chemical shielding anisotropy (CSA) (the CSA is generally larger for serine than for choline and ethanolamine head groups). The CSA appears to be influenced by the chemical nature of the fatty acyl chains [37]. Furthermore, the similarities of the static shielding tensor of phosphatidylserine and -choline taken together with the somewhat larger CSA for phosphatidylserines, suggest that the phosphatidylserine phosphate moiety differs conformationally or motionally from

the phosphatidylcholine phosphate moiety [38,40]. This can be accounted for by greater rigidity of the phosphatidylserine head group than the phosphatidylcholine head group. This rigidity supposedly results from electrostatic interactions and/or hydrogen bonding between or within the phosphatidylserine head groups. Thus, dilution of negatively charged PBPS with neutral DPPC removes some of this interaction and will allow greater freedom of motion of the phosphatidylserine head group. The gel to liquid crystalline phase transition of a phospholipid bilayer upon increase in temperature is accompanied by several structural changes in the lipid molecules. The principal change is the *trans*-gauche isomerization in the saturated carbons in the acyl chains and the average number of gauche conformers can be related to bilayer thickness.

In our previous studies [33,37,39] we deduced from the composition of molecular species in PBPS that it must have been SDPS of the pig brain PS extract (PBPS) that caused the main, strong interaction with CPZ. (We found that POPS and SOPS had only negligible interaction with CPZ). In the study presented here, we employ bilayer samples of DPPC (60%) and the DHA containing synthetic/pure SDPS (40%) as well as the CPZ containing counterpart DPPC (54%)/SDPS (36%)/CPZ (10%) to enhance the possibility of obtaining information on DHA's role in CPZ interaction.

2. Materials and methods

2.1. Liposome preparation

ChlorpromazineHCl (CPZ) (Scheme 1) and synthetic 1,2-dipalmitoyl phosphatidylcholine (DPPC, powder) were obtained from Sigma Chemical Co. (St. Louis, MO, USA). Synthetic 1-stearoyl-2-docosahexenoyl phosphatidylserine (SDPS, dissolved in chloroform) was purchased from Avanti Polar Lipids Inc. (Birmingham, Alabaster, AL, USA). Phospholipid bilayers containing choline and serine head groups were made in a molar composition of 60% PC and 40% PS and dissolved in *t*-butanol and then lyophilized to dryness. The PC/PS and the PC/PS/CPZ bilayers were kept under an argon atmosphere and not exposed to air and light. Each sample of dry powder was then suspended in H_2O. These suspensions contained multilamellar liposomes and unilamellar systems were obtained by freeze-thawing 7 times. At the freeze-thawing stage all samples were adjusted to a pH of 7.4 by adding a small amount of 0.05 M NaOH. Subsequently, the lipid suspension was divided into two equal parts and to one part was added an amount of CPZHCl (dissolved in H_2O) to obtain a 10% molar ratio. Thus a sample of 54% PC, 36% PS and 10% CPZ was obtained as well as the corresponding sample without CPZ. The samples with added CPZHCl were then incubated on a waterbath for 24 h at 317 K. Subsequently, the samples were subjected to 24 h of lyophilization giving partially hydrated liposomes with a hydration level of ~12 water molecules per lipid molecule (determined by ^{1}H–MAS–NMR). Then, water was added to the samples to obtain fully hydrated bilayers (~30 water molecules per lipid molecule) [41,42] and the samples were equilibrated at 315 K for 48 h (above the samples gel to liquid crystalline transition temperature(s)) and packed in NMR rotors.

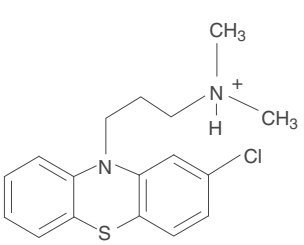

Scheme 1. Chlorpromazine (CPZ).

2.2. CP–MAS–^{13}C NMR spectroscopy

The ^{13}C MAS–NMR experiments were obtained at 100.62 MHz with the Bruker AVANCE DMX 400 instrument equipped with *magic angle spinning* (MAS) hardware and used ZrO_2 spinning rotors with a diameter of 4 mm. Experiments were done at sample temperature of 310 K with sample spinning rate of 1500 Hz. Calibration of the MAS probe temperature has been done by the manufacturer (Bruker, Germany) upon delivery of the solid-state equipment. Confirmation of the MAS probe temperature calibration in the temperature range with relevance to phospholipids bilayer phase transitions was carried out on a pure DPPC sample. ^{13}C NMR spectra were recorded from 293 to 317 K, and the DPPC phase transition was found to occur between 313.6 and 315.6 K. These experiments were carried out with high-power proton decoupling during the acquisition, i.e. without Nuclear Overhauser Effect (NOE). In this study, experiments of the two DPPC/SDPS and DPPC/SDPS/CPZ bilayer systems were carried out with a relaxation delay of 5 s between transients, unless otherwise stated. Typically, a total of 16,000 transients was acquired. The spectra were multiplied with an exponential window function increasing the line-width by 2 Hz to reduce noise prior to Fourier transformation.

^{13}C spin-lattice relaxation times were obtained by a modified inversion-recovery pulse sequence using a composite 180° pulse [43] to counteract potential problems associated with non-uniform excitation across the range of ^{13}C chemical shifts. A recycling delay of 10 s between transients were used between the 256 and 512 transients which were accumulated at a sample temperature of 310 ± 0.5 K. In order to obtain accurate relaxation data on the palmitic acyl chain methyl group, relaxation experiments using a pulse program with broadband ^{1}H-decoupling and a 50 s relaxation delay were also carried out with 128 transients.

2.3. ^{31}P NMR spectroscopy

Static ^{31}P spectra were acquired on these two fully hydrated bilayer samples at the various temperatures ranging from 296 to 318 K at 161.98 MHz and high-power decoupling during acquisition, i.e. without Nuclear Overhauser Effect (NOE).

Typically, 512 transients were collected for each experiment with a relaxation delay of 5 s between transients. These fids were multiplied with an exponential window function increasing the line-width by 50 Hz to reduce noise prior to Fourier transformation. Magic angle spinning ^{31}P experiments (T_1 measurements) were carried out with a rotor spinning speed of 2 KHz. These fids of 64 transients were Fourier transformed without apodization in order to keep spectral resolution. ^{31}P relaxation data were obtained with ^{1}H-cross-polarization at temperatures from 296 to 318 K, and typically 512 transients were accumulated.

3. Results

The ^{13}C Magic Angle Spinning (MAS) spectra of DPPC/SDPS and DPPC/SDPS/CPZ bilayer samples were recorded at a temperature of 310 K and are presented as spectral regions in Figs. 1–3 where the top spectrum shows the phospholipid sample with 10% CPZ and the bottom spectrum the corresponding sample without CPZ. Fig. 1 shows the DPPC and SDPS acyl chain sp^3 carbon resonances in the 12–38 ppm region as well as the phospholipid choline and serine head group carbon resonances and the glycerol moiety resonances

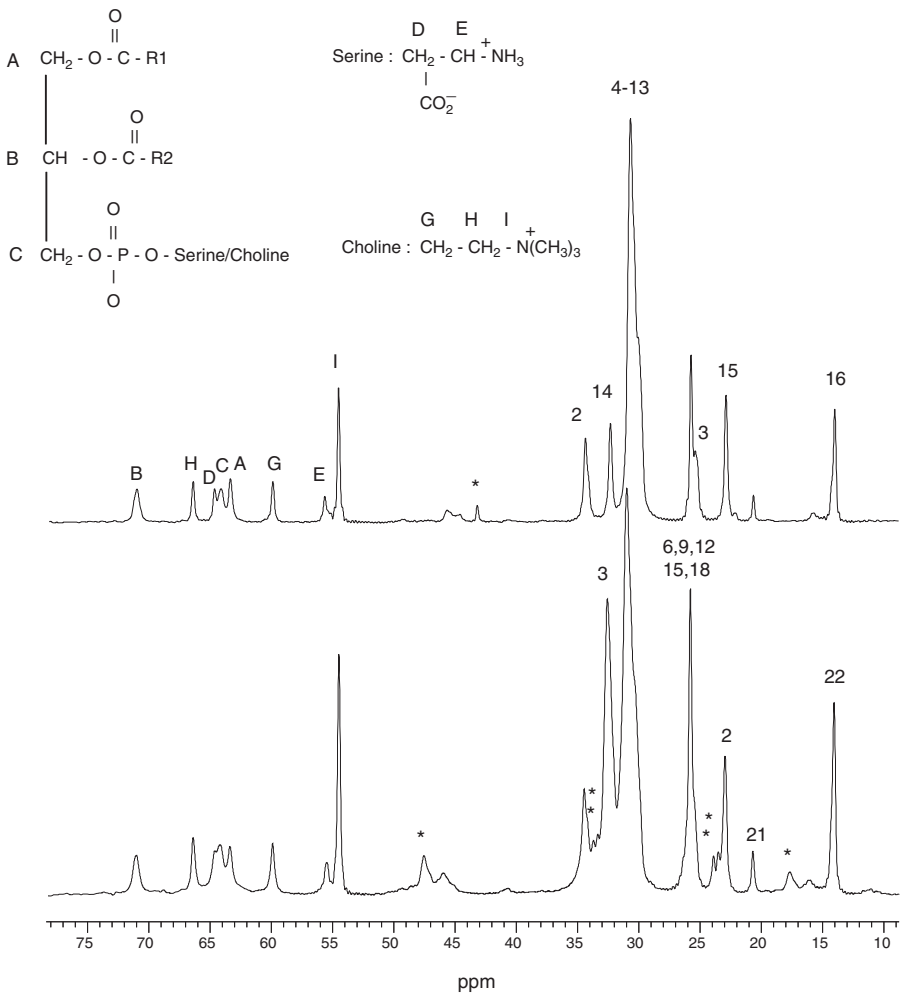

Fig. 1. ^{13}C NMR spectra, acquired at 310 K, displaying spectral region of phospholipid head group, glycerol and saturated acyl chain carbons (10–75 ppm). On top of the figure the structural formula of the glycerol moiety and the two phospholipids head groups, serine and choline, with corresponding assignment letters used in the spectra. Bottom spectrum: resonances of DPPC (60%)/SDPS (40%) sample. Resonances in the 10–35 ppm region of the bottom spectrum are labeled with the DHA (22:6) acyl chain carbon numbers. Resonances labeled with an asterisk "*" denote peaks that change chemical shifts when CPZ is present—compare with top spectrum. Top spectrum: corresponding spectrum of DPPC (54%)/SDPS (36%)/CPZ (10%). Glycerol and phospholipid head group resonances are labeled A–I in top spectrum where the 10–35 ppm region is labeled with the palmitic (16:0) acyl chain resonances of DPPC. Peak labeled with an asterisk "*" denotes a CPZ resonance. See the text for details.

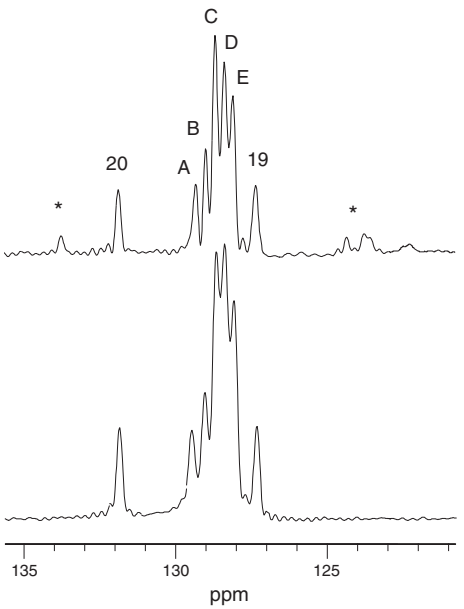

Fig. 2. Double bonded acyl chain carbon resonance region (125–135 ppm) of samples DPPC (60%)/SDPS (40%) (bottom spectrum) and DPPC (54%)/SDPS (36%)/CPZ (10%) (top spectrum). Spectra were acquired at 310 K (samples are in liquid crystalline phase). Assigned DHA resonances are C_{20} and C_{19}. Peaks labeled A–E correspond to carbons 4, 5, 7, 8, 10, 11, 13, 14, 16 and 17 of DHA, these resonances could not be individually assigned. See the text for details.

(in the 52–73 ppm spectral region). Fig. 1 bottom spectrum shows resonances of DPPC (60%)/SDPS (40%) sample and spectrum on top of Fig. 1 shows the corresponding spectrum of DPPC (54%)/SDPS (36%)/CPZ (10%) sample. The two spectra (Fig. 1, top and bottom) are dominated by the palmitic (DPPC) molecular specie. The molar composition of the samples cause the palmitic (16:0) acyl chain resonances to give ~60% of the peak intensities in this spectral region, whereas the contribution from the SDPS species in this spectral region is 40% (20% from each of the 18:0 and 22:6 acyl chains). Fig. 1, bottom spectrum, displays resonances in the 10–35 ppm region labeled with the DHA (22:6) acyl chain carbon numbers of DPPC (60%)/SDPS (40%) sample. Resonances labeled with an asterisk "*" denote peaks that change chemical shifts when CPZ is present—compare with top spectrum. The corresponding top spectrum of Fig. 1 displays resonances in the 10–35 ppm region labeled with the palmitic (16:0) acyl chain resonances of DPPC and glycerol and phospholipid head group resonances are labeled A–I (DPPC (54%)/SDPS (36%)/CPZ (10%) sample). Peak labeled with an asterisk "*" denotes a CPZ resonance. Additionally, Fig. 1 also shows the structural formulas of the glycerol moiety and the two phospholipids head groups, serine and choline, with the corresponding assignment letters used in the spectra. The three glycerol resonances will be composed of the two phospholipid species in the two samples, DPPC and SDPS.

From the T_1 data presented in Table 1, one finds that the carbon T_1 values of the choline head group β carbon and carboxyl carbon both show reduced T_1 values by the addition of CPZ. The glycerol carbon T_1 values, on the other hand, demonstrate a diverse effect of CPZ. The *sn-1* and *sn-3* glycerol carbons display an increased T_1 value due to CPZ in contrast to the *sn-2* glycerol carbon that shows a reduced T_1 value in presence of CPZ.

Resonances in Fig. 1 (bottom spectrum) at 46–48 and 16–18 ppm in the DPPC (60%)/SDPS (40%) spectrum appear at chemical shift values usually not found/reported in ^{13}C NMR spectra of phospholipid bilayers. The largest of these peaks, for example the one at 48 ppm displayed in bottom spectrum of Fig. 1, disappears in presence of CPZ (see Fig. 1, top spectrum). Similarly, the peak at 18 ppm, Fig. 1, bottom spectrum, disappears when CPZ is added to the sample (see Fig. 1, top spectrum). This suggests that the special chemical shifts of these resonances are due to the molecular organization in the DPPC (60%)/SDPS (40%) bilayer, i.e. the peaks at these unusual chemical shifts are due to microdomain formation/molecular segregation of DPPC and SDPS phospholipids. Furthermore, these domains are perturbed by the 10% CPZ present in the DPPC (54%)/SDPS (36%)/CPZ (10%) sample,

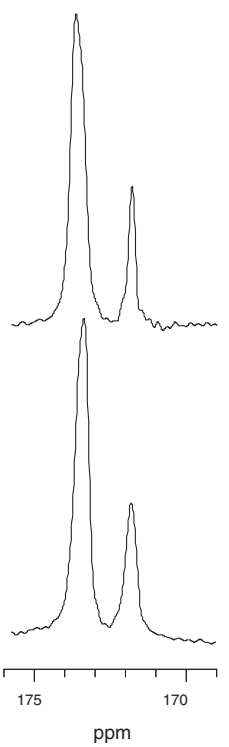

Fig. 3. Carbonyl and carboxyl carbon resonance region (170–176 ppm) of samples DPPC (60%)/SDPS (40%) (bottom spectrum) and DPPC (54%)/SDPS (36%)/CPZ (10%) (top spectrum). Spectra are acquired at 310 K. The molar composition (PC/PS ratio) makes the theoretical ratio between the carbonyl and carboxyl resonances to be 2.5. See the text for details.

Table 1
^{13}C spin-lattice relaxation times T_1 (seconds) at 310 K DPPC/SDPS and DPPC/SDPS/CPZ bilayers

Carbon	DPPC/SDPS	DPPC/SDPS/CPZ
C=O	2.73	2.47
CO_2^-	2.03	0.72
DHA C=C:		
C_{19}	0.83	0.80
C_{20}	0.53	0.61
(A*)	0.88	0.65
(B*)	0.75	0.55
(C*)	1.31	1.55
(D*)	1.69	1.35
(E*)	1.53	1.78
Glycerol carbon:		
sn-1	0.21	0.32
sn-2	0.37	0.27
sn-3	0.16	0.28
Serine carbon:		
α	0.22	0.33
β	1.53	0.73
Choline carbon :		
α	0.17	0.15
β	0.18	0.16
CH_3	0.20	0.24
Palmitic carbon:		
2	0.39	0.46
4–13	0.71	0.82
14	1.50	1.24
15	1.52	1.69
16	4.23	4.46
DHA carbon:		
6, 9, 12, 15, 18	0.56	1.24
21	1.82	1.53

Peaks present in Fig. 1—bottom spectrum that disappear or are reduced when CPZ is added, Fig. 1—top spectrum.

At chemical shift (ppm):		
47.56	1.08	No peak
45.95	0.99	0.80
33.71	1.77	No peak
33.40	1.29	No peak
23.94	0.99	No peak
23.57	0.95	No peak

* Peaks labeled in Fig. 2.

see Fig. 1—top spectrum, where the above-mentioned resonances at 48 and 18 ppm are not present in contrast to the remaining smaller resonances at 46 and 16 ppm. Furthemore, spectral changes of saturated carbon resonances and glycerol/head group resonances, without and with CPZ, shown in Fig. 1, bottom and top spectrum, respectively, indicate that these are due to saturated acyl chain carbons. Hydrophobic mismatch of DPPC domains alongside SDPS domains appears to be the origin of peaks at 48 and 18 ppm (Fig. 1, bottom spectrum). Peak intensity changes (as well as changes in T_1 values—see later) indicate that palmitic carbons 2 and 15 are responsible for the unexpected resonances at 48 and 18 ppm in spectrum of the DPPC (60%)/SDPS (40%) sample. Presumably, SDPS acyl chains experience the microdomain formation as well, as evidenced by the peaks labeled with an asterisk in bottom spectrum of Fig. 1. These assignments, except the assignment of the DHA C6–C18 peak that can be confirmed by comparison with spectra of samples with less DHA content [39], are tentative. The CPZ induced perturbation of the DPPC and the SDPS microdomains cause changes in the above-described resonances—see Fig. 1 top spectrum. Intensities of the assigned resonances displayed in Fig. 1 are in accordance with the molar ratio of SDPS's docosahexenoyl and stearoyl acyl chains at 20% each. The gel to liquid crystalline phase transition temperature of SDPs is not reported in the literature; however, it is likely to be below 0° C. Thus, at a sample temperature of 310 K the SDPS phospholipids would be in the liquid crystalline phase and DPPC just below its transition temperature of 314–315 K. However, the carbon resonances in spectra of DPPC/SDPS and DPPC/SDPS/CPZ have the narrow appearance that corresponds to phospholipids in the liquid (crystalline) state.

Fig. 2 shows the 125–135 ppm region where the C=C resonances of the acyl chains of samples DPPC/SDPS and DPPC/SDPS/CPZ are found. Comparison of the C=C resonances with/without CPZ (see Fig. 2) shows a pronounced intensity change of some of these, the peaks at 127–129 ppm, upon CPZ interaction. The crowded spectral region displayed in Fig. 2 poses an obstacle to a complete resonance assignment. However, in a recent solid-state NMR study, where $^1H-^{13}C$ two dimensional cross-polarization experiments were employed [44], the investigators managed to firmly assign DHA's C_{19} and C_{20}. Thus, the peak at 131.3 ppm is assigned to resonance C_{20} and the peak at 126.8 ppm to resonance C_{19}. The remaining C=C resonances of DHA (C_4–C_5, C_7–C_8, C_{10}–C_{11}, C_{13}–C_{14}, C_{16}–C_{17}) located between 127.4–130.5 ppm (peaks labeled A–E in Fig. 2 top spectrum) could not be individually assigned. As evident in Fig. 2 there is no significant intensity change of DHA's resonances C_{19} and

Table 2
^{13}P chemical shift anisotropy (CSA, in ppm) from 296 to 318 K DPPC/SDPS and DPPC/SDPS/CPZ bilayers

Temperature (K)	DPPC/SDPS	DPPC/SDPS/CPZ
296	99	85
297	99	86
298	97	86
299	98	87
300	95	86
301	95	84
302	94	83
303	94	83
304	91	80
305	90	79
306	88	78
307	88	76
308	86	76
309	86	73
310	84	70
311	82	70
312	82	66
313	80	66
314	79	65
315	78	63
316	76	66
317	73	63
318	71	64

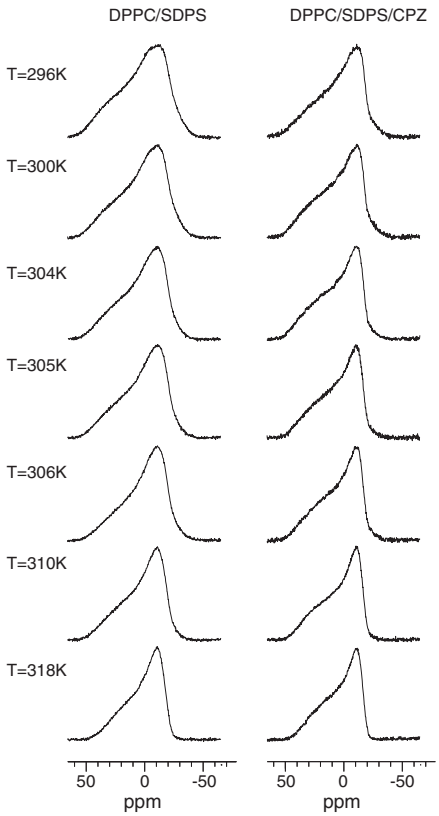

Fig. 4. Static ^{31}P NMR spectra of samples DPPC (60%)/SDPS (40%) (left column) and DPPC (54%)/SDPS (36%)/CPZ (10%) (right column). Sample temperatures from 296 K (top spectra) to 318 K (bottom spectra). See the text for details.

C_{20} upon addition of CPZ. Furthermore, the C=C resonances of DHA (Fig. 2 and Table 1) all display similar T_1 values with and without CPZ. In contrast to this, the DHA's sp^3 carbons in between sp^2 carbons, i.e. carbon 6, 9, 12, 15, and 18 have a combined peak with a T_1 value that more than doubles when CPZ is present. The single resonance peak of DHA's carbon 21 (see Fig. 1 and Table 1), on the other hand, shows a 16% reduction in presence of CPZ. Thus, the part of SDPS's DHA acyl chain that are affected by the presence of CPZ is the part close to the polar region of the bilayer, as demonstrated by the T_1 value increase of these resonances. The appearance of some broad peaks around 124 ppm labeled with an asterisk "*" (Fig. 2, top spectrum) when CPZ is present corresponds to double bonded carbon resonances of the CPZ molecule, as does the peak at ~133.5 ppm also labeled with an asterisk "*".

Fig. 3 shows the carbonyl resonance (~173 ppm) and the serine head group carboxyl (~171 ppm) [45] resonance of samples DPPC/SDPS (bottom spectrum) and DPPC/SDPS/CPZ (top spectrum). The molar composition (PC/PS ratio) makes the theoretical peak ratio of 2.5 between the carbonyl and carboxyl resonances. From the two spectra shown in Fig. 3, it is apparent that resonance intensities are not affected by addition of CPZ. A comparison of both the carbonyl resonance (~173 ppm) the serine head group carboxyl resonance (~171 ppm), without and with CPZ, makes it evident that the 10% CPZ reduces the SDPS's carboxyl resonance T_1 value (Table 1) by 65% (from 2.03 to 0.72 s). The corresponding T_1 values for the combined PC/PS carbonyl resonance show a 10% reduction in presence of CPZ.

In general, the ^{31}P CSA data presented in Table 2 and Fig. 4 show that the sample without CPZ has a higher CSA, than with CPZ, over the whole temperature range measured (296–318 K). The CSA of the sample without CPZ (the DPPC/SDPS sample) displays a fairly steady decrease as temperature increases. In addition to a general decrease in CSA value upon temperature increase, the CPZ-containing sample (the DPPC/SDPS/CPZ sample) displays a sudden drop in CSA of 13 ppm from 304 to 310 K. Thus, the CPZ-containing sample displays this sudden reduction in CSA at a sample temperature of about 305.5 K, in correspondence with the main melting (transition) temperature displayed by this kind of phospholipid sample. The ^{31}P T_1 values were measured at the central band of the MAS spectra, and presented in Table 3. The decrease in T_1 value as sample temperature increases demonstrates that the bilayer phospholipids are in "slow motion" motional regime. In Fig. 5 the three central band peaks are displayed at several of the temperatures investigated. They can be assigned [37,46] to the three molecular species: PC, PS and CPZ–PS complex. Both the PC and the PS species show similar T_1 values with and without CPZ and the CPZ–PS complex shows a T_1 similar to the PC and the PS species—see Table 3.

4. Discussion

The observed, slight decrease of the glycerol carbon resonances of the DPPC/SDPS/CPZ sample (Fig. 1) as compared to the DPPC/SDPS sample is most pronounced for the *sn-3* carbon, i.e. the glycerol carbon where the phosphorus and head group are attached. An explanation for this observation can be found in the possibility of an altered transverse relaxation of dipolar coupled spins under radio-

Table 3
^{13}P T_1 values (seconds) from 296 to 318 K DPPC/SDPS and DPPC/SDPS/CPZ bilayers

Temperature (K)	DPPC/SDPS		DPPC/SDPS/CPZ		
	PC	PS	PC	PS	CPZ–PS
296	1.29	1.03	1.39	1.18	0.99
298	1.03	0.97	1.19	0.99	0.84
300	1.02	1.00	1.02	0.95	0.89
302	0.96	0.85	0.99	0.89	0.74
304	0.96	0.83	0.91	0.88	0.70
306	0.95	0.87	0.87	0.83	1.00
308	0.88	0.80	0.87	0.81	0.71
310	0.93	0.84	0.84	0.76	0.65
312	0.84	0.79	0.84	0.79	0.68
314	0.91	0.84	0.88	0.83	0.64
316	0.82	0.88	0.82	0.79	0.59
318	0.75	0.76	0.79	0.67	0.55

frequency irradiation (decoupling) [47]. In such a case destructive interference effects can cause line broadening due to (molecular) motion interfere with the coherent modulation from radiofrequency decoupling. Even carbons without directly attached protons (such as carbonyl and carboxyl carbons) can to some extent experience these effects when coupled to other nearby protons. Furthermore, dipolar interactions are expected to be weak for non-protonated sp^2 carbons and the main line broadening mechanism will be the chemical shift anisotropy (CSA). (Protonated sp^2 carbons of the acyl chains' olefinic double bonds will experience both the described line broadening mechanisms [44]).

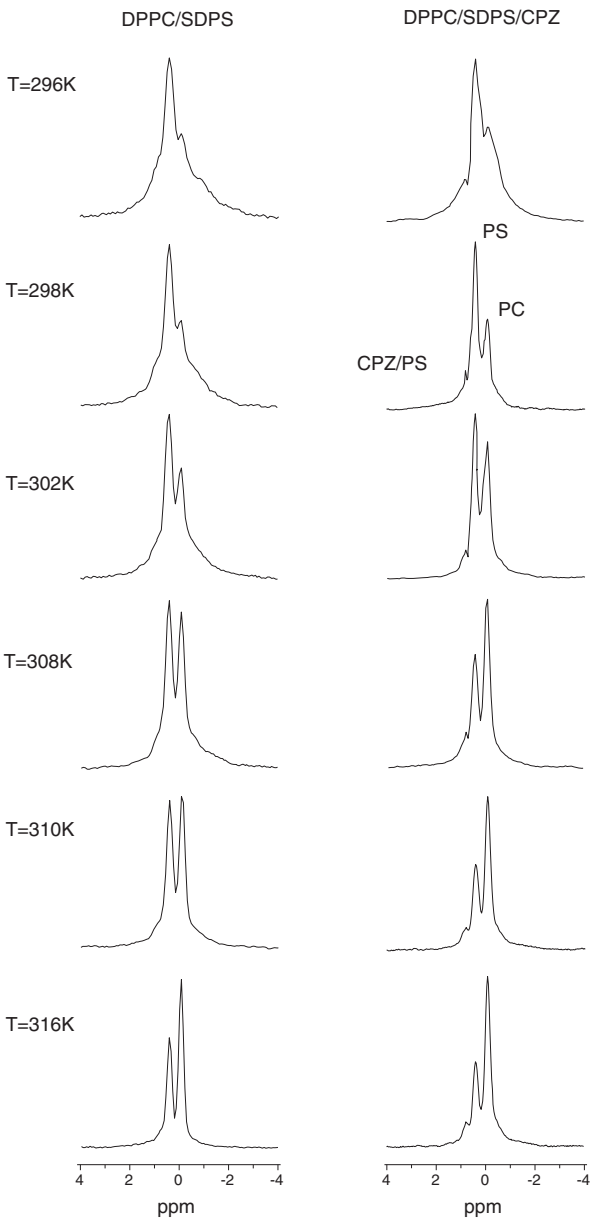

Fig. 5. ^{31}P MAS spectra of samples DPPC (60%)/SDPS (40%) (left column) and DPPC (54%)/SDPS (36%)/CPZ (10%) (right column) between sample temperatures 296 and 318 K. Note sudden decrease in CSA of CPZ-containing sample at 305 K. See the text for details.

Both the choline head group β carbon and the serine head group carboxyl carbon show reduced T_1 values by the addition of CPZ and presumably this is caused by an increased mobility. The glycerol carbon T_1 values, on the other hand, demonstrate a diverse effect of CPZ. The *sn-1* and *sn-3* glycerol carbons display lower mobility (an increased T_1 value) due to CPZ, whereas the *sn-2* glycerol carbon shows higher mobility (a reduced T_1 value) in presence of CPZ. This increased mobility of the *sn-2* moiety is not evident in the C═C resonances of DHA (Fig. 2 and Table 1). These resonances all display similar T_1 values with and without CPZ. However, the DHA's sp^3 carbons in between sp^2 carbons, i.e. carbon 6, 9, 12, 15, and 18 demonstrate reduced mobility in that these resonances have a combined peak with a T_1 value that more than double when CPZ is present. The single resonance peak of DHA's carbon 21 (see Fig. 1 and Table 1), on the other hand, shows a T_1 value with 16% reduction in presence of CPZ. Thus, the part of SDPS's DHA acyl chain that demonstrate a reduced mobility when CPZ is bound to the bilayer is the part close to the polar region of the bilayer, as demonstrated by an increase in the T_1 values of these resonances.

A comparison of both the carbonyl resonance (~173 ppm) the serine head group carboxyl resonance (~171 ppm), without and with CPZ, makes it evident that the 10% CPZ reduces the SDPS's carboxyl resonance T_1 value by 65% (from 2.03 to 0.72 s, see Table 1) indicating an increased mobility of the PS head group when CPZ is bound. The corresponding T_1 values for the combined PC/PS carbonyl resonance show a 10% reduction in presence of CPZ.

The ^{31}P CSA [48] data (Table 2 and Fig. 4) show that the sample without CPZ has a higher CSA, than when CPZ is present, over the whole temperature range measured (296–318 K). Thus, the CSA data support the ^{13}C T_1 data in that they both demonstrate increased mobility of the head groups when CPZ is bound to the bilayer. Resonances that are present in the spectrum of the DPPC (60%)/SDPS (40%) sample (Fig. 1, bottom spectrum) and that disappear in presence of 10% CPZ (Fig. 1, top spectrum) most probably are due to the special interface environment, e.g. the hydrophobic mismatch, at the interface of DPPC and SDPS microdomains. In itself the appearance of resonances at novel chemical shift values is a clear demonstration of a unique chemical environment in the DPPC (60%)/SDPS (40%) bilayer. Rationalizing the effects of microdomains in the DPPC/SDPS sample (see Fig. 1) it is reasonable to expect the existence of special local environments at the interface of microdomains where one predominantly consists of DPPC molecules and a neighboring domain contains SDPS molecules. Taking, for example, the two peaks at 48 and 18 ppm displayed in bottom spectrum of Fig. 1, and assuming that these two resonances are due to acyl chain CH_2 groups of the palmitoyl, stearoyl or C_3/C_{21} of the 22:6 acyl chain. Such a CH_2 group is in a special environment of the interface of two DPPC and SDPS microdomains. In such a case, the 48 ppm peak would come as a result of a CH_2 group that experienced an increased local field due to a neighboring electronegative nucleus, such as oxygen, or the deshielding region of a C=C group with strong magnetic suceptibility. The peak in Fig. 1 bottom spectrum, at 18 ppm, on the other hand, could be due to the special microdomain interface, where the CH_2 spends most of its time in the shielding region of a 22:6 acyl chain C=C group, i.e. this acyl chain resonance is shifted to a lower parts per million value by the environment of the microdomain interface. The demonstrated disappearance of bilayer microdomain ^{13}C peaks in presence of CPZ together with the found CPZ effects on DHA mobility [49] point at the crucial role DHA in *sn-2* position of SDPS has in formation and perseverance of phospholipid microdomains in a bilayer like the DPPC (60%)/SDPS (40%) of this study.

The found tendency of DHA, determined by ^{2}H NMR and X-ray diffraction [31], that the *sn-2* attached (22:6) acyl chain in a (16:0–22:6) PC bilayer has a distribution of mass that is shifted toward the bilayer aqueous interface would imply bending of the DHA acyl chain. In such a process, it is possible that the terminal methyl group can be located somewhere in vicinity of the polar region of the bilayer. The findings of the study presented here suggest CPZ bound to the phosphate of 1-stearoyl-2-docosahexenoyl phosphatidylserine will slow down and partially inhibit such a DHA acyl chain movement in a bilayer. This would affect the area occupied by a SDPS molecule (in the bilayer) and probably the thickness of the bilayer where SDPS molecules reside as well. It is quite likely that such CPZ caused changes can affect the function of proteins embedded in the bilayer.

References

[1] D.B. Jump, The biochemistry of n-3 polyunsaturated fatty acids, J. Biol. Chem. 277 (2002) 8755–8758.
[2] L.A. Witting, C.C. Harvey, B. Century, M.K. Horwitt, Dietary alterations of fatty acids of erythrocytes and mitochondria of brain and liver, J. Lipid Res. 2 (1961) 412–418.
[3] A. Lenzi, L. Gandini, V. Maresca, R. Rago, P. Sgrò, F. Dondero, M. Picardo, Fatty acid composition of spermatozoa and immature germ cells, Mol. Hum. Reprod. 6 (2000) 226–231.
[4] J.S. O'Brien, E.L. Sampson, Fatty acid and fatty aldehyde composition of the major brain lipids in normal human gray matter, white matter, and myelin, J. Lipid Res. 6 (1965) 545–551.
[5] W. Stillwell, S.R. Wassall, Docosahexaenoic acid: membrane properties of a unique fatty acid, Chem. Phys. Lipids 126 (2003) 1–27.
[6] C.E. Borgeson, L. Pardini, R.S. Pardini, R.C. Reitz, Effects of dietary fish oil on human mammary carcinoma and on lipid-metabolizing enzymes, Lipids 4 (1989) 290–295.
[7] M. Neuringer, W.E. Connor, D.S. Lin, L. Barstad, S. Luck, Biochemical and functional effects of prenatal and postnatal ω-3 fatty acid deficiency on retina and brain in rhesus monkeys, Proc. Natl. Acad. Sci. U. S. A. 83 (1986) 4021–4025.
[8] J.A. Glomset, Fish, fatty acids, and human health, N. Engl. J. Med. 312 (1985) 1253–1254.
[9] M. Lagarde, N. Gualde, M. Rigaud, Metabolic interactions between eicosanoids in blood and vascular cells, Biochem. J. 257 (1989) 313–320.
[10] A.M. de Urquiza, S. Liu, M. Sjöberg, R.H. Zetterström, W. Griffiths, J. Sjövall, T. Perlmann, Docosahexaenoic acid, a ligand for the retinoid X receptor in mouse brain, Science 290 (2000) 2140–2144.
[11] S.D. Freedman, H.M. Katz, E.M. Parker, M. Laposata, M.Y. Urman, J.G. Alvarez, A membrane lipid imbalance plays a role in the phenotypic expression of cystic fibrosis in cftr−/− mice, PNAS 96 (1999) 13995–14000.

[12] J.S. Poling, S. Vicini, M.A. Rogawski, N. Salem Jr., Docosahexaenoic acid block of neuronal voltage-gated K+ channels: subunit selective antagonism by zinc, Neuropharmacology 35 (1996) 969–982.
[13] M.C. Garcia, H.Y. Kim, Mobilization of arachidonate and docosahexaenoate by stimulation of the 5-HT2A receptor in rat C6 glioma cells, Brain Res. 768 (1997) 43–48.
[14] A. Salmon, S.W. Dodd, G.D. Williams, J.M. Beach, M.F. Brown, Configurational statistics of acyl chains in polyunsaturated lipid bilayers from deuterium NMR, J. Am. Chem. Soc. 109 (1987) 2600–2609.
[15] C. Leidy, K. Gousset, J. Ricker, W.F. Wolkers, N.M. Tsvetkova, F. Tablin, J.H. Crowe, Lipid phase behavior and stabilization of domains in membranes of platelets, Cell Biochem. Biophys. 40 (2004) 123–148.
[16] M.Ø. Jensen, O.G. Mouritsen, Lipids do influence protein function—the hydrophobic matching hypothesis revisited, Biochim. Biophys. Acta 1666 (2004) 205–226.
[17] P.R. Cullis, M.J. Hope, The bilayer stabilizing role of sphingomyelin in the presence of cholesterol. A ^{31}P NMR study, Biochim. Biophys. Acta 597 (1980) 5335–5542.
[18] B. Mantripragada, B. Sankaram, T.E. Thomson, Cholesterol-induced fluid-phase immiscibility in membranes, Proc. Natl. Acad. Sci. U. S. A. 88 (1991) 8686–8690.
[19] Y.-W. Hsueh, R. Giles, N. Kitson, J. Thewalt, The effect of ceramide on phosphateidylcholine membranes: a deuterium NMR study, Biophys. J. 82 (2002) 3089–3095.
[20] S.R. Shaikh, M.R. Brzustowicz, N. Gustafson, W. Stillwell, S.R. Wassall, Monounsaturated PE does not phase-separate from the lipid raft molecules sphingomyelin and cholesterol: role for polyunsaturation? Biochem. 41 (2002) 10593–10602.
[21] M.R. Brzustowicz, V. Cherezov, M. Caffrey, W. Stillwell, S.R. Wassall, Molecular organization of cholesterol in polyunsaturated membranes: microdomain formation, Biophys. J. 82 (2002) 285–298.
[22] S.R. Shaikh, A.C. Dumaual, D. LoCascio, R.A. Siddiqui, W. Stillwell, Acyl chain unsaturation in PE modulates phase separation from lipid raft molecules, Biochem. Biophys. Res. Commun. 311 (2003) 793–796.
[23] S. Moffett, D.A. Brown, M.E. Linder, Lipid-dependent targeting of G proteins into rafts, J. Biol. Chem. 275 (2000) 2191–2198.
[24] D. Huster, K. Arnold, K. Gawrisch, Influence of docosahexaenoic acid and cholesterol on lateral lipid organization in phospholipid mixtures, Biochem. 37 (1998) 17299–17308.
[25] M.R. Brzustowicz, V. Cherezov, M. Zerouga, M. Caffrey, W. Stillwell, S.R. Wassall, Controlling membrane cholesterol content. A role for polyunsaturated (docosahexaenoate) phospholipids, Biochem. 41 (2002) 12509–12519.
[26] S.R. Shaikh, A.C. Dumaual, A. Castillo, D. LoCascio, R.A. Siddiqui, W. Stillwell, S.R. Wassall, Oleic and docosahexaenoic acid differentially phase separate from lipid raft molecules: a comparative NMR, DSC, AFM, and detergent extraction study, Biophys. J. 87 (2004) 1752–1766.
[27] K.R. Applegate, J.A. Glomset, Computer-based modeling of the conformation and packing properties of docosahexaenoic acid, J. Lipid Res. 27 (1986) 658–680.
[28] K.R. Applegate, J.A. Glomset, Effect of acyl chain unsaturation on the conformation of model diacylglycerols: a computer modeling study, J. Lipid Res. 32 (1991) 635–644.
[29] K.R. Applegate, J.A. Glomset, Effect of acyl chain unsaturation on the packing of model diacylglycerols in simulated monolayers, J. Lipid Res. 32 (1991) 645–655.
[30] B.W. Koening, H.H. Strey, K. Gawrisch, Membrane lateral compressibility determined by NMR and X-ray diffraction. Effect of acyl chain polyunsaturation, Biophys. J. 73 (1997) 1954–1966.
[31] K. Rajamoorthi, H.I. Petrache, T.J. McIntosh, M.F. Brown, Packing and viscoelasticity of polyunsaturated w-3 and w-6 lipid bilayers as seen by 2H NMR and X-ray diffraction, J. Am. Chem. Soc. 127 (2005) 1576–1588.
[32] F.D. Gunstone, M.R. Pollard, C.M. Scrimgeour, H.S. Vedanayagam, Fatty acids. Part 50. ^{13}C nuclear magnetic resonance studies of olefinic fatty acids and esters, Chem. Phys. Lipids 18 (1977) 115–129.
[33] W. Nerdal, S.A. Gundersen, V. Thorsen, H. Høiland, H. Holmsen, Chlorpromazine interaction with glycerophospholipid liposomes studied by magic angle spinning solid state ^{13}C NMR and differential scanning calorimetry, Biochim. Biophys. Acta 1464 (2000) 165–175.
[34] W.-g. Wu, L.-M. Chi, Comparisons of lipid dynamics and packing in fully interdigitated monoarachidoylphosphatidylcholine and non-interdigitated dipalmitoylphosphatidylcholine bilayers: cross polarization/-magic angle spinning ^{13}C-NMR studies, Biochim. Biophys. Acta 1026 (1990) 225–235.
[35] J.R. Silvius, Gagné, Calcium-induced fusion and lateral phase separations in phosphatidylcholine–phosphatidylserine vesicles. Correlation by calorimetric and fusion measurements, Biochem. 23 (1984) 3241–3247.
[36] T.P. Stewart, S.W. Hui, A.R. Portis Jr., D. Papahadjopoulos, Complex phase mixing of phosphatidylcholine and phosphatidylserine in multilamellar membrane vesicles, Biochim. Biophys. Acta 556 (1979) 1–16.
[37] A.U. Gjerde, H. Holmsen, W. Nerdal, Chlorpromazine interaction with phosphatidylserines: a ^{13}C and ^{31}P solid-state NMR study, Biochim. Biophys. Acta 1682 (2004) 28–37.
[38] J.L. Browning, J. Seelig, Bilayers of phosphatidylserine: a deuterium and phosphorus nuclear magnetic resonance study, Biochem. 19 (1980) 1262–1270.
[39] S. Chen, A.U. Gjerde, H. Holmsen, W. Nerdal, Importance of polyunsaturated acyl chains in chlorpromazine interaction with phosphatidylserines: a ^{13}C and ^{31}P solid-state NMR study, Biophys. Chemist. 117 (2005) 101–109.
[40] S.J. Kohler, M.P. Klein, Orientation and dynamics of phospholipid head groups in bilayers and membranes determined from nuclear magnetic resonance chemical shielding tensors, Biochem. 16 (1977) 519–526.
[41] M.J. Janiak, D.M. Small, G.G. Shipley, Temperature and compositional dependence of the structure of hydrated dimyristoyl lecithin, J. Biol. Chem. 254 (1979) 6068–6078.
[42] D.M. Small, Observations on lecithin. Phase equilibria and structure of dry and hydrated egg lecithin, J. Lipid Res. 8 (1967) 551–557.
[43] M. Levitt, Symmetrical composite pulse sequences for NMR population inversion. I. Compensation of radiofrequency field inhomogeneity, J. Magn. Reson. 48 (1982) 234–264.
[44] S. Everts, J.H. davis, 1H and ^{13}C NMR of multilamellar dispersions of polyunsaturated (22:6) phospholipids, Biophys. J. 79 (2000) 885–897.
[45] D.L. Holwerda, P.D. Ellis, R.E. Wuthier, Carbon-13 and phosphorus-31 nuclear magnetic resonance studies on interaction of calcium with phosphatidylserine, Biochem. 20 (1981) 418–428.
[46] T.J.T. Pinheiro, A. Watts, Resolution of individual lipids in mixed phospholipid membranes and specific lipid–cytochrome *c* interactions by magic-angle spinning solid-state phosphorus-31 NMR, Biochem. 33 (1994) 2459–2467.
[47] F. Adebodun, J. Chung, B. Montez, E. Oldfield, X. Shan, Spectroscopic studies of lipids and biological membranes: carbon-13 and proton magic-angle sample sample-spinning nuclear magnetic resonance study of glycolipid-water systems, Biochem. 31 (1992) 4502–4509.
[48] P.R. Cullis, B. de Kruyff, R.E. Richards, Factors affecting the motion of the polar head group in phospholipid bilayers. A ^{31}P NMR study of unsonicated phosphatidylcholine liposomes, Biochim. Biophys. Acta 426 (1976) 433–446.
[49] L.L. Holte, F. Separovic, K. Gawrisch, Nuclear magnetic resonance investigation of hydrocarbon chain packing in bilayers of polyunsaturated phospholipids, Lipids 31 (1996) 199–203.

Paper III

ARTICAINE INTERACTION WITH DSPC BILAYER: A ^{13}C AND ^{31}P SOLID–STATE NMR STUDY[‡]

Chen Song[a], Henning Lygre[b] and Willy Nerdal[a,*]

[a] *Department of Chemistry, University of Bergen, Allégaten 41, N-5007 Bergen, Norway*

[b] *Department of Dental Science–Dental Pharmacology, University of Bergen, Armauer Hansens hus, Haukelandsv. 28, N-5021 Bergen, Norway*

*Author to whom correspondence should be addressed:
Willy Nerdal, Department of Chemistry, University of Bergen, Allégaten 41, N-5007 Bergen, Norway

Tel: +47-55-583353; Fax: +47-55-589400

Email address: Willy.Nerdal@kj.uib.no (W. Nerdal)

Running title: Articaine; Interaction with DSPC Bilayer.

[‡] This work was supported by a grant from the Norwegian Research Council (NFR).

Keywords: ^{13}C-MASNMR; ^{31}P-NMR; bilayers; Articaine bilayer interaction

ABBREVIATIONS

DMPC, 1, 2-Dimyristoyl-*sn*-Glycerol-3-Phosphatidylcholine; DSPC, 1, 2-Distearoyl-*sn*-Glycerol-3-Phosphatidylcholine; PC, Phosphatidylcholine; PS, Phosphatidylserine; MAS, Magic-angle Spinning; NMR, Nuclear Magnetic Resonance; CSA, Chemical Shift Anisotropy; NOE, Nuclear Overhauser Effect.

ABSTRACT

Articaine hydrochloride, 4-methyl-3(2-[propylamino]propionamido)-2-thiophenecarboxylic acid, methyl ester hydrochloride, is a local anaesthetic commonly used in dentistry, and is classified as an amide local anaesthetic. Solid-state ^{13}C and ^{31}P NMR were used to investigate the uncharged articaine species (sample pH=10.0) when interacting with distearoylphosphatidylcholine (DSPC) model membranes. The DSPC phospholipid bilayer was studied at four different molar ratios of articaine, 10, 25, 40, and 55 mol%, respectively. The articaine concentration dependent decrease in the DSPC bilayer gel-to-liquid-crystalline phase-transition temperature demonstrates substantial articaine interaction with this bilayer.

A DSPC bilayer contains a large hydrophobic core and the ^{13}C and ^{31}P NMR spectra of the 40 mol% articaine−containing sample demonstrate a disturbance in the molecular packing of the polar bilayer region that extends into the hydrophobic region, evidenced by carbon 2 and 3 of the stearoyl acyl chains. Observed ^{31}P and ^{13}C NMR spectral changes when articaine is increased from 40 to 55 mol%, suggest formation of articaine aggregates and decrease in DSPC bilayer perturbation at the latter articaine level.

1. INTRODUCTION

Local anesthetics are used to prevent generation of the nerve impulse by their binding to the voltage-gated sodium channel and blocking the inward sodium transport that creates the action potential of axons (Butterworth and Strichartz, 1990). Other membrane proteins are also targets of local anesthetics (Papahadjoupoulos et al., 1975; Tanaka and Hidaka, 1981; Vanderkooi and Adade, 1986; Arias et al., 1990; Bräu et al., 1995; Hollman et al., 2001) and the packing of phospholipids in biological bilayers is perturbed by these compounds (Boulanger et al., 1981; Auger et al., 1990; de Paula and Schreier, 1995; Pinto et al., 2000) with a possible change in membrane protein structure and function. Thus, perturbation of phospholipid packing in bilayers is intimately tied to a compound's anesthetic effect. In general, depression of bilayer gel-to-liquid-crystalline phase-transition temperature by local anesthetics has been found to correlate with the hydrophobicity of the anesthetic (Gupta, 1991; Hata et al., 2000a). The hemolytic effect of several local anesthetics on rat erythrocytes has been found to be greatly influenced by the uncharged species, even at a pH of 7.4, where there is a predominance of the positively charged species, indicating that the disrupting effect on the erythrocyte membranes is mainly due to hydrophobic interactions (Malheiros et al., 2004).

Articaine hydrochloride, 4-methyl-3(2-[propylamino]propionamido)-2-thiophenecarboxylic acid, methyl ester hydrochloride (Scheme 1), is a local anesthetic commonly used in dentistry (Malamed et al., 2000a, 2001), and is classified as an amide local anesthetic. However, unlike many other local anesthetics, a thiophene group increases articaine's liposolubility (Malamed et al., 2000b), and ability to penetrate the nerve sheath. In contrast to most local anesthetics, articaine contains an ester linkage that causes articaine to be hydrolyzed by plasma esterase (Vree et al., 1988; Grossmann et al., 2004) to articainic acid. In studies of local anesthetics interacting with model membranes, several methods have been employed, such as fluorescence spectroscopy (Westman et al., 1982; Fraceto et al., 2002), infrared spectroscopy (Fraceto et al., 2002; Suwalsky et al., 2002), X-ray diffraction (Coster et al., 1981; Suwalsky et al., 2002, 2005), electron spin resonance (Neal et al., 1976; Pinto et al.,

2000; Fraceto et al., 2002), ultraviolet light absorption spectroscopy (Westman et al., 1982) and nuclear magnetic resonance (Boulanger et al., 1981; Kelusky et al., 1984; Yoshino et al., 1998; Fraceto et al., 2002, 2005). Here, we employ solid-state ^{13}C (Wu and Chi, 1990) and ^{31}P NMR (Browning and Seelig, 1980) to study the uncharged articaine species interacting with distearoylphosphatidylcholine (DSPC) model membranes.

The DSPC bilayer samples subjected to NMR experiments were adjusted to a pH of 10.0 where more than 99% of the articaine molecules are in the uncharged form (pK_a of 7.8 (Malamed et al., 2000)). In the uncharged form, articaine is more hydrophobic (Butterworth and Strichartz, 1990; Pinto et al., 2000) and more potent (Kaneshina et al., 1997; Hata et al., 2000b) for phospholipid bilayer interaction than the charged species.

The hydrophobicity of articaine, and thereby its potential for interaction with the hydrophobic part of the phospholipid bilayer (articaine's lipophilicity) can be evaluated by the corresponding octanol/water partition coefficient. An octanol/water partition coefficient of 257 has been found for articaine and this high articaine preference for octanol over water was furthermore found to correlate well with articaine binding to isolated guinea pig atria tissue (Lüllman et al., 1980). Thus, more than 99% of the articaine added to the DSPC phospholipid samples used in this study will prefer the hydrophobic environment provided by the phospholipid bilayer and only a negligible fraction will prefer the water phase.

An amphiphilic compound like articaine will, depending on pH, have an ionic or nonionic polar moiety and a hydrophobic part. In an aqueous medium, amphiphilic molecules are able to organize themselves as micelles, bilayers, monolayers, hexagonal or cubic phases. Thus, it is likely that at certain conditions, e.g. concentration, an amphiphile like articaine can form self-aggregated structures. This has been observed for other local anesthetics like dibucaine and tetracaine (Schreier et al., 2000), where the critical micelle concentrations (CMC) were found to be 0.066 and 0.130 M, respectively.

In the present study, the DSPC phospholipid bilayer was prepared at four different molar ratios of articaine, 10, 25, 40, and 55 mol%, respectively. In the clinic, a 4 % articaine solution is used (Malamed et al., 2000), and both the water/lipid partitioning coefficient of local anesthetics (Malheiros et al., 2004) and the amount of bilayers in myelinized nervous fibers ensures that the injected anesthetic will reside in the bilayer. In addition to study the interaction of articaine with the DSPC bilayer, the experiments can also provide information about uncharged articaine self-association when interacting with the DSPC bilayer (de Verteuil et al., 1981; Garcia-Soto and Fernández, 1983).

2. EXPERIMENTAL

2.1 Sample preparation. Pure DSPC and DSPC with (10, 25, 40, and 55 mol%) articaine

Articaine Hydrochloride was obtained from Septodont (Saint-Maur-des-Fossés, France), and synthetic 1,2-Distearoyl-*sn*-Glycerol-3-Phosphatidylcholine (DSPC, powder) was purchased from Sigma Chemical Co. (St. Louis, MO, USA) and used without further purification. The desired amount of DSPC was dissolved in spectroscopic grade chloroform and then lyophilized to dryness, and the DSPC bilayer was kept under an argon atmosphere and not exposed to air and light. The sample of dry powder was then suspended in degassed distilled water. Subsequently, the lipid suspension of DSPC was divided into eight equi-amount samples and to four, the appropriate amounts of articaine (dissolved in degassed distilled water) were added to obtain four bilayer samples with an articaine molar ratio of 10, 25, 40 and 55 mol%, respectively. The suspensions contained multilamellar liposomes and unilamellar systems were obtained by freeze−thawing nine times. This sample preparation procedure gives large unilamellar liposomes of unequal size. However, in the final samples, bulk water is eliminated and the bilayers procedures are found to both stable and without artefacts, i. e. without different bilayer structures (Song et al., 2006) such as high curvature liposomes, i. e. small diameter liposomes that tend to change to larger diameter liposomes of higher stability. In our experience, employing an additional step in the sample preparation procedure of extrusion through a

(1000 nm) carbonate filter does not change or improve the subsequent NMR spectra, i.e. the sample at the time of data acquisition (Nerdal et al., 2000; Gjerde et al., 2004). In fact, some phospholipids (phosphatidylserines) tend to adhere to the carbonate filter and not pass the filter quantitatively (Gjerde et al., 2004).

At the freeze–thawing stage, one of the pure DSPC samples and all articaine–containing samples were adjusted to a pH of 10.0 by adding a small amount of 0.05 M NaOH, and the remaining sample of the pure DSPC bilayer was adjusted to a pH of 7.4. Furthermore, two DSPC samples containing 40 mol% articaine at sample pH of 5.0 and 7.4, respectively, were prepared in a similar manner.

Thus, four samples of DSPC and articaineHCl at a sample pH of 10.0, two DSPC samples with 40 mol% articaine at pH of 5.0 and at 7.4, were obtained as well as two pure DSPC samples of pH values of 7.4 and 10.0. All samples were equilibrated on an oil bath for 24 hours at 60 °C. Subsequently, the samples were subjected to 24 hours of lyophilization giving partially hydrated liposomes with a hydration level of ~12 water molecules per lipid molecule (determined by ^{1}H MASNMR). Water was added to the each sample to obtain fully hydrated bilayers (~30 water molecules per lipid molecule) (Small, 1967; Janiak et al., 1979) and the samples were equilibrated at 60 °C for another 48 hours (above the samples gel-to-liquid-crystalline transition temperature(s)) and packed into NMR rotors.

2.2 ^{13}C MASNMR Spectroscopy

The ^{13}C MASNMR experiments were obtained at 125.76 MHz on a Bruker 500 MHz Ultrashield Plus instrument equipped with magic-angle spinning hardware and using ZrO_2 rotors with a diameter of 4 mm. These rotors (and lids) are guaranteed by the manufacturer (Bruker) for use up to 50 °C. Above this temperature, we have experienced that the lid may come off during NMR acquisition, especially overnight (^{13}C) NMR experiments. Experiments were done at a sample temperature of 44 °C with sample spinning rate of 2 kHz. The experiments of this study were carried out with high-power proton decoupling during the acquisition i.e. without NOE and with a relaxation delay of six

seconds between transients. Acquisition of 16384 transients was carried out in each experiment, with the exception of the experiments on pure articaine, where 12288 transients were acquired in each. The fids were subjected to Fourier transformation without the use of an exponential window function in order to keep spectral resolution.

2.3 ^{31}P NMR Spectroscopy

^{31}P experiments were carried out on a Bruker 500 MHz Ultrashield Plus instrument and on a Bruker AVANCE DMX 400 instrument. Magic-angle spinning ^{31}P experiments were carried out at 161.98 MHz with a rotor spinning rate of 1.5, 2, and 3 kHz, respectively. Typically, 1024 transients with a relaxation delay of four seconds between transients were accumulated at 44°C and 57 °C, and Fourier transformed without apodization in order to keep spectral resolution. The majority of the static ^{31}P spectra were carried out at 161.98 MHz with 10240 transients and a relaxation delay of five seconds between transients. These experiments were acquired on samples with a pH of 10.0 at temperatures 42−57 °C. Static ^{31}P experiments were acquired at 202.47 MHz on DSPC bilayer with 40 mol% articaine at sample temperatures of 42 and 52 °C, respectively. In these two latter experiments the amount of sample was ∼1/3 of the other samples, 12288 transients were collected with a relaxation delay of five seconds between transients and the probe-head was a flat-coil (shown in Figure 3-panel B). All ^{31}P experiments were acquired with high-power decoupling during acquisition, i.e. without NOE. The static ^{31}P fids were multiplied with an exponential window function increasing the linewidth by 50 Hz to reduce noise prior to Fourier transformation. The ^{31}P chemical shifts were referenced to 85% phosphoric acid (H_3PO_4, 0 ppm).

3. RESULTS

Articaine has a pK_a of 7.8, and consequently, at a pH of 7.4, two articaine species will be present, the positively charged and the neutral species, at about 70% and 30%, respectively. Figure 1-a shows the 120−180 ppm region of a ^{13}C MASNMR spectrum of pure articaine (with 15 wt% D_2O). Displayed in Figure 1-b and Figure 1-c are the 120−180 ppm regions of ^{13}C MASNMR spectra of fully hydrated DSPC bilayer with 40 mol% articaine added, at sample pH's of 7.4 and 5.0, respectively. All spectra of Figure 1 are acquired at 44 ℃, where the DSPC bilayer is in the gel state (DSPC has a T_m of 54 ℃ and will depend on pH). The asterisks in Figure 1-c label articaine resonances that have a pronounced change in chemical shifts upon increased sample acidity. In a ^{13}C MASNMR spectrum of dipalmitoylphosphatidylcholine (DMPC) bilayer at pH of 7.4 (data not shown) acquired at 44 ℃ (above DMPC's T_m of 34 ℃), the 70%/30% distribution was demonstrated by two articaine resonances (with this peak intensity ratio) at ~163 ppm. The articaine carbonyl (Scheme 1) will most likely be influenced by protonation of the amide nitrogen three covalent bonds away in the molecule and this identifies the articaine carbonyl resonance, see Figure 1-a. Furthermore, the articaine carboxyl resonance can now be identified to be the resonance at ~170 ppm, see top spectrum. The left-most resonance in Figure 1-b and Figure 1-c, is the carbonyl resonance of DSPC. In order to study the interaction of the neutral and most potent articaine species with the DSPC bilayer, and at the same time avoid drawbacks due to the presence of two articaine species in the sample, a sample pH of 10.0 was chosen for the articaine interaction study with the DSPC bilayer. Figure 2-top, shows a ^{13}C MASNMR spectrum of DSPC at pH of 7.4, note that the spectral region without resonances, 76−170 ppm, is omitted in the spectrum and that the DSPC molecule is displayed on top of the spectrum. The corresponding spectrum of DSPC at a sample pH of 10.0 is displayed in Figure 2-bottom. Some resonances that are due to changed packing of the phospholipids in the polar bilayer region at a pH of 10.0 are marked with an asterisk in Figure 2-bottom. See for example the resonance at ~173 ppm in Figure 2-bottom, this is presumably a DSPC carbonyl resonance from molecular pacing specific to a sample at a pH of 10.0. Similarly, resonances marked with an asterisk in the glycerol/headgroup

region, i.e. the molecular packing of a minor part of the DSPC molecules that takes place at a pH of 10.0 are visible in the glycerol/headgroup region. Whereas, the hydrophobic part of the bilayer, reported by the resonances in the 14−36 ppm region displays no changes due to the high pH. A further documentation of alterations in the polar region of the bilayer is found in the ^{31}P static NMR spectra displayed in Figure 3. In Figure 3-A, all four spectra are acquired on samples with a pH of 10.0. The two spectra in the top row are acquired at 42 ^{o}C (below T_m) and the two spectra of the top row at 57 ℃ (above T_m). The CSA of the static ^{31}P spectra shown in Figure 3-A are: 97 ppm in top left spectrum (pure DSPC at 42 ℃), 80 ppm in top right spectrum (DSPC/40 mol% articaine at 42 ℃), 68 ppm in lower left spectrum (pure DSPC at 57 ℃) and 60 ppm in lower right spectrum (DSPC/40 mol% articaine at 57 ℃). Furthermore, the two spectra in the left column are acquired on pure DSPC bilayer and the two spectra in the right column on DSPC bilayer with 40 mol% articaine.

The corresponding spectra of samples at a pH of 7.4 are displayed in Figure 3-B where the observed CSA of these static ^{31}P spectra are: 97 ppm in top left spectrum (pure DSPC at 42 ℃), 95 ppm in top right spectrum (DSPC/40 mol% articaine at 42 ℃), 62 ppm in lower left spectrum (pure DSPC at 57 ℃) and 60 ppm in lower right spectrum (DSPC/40 mol% articaine at 57 ℃). Thus, the most pronounced reduction of the phospholipid phosphorous CSA in presence of 40 mol% articaine is found at a sample pH of 10.0 at 42 ℃ (below T_m) (Figure 3-A, top row). The corresponding increase in mobility of the phospholipid phosphorous atom causing the reduction in the observed CSA is most pronounced at a pH of 10.0 and 42 ℃. Furthermore, at a sample pH of 10.0 and in presence of 40 mol% articaine a small fraction of the phospholipids will be highly mobile and give rise to an isotropic lipid phase (Figure 3-A, right column). The isotropic peak in the two spectra at pH of 10.0 (Figure 3-A, left column) can be corroborated with the minor resonances in the ^{13}C MASNMR spectra shown in Figure 2-bottom, in that a pH of 10.0 has some effect on the molecular packing in the glycerol/headgroup part of the DSPC bilayer. Figure 4 shows the ^{31}P CSA as a function of sample temperature. The CSA of pure DSPC (□ in Figure 4) displays a sudden drop at the DSPC's gel-to-liquid-crystalline

phase-transition temperature of 56 ℃. CSA values of DSPC bilayer with 10 mol% articaine (∗ in Figure 4) and 40 mol% articaine (△ in Figure 4) display a bilayer phase transition temperature of 52 ℃ and 48 ℃, respectively. The DSPC bilayer samples with articaine contents of 25 and 55 mol%, show gel-to-liquid-crystalline phase-transition temperatures of 48 and 46 ℃, respectively (data not shown). Thus, the observed concentration−dependent reduction in bilayer gel-to-liquid-crystalline phase-transition temperature demonstrates articaine interaction with the DSPC bilayer.

Figure 5 shows ^{31}P MASNMR spectra of DSPC bilayer without (Figure 5-a) and with 10−55 mol% articaine (Figure 5, b−e) at samples temperatures of 44 ℃ (left column) and 57℃ (right column), respectively. In these spectra, the central band peak(s) and the corresponding spinning sideband(s) on one side of the central band peak(s) are displayed. The MAS spinning rate for all spectra is 3 kHz. Two central band peaks are present in spectra of DSPC with 10 mol% articaine (Figure 5-b), and three central band peaks in DSPC samples with 25 (Figure 5-c) and 40 mol% (Figure 5-d) articaine, whereas two such peaks are found in spectra of DSPC with 55 mol% (Figure 5-e) articaine. In general, the central band peaks caused by the presence of articaine demonstrate chemical environments for the phospholipid phosphate-group that are due interaction with the anesthetic. The change in spectra of Figure 5 when articaine content is increased from 40 mol% (Figure 5-d) to 55 mol% (Figure 5-e) shows a reduction from three central band peaks to two. This could indicate articaine self-association/phase separation in DSPC bilayer at high (55 mol%) articaine levels (see later).

The ^{13}C MASNMR spectra of the 159−181 ppm region (shown in Figure 6) show on top spectrum a, pure DSPC bilayer at pH of 10.0. The carbonyl resonance is found at ∼174.1 ppm and an additional smaller resonance at ∼175.9 ppm. The latter corresponds with the already described phospholipid packing in a DSPC bilayer at pH of 10.0. The resonance at ∼175.9 ppm in spectrum shown in Figure 6-a, disappears with 10 mol% articaine, suggesting that the pH related disturbance of the DSPC bilayer is located mainly to the polar region. The resonance at ∼163.0 ppm in spectra b-e of Figure 6 is the articaine carbonyl

resonance (see Scheme 1 and Figure 1-a). Furthermore, at 40 mol% articaine, the influence of the phospholipid packing of the phosphate/headgroup region of the DSPC bilayer appears to be severely affected in that the articaine carboxyl resonance appears at ~178.8 ppm and two other (carboxyl) peaks are found at ~174.7 and ~175.3 ppm (Figure 6-d). The articaine carboxyl resonance at 40 mol% articaine in the DSPC bilayer demonstrates that the articaine carboxyl group is likely to be the main articaine moiety with DSPC interaction in the polar region of this bilayer. The articaine carboxyl resonance is greatly reduced in spectrum of 55 mol% articaine, Figure 6-e.

A further demonstration of articaine influence on DSPC bilayer's (at pH=10.0) polar region is found in the ^{13}C MASNMR spectra in Figure 7 showing spectral region 47−73 ppm of pure DSPC in spectrum a, 25 mol% articaine-containing spectrum shown in Figure 7-b, 40 mol% articaine in Figure 7-c and 55 mol% articaine in Figure 7-d. In Figure 7-a the glycerol and choline headgroup carbon resonances are labeled A−C, G, H and I, and smaller resonances in this spectral region are due to some perturbation of phospholipids packing at a pH of 10.0. Articaine resonances are present in spectra of Figure 7-b, -c and -d at ~58.5, ~52.2, ~49.9 and ~49.5 ppm, respectively.

Evidence for articaine influence on phospholipid packing in DSPC bilayer (at pH=10.0) hydrophobic region is found when comparing ^{13}C MASNMR spectra shown in Figure 8. Spectrum of pure DSPC shown in Figure 8-a, DSPC with 40 mol% articaine in Figure 8-b, DSPC with 55 mol% articaine in Figure 8-c and pure articaine (with 15 wt% D_2O) in Figure 8-d. These spectra of Figure 8 show spectral regions 9−27 and 34−37 ppm. Major spectral changes are evident for acyl chain carbon resonances 2 and 3, in Figure 8-b, where the two resonances that can be assigned to carbon 2 of the stearoyl acyl chain, and similarly the two resonances assigned to carbon 3, suggest conversion between two mesomorphic lipid states at a rate slower than the NMR timescale. Furthermore, smaller articaine resonances are present at ~20.0, ~16.8, ~11.5 and ~11.0 ppm. As demonstrated in Figure 8-c, the large molecular packing effect on the phospholipids by the 40 mol % articaine (Figure 8-b) is reduced in 55 mol% articaine−containing sample (Figure 8-c). The arrows in Figure 8-c

point at broad resonances that are not present in spectrum 40 mol% articaine containing sample (Figure 8-b). Accompanying these spectral changes is a marked reduction in articaine resonances (marked with '#' in Figure 8-c) even though the total articaine molar ratio increases from 40 mol% (Figure 8-b) to 55 mol% (Figure 8-c). The broad resonances only present in spectrum of the 55 mol% DSPC sample (indicated by arrows in Figure 8-c) could very well come from self-aggregated articaine molecules, such an interpretation is supported by the observed reduction in signal intensity of articaine resonances (marked with '#' in Figure 8-c) as articaine mol% is increased from 40 to 55.

4. Discussion

Our samples contain phospholipids hydrated with ~32 water molecules per phospholipids i.e. without bulk water present the amount of articaine that can be accommodated in the bilayer can be followed in the NMR spectra of our samples with 10, 25, 40 and 55 mol% articaine. Thus, the absence of bulk water in our samples makes a lipid (or octanol)/water partition coefficient not directly applicable. Apparently, an articaine molar ratio of 55 is above the amount that can be accommodated in the DSPC bilayer and some form of articaine aggregates coexists with the articaine saturated bilayer. This comes into effect when the articaine molar ratio is increased from 40 to 55. In case of hydrolysis of the articaine at a pH of 10.0, formation of free carboxylic acid will follow. Evidence of free carboxylic acid is not found in our ^{13}C NMR spectra in that an eventual free carboxylic acid carbon resonance would appear in the carbonyl chemical shift region (Figure 6), and would increase with increasing articaine molar ratio as well as show a narrow line-shape compared with the other resonances due to the high mobility of a small molecule. No carbon resonance with these characteristics can be found in our spectra (Figure 6). The uncharged articaine concentration−dependent reduction in the DSPC bilayer gel-to-liquid-crystalline phase-transition temperature demonstrates substantial articaine interaction with this bilayer. In general, depression of gel-to-liquid-crystalline phase-transition temperature by local anesthetics has been found to correlate with the anesthetic hydrophobicity (Malheiros et al., 2004). However, hydrophobicity of the anesthetic as well as steric effects in the anesthetic−

phospholipid interaction will determine the preferential positioning of the anesthetic in the bilayer (Fraceto et al., 2005). The importance of articaine hydrophobicity can be seen when comparing the ^{13}C MASNMR spectra of DMPC/40 mol% articaine at a pH of 7.4 (Figure 1-bottom) with that DSPC/40 mol% articaine at a pH of 10.0 (Figure 6-d). Articaine carboxyl group interaction with the PC bilayer appears to be substantial at a sample pH of 10.0, with uncharged articaine, and not present/minor at a sample pH of 7.4. A DSPC bilayer contains a large hydrophobic core and the NMR spectra of the 40 mol% articaine−containing sample demonstrate a large disturbance in the molecular packing of the polar bilayer region that extends into the hydrophobic region, evidenced by carbon 2 and 3 of the acyl chains. Observed ^{31}P and ^{13}C NMR spectral changes when articaine is increased from 40 to 55 mol%, suggest formation of articaine aggregates and decrease in DSPC bilayer perturbation at the latter articaine level.

REFERENCES

Arias, H.R., Sankaram, M.B., Marsh, D., Barrantes, F.J., 1990. Effect of local anaesthetics on steroid-nicotinic acetylcholine receptor interactions in native membranes of *Torpedo marmorata* electric organ. *Biochim. Biophys. Acta* 1027(3), 287−294.

Auger, M., Smith, I.C.P., Mantsch, H.H., Wong, P.T.T., 1990. High-pressure infrared study of phosphatidylserine bilayers and their interactions with the local anesthetic tetracaine. *Biochemistry* 29(8), 2008−2015.

Boulanger, Y., Schreier, S., Smith, I.C.P., 1981. Molecular details of anesthetic-lipid interaction as seen by deuterium and phosphorus-31 nuclear magnetic resonance. *Biochemistry* 20(24), 6824−6830.

Bräu, M.E., Nau, C., Hempelmann, G., Vogel, W., 1995. Local anesthetics potently block a potential insensitive potassium channel in myelinated nerve. *J. Gen. Physiol.* 105(4), 485−505.

Browning, J.L., Seelig, J., 1980. Bilayers of phosphatidylserine: a deuterium and phosphorus nuclear magnetic resonance study. *Biochemistry* 19(6), 1262−1270.

Butterworth, J.F. IV, Strichartz, G.R., 1990. Molecular mechanisms of local anesthesia: a review. *Anesthesiology* 72(4), 711−734.

Coster, H.G.L., James, V.J., Berthet, C., Miller, A., 1981. Location and effect of procaine on lecithin/cholesterol membranes using X-ray diffraction methods. *Biochim. Biophys. Acta* 641(1), 281−285.

de Paula, E., Schreier, S., 1995. Use of a novel method for determination of partition coefficients to compare the effect of local anesthetics on membrane structure. *Biochim. Biophys. Acta* 1240(1), 25−33.

de Verteuil, F., Pink, D.A., Vadas, E.B., Zuckermann, M.J., 1981. Phase diagrams for impure lipid systems. Application to lipid/anaesthetic mixtures. *Biochim. Biophys. Acta* 640(1), 207−222.

Fraceto, L.F., Pinto, L. de. M.A., Franzoni, L., Braga, A.A.C., Spisni, A., Schreier, S., de Paula, E., 2002. Spectroscopic evidence for a preferential location of lidocaine inside phospholipid bilayers. *Biophys. Chem.* 99(3), 229−243.

Fraceto, L.F., Spisni, A., Schreier, S., de Paula, E., 2005. Differential effects of uncharged aminoamide local anesthetics on phospholipid bilayers, as monitored by ^{1}H-NMR measurements. *Biophys. Chem.* 115(1), 11−18.

Garcia-Soto, J., Fernández, M.S., 1983. The effect of neutral and charged micelles on the acid-base dissociation of the local anesthetic tetracaine. *Biochim. Biophys. Acta* 731(2), 275−281.

Gjerde, A.U., Holmsen, H., Nerdal, W., 2004. Chlorpromazine interaction with phosphatidylserines: A ^{13}C and ^{31}P solid-state NMR study. *Biochim. Biophys. Acta* 1682(1−3), 28−37.

Grossmann, M., Sattler, G., Pistner, H., Oertel, R., Richter, K., Schinzel, S., Jacobs, L.-D., 2004. Pharmacokinetics of articaine hydrochloride in tumescent local anesthesia for liposuction. *J. Clin. Pharmacol.* 44(11), 1282−1289.

Gupta, S.P., 1991. QSAR (quantitative structure-activity relationship) studies on local anesthetics. *Chem. Rev.* 91(6), 1109−1119.

Hata, T., Matsuki, H., Kaneshina, S., 2000a. Effect of local anesthetics on the phase transition temperatures of ether- and ester-linked phospholipid bilayer membranes. *Colloids Surf. B* 18(1), 41−50.

Hata, T., Sakamato, T., Matsuki, H., Kaneshina, S., 2000b. Partition coefficients of charged and uncharged local anesthetics into dipalmitoylphosphatidylcholine bilayer membrane: estimation from pH dependence on the depression of phase transition temperatures. *Colloids Surf. B* 22(1), 77–84.

Hollman, M.W., Wieczorek, K.S., Berger, A., Durieux, M.E., 2001. Local anesthetic inhibition of G protein-coupled receptor signaling by interference with $G\alpha_q$ protein function. *Mol. Pharmacol.* 59(2), 294−301.

Janiak, M.J., Small, D.M., Shipley, G.G., 1979. Temperature and compositional dependence of the structure of hydrated dimyristoyl lecithin, *J. Biol. Chem.* 254(13), 6068−6078.

Kaneshina, S., Satake, H., Yamamoto, T., Kume, Y., Matsuki, H., 1997. Partitioning of local anesthetic dibucaine into bilayer membranes of dimyristoylphosphatidylcholine. *Colloids Surf. B* 10(1), 51−57.

Kelusky, E.C., Smith, I.C.P., 1984. The influence of local anesthetics on molecular organization in phosphatidylethanolamine membranes. *Mol. Pharmacol.* 26(2), 314−321.

Lüllman, H., Timmermans, P.B.M.W.M., Weikert, G.M., Ziegler, A., 1980. Accumulation of drugs by guinea pig isolated atria. Quantitative correlations. *J. Med. Chem.* 23(5), 560−565.

Malamed, S.F., Gagnon, S., Leblanc, D., 2000a. Efficacy of articaine: a new amide local anesthetic. *J. Am. Dent. Assoc.* 131(5), 635−642.

Malamed, S.F., Gagnon, S., Leblanc, D., 2000b. A comparison between articaine HCl and lidocaine HCl in pediatric dental patients. *Pediatr. Dent.* 22, 307−311.

Malamed, S.F., Gagnon, S., Leblanc, D., 2001. Articaine hydrochloride: a study of the safety of a new amide local anesthetic. *J. Am. Dent. Assoc.* 132(2), 177−185.

Malheiros, S.V.P., Pinto, L.M.A., Gottardo, L., Yokaichiya, D.K., Fraceto, L.F., Meirelles, N.C., de Paula, E., 2004. A new look at the hemolytic effect of local anesthetics, considering their real membrane/water partitioning at pH 7.4. *Biophys. Chem.* 110(3), 213–221.

Neal, M.J., Butler, K.W., Polnaszek, C.F., Smith, I.C.P., 1976. The influence of anesthetics and cholesterol on the degree of molecular organization and mobility of ox brain white matter. Lipids in multibilayer membranes: a spin probe study using spectral simulation by the stochastic method. *Mol. Pharmacol.* 12(1), 144−155.

Nerdal, W., Gundersen, S. A., Thorsen, V., Høiland, H., Holmsen, H., 2000. Chlorpromazine interaction with glycerophospholipid liposomes studied by magic angle spinning solid-state ^{13}C-NMR and differential scanning calorimetry. *Biochim. Biophys. Acta* 1464(1), 165−175.

Papahadjoupoulos, D., Jacobson, K., Poste, G., Shepherd, G., 1975. Effects of local anesthetics on membrane properties I. Changes in the fluidity of phospholipid bilayers. *Biochim. Biophys. Acta.* 394(4), 504−519.

Pinto, L. de M.A., Yokaichiya, D.K., Fraceto, L.F, de Paula, E., 2000. Interaction of benzocaine with model membranes. *Biophys. Chem.* 87(2−3), 213−223.

Schreier, S., Malheiros, S.V.P., de Paula, E., 2000. Surface active drugs: self-association and interaction with membranes and surfactants. Physicochemical and biological aspects. *Biochim. Biophys. Acta* 1508(1−2), 210−234.

Small, D.M., 1967. Phase equilibria and structure of dry and hydrated egg lecithin. *J. Lipid Res.* 8(6), 551−557.

Song, C., Holmsen, H., Nerdal, W., 2006. Existence of lipid microdomains in bilayer of dipalmitoylphosphatidylcholine (DPPC) and 1-stearoyl-2-docosahexenoyl phosphatidylserine (SDPS) and their perturbation by chlorpromazine: A ^{13}C and ^{31}P solid-state NMR study. *Biophys. Chem.* 120(3), 178−187.

Suwalsky, M., Schneider, C., Villena, F., Norris, B., Cárdenas, H., Cuevas, F., Sotomayor, C.P., 2002. Structural effects of the local anesthetic bupivacaine

hydrochloride on the human erythrocyte membrane and molecular models. *Blood Cells Mol. Diseases* 29(1), 14−23.

Suwalsky, M., Schneider, C., Villena, F., Norris, B., Cárdenas, H., Cuevas, F., Sotomayor, C.P., 2005. A study of the perturbation effects of the local anesthetic procaine on human erythrocyte and model membranes and of modifications of the sodium transport in toad skin. *Biophys. Chem.* 116(3), 227−235.

Tanaka, T., Hidaka, H., 1981. Interaction of local anesthetics with calmodulin. *Biochem. Biophys. Res. Commun.* 101(2), 447−453.

Vanderkooi, G., Adade, A.B., 1986. Stoichiometry and dissociation constants for interaction of tetracaine with mitochondrial adenosinetriphosphatase as determined by fluorescence. *Biochemistry* 25(22), 7118−7124.

Vree, T.B., Baars, A.M., Van Oss, G.E., C.J.M., Booij, L.H.D.J., 1988. High-performance liquid chromatography and preliminary pharmacokinetics of articaine and its 2-carboxy metabolite in human serum and urine. *J. Chromatogr.* 424(2), 440−444.

Westman, J., Boulanger, Y., Ehrenberg, A., Smith, I.C.P., 1982. Charge and pH dependent drub binding to model membranes. A ^{2}H-NMR and light absorption study. *Biochim. Biophys. Acta* 685(3), 315−328.

Wu, W.-g., Chi, L.-M., 1990. Comparisons of lipid dynamics and packing in fully interdigitated monoarachidoylphosphatidylcholine and non-interdigitated dipalmitoylphosphatidylcholine bilayers: cross polarization/magic angle spinning $^{13+}$C-NMR studies. *Biochim. Biophys. Acta* 1026(2), 225−235.

Yoshino, A., Yoshida, T., Okabayashi, H., Kamaya, H., Ueda, I., 1998. ^{19}F and ^{1}H NMR and NOE study on halothane-micelle interaction: residence location of anesthetic molecules. *J. Colloid. Interface Sci.* 198(2), 319−322.

FIGURE LEGENDS

Scheme 1. Structural formula of positively charged articaine hydrochloride.

Figure 1. ^{13}C MASNMR spectra acquired at 44 ℃, displaying spectral region of 122−178 ppm. a: Spectrum of articaine (with 15 wt% D_2O) with assigned resonances of carboxyl (O−C=O) and carbonyl (C=O) group, see Scheme 1. b: Spectrum of DSPC and 40 mol% articaine at a sample pH of 7.4. c: Spectrum of DSPC and 40 mol% articaine at a sample pH of 5.0. Articaine resonances labeled with an asterisk '*' are resonances that change chemical shifts upon a decrease in pH from 7.4 to 5.0. See the text for details.

Figure 2. ^{13}C MASNMR spectra, acquired at 44 ℃, displaying spectral regions from 12−76 ppm, and 170−178 ppm. On top of the figure, the molecular structure of DSPC with corresponding spectral assignment letters. Top: Spectrum of DSPC at a pH of 7.4, where resonances labelled with numbers identify the acyl chain carbons and capital letters identify glycerol and headgroup resonances. Bottom: Spectrum of DSPC, at a sample pH of 10.0. Resonances labelled with an asterisk '*' denote resonances present only at pH 10.0, and the spinning sidebands are labelled as '*SSB*'. See the text for details.

Figure 3. Panel A: Static ^{31}P NMR spectra acquired at a sample pH of 10.0 at 42℃ (top row) and at 57 ℃ (lower row). The two spectra of the left column are of pure DSPC. The corresponding two spectra of the right column are acquired on DSPC with 40 mol% articaine. The asterisk '*' in right column spectra denotes an isotropic phase resonance. Panel B: Static ^{31}P NMR spectra acquired at a sample pH of 7.4 at 42 ℃ (top row) and at 57 ℃ (lower row). The two spectra of the left column are of pure DSPC. The corresponding two spectra of the right column are acquired on DSPC with 40 mol% articaine. See the text for details.

Figure 4. ^{31}P chemical shift anisotropy (CSA, in ppm) from 42−57/60 ℃, pH=10.0, □: DSPC (42−60 ℃), ∗: DSPC/10 mol% articaine (42−57 ℃), △: DSPC/40 mol% articaine (42−57 ℃).

Figure 5. ^{31}P MASNMR spectra of sample DSPC (a), and the spectra of DSPC with 10 mol%, 25 mol%, 40 mol%, and 55 mol% (b-e), from top to bottom, at

temperatures below (44 ℃), left column, and above (57 ℃), right column, the gel-to-liquid-crystalline phase-transition temperatures of DSPC with/without articaine. All spectra were obtained with a 3 kHz MAS spinning rate. The symbol '†' marks unidentified resonances and the symbol '*' in spectra shown in row d, marks two isotropic phase resonances. See the text for details.

Figure 6. Carbonyl carbon resonance region (159−181 ppm) of sample DSPC (a), and the spectra of DSPC with 10 mol%, 25 mol%, 40 mol%, and 55 mol% (b−e), from top to bottom. In spectrum d, the resonance labeled '†' denotes the articaine carboxyl resonance, and the resonance labelled '#' denotes the articaine carbonyl resonance. In spectrum d, two smaller resonances appear at ∼175 ppm; these can be articaine carboxyl and/or DSPC carbonyl resonances. See the text for the details.

Figure 7. Resonance region of glycerol moiety and the choline headgroup (48−74 ppm) of a: pure DSPC sample where resonances are labelled A−C, H, G and I (see DSPC structure on top of Figure 2), and b, c and d show spectra of DSPC with 25 mol%, 40 mol%, and 55 mol%, from top to bottom. Resonances labelled with an asterisk '*' denote DSPC resonances present only at a pH of 10.0, and the resonances labeled '#' denote articaine resonances. See the text for details.

Figure 8. Acyl chain carbon resonance in regions, 9−27 ppm, and 34−37 ppm (main acyl chain peak not shown), of a: pure DSPC sample; b: DSPC with 40 mol% articaine; and c: DSPC with 55 mol% articaine. Resonances labeled with '†' denote new DSPC resonances when articaine is present, and resonances labelled with '#' denote articaine resonances. Arrows point at broad articaine resonances that appear at high articaine ratios (55 mol%). These resonances could be due to presence of articaine aggregates. d: Spectrum of pure articaine showing regions, 9−27 ppm, and 34−37 ppm. See the text for the details.

Scheme 1

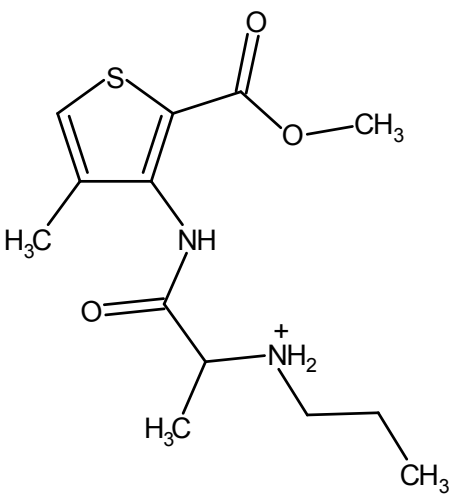

Figure 1

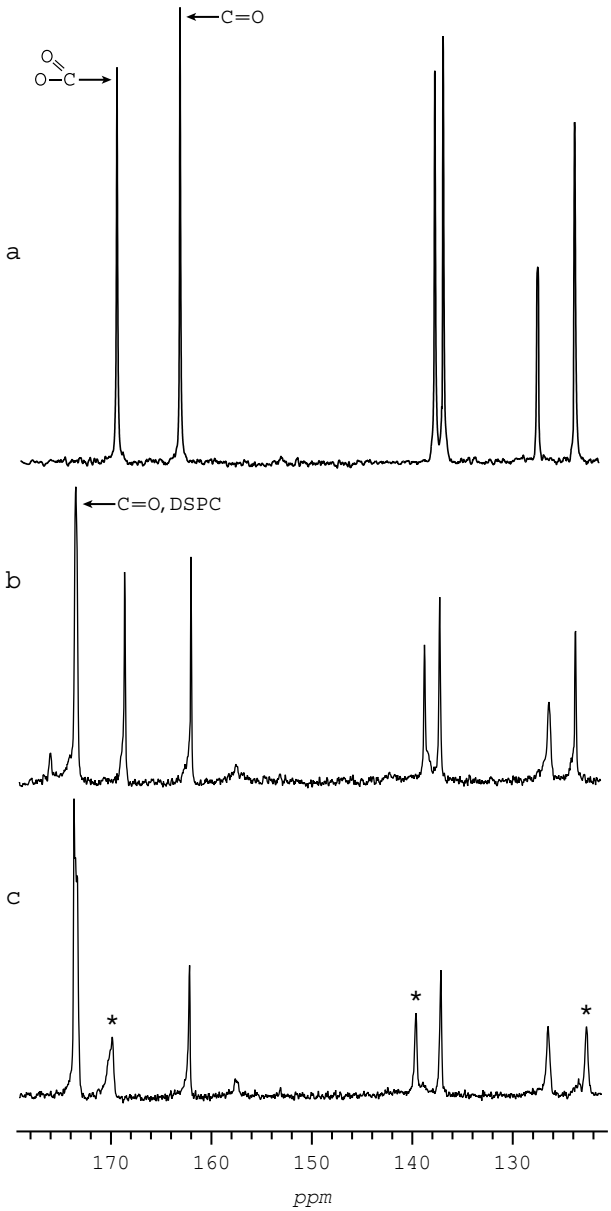

Figure 2

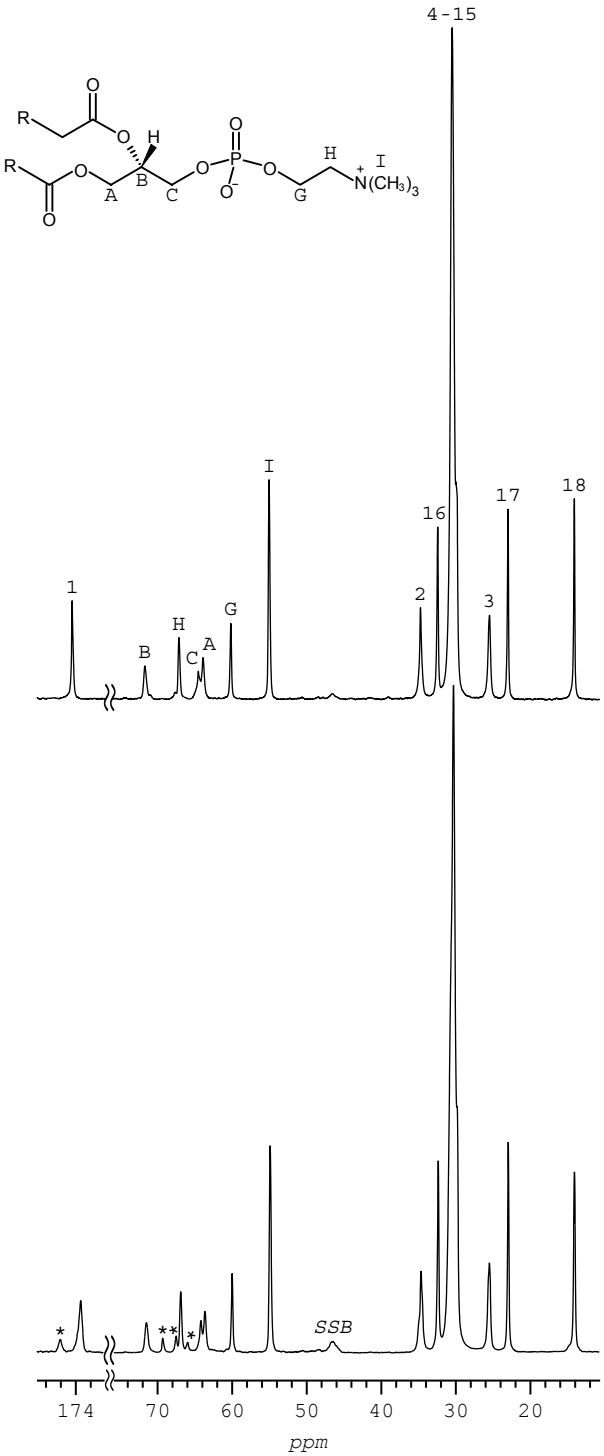

Figure 3

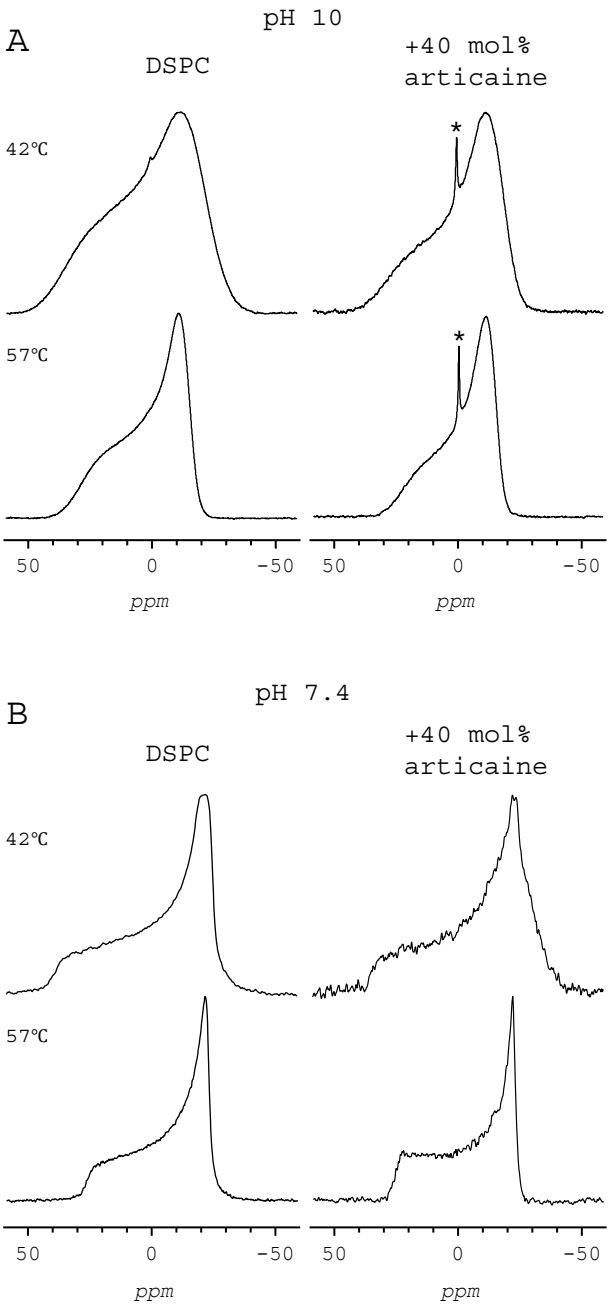
A
pH 10
DSPC
+40 mol%
articaine
42℃
57℃
*
*
50
0
-50
ppm
B
pH 7.4
DSPC
+40 mol%
articaine
42℃
57℃
50
0
-50
ppm

Figure 4

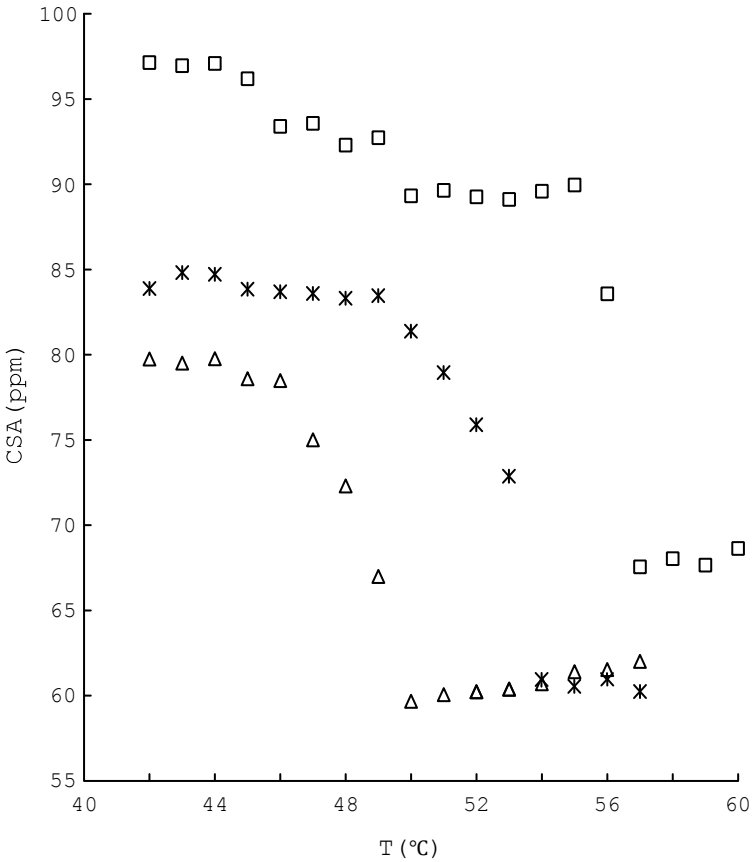

Figure 5

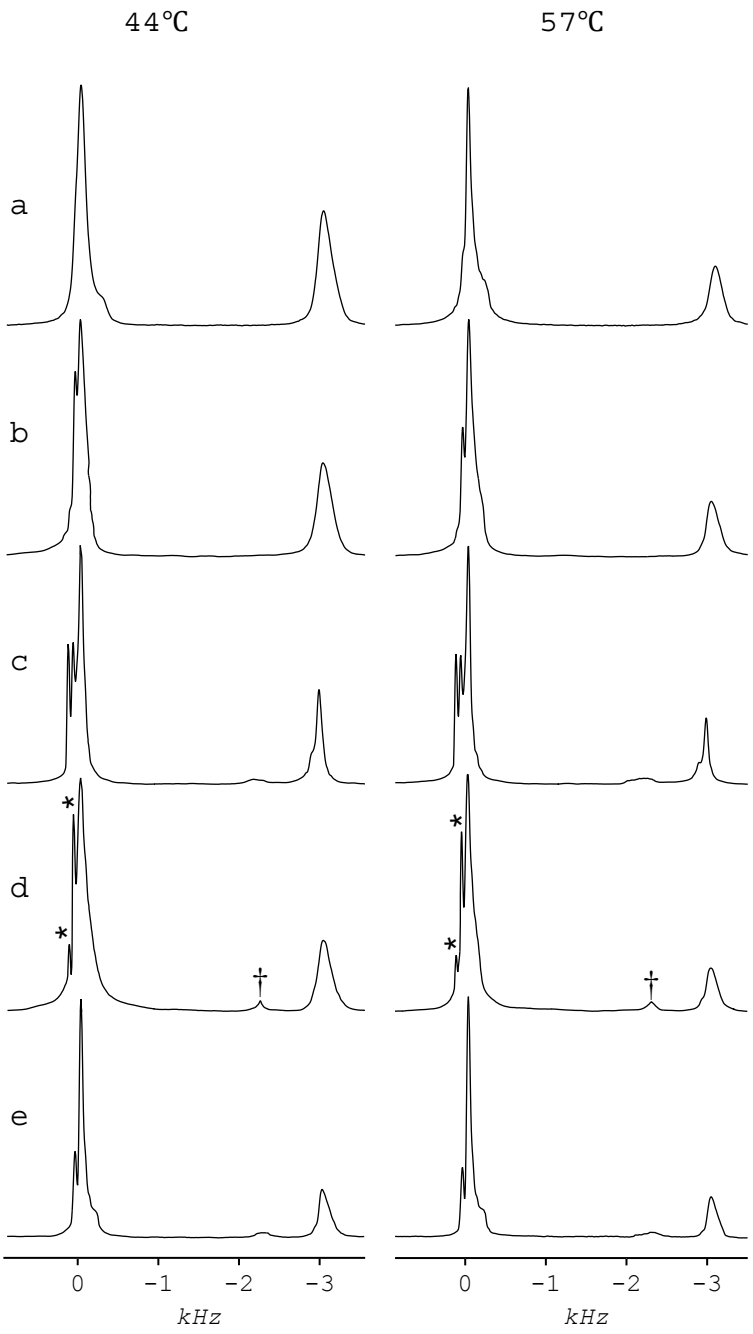

Figure 6

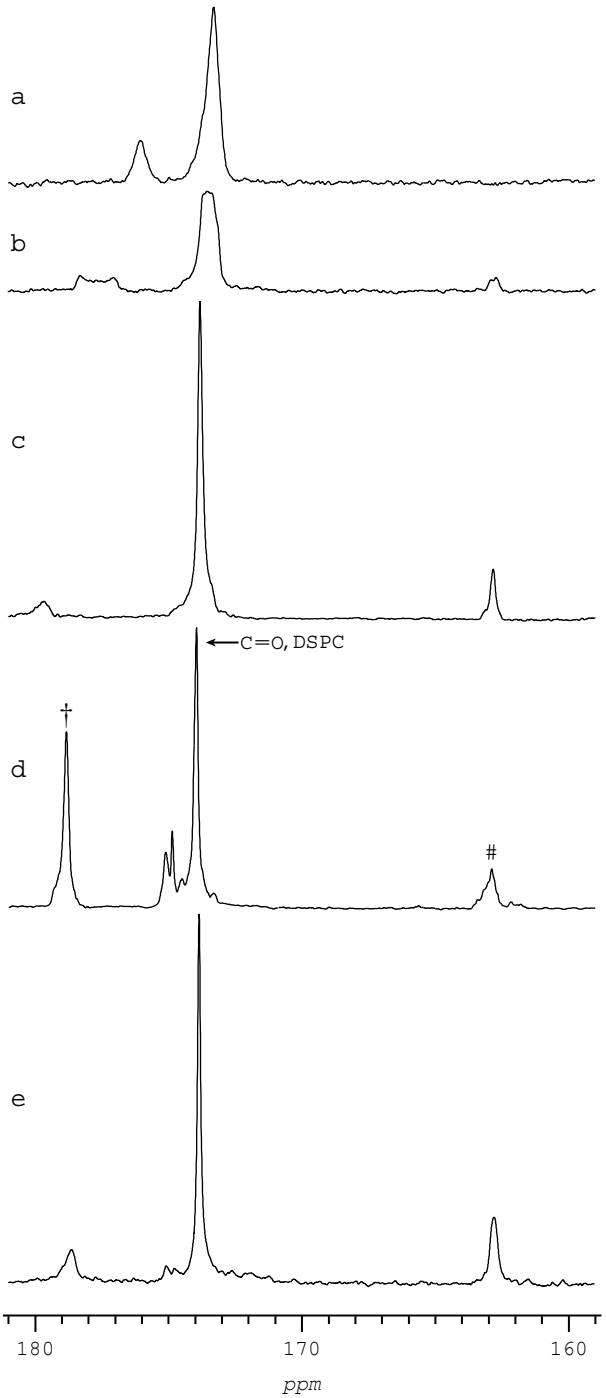

Figure 7

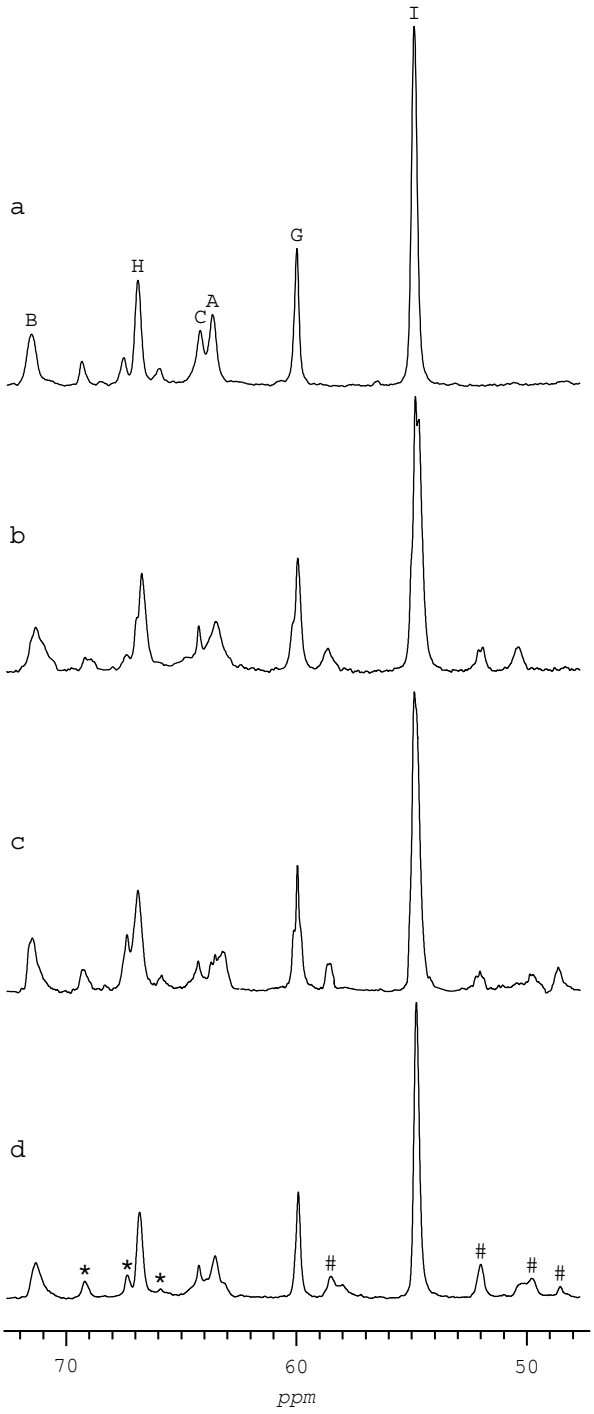

Figure 8

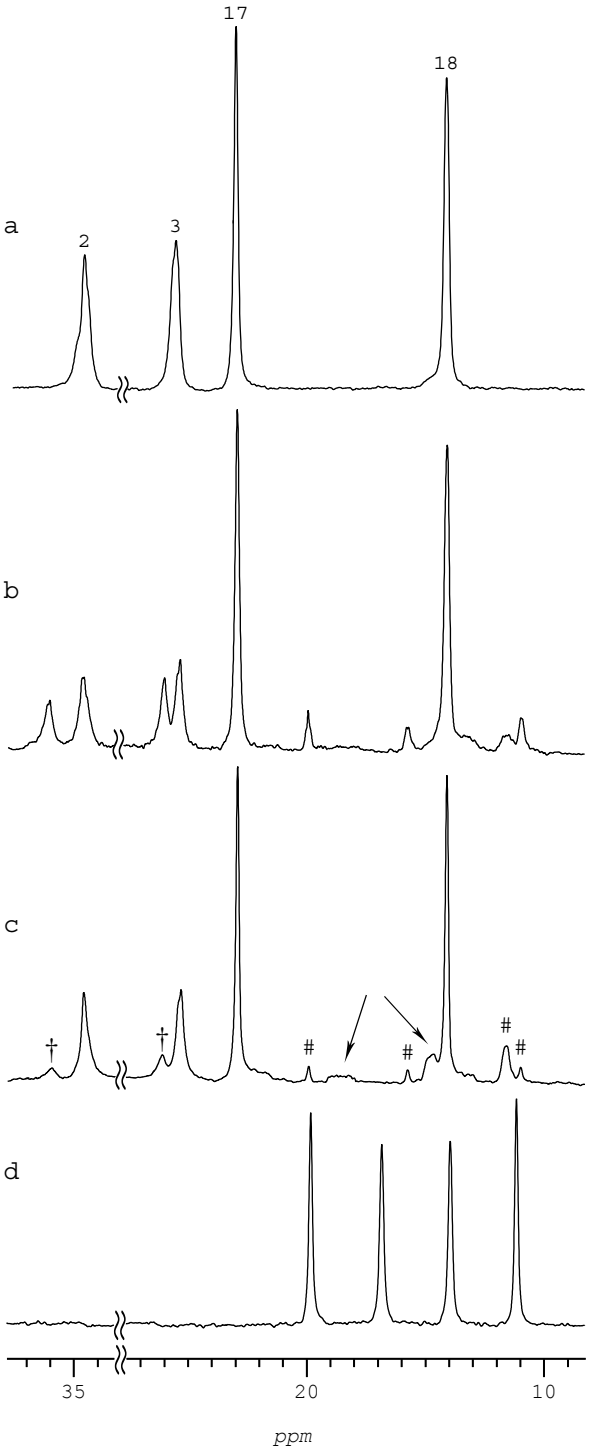

Paper IV

OLANZAPINE INTERACTION WITH DPPC/DPPS AND DPPC/POPS BILAYERS: A ^{13}C AND ^{31}P SOLID–STATE NMR STUDY[‡]

Chen Song[1] and Willy Nerdal[1,*]

[1] *Department of Chemistry, University of Bergen, Allégaten 41, N-5007 Bergen, Norway*

*Author to whom correspondence should be addressed:
Willy Nerdal, Department of Chemistry, University of Bergen, Allégaten 41, N-5007 Bergen, Norway

Tel: +47-55-583353; Fax: +47-55-589400

Email address: Willy.Nerdal@kj.uib.no (W. Nerdal)

Running title: Olanzapine Interaction with DPPC/DPPS and DPPC/POPS Bilayers.

[‡] This work was supported by a grant from the Norwegian Research Council (NFR).

Keywords: ^{13}C-MASNMR; ^{31}P-NMR; bilayers; Olanzapine bilayer interaction

ABBREVIATIONS

DPPC, 1,2-Dipalmitoyl-*sn*-Glycerol-3-Phosphatidylcholine; DPPS, 1,2-Dipalmitoyl-*sn*-Glycerol-3-Phosphatidylserine; POPS, 1-Palmitoyl, 2-oleoyl-*sn*-Glycerol-3-Phosphatidylserine;PC, Phosphatidylcholine; PS, Phosphatidylserine; MAS, Magic-angle Spinning; NMR, Nuclear Magnetic Resonance; CSA, Chemical Shift Anisotropy; NOE, Nuclear Overhauser Effect; T_m, gel-to-liquid-crystalline phase-transition

ABSTRACT

Olanzapine (OLZ), a thienobenzodiazepine derivative, widely used as an antipsychotic agent has been studied with ^{13}C and ^{31}P solid-state NMR techniques when interacting with a DPPC (60%)/ POPS (40%) bilayer at two hydrations (36 and 50 wt.% H_2O) with and without 10 mol% OLZ as well as a bilayer with saturated acyl chains, a DPPC (60%)/DPPS (40%) bilayer with and without 10 mol% OLZ, at a hydration of 36 wt.% H_2O. The results reveal that the serine headgroup is directly affected by OLZ interdigitation of the bilayer, and that the OLZ interaction with PS is to a great extent caused by electrostatic attraction to the serine headgroup.

The experiments of this study were carried out at a sample pH of 7.4 where a neutral and a positively charged form of OLZ are present. ^{31}P MASNMR experiments show two new ^{31}P resonances both for the PS and the PC phosphorous in presence of OLZ. Static ^{31}P NMR spectra demonstrate a substantial decrease in chemical shift anisotropy (CSA) of the OLZ−containing bilayer. The corresponding increased phospholipid headgroup mobilities producing such a reduction in CSA could very well lead to a changed lateral phospholipid organization of the bilayer. This is supported by ^{31}P MASNMR spectra indicating that imperfections in DPPC and POPS mixing are reduced in presence of OLZ.

1. INTRODUCTION

Olanzapine (OLZ, see Scheme 1), a relatively new thienobenzodiazepine derivative, is widely used as an antipsychotic agent and has become one of the most commonly used atypical antipsychotics [1] with antagonism of dopamine D_1, muscarinic $M_{1\text{-}5}$, α_1-adrenoceptors and histamine H_1 receptors [2]. OLZ exhibits relatively high affinity for several neurotransmitter receptors, such as $D_{1\text{-}5}$ dopaminergic, 5-HT_{2A-2C} and 5-$HT_{3,\,6,\,7}$ serotonergic, α_1-adrenoceptors and histamine H_1 [1–7], as well as moderate affinity for the five muscarinic receptor subtypes, M_{1-5} [8]. The functional blockade of these receptors may contribute to its broad efficacy in the treatment of schizophrenia and related psychoses [9–12]. However, in therapeutic concentrations OLZ affects other cellular responses, like inhibition of the integral membrane protein that acts specifically on phosphatidylcholine [13], phospholipase D (PLD), elevation of serum creatine kinase (CK) level [14], the latter effect may cause or induce cell membrane damage. Furthermore, OLZ is found to elevate apolipoprotein-D (apoD) levels [15]. Thus, OLZ can interfere with phospholipid metabolism, in that apoD binds to arachidonic acid (AA) and cholesterol [16–18]. Recently, Parikh et al. [19] found that OLZ prevented loss of antioxidant enzymes in rat brain. Evans et al. [20] indicated that reduced levels of antioxidant enzymes can be associated with increased plasma lipid peroxides and reduced level of essential polyunsaturated fatty acids (EPUFA) in membranes, omega-3 fatty acids in particular. Studies in rats have shown that atypical antipsychotic agents (olanzapine, clozapine, and risperidone) have antioxidant effects and reduce lipid peroxidation [21,22], affecting membrane 5-HT_2 receptor affinity [23]. Furthermore, OLZ, clozapine and risperidone were found to improve the levels of erythrocyte EPUFAs [24], possibly a contributing effect in the treatment of schizophrenia [25,26]. On the other hand, the activity of membrane-bound proteins (receptors, channels, enzymes) is often dependent on the class of phospholipid, the particular acyls and the physical state of the phospholipids. Thus, C_{55}-isoprenoid alcohol kinase from *Staphylococcus aureus* requires glycerophospholipids for activity and gives far higher activity with phosphatidylcholine than phosphatidylethanolamine or phosphatidylserine,

and maximal activity with phosphatidylcholine is obtained with short chain acyls while hexadecanoyl- and octadecanoyl- containing phosphatidylcholine gave no activation [27]. Furthermore, the activity of phospholipase A_2 (PLA_2) is highly dependent on the structure of its membrane substrate [28, 29], and subtle variations in the acyl composition substantially affect the physical state of the substrates and thereby the activity of cytochrome b_5 reconstituted in phosphatidylcholine liposomes [30], this is also shown in *P*-glycoprotein [31] and opioid receptor [32]. Anionic glycerophospholipids determine the topology, and hence activity, of membrane proteins in general [33], and these phospholipids alter the structure of human recombinant prion protein associated with membranes in living cells [34]. The nicotinic acetylcholine receptor in reconstituted membranes from egg phosphatidylcholine and di-oleoyl phosphatidylacid has been found to be affected by variations in cholesterol content (which changes membrane fluidity) and its conformation altered to inactive and desensitized forms [35]. For the reconstitution of the dopaminergic receptor (D_2), phosphatidylserine is particularly important, in that a lipid composition of phosphatidylcholine, phosphatidylethanolamine and phosphatidylserine will almost fully restore the receptor binding, which is about six-fold higher than in a phospholipid bilayer without phosphatidylserine species. Thus, depletion of phosphatidylserine from bilayers with dopamine D_2-receptor weaken the ligand affinity [36]. Influence of bilayer lipid composition on membrane protein activities has recently been reviewed by Lee [37].

The above observations indicate that the activity of membrane-bound proteins bound to lipid bilayers can be influenced by changes in phospholipid composition of the bilayer. Therefore, it is likely that perturbation of the lipid bilayer by amphiphilic OLZ molecules could influence the activity or catalyzed processes of bilayer-bound proteins, even without direct interaction between the protein and the amphiphile. Thus, some of the effects of OLZ on dopaminergic receptors can be due to OLZ perturbation of the lipid bilayer that contains the receptor. The effects of OLZ on processes taking place in biological membranes are scarcely investigated. This is contrasted by the typical antipsychotic agent chlorpromazine (CPZ), that has prompted several physiochemical studies of interactions with glycerophospholipids by various

techniques, such as Electron Spin Resonance (ESR) [38], Electron Paramagnetic Resonance (EPR) [39], X-ray [40], and NMR [41,42].

In the present study, ^{13}C [43] and ^{31}P [44] solid-state NMR techniques were employed to study the interaction of 10 mol% OLZ on a DPPC (60%)/POPS (40%) bilayer at two hydrations, at 36 and at 50 wt.% H_2O, as well as on a bilayer with fully saturated acyl chains, a DPPC (60%)/DPPS (40%) bilayer at a hydration of 36 wt.% H_2O. All samples were pH adjusted to 7.4 in order to ensure that the serine headgroup carboxyl group was deprotonated (pK_a of 4.4). The current study is aimed at molecular mechanisms involved in the interaction of the amphiphilic drug OLZ interacting with phospholipid model membranes. Previously, we have carried out NMR studies on the interaction of chlorpromazine with model membranes at two different hydrations, with 36 wt.% H_2O [41] and even a lower water content of 15 wt.% H_2O (12 H_2O per phospholipid) [42]. The water content is found to influence CPZ interdigitation in phospholipids bilayers, suggesting that structural and dynamic properties of the bilayer change with hydration. Furthermore, in a previous study in our laboratory of a DPPC (60%)/SDPS (40%) bilayer using 36 wt.% H_2O (30 water molecules per lipid molecule), certain spinning sideband resonances were mis-assigned to be due to phospholipid domain formation. Without consequences for the evidences indicating domain formation in that previous study [45], we clarify this by comparing a DPPC/POPS bilayer system at two different hydrations.

A PC (60%)/PS (40%) sample composition can be expected to be fully miscible in that phase diagrams for DMPC−DMPS [46] and DEPC−DEPS [47] mixtures were found highly miscible in both the gel and liquid-crystalline phases in presence of only monovalent cations. However, in presence of 30 mM calcium ions PS−PS samples containing 40−70% PS show both lamellar and cochleate structures at temperatures well above 37 ℃ and at lower temperatures (than 37 ℃), two solid phases will form for samples with PS content up to about 40% PS [46].

2. MATERIALS AND METHODS

2.1 Chemicals

Olanzapine (OLZ, powder) was obtained from *SynFine* Research Inc. (Ontario, Canada), synthetic 1,2-Dipalmitoyl-*sn*-Glycero-3-Phosphatidylcholine (DPPC, lyophilized powder) and synthetic 1-Palmitoyl-2-Oleoyl-*sn*-Glycero-3-[Phospho-L-Serine] (POPS, lyophilized powder) were purchased from Avanti Polar Lipids Inc. (Birmingham, Alabaster, AL, USA), synthetic 1,2-Dipalmitoyl-*sn*-Glycero-[Phospho-L-Serine] (DPPS, powder) was obtained from Sigma Chemical Co. (St. Louis, MO, USA). All lipids were kept at −20 ℃ and used without further purification.

2.2 Sample preparation

2.2.1 Fully hydrated samples (50 wt.% H_2O): DPPC (60%)/POPS (40%) and DPPC (54%)/POPS (36%)/OLZ (10%)

The desired amounts of DPPC and POPS phospholipid bilayers containing choline and serine headgroups were weighed into a plastic tube with a molar composition of 60% phosphatidylcholine and 40% phosphatidylserine, and dissolved in spectroscopic grade chloroform and then dried under a stream of argon gas to form a thin film around the bottom of the plastic tube, followed by the overnight lyophilization in the vacuum chamber to dryness. The sample of dry powder was then suspended in degassed distilled water, and the calculated amount of sodium perchlorate salt ($NaClO_4$) was added (equi-molar to the serine headgroups of POPS). Subsequently, the lipid suspension of DPPC/POPS was divided into two equi-amount parts, and the appropriate amount of OLZ (dissolved in degassed distilled water) was added to obtain the bilayer sample DPPC/POPS/OLZ with an OLZ content of 10 mol%. The suspensions contained multilamellar liposomes and unilamellar systems were obtained by ten freeze-thawing cycles from −196 to 22 ℃. At the freeze-thawing stage, both samples were adjusted to a pH of 7.4 by adding a small amount of 0.05 M NaOH, and the bilayers were kept under an argon atmosphere and not exposed to air and light. Thus, a sample of PC (54%), PS

(36%) and OLZ (10%) was obtained as well as the corresponding sample without OLZ (PC (60%), PS (40%)). Subsequently, the samples were subjected to 24−hours of lyophilization giving partially hydrated liposomes with a hydration level of 12 water molecules per lipid molecule (determined by ^{1}H-MASNMR). The appropriate amount of degassed distilled water was added to the each sample to obtain hydrated bilayers with 50 wt.% H_2O followed by equilibration above the samples gel-to-liquid-crystalline transition temperatures (T_m) at 50 ℃ for 48 hours and packed into NMR rotors.

2.2.2 Partially hydrated (36 wt.% H_2O) samples: DPPC (60%)/POPS (40%) and DPPC (54%)/POPS (36%)/OLZ (10%)

The main preparation procedure of this sample was the same as for the fully hydrated DPPC/POPS sample (described above), except that no sodium perchlorate salt ($NaClO_4$) was added, and after the 24−hours of lyophilization, 36 wt.% H_2O was achieved by adding the appropriate amount of distilled degassed water followed by equilibration for 48 hours at 50 ℃.

2.2.3 Partially hydrated (36 wt.% H_2O) samples: DPPC (60%)/DPPS (40%) and DPPC (54%)/DPPS (36%)/OLZ (10%)

The preparation procedure of this sample was the same as for the partially hydrated DPPC (60%)/POPS (40%) and DPPC (54%)/POPS (36%)/OLZ (10%) samples (described in *Section 2.2.2*), except that these samples were equilibrated at 60 ℃ for 48 hours.

2.3 NMR Spectroscopy

2.3.1 ^{13}C MASNMR Spectroscopy

The ^{13}C MASNMR experiments were obtained at 125.76 MHz on Bruker 500 MHz Ultrashield Plus instrument (11.75 T) equipped with magic angle spinning (MAS) hardware and using ZrO_2 rotors with a diameter of 4 mm. Experiments were done at a sample temperature of 43 ℃, with a sample spinning rate of 2 kHz. The ^{13}C NMR experiments were carried out with high-power proton decoupling during the acquisition i.e. without Nuclear Overhauser Effect (NOE).

In this study, experiments were carried out with a relaxation delay of six seconds between transients, and a total of 16384 transients were accumulated for each experiment. The fids were multiplied with an exponential window function increasing the linewidth by 2 Hz to reduce noise prior to Fourier transformation.

^{13}C spin-lattice relaxation time constants (T_1) were obtained by a modified inversion-recovery pulse sequence using a composite 180-pulse [48] to counteract potential problems associated with non-uniform excitation across the range of ^{13}C chemical shifts. A ^{13}C-NMR 90° pulse was approximately 7−9 μs and the recycling time was set to five times the largest T_1, typically ten seconds between transients, and 2048 transients accumulated at sample temperatures of 23, 33 and 43 ℃, respectively. In order to obtain accurate relaxation data on the palmitic acyl chain methyl group, relaxation experiments employing a 50 s relaxation delay were also carried out with 32 transients.

2.3 ^{31}P NMR Spectroscopy

^{31}P experiments were carried out at 202.47 MHz on a Bruker 500 MHz Ultrashield Plus instrument. Magic angle spinning ^{31}P experiments were carried out with a rotor spinning rate of 2 kHz. Typically, 2048 transients with a relaxation delay of five seconds between transients were accumulated at the various temperatures ranging from 23 ℃ to 43 ℃, and Fourier transformed without apodization in order to keep spectral resolution.

Static ^{31}P spectra were acquired on these bilayer samples at 27 ℃ and 43 ℃ with high-power decoupling during acquisition, i.e. without NOE. Typically, 2048 transients were collected for each experiment with a relaxation delay of six seconds between transients. These fids were multiplied with an exponential window function increasing the linewidth by 50 Hz to reduce noise prior to Fourier transformation.

^{31}P relaxation data were obtained by employing the same pulse program as for ^{13}C T_1 measurements at temperatures of 23−43 ℃ and with rotor spinning speed of 2 kHz. A ^{31}P-NMR 90° pulse was approximately 4−5 μs and the recycling time was set to five times the largest T_1, typically eight seconds

between a total of 1024 transients. The ^{31}P chemical shifts were referenced to 85% phosphoric acid (H_3PO_4, 0 ppm).

3. RESULTS

Figure 1-top shows ^{13}C MASNMR spectrum of partially hydrated (36 wt.% H_2O) bilayer samples DPPC (60%)/DPPS (40%) and Figure 1-bottom shows the corresponding spectrum of DPPC (54%)/DPPS (36%)/OLZ (10%) at a sample temperature of 43 °C. Figure 1 displays spectral regions 12−74 ppm and 170−180 ppm as well as the molecular structures of the phospholipids DPPC and DPPS with capital letters next to glycerol and headgroup carbons corresponding to resonance assignments in spectrum of Figure 1-top. Furthermore, in spectrum of Figure 1-top, the acyl chain sp^3 carbon resonances in the 12−38 ppm region are assigned. Similarly, in the 52−74 ppm spectral region [49,50] the phospholipid choline headgroup carbons resonances are labeled G, H and I, the serine headgroup carbons resonances are labeled D and E and the glycerol moiety carbons resonances are labeled A, B and C. In the 169−180 ppm spectral region of Figure 1-top, the carbonyl resonance is labeled 1 (173.82 ppm) and the serine headgroup carboxyl resonance is labeled F (171.69 ppm) [51].

In presence of 10 mol% OLZ (Figure 1-bottom) two new resonances are found at 178.57 and 174.48 ppm, these are indicated by a double dagger '‡'. These two new resonances most likely are serine headgroup carboxyl resonances in environments caused by presence of OLZ. This is supported by the molar ratio of PC/PS in the sample giving a peak ratio of 1.5 between carbonyl and carboxyl resonances. Furthermore, OLZ affects the chemical shift of the main DPPS carboxyl carbon resonance (see Figure 1-top, resonance F), in that this resonance shifts to higher ppm values by 0.38 ppm in presence of OLZ (see Figure 1-bottom). Additional OLZ caused changes of serine headgroup resonances are found in the pronounced intensity reductions of resonance D and E, compare Figure 1-top and Figure 1-bottom (spectral region 52−74 ppm). For the DPPC and DPPS acyl chain sp^3 carbon resonances (in 12−38 ppm), several small resonances at unusual chemical shift values are present in the top spectrum, such as the resonances at 26.11 and 23.78 ppm, labelled with a

dagger '†'. The acyl chain carbons giving rise to these resonances are primarily associated with an order−disorder exchange of the palmitic acyl chains of the bilayer system DPPC/DPPS at a sample temperature of 43 °C. In addition, the disappearance of spinning sidebands (labelled as '*SSB*' in Figure 1, top) at 46.82 and 48.39 ppm caused by low mobility of carbons 4−13 and carbon 14 of the acyl chains, respectively, demonstrates increased mobility of these acyl chain carbons in the presence of OLZ. Comparison of the spectrum in Figure 1, bottom and ^{13}C MASNMR spectrum of the pure OLZ powder with 15 wt.% D_2O (data not shown), the resonances within the spectral region of 42−52 ppm and the resonance at 16.79 ppm can be assigned as OLZ resonances [52]. Scheme 1 shows the chemical structure of OLZ, with the corresponding assignment numbers used in the bottom spectrum (in brackets).

In order to investigate OLZ interaction with PC/PS bilayer and the influence of acyl chain unsaturation [53] bilayer samples DPPC (60%)/POPS (40%) at two hydrations, partially hydrated, with 36 wt.% H_2O and fully hydrated, with 50 wt.% H_2O, as well as fully hydrated DPPC (54%)/POPS (36%)/OLZ (10%) bilayer sample were employed. Figure 2 displays ^{13}C MASNMR of these three samples at 43 °C. Figure 2 displays the 12−74 ppm spectral region as well as the molecular structure of the POPS molecule together with capital letters next to glycerol and serine headgroup carbons corresponding to resonance assignments in spectrum of Figure 2-b. In addition, Figure 2-a has resonances labelled '*SSB*', these are spinning sideband resonances of the main acyl chain resonances. Figure 2-b shows resonance assignments of acyl chain sp^3 carbon resonances, some of these acyl chain resonances are also labelled in spectrum of Figure 2-c. The palmitic acyl chain contributes 80% to the resonance intensities of spectra in Figure 2-a, -b and -c, and these are assigned in Figure 2-b, as well as resonances 8 and 11 of the oleic acyl chain. (The oleoyl chain carbon resonances 9 and 10, labelled in the POPS structure on Figure 2, are presented in Figure 4, see later). The molar composition of the bilayer system gives a PC/PS peak ratio of 1.5, this is confirmed in Figure 2-b, 54−74 ppm spectral region.

Comparison of the DPPC (60%)/POPS (40%)/36 wt.% H_2O sample (Figure 2-a) and the DPPC (60%)/POPS (40%)/50 wt.% H_2O sample (Figure 2-b), the

disappearance of spinning sidebands (labelled as '*SSB*' in Figure 2-a) in spectrum of 50 wt.% H_2O bilayer sample demonstrating higher mobility of the phospholipids in fully hydrated bilayer (Figure 2-b). This is also evident from the narrow lineshapes of some resonances of the fully hydrated bilayer, such as the internal methylene $(CH_2)_n$. In Figure 2-a (partially hydrated sample) four resonances in the acyl chain region are labelled with a dagger '†', these resonances could be due to molecular packing effects in the DPPC (60%)/POPS (40%) bilayer possibly due to existence of phospholipids microdomains [47]. Increasing the hydration of the bilayer (from 36 wt.% H_2O to 50 wt.% H_2O), causes the resonances labelled with a dagger '†' in Figure 2-a, to disappear, see Figure 2-b.

Figure 3 displays ^{13}C MASNMR spectra of bilayer samples DPPC (60%)/POPS (40%) (36 wt.% H_2O) in Figure 3-a, DPPC (60%)/POPS (40%) (50 wt.% H_2O) in Figure 3-b, as well as fully hydrated DPPC (54%)/POPS (36%)/OLZ (10%) (50 wt.% H_2O) in Figure 3-c, at a sample temperature of 43 °C. In Figure 3-b, the two carbonyl resonances can be identified (labelled *sn*-1 and *sn*-2) [54] as well as the serine carboxyl resonance, labelled F. Effects of more than one form of phospholipid packing at 36 wt.% H_2O in the DPPC (60%)/POPS (40%) bilayer can be seen in the spectrum of Figure 3-a, where three identifiable carbonyl resonances are present. The dagger '†' identifies the carbonyl resonance caused by more than one form of molecular packing at 36 wt.% H_2O in the DPPC (60%)/POPS (40%) bilayer. A comparison of the serine headgroup carboxyl F resonance, Figure 3-b, with the OLZ–containing bilayer spectrum of Figure 3-c, makes it evident that the main part of this carboxyl resonance is shifted 5.80 ppm to higher ppm values (labelled with an asterisk '*' in Figure 3-c). A similar effect can be found in spectra of DPPC (60%)/DPPS (40%) in Figure 1-top and its counterpart DPPC (54%)/DPPS (36%)/OLZ (10%) in Figure 1-bottom i.e. in spectra of bilayers with saturated acyl chains. The corresponding changes in ^{13}C T_1 values for both carbonyl resonances by adding OLZ to the bilayer suggest reduced phospholipid mobility (see Table 1). Furthermore, the changes in the *sn*-2 carbonyl chemical shift (see Figure 3) and T_1 value (Table 1) strongly suggest phospholipid conformational changes as well as changes in the chemical environment for the phospholipids due to OLZ interaction [55]. This is supported by the observed behaviour of the serine carboxyl carbon,

where the T_1 value (Table 1) of the carboxyl group at 171.71 ppm (Figure 3-b) increases by 51% (from 1.66 s to 2.51 s) with the addition of OLZ, (Figure 3-b) and the T_1 value of the new carboxyl resonance (labelled with an asterisk '*') at 177.51 ppm is found to be 3.24 s (Table 1).

Figure 4 shows the 128−132 ppm spectral region of ^{13}C MASNMR spectra of bilayer samples DPPC (60%)/POPS (40%) (36 wt.% H_2O) in Figure 4-a, DPPC (60%)/POPS (40%) (50 wt.% H_2O) in Figure 4-b, as well as fully hydrated DPPC (54%)/POPS (36%)/OLZ (10%) (50 wt.% H_2O) in Figure 4-c, at a sample temperature of 43 ℃. In the spectral region displayed in Figure 4, the C=C resonances of the oleic acyl chain carbons 9 and 10 of samples DPPC/POPS and DPPC/POPS/OLZ are found, these are assigned in Figure 4-b. Comparison of the C=C resonances from the DPPC/POPS samples with different hydrations (spectra in Figure 4-a and Figure 4-b) shows no change in resonance intensities or chemical shifts. However, spectrum in Figure 4-c of DPPC (54%)/POPS (36%)/OLZ(10%) the 50 wt.% H_2O sample, display a reduction of 0.16 ppm in the chemical shift separation (Δδ) of carbon 9 and 10 resonances in presence of OLZ (compare spectra in Figure 4-b and -c). Furthermore, T_1 values for these oleic chain carbons 9 and 10 (Table 1) show that 10 mol% OLZ in the DPPC/POPS bilayer increases the T_1 values for these two C=C resonances in that carbon 9 experience an increase in T_1 from 0.71 s to 0.81 s (14%) and carbon 10 an increase in T_1 from 0.60 s to 0.80 s (33%), see Table 1. The small broad peak at 128.78 ppm, labelled as (2) in Figure 4-c is an OLZ carbon resonance (see Scheme 1 for the assignment).

Figure 5 displays the central band region of ^{31}P MASNMR spectra acquired on bilayer samples DPPC (60%)/POPS (40%) with 36 wt.% H_2O (Figure 5, left column), DPPC (60%)/POPS (40%) with 50 wt.% H_2O (Figure 5, middle column) and DPPC (54%)/POPS (36%)/OLZ (10%) with 50 wt.% H_2O (Figure 5, right column) at temperatures 23−43 ℃ (top row to bottom row). In Figure 5, the experimental temperature is labelled to the left of the three spectra on the same row in Figure 5 that are acquired at the given temperature. All spectra were obtained with a 2 kHz MAS spinning rate. The phosphatidylcholine and phosphatidylserine components are assigned in the spectra shown in the bottom row of Figure 5, i.e. at 43 ℃ where the bilayer is in the liquid-crystalline

state. In Figure 5, left column and bottom row, the PS and PC ^{31}P resonances in the partially hydrated bilayer are labelled. These two resonances display a chemical shift difference of 0.48 ppm, a value that correlates well with earlier findings on this type of phospholipid composition as well as with similar bilayers [47]. In spectra of 50 wt.% H_2O DPPC/POPS sample displayed in Figure 5, middle column and bottom row, the corresponding chemical shift difference between PS and PC is 1.21 ppm. Furthermore, it is the PS phosphorous chemical shift that shows this sensitivity on increasing hydration from 36 wt.% (Figure 5, left column and bottom row) to 50 wt.% H_2O (Figure 5, middle column and bottom row). Existence of several lipid packing conformations is demonstrated in the ^{31}P MASNMR spectra of Figure 5, middle column and bottom row, in the somewhat broad appearance of the PS and PC resonances, even at 43 ℃ where the bilayer is in the liquid-crystalline state. This tendency of several lipid packing conformations is becoming more pronounced at lower temperatures where the bilayer is in the gel state, see Figure 5, middle column and top row, at a sample temperature of 23 ℃ where a new resonance appears in between the PS and PC resonances that are identified in the liquid-crystalline bilayer state (Figure 5, middle column and bottom row). The co-existence of several molecular packing arrangements in the DPPC/POPS bilayer at 23 ℃ is further supported by the molecular composition of the bilayer that is a 1.5 PC/PS ratio. Thus, the resonance between PS and PC of Figure 5, middle column and top row, at a sample temperature of 23 ℃ must have PS as well as PC phosphorous resonances contributing to the peak intensity.

Comparing spectrum of DPPC/POPS/OLZ sample shown in Figure 5, right column and bottom row, i.e. at 43 ℃, with corresponding spectrum of sample without OLZ shown in Figure 5, middle column and bottom row, resonances labelled a−c and d−f (Figure 5, right column and bottom row) are PS and PC ^{31}P resonances, respectively. Of the three ^{31}P resonances attributed to PS, resonances a−c, the resonance labelled b is at the same chemical shift as the PS resonance in spectrum without OLZ, see Figure 5, middle column and bottom row. Similarly, the resonance labelled d (Figure 5, right column and bottom row) is at the same chemical shift as the resonance labelled PC in spectrum without OLZ, see Figure 5, middle column and bottom row. Thus, the presence of OLZ in the bilayer gives rise to chemical environments in the bilayer polar

region that affects both PS and PC headgroups. Furthermore, lowering sample temperature from 43 to 23 ℃ (Figure 5, right column and top row) broadens all PS resonances (labelled a−c) and two PC resonances (labelled e and f) without affecting the PC resonance labelled d in Figure 5, right column and bottom row. The OLZ affected ^{31}P resonances a−c of PS as well as e and f of PC are presumably broadened in spectra at lower temperatures due to chemical exchange caused by presence of OLZ. The exchange rates can be estimated by the difference in resonance position (Hz) from resonances a and c of PS, c and e of PC to be in the 5−9 ms range.

^{31}P T_1 values of the central band peaks displayed in Figure 5, listed in Table 2, show that both PS and PC phosphorous mobilities are sensitive to sample temperature. The ^{31}P T_1 values for all of the phosphatidylserine resonances decrease with increasing temperature, indicating an increase in phosphorous mobility (slow motional regime, Scheme 2). This behaviour is contrasted by the OLZ−containing sample, where some T_1 values increase and other decrease with increasing temperature (fast motional regime, Scheme 2). The T_1 value of the peak labelled PC of the 50 wt.% H_2O sample (Figure 5, middle column) decreases from 1.04 s at 23 ℃ to 0.59 s at 35 ℃ and then increases to 0.74 s at 39 ℃ and 0.78 s at 43 ℃. The DPPC gel-to-liquid-crystalline phase transition is at 38−41 ℃ [58]. Comparison of the ^{31}P T_1 values of the two DPPC/POPS samples with 36 wt.% H_2O and 50 wt.% H_2O (Table 2), demonstrates higher mobilities for both phosphatidylserine and phosphatidylcholine phosphorous at 50 wt.% H_2O.

Figure 6 shows static ^{31}P spectra of samples DPPC (60%)/POPS (40%) with 36 wt.% H_2O (Figure 6-a), DPPC (60%)/POPS (40%) with 50 wt.% H_2O (Figure 6-b) and DPPC (54%)/POPS (36%)/OLZ (10%) with 50 wt.% H_2O (Figure 6-c) spectra in left column of Figure 6 at 27 ℃, and spectra in right column of Figure 6 at 43℃. The ^{31}P CSA values of DPPC (60%)/POPS (40%) with 36 wt.% H_2O (Figure 6-a) are 87 and 65 ppm at 27 and 43 ℃, respectively. Higher hydration reduces the CSA values in that the ^{31}P CSA values of DPPC (60%)/POPS (40%) with 50 wt.% H_2O (Figure 6-b) are 64 and 58 ppm at 27 and 43 ℃, respectively. Incorporation of OLZ in the bilayer causes a further reduction of CSA shown by

the ^{31}P CSA values of DPPC (54%)/POPS (36%)/OLZ (10%) with 50 wt.% H_2O (Figure 6-c) that are 63 and 51 ppm at 27 and 43 °C, respectively.

4. DISCUSSION

The results of this study reveal that the serine headgroup is directly affected by OLZ interdigitation of the bilayer, and that the OLZ interaction with PS is to a great extent caused by electrostatic attraction to the serine headgroup.

The DPPC/DPPS bilayer (Figure 1) displayed substantial effects of OLZ on the serine headgroup carbon resonances (D and E in Figure 1) and a smaller effect is found for the DPPC/POPS bilayer (Figure 2) on the choline headgroup resonances (G, H and I in Figure 1).

The experiments of this study were carried out at a sample pH of 7.4 where a neutral and a positively charged form of OLZ are present. The ^{31}P MASNMR experiments presented in Figure 5 show two (major) new ^{31}P resonances both for the PS and the PC phosphorous in presence of OLZ. In addition, OLZ is found to form dimers in the solid-state and such dimer formation is possible through intermolecular interactions, such as hydrogen bonding and electrostatic forces where stabilization appears to be achieved by interactions between *N*-methylpiperazine moiety and the phenyl/thiophene systems [56]. Furthermore, OLZ displays polymorphism and can form both dehydrated and hydrated dimers in the solid-state [52]. Thus, in light of such a tendency to dimer-formation, it cannot be ruled out that some of the bilayer interaction of OLZ is carried out by OLZ−dimers. The static ^{31}P NMR spectra presented in Figure 6 demonstrate a substantial decrease in CSA of the OLZ−containing bilayer. The corresponding increased phospholipids headgroup mobilities producing such a CSA reduction by presence of OLZ could very well lead to a changed lateral phospholipid organization of the bilayer [57]. In fact, the ^{31}P MASNMR spectra presented in Figure 5 indicate that imperfections in DPPC and POPS mixing (see Figure 5, middle column and top row) are reduced in presence of OLZ (see Figure 5, right column and top row).

REFERENCES

[1] N.A. Moore, N.C. Tye, M.S. Axton, F.C. Risius, The behavioral pharmacology of olanzapine, a novel "atypical" antipsychotic agent. *J. Pharmacol. Exp. Ther.* 262(2) (1992) 545–551.

[2] F.P. Bymaster, D.L. Nelson, N.W. DeLapp, J.F. Falcone, K. Eckols, L.L. Truex, M.M. Foreman, V.L. Lucaites, D.O. Calligaro, Antagonism by olanzapine of dopamine D_1, serotonin$_2$, muscarinic, histamine H_1 and α_1-adrenergic receptors in vitro. *Schizophr. Res.* 37(1) (1999) 107−122.

[3] A. Fuller, H.D. Snoddy, Neuroendocrine evidence for antagonism of serotonin and dopamine receptors by olanzapine (LY170053), an antipsychotic drug candidate. *Res. Commun. Chem. Pathol. Pharmacol.* 77(1) (1992) 87−93.

[4] F.P. Bymaster, D.O. Calligaro, J.F. Falcone, R.D. Marsh, N.A. Moore, N.C. Tye, P. Seeman, D.T. Wong, Radioreceptor binding profile of the atypical antipsychotic olanzapine. *Neuropsychopharmacol.* 14(2) (1996) 87−96.

[5] F.P. Bymaster, K.W. Perry, D.L. Nelson, D.T. Wong, K. Rasmussen, N.A. Moore, D.O. Calligaro, Olanzapine: a basic science update. *Br. J. Psychiat., Suppl.* 37 (1999) 36−40.

[6] B.L. Roth, S.C. Craigo, M.S. Choudhary, A.Uluer, F.J. Monsma, Jr., Y. Shen, H.Y. Meltzer, D.R. Sibley, Binding of typical and atypical antipsychotic agents to 5-hydroxytryptamine-6 and 5-hydroxytryptamine-7 receptors. *J. Pharmacol. Exp. Ther.* 268(3) (1994) 1403−1410.

[7] F.P. Bymaster, J.F. Falcone, D. Bauzon, J.S. Kennedy, K. Schenck, N.W. DeLapp, M.L. Cohen, Potent antagonism of 5-HT_3 and 5-HT_6 receptors by olanzapine. *Eur. J. Pharmacol.* 430(2−3) (2001) 341−349.

[8] F.P. Bymaster, J.F. Falcone, Decreased binding affinity of olanzapine and clozapine for human muscarinic receptors in intact clonal cells in physiological medium. *Eur. J. Pharmacol.* 390(3) (2000) 245−248.

[9] B. Fulton, K.L. Goa, Olanzapine. A review of its pharmacological properties and therapeutic efficacy in the management of schizophrenia and related psychoses. *Drugs* 53(2) (1997) 281−298.

[10] G.D. Tollefson, C.M. Beasley, Jr., P.V. Tran, J.S. Street, J.A. Krueger, R.N. Tamura, K.A. Graffeo, M.E. Thieme, Olanzapine versus haloperidol in the treatment of schizophrenia and schizoaffective and schizophreniform disorders: results of an international collaborative trial. *Am. J. Psychiatry* 154(4) (1997) 457−465.

[11] M. Tohen, T.M. Sanger, S.L. McElroy, G.D. Tollefson, K.N.R. Chengappa, D.G. Daniel, F. Petty, F. Centorrino, R. Wang, S.L. Grundy, M.G. Greaney, T.G. Jacobs, S.R. David, V. Toma, and The Olanzapine HGEH study group, Olanzapine versus placebo in the treatment of acute mania. *Am. J. Psychiatry* 156(5) (1999) 702−709.

[12] C.M. Beasley, Jr., G. Tollefson, P. Tran, W. Satterlee, T. Sanger, S. Hamilton, and the Olanzapine HGAD study group, Olanzapine versus placebo and haloperidol: acute phase results of the North American double-blind olanzapine trial. *Neuropsychopharmacol.* 14(2) (1996) 111−123.

[13] M. Krzystanek, H.I. Trzeciak, I. Krupka-Matuszczyk, E. Krzystanek, Antidepressant-like influence of olanzapine on membrane phospholipase D activity in rat brain. *Eur. Neuropsychopharmacol.* 12(Suppl. 3) (2002) 297−298.

[14] K. Melkersson, Serum creatine kinase levels in chronic psychosis patients−a comparison between atypical and conventional antipsychotics. *Prog. Neuro-Psychopharmacol. & Biol. Psychiat.* 30(7) (2006) 1277−1282.

[15] M.M. Khan, V.V. Parikh, S.P. Mahadik, Antipsychotic drugs differentially modulate apolipoprotein D in rat brain. *J. Neurochem.* 86(5) (2003) 1089–1100.

[16] J.K. Boyles, L.M. Notterpek, M.R. Wardell, S.C. Rall, Jr., Identification, characterization and tissue distribution of apolipoprotein D in the rat. *J. Lipid Res.* 31(12) (1990) 2243−2256.

[17] P.P. Desai, C.H. Bunker, F.A.M. Ukoli, M.I. Kamboh, Genetic variation in the apolipoprotein D gene among African blacks and its significance in lipid metabolism. *Atherosclerosis* 163(2) (2002) 329−338.

[18] W.Y. Ong, C.P. Lau, S.K. Leong, U. Kumar, S. Suresh, S.C. Patel, Apolipoprotein D gene expression in the rat brain and light and electron microscopic immunocytochemistry of apolipoprotein D expression in the cerebellum of neonatal, immature and adult rats. *Neuroscience* 90(3) (1999) 913−922.

[19] V.V. Parikh, M.M. Khan, S.P. Mahadik, Differential effects of antipsychotics on expression of antioxidant enzymes and membrane lipid peroxidation in rat brain. *J. Psychiatric Res.* 37(1) (2003) 43−51.

[20] D.R. Evans, V.V. Parikh, M.M. Khan, C. Coussons, P.F. Buckley, S.P. Mahadik, Red blood cell membrane essential fatty acid metabolism in early psychotic patients following antipsychotic drug treatment. *Prostag. Leukotr. Essential Fatty Acids* 69(6) (2003) 393−399.

[21] S.P. Mahadik, D.R. Evans, H. Lal, Oxidative stress and role of antioxidant and ω-3 essential fatty acid supplementation in schizophrenia. *Prog. Neuro-Psychopharmacol. & Biol. Psychiat.* 25(3) (2001) 463−493.

[22] S.P. Mahadik, D.R. Evans, A. Terry, W. Hill, Neuroprotective actions of atypical antipsychotics in schizophrenia: improved cognitive performance and underlying mechanisms of action. *Schizophr. Res.* 49(2) (Suppl. 1) (2001) 94.

[23] A.C. Rego, C.R. Oliveira, Influence of lipid peroxidation on [^{3}H]ketanserin binding to 5-HT$_2$ prefrontal cortex receptors. *Neurochem. Int.* 27(6) (1995) 489–496.

[24] D.R. Evans, S.P. Mahadik, J. Akin, W. Evans, D. Jain, Cell membrane essential fatty acid status in drug-naive first-episode psychotic patients and its relation to outcome. *Schizophr. Res.* 49(2) (Suppl. 1) (2001) 83.

[25] M.M. Khan, D.R. Evans, V. Gunna, R.E. Scheffer, V.V. Parikh, S.P. Mahadik, Reduced erythrocyte membrane essential fatty acids and increased lipid

peroxides in schizophrenia at the never-medicated first-episode of psychosis and after years of treatment with antipsychotics. *Schizophr. Res.* 58(1) (2002) 1−10.

[26] D.F. Horrobin, The membrane phospholipid hypothesis as a biochemical basis for the neurodevelopmental concept of schizophrenia. *Schizophr. Res.* 30(3) (1998) 193−208.

[27] R.B. Genniss, J.L. Strominger, Activation of C_{55}-isoprenoid alcohol phosphokinase from *Staphylococcus aureus*: I. Activation by phospholipids and fatty acids. *J. Biol. Chem.* 251(5) (1976) 1264−1282.

[28] D.W. Grainger, A. Reichert, H. Ringsdorf, S. Salesse, Hydrolytic action of phospholipase A_2 in monolayers in the phase transition region: direct observation of enzyme domain formation using fluorescence microscopy. *Biochim. Biophys. Acta* 1023(3) (1990) 365−379.

[29] W.R. Burack, R.L. Biltonen, Lipid bilayer heterogeneities and modulation of phospholipase A_2 activity. *Chem. Phys. Lipids* 73(1−2) (1994) 209−222.

[30] K.M.P. Taylor, M.A. Roseman, Effect of cholesterol, fatty acyl chain composition, and bilayer curvature on the interaction of cytochrome b_5 with liposomes of phosphatidylcholines. *Biochemistry* 34(11) (1995) 3841–3850.

[31] Y. Romsicki, F.J. Sharom, The membrane lipid environment modulates drug interactions with the *P*-glycoprotein multidrug transporter. *Biochemistry* 38(21) (1999) 6887−6896.

[32] D.F. Lazar, F. Medzihradsky, Altered microviscosity at brain membrane surface induces distinct and reversible inhibition of opioid receptor binding. *J. Neurochem.* 59(4) (1992) 1233−1240.

[33] W. van Klompenburg, I.M. Nilsson, G. von Heijne, B. de Kruijff, Anionic phospholipids are determinants of membrane protein topology. *EMBO J.* 16(14) (1997) 4261−4266.

[34] M. Morillas, W. Swietnicki, P. Gambetti, W.K. Surewicz, Membrane environment alters the conformational structure of the recombinant human prion protein. *J. Biol. Chem.* 274(52) (1999) 36859−36865.

[35] J.R. Baenziger, M.-L. Morris, T.E. Darsaut, S.E. Ryan, Effect of membrane lipid composition on the conformational equilibria of the nicotinic acetylcholine receptor. *J. Biol. Chem.* 275(2) (2000) 777–784.

[36] L.K. Srivastava, S.M.I. Kazmi, A.J. Blume, R.K. Mishra, Reconstitution of affinity-purified dopamine D_2 receptor binding activities by specific lipids. *Biochim. Biophys. Acta* 900(2) (1987) 175−182.

[37] A.G. Lee, Lipid–protein interactions in biological membranes: a structural perspective. *Biochim. Biophys. Acta* 1612(1) (2003) 1–40.

[38] M. Luxnat, H.-J. Galla, Partition of chlorpromazine into lipid bilayer membranes: the effect of membrane structure and composition. *Biochim. Biophys. Acta* 856(2) (1986) 274−282.

[39] K. Ondrias, A. Staško, V. Mišik, J. Reguli, E. Švajdlenka, Comparison of perturbation effect of propranolol, verapamil, chlorpromazine and carbisocaine on lecithin liposomes and brain total lipid liposomes. an EPR spectroscopy study. *Chem.-Biol. Interact.* 79(2) (1991) 197−206.

[40] M. Suwalsky, L. Gimenez, V. Saenger, F. Neira, X-ray studies on phospholipid bilayers. VIII. Interactions with chlorpromazine.HCl. *Z. Naturforsch[c]* 43 (1988) 742−748.

[41] A.U. Gjerde, H. Holmsen, W. Nerdal, Chlorpromazine interaction with phosphatidylserines: a ^{13}C and ^{31}P solid-state NMR study. *Biochim. Biophys. Acta* 1682(1−3) (2004) 28−37.

[42] W. Nerdal, S.A. Gundersen, V. Thorsen, H. Høiland, H. Holmsen, Chlorpromazine interaction with glycerophospholipid liposomes studied by magic angle spinning solid state ^{13}C-NMR and differential scanning calorimetry. *Biochim. Biophys. Acta* 1464(1) (2000) 165−175.

[43] W.-g. Wu, L.-M. Chi, Comparisons of lipid dynamics and packing in fully interdigitated monoarachidoylphosphatidylcholine and non-interdigitated dipalmitoylphosphatidylcholine bilayers: cross polarization/magic angle spinning ^{13}C-NMR studies. *Biochim. Biophys. Acta* 1026(2) (1990) 225−235.

[44] J.L. Browning, J. Seelig, Bilayers of phosphatidylserine: a deuterium and phosphorus nuclear magnetic resonance study. *Biochemistry* 19(6) (1980) 1262−1270.

[45] C. Song, H. Holmsen, W. Nerdal, Existence of lipid microdomains in bilayer of dipalmitoylphosphatidylcholine (DPPC) and 1-stearoyl-2-docosahexenoylphosphatidylserine (SDPS) and their perturbation by chlorpromazine: A ^{13}C and ^{31}P solid-state NMR study. *Biophy. Chem.* 120(3) (2006) 178−187.

[46] J.R. Silvius, J. Gagné, Calcium-induced fusion and lateral phase separations in phosphatidylcholine-phosphatidylserine vesicles. Correlation by calorimetric and fusion measurements. *Biochemistry* 23(14) (1984) 3241−3247.

[47] J. Gagné, L. Stamatatos, T. Diacovo, S.W. Hui, P.L. Yeagle, J.R. Silvius, Physical properties and surface interactions of bilayer membranes containing N-methylated phosphatidylethanolamines. *Biochemistry* 24(16) (1985) 4400−4408.

[48] M. Levitt, Symmetrical composite pulse sequences for NMR population inversion: I. Compensation of radiofrequency field inhomogeneity. *J. Magn. Reson. (1969)* 48(2) (1982) 234−264.

[49] L.R. Brown, K. Wüthrich, NMR and ESR studies of the interactions of cytochrome *c* with mixed cardiolipin-phosphatidylcholine vesicles. *Biochim. Biophys. Acta* 468(3) (1977) 389−410.

[50] T. Mavromoustakos, E. Theodoropoulou, D.-P. Yang, The use of high-resolution solid-state NMR spectroscopy and differential scanning calorimetry to study interactions of anesthetic steroids with membrane. *Biochim. Biophys. Acta* 1328(1) (1997) 65−73.

[51] D.L. Holwerda, P.D. Ellis, R.E. Wuthier, Carbon-13 and phosphorus-31 nuclear magnetic resonance studies on the interaction of calcium with phosphatidylserine. *Biochemistry* 20(2) (1981) 418−428.

[52] S.M. Reutzel-Edens, J.K. Bush, P.A. Magee, G.A. Stephenson, S.R. Byrn, Anhydrates and hydrates of olanzapine: crystallization, solid-state characterization, and structural relationships. *Cryst. Growth Des.* 3(6) (2003) 897−907.

[53] L.L. Holte, F. Separovic, K. Gawrisch, Nuclear magnetic resonance investigation of hydrocarbon chain packing in bilayers of polyunsaturated phospholipids. *Lipids* 31(1) (1996) Suppl: S199−S203.

[54] C.F. Schmidt, Y. Barenholz, C. Huang, T.E. Thompson, Phosphatidylcholine ^{13}C-labeled carbonyls as a probe of bilayer structure. *Biochemistry* 16(18) (1977) 3948−3954.

[55] B.A. Cornell, M. Keniry, The effect of cholesterol and gramicidin A′ on the carbonyl groups of dimyristoylphosphatidylcholine dispersions. *Biochim. Biophys. Acta* 732(3) (1983) 705−710.

[56] I. Wawrzycka-Gorczyca, P. Borowski, J. Osypiuk-Tomasik, L. Mazur, A.E. Koziol, Crystal structure of olanzapine and its solvates. Part 3. Two and three-component solvates with water, ethanol, butan-2-ol and dichloromethane. *J. Mol. Struct.* 830(1−3) (2007) 188−197.

[57] A. Jutila, T. Söderlund, A.L. Pakkanen, M. Huttunen, P.K.J. Kinnunen, Comparison of the effects of clozapine, chlorpromazine, and haloperidol on membrane lateral heterogeneity. *Chem. Phys. Lipids* 112(2) (2001) 151−163.

[58] A. Aroti, E. Leontidis, E. Maltseva, G. Brezesinski, Effects of Hofmeister anions on DPPC Langmuir monolayers at the air-water interface. *J. Phys. Chem. B.* 108(39) (2004) 15238−15245.

FIGURE LEGENDS

Scheme 1. Molecular structure of olanzapine (OLZ) with corresponding assignment letters.

Scheme 2. A pictorial representation of spin-lattice relaxation time constant (T_1, in seconds) as the function of correlation time (τ_c, in nanoseconds). The plot shows a T_1 minimum at $\tau_c = \omega^{-1}$ (≈1.3 ns).

Figure 1. Proton-decoupled ^{13}C MASNMR spectra of partially hydrated bilayers at 316 K (43℃, above T_m) with top spectrum: DPPC (60%)/DPPS (40%), and the bottom spectrum: DPPC (54%)/DPPS (36%)/OLZ (10%), displaying spectral regions from 12−74 ppm, and 170−180 ppm. On the upper part of figure, the molecular structures of DPPC and DPPS with corresponding assignment letters shown. In the top spectrum, the spinning sidebands are labelled as '*SSB*', and the resonances marked with dagger '†' provide the evidence of the order−disorder exchange of the palmitic acyl chains. In the bottom spectrum, peaks labelled with the asterisk '*' or double dagger '‡' denote the new resonance compared with the top spectrum, and the selected OLZ signals are indicated by the number(s) in the parenthesis. See the text for details.

Figure 2. Proton-decoupled ^{13}C MASNMR spectra acquired at 316 K (43℃, above T_m), displaying spectral region of phospholipid headgroups, glycerol and saturated acyl chain carbons (12−74 ppm) of samples DPPC (60%)/POPS (40%) with 36 wt.% H_2O (spectrum a) and DPPC (60%)/POPS (40%) with 50 wt.% H_2O (spectrum b), and DPPC (54%)/POPS (36%)/OLZ (10%) with 50 wt.% H_2O (spectrum c). On top of the figure the structural formula of POPS phospholipid is shown. Glycerol and phospholipid headgroup resonances are labelled A−I in spectrum b, where the 12−38 ppm region is labelled with the palmitic (16:0) acyl chain resonances of DPPC. In spectrum a, the resonances labelled with the dagger '†' denote the hydrophobic mismatch of the acyl chains, and the spinning sidebands are labelled as '*SSB*'. In spectrum c, resonances labelled with an asterisk '*' denote new peaks when OLZ is present−compare with spectrum b, and the selected OLZ signals are indicated by the numbers in the parenthesis. See the text for details.

Figure 3. Proton-decoupled ^{13}C MASNMR spectra acquired at 316 K (43°C, above the main phase transition temperature, T_m): carbonyl and carboxyl carbon resonance region (171−179 ppm) of samples DPPC (60%)/POPS (40%) with 36 wt.% H_2O (spectrum a) and DPPC (60%)/POPS (40%) with 50 wt.% H_2O (spectrum b), and DPPC (54%)/POPS (36%)/OLZ (10%) with 50 wt.% H_2O (spectrum c). The two carbonyl (*sn*-1 and *sn*-2) and carboxyl resonances are assigned in spectrum b, and the peak labelled with an asterisk '*' in spectrum c indicates the new carboxyl resonance compared with the spectrum b. The molar composition (PC/PS ratio) makes the theoretical ratio between the carbonyl and carboxyl resonances to be ∼5, the ^{13}C chemical shift values of relevant peaks in this region listed at the bottom part of the figure. See the text for details.

Figure 4. Proton-decoupled ^{13}C MASNMR spectra acquired at 316 K (43°C, above T_m): double bonded acyl chain carbon resonance region (128−132 ppm) of samples DPPC (60%)/POPS (40%) with 36 wt.% H_2O (spectrum a) and DPPC (60%)/POPS (40%) with 50 wt.% H_2O (spectrum b), and DPPC (54%)/POPS (36%)/OLZ (10%) with 50 wt.% H_2O (spectrum c). The two carbons resonances are assigned in spectrum b, and spectrum c, an OLZ signal is indicated by the number in the parenthesis. The ^{13}C chemical shift values of relevant peaks in this region listed at the bottom part of the figure. See the text for details.

Figure 5. ^{31}P MASNMR spectra of samples DPPC (60%)/POPS (40%) with 36 wt.% H_2O (left column) and DPPC (60%)/POPS (40%) with 50 wt.% H_2O (middle column), and DPPC (54%)/POPS (36%)/OLZ (10%) with 50 wt.% H_2O (right column) between sample temperatures 296 K (23°C) and 316 K (43°C), the experimental temperature is labelled with the corresponding spectrum. All spectra were obtained with a 2 kHz MAS spinning rate. The phosphatidylcholine and phosphatidylcholine components are assigned in the spectra at the temperature of 43 °C. See the text for details.

Figure 6. Static ^{31}P spectra of samples a) DPPC (60%)/POPS (40%) with 36 wt.% H_2O, b) DPPC (60%)/POPS (40%) with 50 wt.% H_2O, and c) DPPC (54%)/POPS (36%)/OLZ (10%) with 50 wt.% H_2O at 300 K (27°C, left column) and 316 K (43°C, right column), and ^{31}P CSA values (± 1 ppm) listed at the bottom region.

Table 1. ^{13}C spin-lattice relaxation time constants T_1 (seconds) of the 50 wt.% H_2O bilayers DPPC (60%)/POPS (40%) and DPPC (54%)/POPS (36%)/OLZ (10%) at the temperatures of 23, 33 and 43 ℃. T_1 constants above the liquid-crystalline phases (43℃) are underlined.

Carbon (s)	DPPC / POPS *(50 wt.% H_2O)*			DPPC / POPS / OLZ (10%) (*50 wt.% H_2O*)		
	23 ℃	33℃	43℃	23℃	33℃	43℃
Carbonyl (1):						
sn-1 C=O *(1[a])*	1.18	1.30	1.34	2.57	2.08	1.41
sn-2 C=O *(1[b])*	1.55	1.60	1.77	0.88	0.36	0.42
Carboxyl (F)	1.03	1.55	1.66	1.41	1.88	2.51
POPS C=C:						
C_9	0.55	0.59	0.71	0.69	0.73	0.81
C_{10}	0.47	0.55	0.60	0.67	0.71	0.80
Glycerol Carbons:						
sn-1 *(A)*	0.12	0.15	0.15	0.11	0.11	0.16
sn-2 *(B)*	0.36	0.39	0.50	0.57	0.72	0.87
sn-3 *(C)*	0.09	0.11	0.10	0.22	0.18	0.04
Serine Carbons:						
α *(D)*	0.12	0.18	0.21	0.42	0.55	0.66
β *(E)*	0.39	0.37	0.40	0.49	0.68	0.93
Choline Carbons:						
α *(G)*	0.18	0.21	0.23	0.29	0.28	0.33
β *(H)*	0.23	0.24	0.32	0.35	0.35	0.38
CH_3 *(I)*	0.25	0.30	0.36	0.32	0.36	0.49
Palmitic Carbons:						
2	0.34	0.23	0.21	0.91	0.61	0.48
3	0.77	0.61	0.52	0.63	0.53	0.64
4−7	0.85	0.83	0.72	0.88	0.85	0.83
12, 13	0.68	0.71	0.70	0.64	0.65	0.74
14	1.05	1.11	1.17	0.99	1.04	1.24
15	0.92	0.99	1.08	0.96	1.24	1.19
16	1.73	1.88	3.51	2.20	2.25	4.35
Oleic Carbons:						
8, 11	0.73	0.71	0.66	0.71	0.66	0.67

A−I: Resonances assigned in Figures 1 and 2.

Table 2. ^{31}P spin-lattice relaxation time constants T_1 (seconds) of DPPC (60%)/POPS (40%) with 36 wt.% H_2O, DPPC (60%)/POPS (40%) and DPPC (54%)/POPS (36%)/OLZ (10%) with 50 wt.% H_2O at 23−43 ℃.

T(℃)	DPPC/POPS *(36 wt.% H_2O)*		DPPC/POPS *(50 wt.% H_2O)*			DPPC/POPS/OLZ *(50 wt.% H_2O)*‡					
						PS region			*PC region*		
	PS	PC	PS	PS*	PC	Peak a	Peak b	Peak c	Peak d	Peak e	Peak f
23	0.94	1.15	0.96	1.08	1.04	0.88	1.00	0.99	0.72	0.68	0.94
27	0.85	1.02	0.88	0.93	0.94	0.80	0.76	0.93	0.79	0.68	0.95
31	0.78	0.92	0.76	0.76	0.65	0.82	0.77	0.88	0.78	0.76	0.83
35	0.68	0.81	0.64	0.64	0.59	0.76	0.73	0.83	1.09	0.75	0.81
39	0.65	0.63	0.64	0.55	0.74	0.72	0.66	0.81	1.24	0.79	0.63
43	0.63	0.57	0.61	0.53	0.78	0.67	0.54	0.71	1.96	0.88	0.62

‡ Peaks labled in Figure 5.

Scheme 1

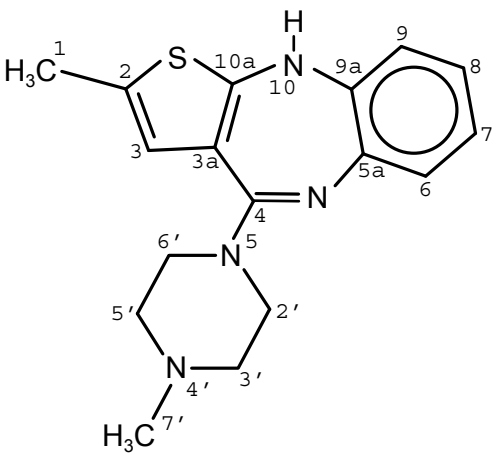

Scheme 2

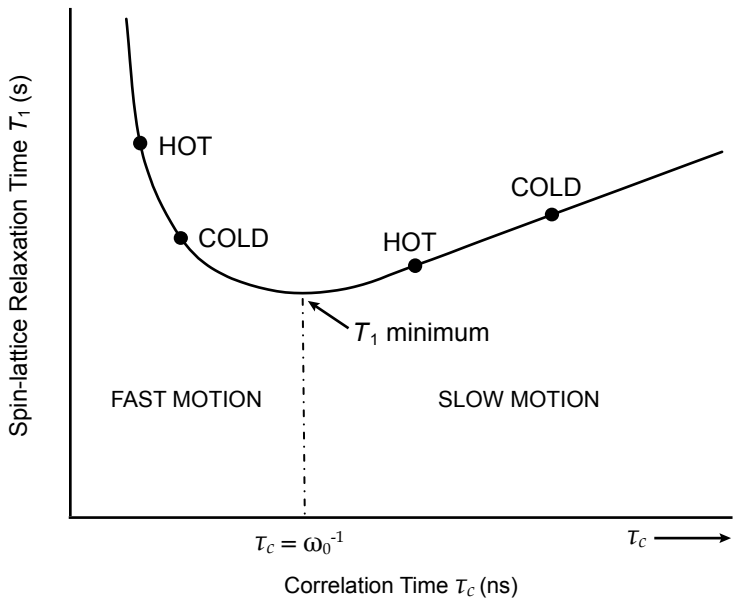
Spin-lattice Relaxation Time T_1 (s)
HOT
COLD
HOT
COLD
T_1 minimum
FAST MOTION
SLOW MOTION
$\tau_c = \omega_0^{-1}$
τ_c
Correlation Time τ_c (ns)

Figure 1

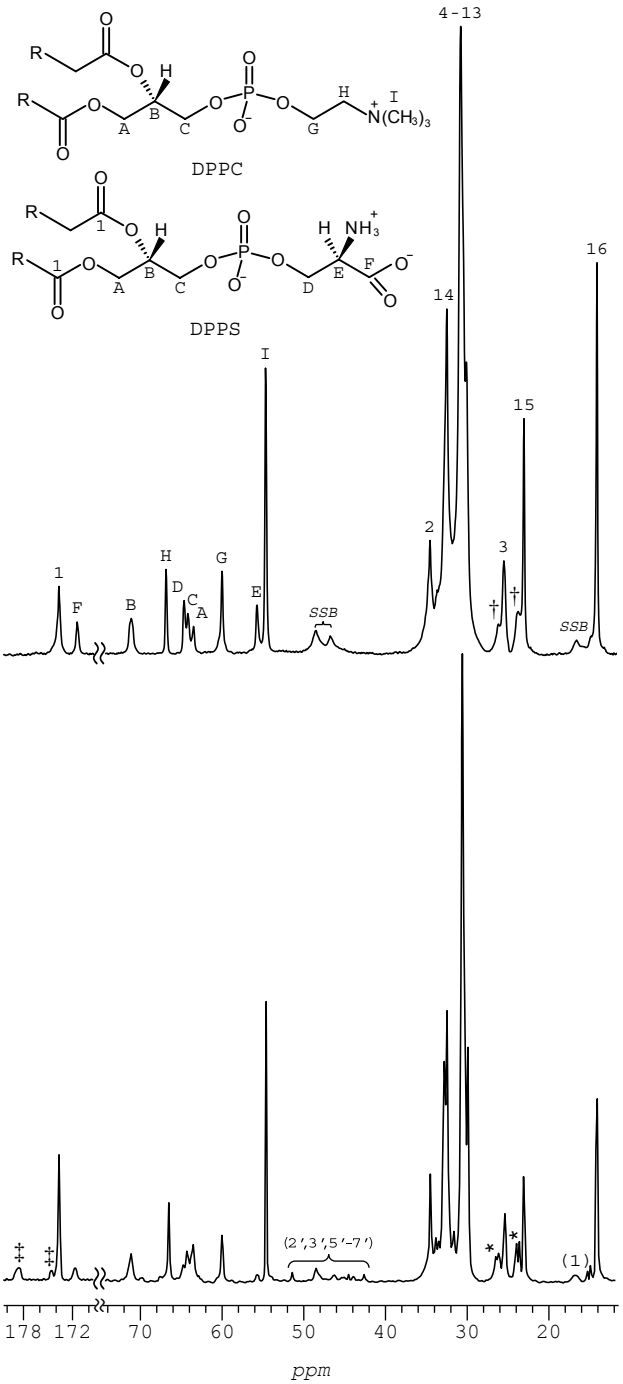
DPPC
DPPS
4-13
14
16
15
2
3
I
1
F
B
H
D
C
A
G
E
SSB
SSB
†
†
(2',3',5'-7')
(1)
*
*
‡
‡
178 172 70 60 50 40 30 20
ppm

Figure 2

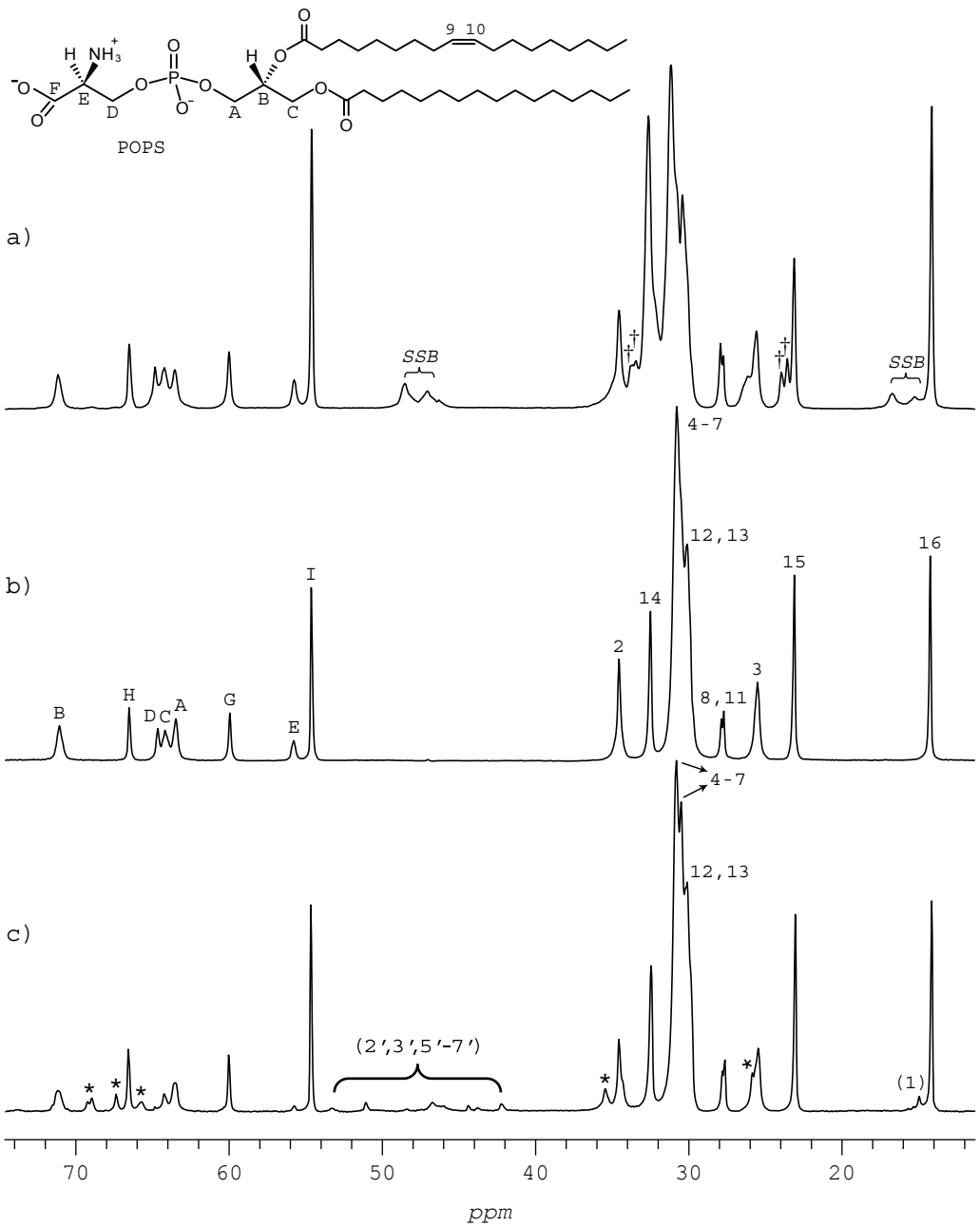
POPS
a)
SSB
SSB
4-7
b)
B
H
D C
A
G
E
I
2
14
12,13
8,11
3
15
16
c)
4-7
12,13
(2′,3′,5′-7′)
(1)
70
60
50
40
30
20
ppm

Figure 3

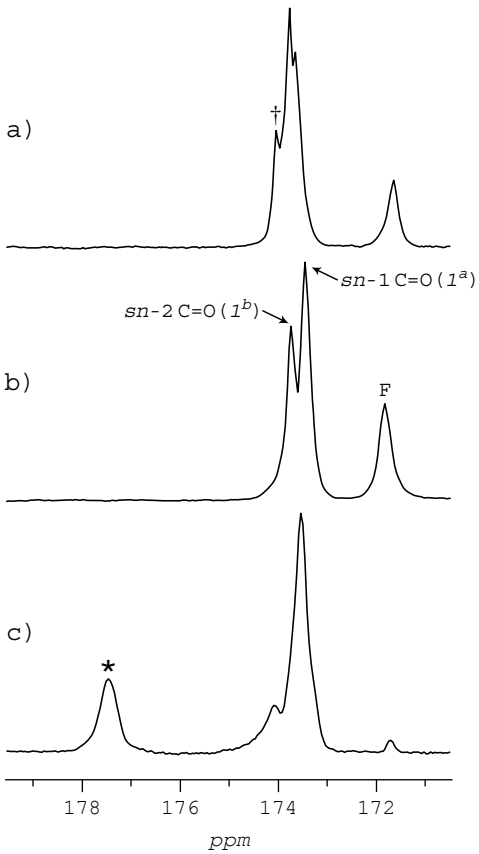

^{13}C chemical shift values of relevant peaks listed below (in *ppm*),

	1^a	1^b	Carboxyl *(F)*
a) DPPC/POPS (~*36 wt.% H_2O*)	173.63	174.05†,173.79	171.64
b) DPPC/POPS (~*50 wt.% H_2O*)	173.42	173.70	171.80
c) DPPC/POPS/OLZ (~*50 wt.% H_2O*)	173.54	174.08	177.51*,171.71

Figure 4

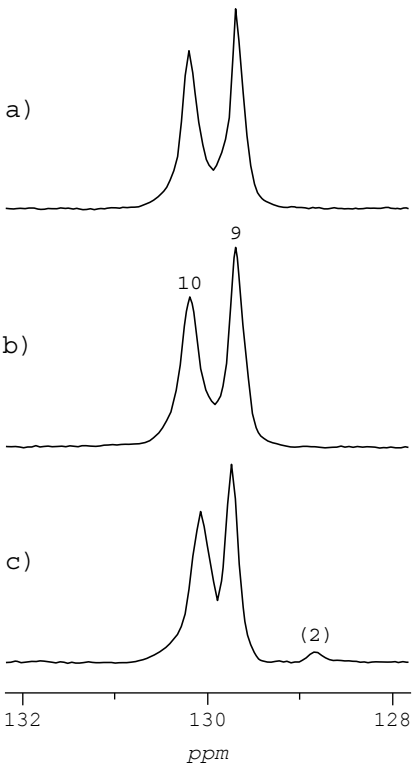

^{13}C chemical shift values of relevant peaks listed below (in ppm)

	C_{10}	C_9
a) DPPC/POPS (*36 wt.% H_2O*)	130.16	129.68
b) DPPC/POPS (*50 wt.% H_2O*)	130.15	129.68
c) DPPC/POPS/OLZ (*50 wt.% H_2O*)	130.06	129.73

Figure 5

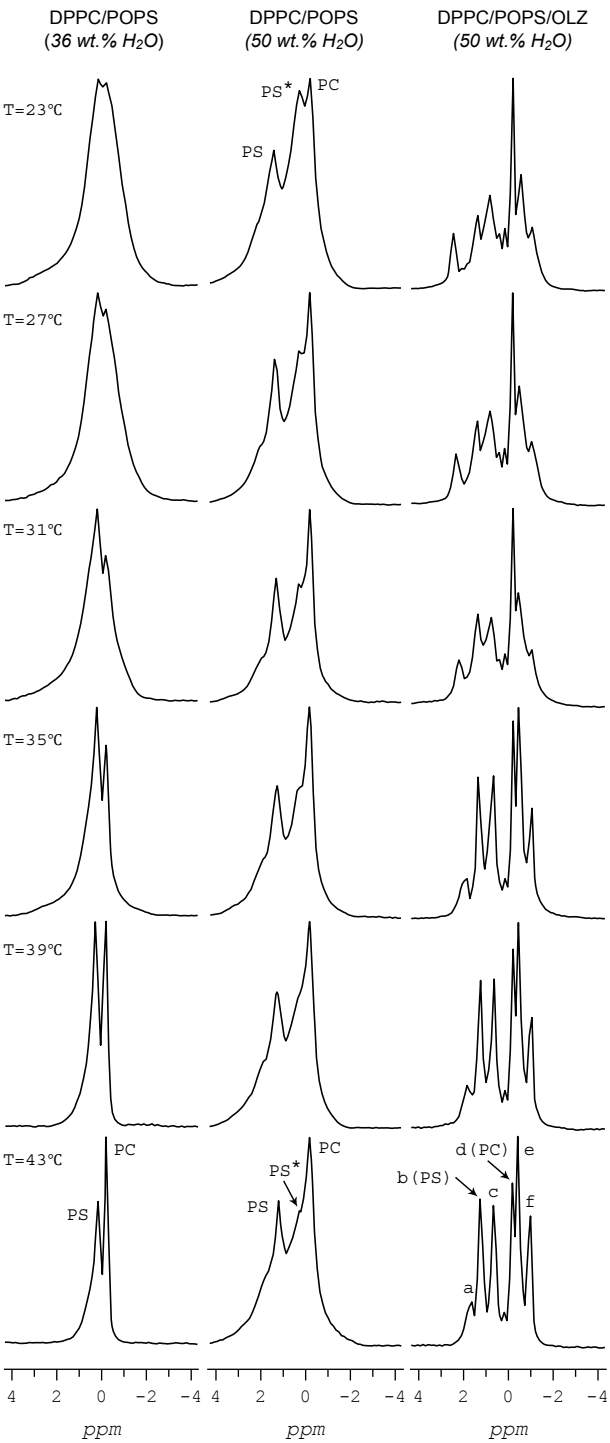
DPPC/POPS
(36 wt.% H2O)
DPPC/POPS
(50 wt.% H2O)
DPPC/POPS/OLZ
(50 wt.% H2O)
T=23°C
T=27°C
T=31°C
T=35°C
T=39°C
T=43°C
PS*
PC
PS
PC
PS
PS*
PC
PS
d (PC)
e
b (PS)
c
f
a
4 2 0 −2 −4
ppm

Figure 6

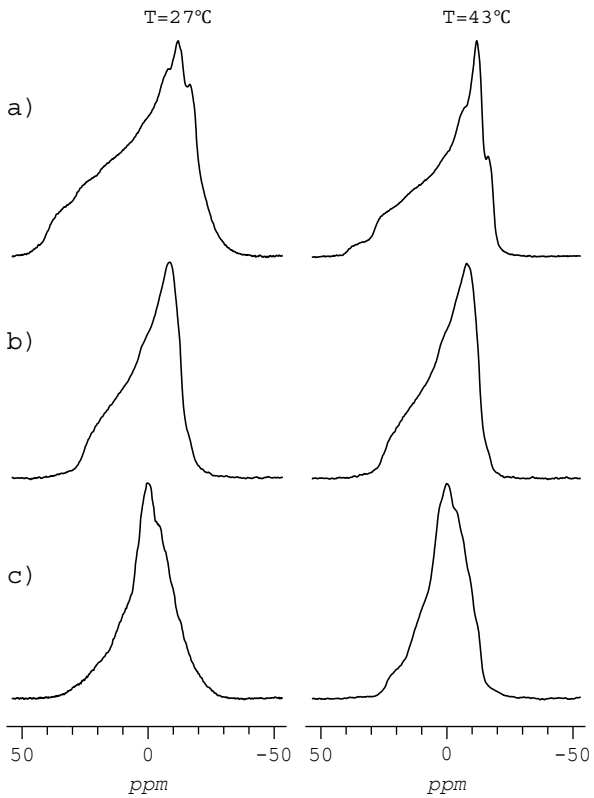

CSA values (±1 ppm) of static ^{31}P NMR spectra listed below

T (℃)	a) DPPC/POPS *(36 wt.% H_2O)*	b) DPPC/POPS *(50 wt.% H_2O)*	c) DPPC/POPS/OLZ *(50 wt.% H_2O)*
23	87	64	63
43	65	58	51